International Journal of Polymer Science

Polymeric Biomaterials for Tissue Engineering Applications

Guest Editors: Shanfeng Wang, Lichun Lu, Chun Wang, Changyou Gao, and Xiaosong Wang

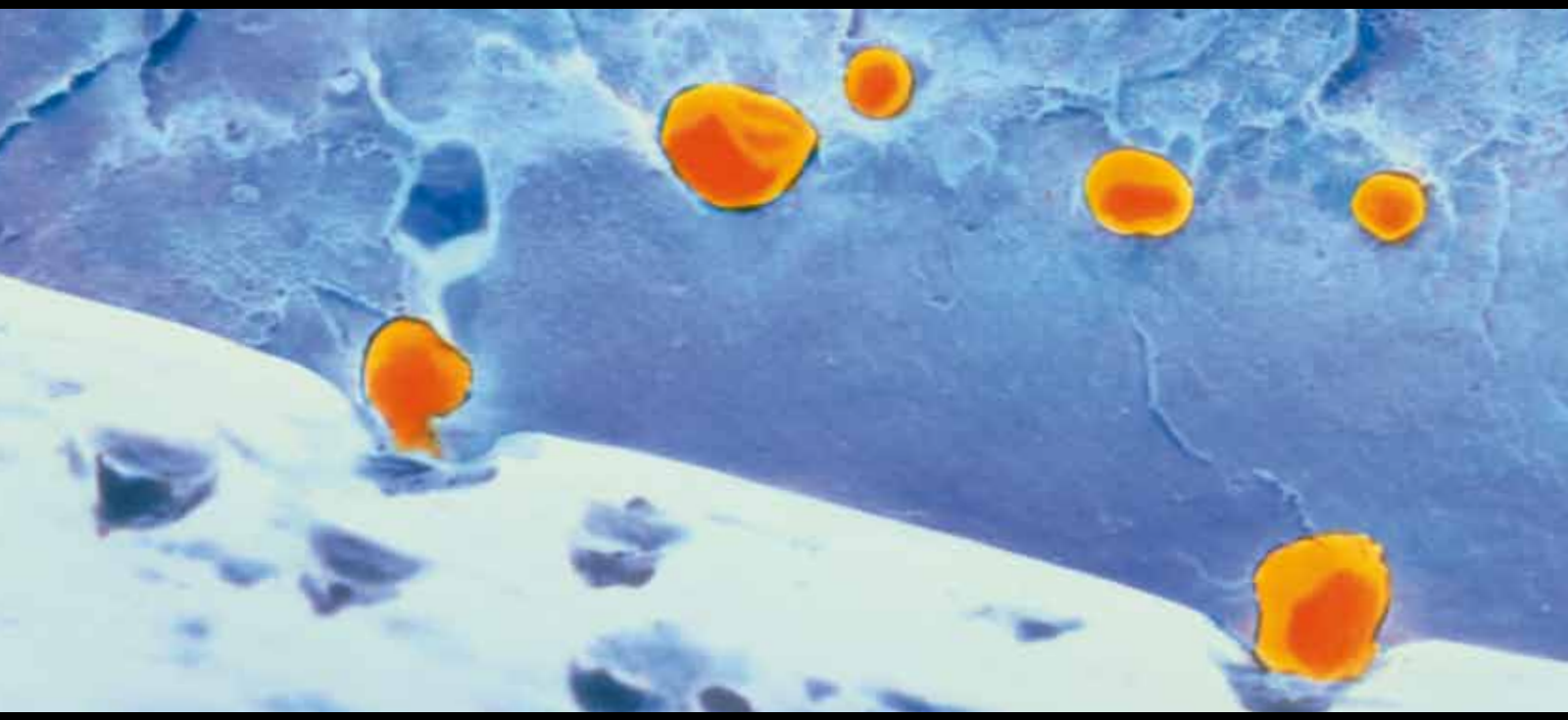

Polymeric Biomaterials for Tissue Engineering Applications

International Journal of Polymer Science

Polymeric Biomaterials for Tissue Engineering Applications

Guest Editors: Shanfeng Wang, Lichun Lu, Chun Wang, Changyou Gao, and Xiaosong Wang

Editorial Board

Contents

Hindawi Publishing Corporation
International Journal of Polymer Science
Volume 2010, Article ID 148513, 2 pages
doi:10.1155/2010/148513

Editorial

Polymeric Biomaterials for Tissue Engineering Applications

Shanfeng Wang,[1] Lichun Lu,[2] Chun Wang,[3] Changyou Gao,[4] and Xiaosong Wang[5]

[1] *Department of Materials Science & Engineering, The University of Tennessee, Knoxville, TN 37996, USA*
[2] *Departments of Biomedical Engineering and Orthopaedic Surgery, Mayo Clinic College of Medicine, Rochester, MN 55905, USA*
[3] *Department of Biomedical Engineering, University of Minnesota, Minneapolis, MN 55455, USA*
[4] *Department of Polymer Science and Engineering, Zhejiang University, Hangzhou 310027, China*
[5] *School of Chemistry, University of Leeds, Leeds LS2 9JT, UK*

Correspondence should be addressed to Shanfeng Wang, swang16@utk.edu

Received 24 August 2010; Accepted 24 August 2010

The interdisciplinary field of biomaterials and tissue engineering has been one of the most dynamic and rapidly expanding disciplines during the past two decades. Polymers are especially useful in this area mainly because of their flexibility in chemical structure engineering and physical property design. Many noncytotoxic and biodegradable polymers can be fabricated into medical devices for numerous applications, including tissue replacement, drug delivery, cancer therapy, and nonviral gene therapy. As a result of rapid growth of polymer science and engineering in recent years, synthetic and supramolecular strategies have been developed for polymeric biomaterial exploration. By tuning polymer structural parameters and morphologies at different length scales, controllable physical properties for satisfying diverse clinical needs have been demonstrated. Polymeric biomaterials can also be incorporated with natural materials and inorganic nanoparticles to achieve novel, unique, and synergetic properties for better performance. Biomimetic and intelligent polymeric systems have also been investigated to advance our material design strategies.

Cell/tissue-material interactions are crucial in applying biomaterials to clinical uses. There are major factors such as surface chemistry, topology, and mechanical cues to influence cell responses to biomaterial substrates collectively. Through rational design of polymer surface properties, cell-material interactions such as cell adhesion, spreading, proliferation, migration, and differentiation can be modulated. Vesicular colloids self-assembled from amphiphilic block copolymers can be used as carriers for delivering drugs to desired targets. Polycations such as polyethylenimine can be used as nonviral gene delivery carriers. Polymer scaffolds with predesigned geometries and nanometer-scale or micron-scale structural parameters can be fabricated for bone, nerve, cardiovascular, skin, ligament, and cartilage tissue engineering applications.

The aim of this special issue is to highlight recent significant progress in the synergy between material design strategies and biological evaluations through contributions from active researchers in the field. This issue covers various topics related to biomaterials for tissue engineering applications. Six original research papers and three reviews are included to stimulate the continuing efforts in developing novel polymeric systems, which are crucial to improve our understanding on cell/tissue-material interactions and biomedical applications.

Combination of naturally derived and synthetic polymers is an efficient way to produce biomaterials that integrate excellent biocompatibility from the former component and good processing properties from the later. All of the six original research papers demonstrate the importance of this approach. The first three papers describe different polymer composites containing natural polymers and focus on their mechanical properties. In the first paper (ID 270273), X. Zhu et al. report the effects of composite formulation on the mechanical properties of biodegradable poly(propylene fumarate) (PPF)/bone fiber scaffolds. PPF is an unsaturated linear polyester that can be cross-linked. Mineralized bone fibers (MBFs) were from allograft bone while demineralized bone fibers (DMFs) were obtained from acidification of MBF. In this study, the authors studied the effects of various

parameters such as PPF molecular weight, incorporation of bone fibers (MBFs or DBFs), and the amounts of cross-linker, initiator, and porogen on the ultimate strength and compressive modulus of the composite scaffolds. In the second paper (ID 369759), Z. Wang et al. report chitin fiber enhanced chitosan 3D composite rods. In this study, chitin fiber/chitosan composite rods with a layered structure were constructed using an *in situ* precipitation method. The bending strength and modulus were increased by 23.6% and 26.8% by adding 0.5% chitin fiber to the chitosan matrix. In the third paper (ID175264), R. Khanna et al. report the *in situ* swelling behavior of chitosan-polygalacturonic acid/hydroxyapatite nanocomposites in cell culture media. Nanocomposite films were soaked in cell culture media, and *in situ* characterization was performed to demonstrate that nanoscale elastic modulus decreased by ~2 GPa over 48 days.

Electrospinning and salt-leaching are widely used techniques for the fabrication of porous structures for tissue engineering applications. In the fourth paper (ID 436178), B. Wulkersdorfer et al. applied a combined electrospinning/particulate leaching technique to fabricate biomodal porous scaffolds. In this technique, sucrose particles were mixed with poly(glycolic acid) and electrospun into fiber mesh. Deep cellular penetration was found in these biomodal porous scaffolds while no cellular penetration was found in the spun scaffolds without using sucrose particles.

In cardiovascular tissue engineering applications, surface modification is an effective approach to improve the blood compatibility of the polymers such as polyurethanes (PUs). In the fifth paper (ID 807935), F. Gong et al. report a method to immobilize hyaluronic acid (HA), a nonimmunogenic biomaterial naturally derived from mammalian tissues, onto the surface of amino-functionalized PU films. The modified PU films, without detectable cytotoxicity, could prolong the coagulation time in platelet-poor plasma and better support human vein endothelial cell adhesion and proliferation. HA immobilized PU is promising as a blood-contacting material for cardiovascular tissue engineering applications.

As one tissue engineering approach, oral therapy by delivering engineered microorganisms such as viable cells in microcapsules is promising in treating many diseases. In the sixth paper (ID 985137), H. Chen et al. report the investigation of genipin cross-linked alginate-chitosan microcapsule for oral delivery of live bacterial cells. The potential of this microcapsule system with strong stability was evaluated using a dynamic human gastrointestinal (GI) model for GI applications.

Review papers in this issue cover three different fields: chemical modification of polymer biomaterials, surface modification, and polymers for fabricating nerve conduits. The seventh paper (ID 423460) contributed by B. Hazer surveys chemical methods used to modify hydrophobic, semicrystalline poly(3-hydroxy alkanoate)s, a series of degradable biomaterials produced by microorganisms, to be amphiphilic. These amphiphilic poly(3-hydroxy alkanoate)s can be used for different tissue engineering applications. In the eighth paper (ID 296094), T. G. Vladkova reviews surface engineered polymeric biomaterials with improved biocontact properties. Numerous methods such as physicochemical modification and immobilization of biomacromolecules are discussed. The final paper of this issue (ID 138686) contributed by S. Wang et al. provides a comprehensive summary of polymeric biomaterials and fabrication methods that have been used for making synthetic nerve conduits. Learning from the existing polymer candidates, we can improve our material design strategies for developing novel biomaterials with optimal properties for nerve regeneration and repair.

Acknowledgments

The authors thank all the contributing authors and reviewers for their efforts in putting together this special issue.

Shanfeng Wang
Lichun Lu
Chun Wang
Changyou Gao
Xiaosong Wang

Hindawi Publishing Corporation
International Journal of Polymer Science
Volume 2010, Article ID 270273, 6 pages
doi:10.1155/2010/270273

Research Article

Effects of Composite Formulation on Mechanical Properties of Biodegradable Poly(Propylene Fumarate)/Bone Fiber Scaffolds

Xun Zhu, Nathan Liu, Michael J. Yaszemski, and Lichun Lu

Departments of Orthopedic Surgery and Biomedical Engineering, Mayo Clinic College of Medicine, 200 First Street SW, Rochester, MN 55905, USA

Correspondence should be addressed to Lichun Lu, lu.lichun@mayo.edu

Received 15 March 2010; Accepted 9 May 2010

Academic Editor: Shanfeng Wang

The objective of our paper was to determine the effects of composite formulation on the compressive modulus and ultimate strength of a biodegradable, in situ polymerizable poly(propylene fumarate) (PPF) and bone fiber scaffold. The following parameters were investigated: the incorporation of bone fibers (either mineralized or demineralized), PPF molecular weight, N-vinyl pyrrolidinone (NVP) crosslinker amount, benzoyl peroxide (BP) initiator amount, and sodium chloride porogen amount. Eight formulations were chosen based on a resolution III two-level fractional factorial design. The compressive modulus and ultimate strength of these formulations were measured on a materials testing machine. Absolute values for compressive modulus varied from 21.3 to 271 MPa and 2.8 to 358 MPa for dry and wet samples, respectively. The ultimate strength of the crosslinked composites varied from 2.1 to 20.3 MPa for dry samples and from 0.4 to 16.6 MPa for wet samples. Main effects of each parameter on the measured property were calculated. The incorporation of mineralized bone fibers and an increase in PPF molecular weight resulted in higher compressive modulus and ultimate strength. Both mechanical properties also increased as the amount of benzoyl peroxide increased or the NVP amount decreased in the formulation. Sodium chloride had a dominating effect on the increase of mechanical properties in dry samples but showed little effects in wet samples. Demineralization of bone fibers led to a decrease in the compressive modulus and ultimate strength. Our results suggest that bone fibers are appropriate as structural enforcement components in PPF scaffolds. The desired orthopaedic PPF scaffold might be obtained by changing a variety of composite formulation parameters.

1. Introduction

There has been a great need for the treatment of skeletal defects which may result from tumors, trauma, or abnormal development [1]. The current methods for restoring tissue structure and function rely mostly on autograft and allograft [2–4]. Both methods, while appropriate for management of many bone defects, do have certain limitations. These include donor site morbidity after autograft harvesting and slow incorporation of cortical allograft. The other materials commonly used such as polymers, ceramics, and metals all have their associated drawbacks, such as poor integration with the host tissue, stress shielding of adjacent bone, and osteolysis from particulate wear debris [5]. The treatment regimen could be improved with the availability of a skeletal regeneration biomaterial that could be processed into the specific shape needed, provide structural support required, be replaced by new, vascularized bone tissue, and then disappear to allow the new bone to remodel along local stress lines.

Poly(propylene fumarate) (PPF) is an unsaturated linear polyester with fumarate double bonds that can be crosslinked *in situ*. It is biocompatible, biodegradable, osteoconductive, and capable of both preformed and injectable applications [6–9]. PPF scaffolds can be used to fill irregularly shaped defects with minimal surgical intervention. They possess mechanical properties on the order of magnitude of human trabecular bone. The fabrication of biodegradable polymer composites based on PPF for orthopaedic applications has been the subject of investigation in our laboratory [10–12]. The properties of the produced composites can be tailored for specific applications by varying different parameters

including crosslinking density and fillers [10, 11, 13, 14]. The composite formulation can include a porogen such as NaCl for initial porosity and a particulate ceramic such as β-tricalcium phosphate (TCP) for mechanical reinforcement and increased osteoconductivity.

Mineralized bone fibers (MBFs) are obtained by processing allograft bone. The technique involves shaving the cortical bone to produce bone fibers. MBFs have a composition identical to bone and may be used for structural reinforcement of scaffolds. They have been shown to increase the initial compressive strength of PPF/PPF-DA scaffolds [11]. The acidification of MBF produces demineralized bone fibers (DBF), which consist of nonmineral components of MBF and have accessible bone inductive factors. Demineralized bone matrices (DBMs) have extremely high-osteoinductive properties and greatly improve the integration of autogenous bone grafts in the skull [15]. In the various forms of DBM, the fiber-based grafts produced the largest new bone in a critical size cranial defect in athymic rats [16]. These grafts were found to perform as well as autografts [16]. Therefore, the incorporation of bone fibers in PPF scaffolds not only provides a structural support component but could also promote bone regeneration in bone defects.

In this study, experiments were designed to study the effects of various processing parameters, such as PPF molecular weight, incorporation of bone fibers (MBF or DBF), crosslinker amount, initiator amount, and porogen amount, on the ultimate strength and compressive modulus of PPF/bone fiber scaffolds.

2. Materials and Methods

2.1. Raw Materials. Fumaryl chloride (Aldrich, Milwaukee, WI) was purified by distillation under nitrogen atmosphere. Demineralized bone fibers (DBFs) were obtained through acidification wash of mineralized bovine bone fibers (MBF) (OsteoTech Inc.). Propylene glycol, N-vinyl pyrrolidinone (NVP), *N*,*N*-dimenthyl-*p*-toluidene (DMT), benzoyl peroxide (BP) and sodium chloride were purchased from Aldrich Chemical (Milwaukee, WI) and used as received. All solvents were purchased from Fisher (Pittsburgh, PA) as reagent grade and used as received. Sodium chloride was sieved to obtain particles in a 106–300 μm size range and used as porogen. All experiments described below were based on a Resolution III two-level fractional factorial design varying six parameters. The six parameters included PPF molecular weight, NVP to PPF ratio, BF to polymer (PPF/NVP) ratio, BF type, BP to PPF ratio, and the percentage of NaCl in the composites. The experimental design and the values for all parameters are presented in Table 1

2.2. PPF Synthesis. PPF was synthesized by a two-step reaction process as described previously in [17]. Briefly, fumaryl chloride was added dropwise to a solution of propylene glycol in methylene chloride at 0°C under nitrogen in the presence of K_2CO_3. After addition of fumaryl chloride, the reaction mixture was stirred for an additional 2 h at 0°C before water was added to dissolve the inorganic salt. The organic phase was separated and dried over Na_2SO_4. After filtration of the mixture and evaporation of the solvent, the formed di(2-hydroxylpropyl) fumarate was converted to PPF by transesterification at 160°C and 0.5 mmHg. The produced polymer was purified by solution precipitation forming a viscous liquid. Gel permeation chromatography with a differential refractometer (Waters 410, Milford, MA) was used to determine polymer molecular weight distributions. A Phenogel column (300 × 7.8 mm, 5 nm, mixed bed, Phenomenex, Torrance, CA) and a Phenogel guard column (7.8 mm, 5 nm, mixed bed, Phenomenex) were employed for the elution of polymer solution in chloroform at flow rate of 1 ml/min. Polystyrene standards were utilized to obtain a calibration curve for calculating the polymer molecular weights.

2.3. Demineralization of Bone Fibers. MBF were weighed to the nearest gram and soaked in 15 volume of a 0.6 N HCl solution with 0.025% Triton X-100. When the pH of the solution was more than 1, the acid was decanted and replaced with another 15 volume of fresh 0.6 N HCl without triton. PH readings were taken every ten minutes until it is more than 1. The acid was carefully decanted and the same volume of distilled, deionized water (ddH_2O) was added. The water wash was repeated several times until the pH is greater than 3. The resulting DMF were soaked in 70% ethanol for 30 min. and collected on a 106 μm sieve. DMF were washed again with ddH_2O and freeze-dried for 24 hrs.

2.4. Experimental Design. All experiments described below were based on a Resolution III two-level fractional factorial design varying six parameters [18]. The experimental design and the values for all parameters are presented in Table 1. Six processing parameters were varied to determine their effects on mechanical properties of the composite scaffolds. The high (+) and low (−) values for all parameters are listed (Table 1(a)). The number average molecular weights (Mn) of PPF were chosen as 4000 and 2000. The ratios of NVP to PPF were 0.7 and 0.5 ml per gram. The weight percentages of bone fibers to polymer were 20% and 0%. The weight percentages of BP were 0.5% and 0.1%. The weight percentages of NaCl were 30% and 0%. The two levels for the factor called bone fiber type are DMF and MBF. High and low levels were then combined according to the resolution III design to create eight formulations (Table 1(b)). This factorial design will demonstrates the effect that each parameter exhibits while minimizing the numbers of trials. The results from each experiment were examined to determine the main effects of each parameter on the measured property [18].

2.5. Scaffold Preparation. The designated amount of monomer (NVP) was divided into two portions. Three-fourths of the monomer was combined with the PPF. The initiator (BP) was dissolved in the remaining one-fourth of the monomer and added to the polymer solution. The solid phase components (BF, NaCl) were added, followed by DMT. The resulting paste was immediately placed in 8-mm diameter glass vials. The resulting PPF cylinders (*dry* samples) were removed from the vials after overnight

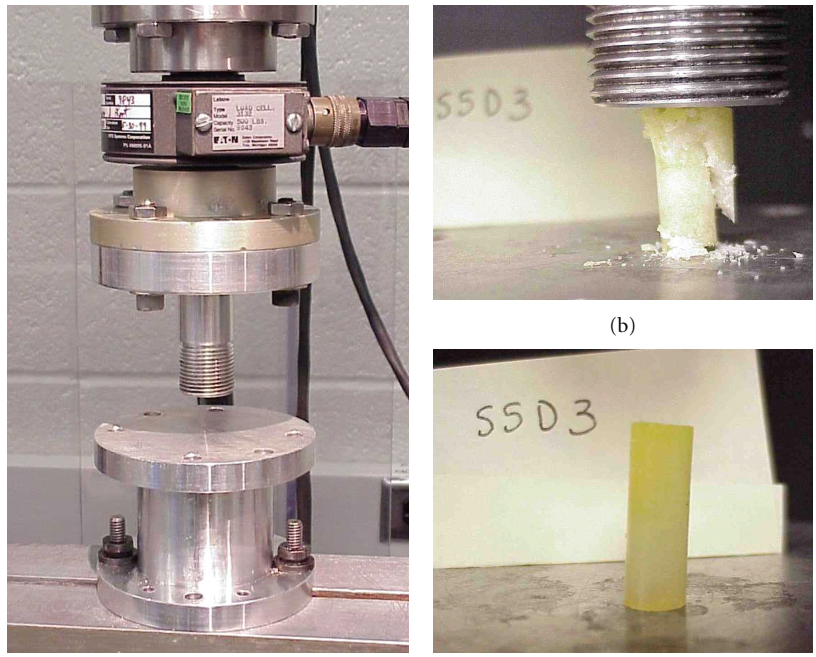

(a) (b) (c)

Figure 1: (a) The servohydraulic materials testing machine used in this study. (b) A representative PPF composite scaffold incorporating mineralized bone fibers and sodium chloride porogen. The PPF cylinder was approximately 6 mm in diameter and 20 mm in height. (c) The specimen was placed between two solid platens and compressed at a rate of 0.1 mm/second.

Table 1

(a) High and Low Levels for Six Parameters Tested in a Resolution III, Two-level Fractional Factorial Design

Level	PPF Mn	NVP/PPF	BF/polymer	BF Type	BP/PPF	NaCl
+	4000	0.7 ml/g	2/8	DBF	0.5%	30%
−	2000	0.5 ml/g	0	MBF	0.1%	0

(b) Combinations of the Experimental Variables in the Resolution III, Two-level Fractional Factorial Design

Formula	PPF Mn	NVP/PPF	BF/polymer	BF Type	BP/PPF	NaCl
1	+	+	+	+	+	+
2	+	+	−	none	−	−
3	+	−	+	−	+	−
4	+	−	−	none	−	+
5	−	+	+	−	−	+
6	−	+	−	none	+	−
7	−	−	+	+	−	−
8	−	−	−	none	+	+

crosslinking. Half of the samples were incubated with phosphate buffered saline (PBS) for one day to leach out some of sodium chloride (*wet* samples). The scaffolds tested in this study had a diameter of 6 mm and a height of 20 mm.

2.6. Mechanical Testing. Mechanical properties of both dry and wet samples were analyzed using a servohydraulic testing machine (MTS, Minneapolis, MN), as shown in Figure 1 (a). Sample length and diameter were measured before testing (Figure 1 (b)). The specimens were placed between two solid platens and compressed at a rate of 0.1 mm/second (Figure 1 (c)). Load and displacement were recorded using a digital computer (Figure 2). The stress-strain curve was plotted by determining stress as the load divided by the cross-sectional area and strain as the displacement divided by the initial length of the cylinder. Compressive modulus was calculated as the slope of the initial linear portion of the stress-strain curve, beginning at 1.0% strain. The highest strength achieved was the ultimate strength.

2.7. Statistical Analysis. All data are reported as means ± standard deviations (SDs) for $n = 4$, except for size

Table 2: Summary of Results for Ultimate Strength and Compressive Modulus.

	Dry Samples		Wet Samples	
Formulation	Modulus (MPa)	Ultimate Strength (MPa)	Modulus (MPa)	Ultimate Strength (MPa)
1	117 ± 39	9.9 ± 0.3	24.5 ± 4.6	3.3 ± 0.4
2	108 ± 15	13.2 ± 14	66.0 ± 7.7	7.0 ± 0.7
3	246 ± 1.0	11.1 ± 0.6	358 ± 5.2	16.6 ± 4.4
4	271 ± 29	20.3 ± 8.0	184 ± 1.3	12.0 ± 0.5
5	258 ± 25	13.3 ± 1.0	157 ± 22	8.7 ± 2.1
6	184 ± 0.5	13.0 ± 0.5	101 ± 0.2	9.2 ± 0.6
7	21.3 ± 5.7	2.1 ± 0.9	2.8 ± 0.1	0.4 ± 0.0
8	220 ± 17	18.4 ± 4.0	157 ± 8.2	11.0 ± 2.0

Values are given as means ± standard deviations for $n = 4$.

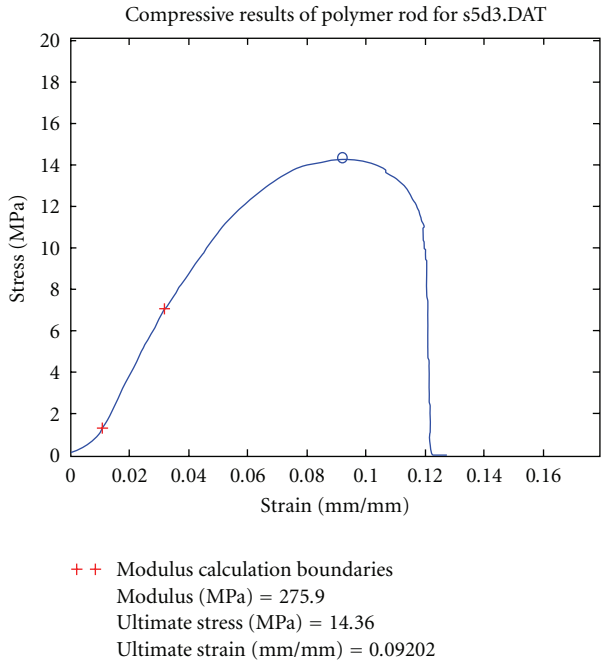

Figure 2: Load and displacement of the representative sample shown in Figure 1 were recorded during compression. The stress-strain curve was then plotted and compressive modulus was calculated as the slope of the initial linear portion of the stress-strain curve, beginning at 1.0% strain. The highest strength achieved was the ultimate strength.

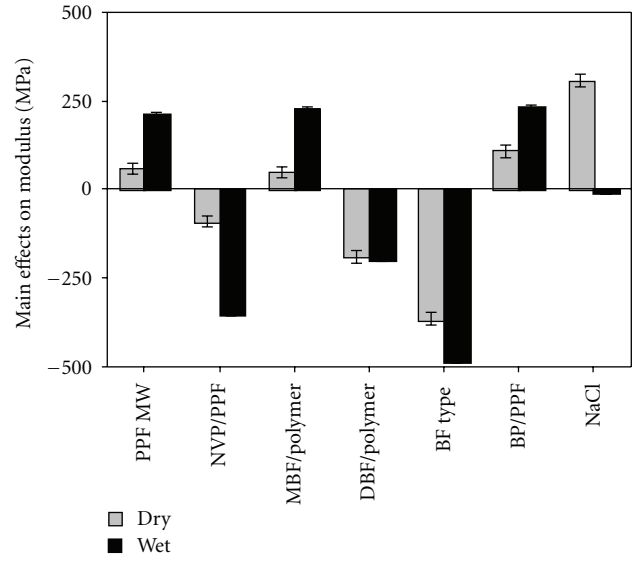

Figure 3: The main effects of the parameters on the compressive modulus of the crosslinked PPF composites. A positive number indicates an increase in the modulus as the parameter was changed from a low (−) level to a high (+) level. A negative number indicates a decrease in the modulus as the parameter was changed from a low (−) level to a high (+) level. Error bars represent the standard error of the effect (dry ± 16.5 MPa, wet ± 6.2 MPa).

distribution measurements where SD was calculated based on normal distribution. Single factor analysis of variance (ANOVA) was used to assess the statistical significance of results. Scheffé's method was employed for multiple comparison tests at significance levels of 95 and 99%.

3. Results

This study was designed to determine the effects of six parameters on the ultimate stress and compressive modulus of PPF/bone fiber composite scaffolds. The six parameters included PPF molecular weight, NVP to PPF ratio, BF to polymer (PPF/NVP) ratio, BF type, BP to PPF ratio, and the percentage of NaCl in the composites. The ultimate stress and compressive modulus of all formulations were measured and values are given in Table 2.

3.1. Compressive Modulus. Absolute values of compressive moduli varied from 21.3 to 271 MPa and 2.8 to 358 MPa for dry and wet samples, respectively (Table 2). The results from each formulation were calculated to determine the effects of each parameter on the measured property (Figure 3). In dry samples, the presence of NaCl significantly increased the observed modulus values and overshadowed the effects contributed by other factors. This increased modulus was not seen in the corresponding wet samples. Therefore, the mechanical data from wet samples are more suitable for

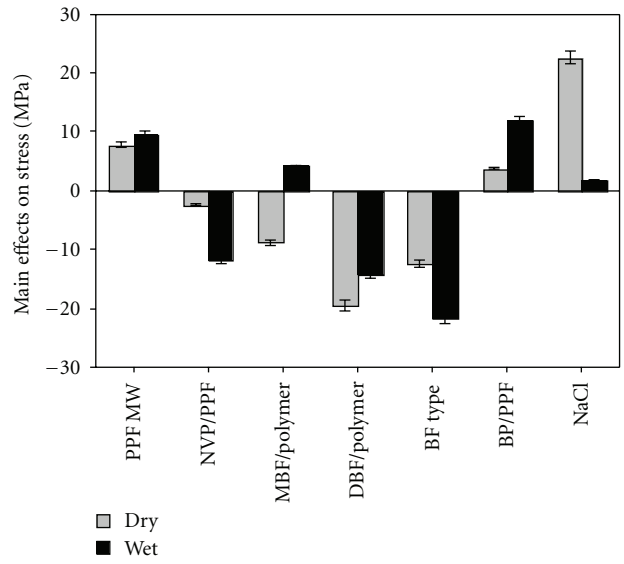

Figure 4: The main effects of the parameters on the ultimate strength of the crosslinked PPF composites. A positive number indicates an increase in the strength as the parameter was changed from a low (−) level to a high (+) level. A negative number indicates a decrease in the strength as the parameter was changed from a low (−) level to a high (+) level. Error bars represent the standard error of the effect (dry ± 16.5 MPa, wet ± 6.2 MPa).

analysis of other effects. The incorporation of mineralized bone fibers and the increase of PPF molecular weight significantly increased the compressive modulus of PPF/NVP scaffolds. A decrease in monomer (NVP) led to an increase in compressive modulus. An increase in radical initiator (BP) was also found to increase the compressive modulus. Demineralization of bone fibers significantly decreased the compressive modulus of the scaffolds.

3.2. Ultimate Strength. The ultimate strength of the crosslinked composites varied from 2.1 to 20.3 MPa for dry samples and from 0.4 to 16.6 MPa for wet samples (Table 2). Very similar to compressive modulus, the presence of NaCl in dry samples significantly increased the observed modulus values and overshadowed the effects contributed by other factors (Figure 4), a phenomena not observed in the corresponding wet samples. The incorporation of MBF and the increase of PPF molecular weight were found to increase the ultimate strength of PPF/NVP scaffolds dramatically. Ultimate strength also increased as the amount of benzoyl peroxide increased or the amount of NVP decreased in the composites. Demineralization of bone fibers significantly decreased the ultimate strength of the scaffolds.

4. Discussion

Biodegradable PPF is a promising orthopedic material that may be used as injectable or preformed scaffolds to repair and regenerate bone defects [19–21]. The components used to form PPF scaffolds have a large influence on their mechanical properties. The objective of our study was to measure the compressive modulus and ultimate strength to determine the effects of the incorporation of bone fibers, PPF molecular weight, NVP amount, BP amount, NaCl amount, and demineralization of bone fibers on these measured properties. It was the first time that the effects of the incorporation of bone fibers and demineralization of bone fibers on PPF scaffolds were investigated.

New and important factors have been identified to affect the mechanical properties of PPF/NVP scaffolds. The incorporation of mineralized bone fibers and an increase in PPF molecular weight resulted in higher compressive modulus and ultimate strength. Both mechanical properties also increased when the amount of benzoyl peroxide increased or the amount of NVP decreased. Sodium chloride had a dominating effect on the increase of mechanical properties in dry samples but showed little effects in wet samples. Demineralized bone fibers led to a decrease in the compressive modulus and ultimate strength.

Our results are consistent with a previous finding that compressive modulus and ultimate strength increased with increasing the amount of benzoyl peroxide and a decrease in NVP amount [13]. PPF molecular weight was also found to have great influence on the mechanical properties. At higher molecular weights (2000 to 5000), it was reported that PPF molecular weight did not affect the mechanical strength [13]. This result, however, was based on dry samples incorporating NaCl to determine the main effects. As shown in our study, the dominating effect of NaCl in dry samples masked the effects of other factors. Therefore, wet samples are more appropriate to determine the effects of factors other than NaCl.

We demonstrated for the first time that the incorporation of mineralized bone fibers in PPF/NVP scaffolds increases the mechanical properties significantly and in contrast, the incorporation of demineralized bone fibers decrease the mechanical properties significantly. Considering the fact that both bone fibers are biodegradable and DMF are osteoinductive, our results showed that PPF/bone fiber composites with a wide range of mechanical properties could be fabricated for different clinical uses.

In summary, we have identified the important factors that affect the compressive modulus and ultimate strength of PPF/bone fiber scaffolds. The desired orthopedic PPF scaffold might be obtained by varying these factors. Our results suggest that bone fibers are appropriate as structural enforcement components in PPF scaffolds, and may modulate other aspects of the synthetic biomaterials such as osteoconductivity.

Acknowledgments

This paper was supported by the John Smith Foundation, Mayo Foundation, and National Institutes of Health (R01 EB30005 and AR 45871).

References

[1] L. Lu, B. L. Currier, and M. J. Yaszemski, "Synthetic bone substitutes," *Current Opinion in Orthopaedics*, vol. 11, no. 5, pp. 383–390, 2000.

[2] A. G. Mikos, L. Lu, J. S. Temenoff, and J. K. Tessmar, "Synthetic bioresorbable polymer scaffolds," in *Biomaterials Science*, B. D. Ratner, A. S. Hoffman, F. J. Schoen, and J. E. Lemons, Eds., pp. 735–749, Elsevier, New York, NY, USA, 2nd edition, 2004.

[3] L. Lu, E. Jabbari, M. J. Moore, and M. J. Yaszemski, "Animal models for evaluation of tissue engineered orthopedic implants," in *The Biomedical Engineering Handbook*, J. D. Bronzino, Ed., chapter 45, pp. 1–10, CRC Press, Boca Raton, Fla, USA, 3rd edition, 2006.

[4] S. Wang, L. Lu, B. L. Currier, and M. J. Yaszemski, "Orthopedic prosthesis and joint implants," in *An Introduction to Biomaterials*, S. A. Guelcher and J. O. Hollinger, Eds., Biomedical Engineering Series, pp. 369–393, CRC /Taylor & Francis, Boca Raton, Fla, USA, 2006.

[5] M. Light and I. O. Kanat, "The possible use of coralline hydroxyapatite as a bone implant," *Journal of Foot Surgery*, vol. 30, no. 5, pp. 472–476, 1991.

[6] S. Wang, L. Lu, and M. J. Yaszemski, "Bone-tissue-engineering material poly(propylene fumarate): correlation between molecular weight, chain dimension, and physical properties," *Biomacromolecules*, vol. 7, no. 6, pp. 1976–1982, 2006.

[7] K.-W. Lee, S. Wang, L. Lu, E. Jabbari, B. L. Currier, and M. J. Yaszemski, "Fabrication and characterization of poly(propylene fumarate) scaffolds with controlled pore structures using 3-dimensional printing and injection molding," *Tissue Engineering*, vol. 12, no. 10, pp. 2801–2811, 2006.

[8] K.-W. Lee, S. Wang, M. J. Yaszemski, and L. Lu, "Physical properties and cellular responses to crosslinkable poly(propylene fumarate)/hydroxyapatite nanocomposites," *Biomaterials*, vol. 29, no. 19, pp. 2839–2848, 2008.

[9] S. Wang, D. H. R. Kempen, M. J. Yaszemski, and L. Lu, "The roles of matrix polymer crystallinity and hydroxyapatite nanoparticles in modulating material properties of photo-crosslinked composites and bone marrow stromal cell responses," *Biomaterials*, vol. 30, no. 20, pp. 3359–3370, 2009.

[10] X. Zhu, L. Lu, N. Liu, P. Chu, B. L. Currier, and M. J. Yaszemski, "Mechanical properties of biodegradable poly(propylene fumarate/bone fiber composites," *Transactions Society of Biomaterials*, vol. 25, p. 260, 2002.

[11] S. He, J. Ulrich, R. G. Valenzuela, et al., "Mechanical properties of biodegradable poly(propylene fumarate)-bone fiber composites during the degradation process," *Transactions Society of Biomaterials*, vol. 24, p. 149, 2001.

[12] B. D. Porter, J. B. Oldham, S.-L. He et al., "Mechanical properties of a biodegradable bone regeneration scaffold," *Journal of Biomechanical Engineering*, vol. 122, no. 3, pp. 286–288, 2000.

[13] S. Wang, L. Lu, J. A. Gruetzmacher, B. L. Currier, and M. J. Yaszemski, "A biodegradable and cross-linkable multiblock copolymer consisting of poly(propylene fumarate) and poly(ε-caprolactone): synthesis, characterization, and physical properties," *Macromolecules*, vol. 38, no. 17, pp. 7358–7370, 2005.

[14] S. Wang, D. H. Kempen, N. K. Simha, et al., "Photo-crosslinked hybrid polymer networks for bone and nerve tissue-engineering applications: controlled physical properties and regulated cell responses," *Biomacromolecules*, vol. 9, pp. 1229–1241, 2008.

[15] A. B. M. Rabie, R. W. K. Wong, and U. Hägg, "Composite autogenous bone and demineralized bone matrices used to repair defects in the parietal bone of rabbits," *British Journal of Oral and Maxillofacial Surgery*, vol. 38, no. 5, pp. 565–570, 2000.

[16] K. D. Chesmel, J. Branger, H. Wertheim, and N. Scarborough, "Healing response to various forms of human demineralized bone matrix in athymic rat cranial defects," *Journal of Oral and Maxillofacial Surgery*, vol. 56, no. 7, pp. 857–865, 1998.

[17] S. J. Peter, L. J. Suggs, M. J. Yaszemski, P. S. Engel, and A. G. Mikos, "Synthesis of poly(propylene fumarate) by acylation of propylene glycol in the presence of a proton scavenger," *Journal of Biomaterials Science, Polymer Edition*, vol. 10, no. 3, pp. 363–373, 1999.

[18] G. Box, W. Hunter, and J. S. Hunter, *Statistics for Experimenters*, John Wiley & Sons, New York, NY, USA, 1978.

[19] D. H. R. Kempen, M. C. Kruyt, L. Lu et al., "Effect of autologous bone marrow stromal cell seeding and bone morphogenetic protein-2 delivery on ectopic bone formation in a microsphere/poly(propylene fumarate) composite," *Tissue Engineering, Part A*, vol. 15, no. 3, pp. 587–594, 2009.

[20] D. H. R. Kempen, M. J. Yaszemski, A. Heijink et al., "Non-invasive monitoring of BMP-2 retention and bone formation in composites for bone tissue engineering using SPECT/CT and scintillation probes," *Journal of Controlled Release*, vol. 134, no. 3, pp. 169–176, 2009.

[21] D. H. R. Kempen, L. Lu, A. Heijink et al., "Effect of local sequential VEGF and BMP-2 delivery on ectopic and orthotopic bone regeneration," *Biomaterials*, vol. 30, no. 14, pp. 2816–2825, 2009.

Hindawi Publishing Corporation
International Journal of Polymer Science
Volume 2010, Article ID 369759, 7 pages
doi:10.1155/2010/369759

Research Article

Chitin Fiber and Chitosan 3D Composite Rods

Zhengke Wang,[1] Qiaoling Hu,[1] and Lei Cai[2]

[1] *Department of Polymer Science and Engineering, Key Laboratory of Macromolecule Synthesis and Functionalization, Zhejiang University, Ministry of Education, Hangzhou 310027, China*
[2] *Department of Materials Science and Engineering, The University of Tennessee, Knoxville, TN 37996, USA*

Correspondence should be addressed to Qiaoling Hu, huql@zju.edu.cn

Received 15 March 2010; Accepted 21 April 2010

Academic Editor: Shanfeng Wang

Chitin fiber (CHF) and chitosan (CS) 3D composite rods with layer-by-layer structure were constructed by in situ precipitation method. CHF could not be dissolved in acetic acid aqueous solution, but CS could be dissolved due to the different deacetylation degree (D.D) between CHF and CS. CHF with undulate surfaces could be observed using SEM to demonstrate that the sufficiently rough surfaces and edges of the fiber could enhance the mechanical combining stress between fiber and matrix. XRD indicated that the crystallinity of CHF/CS composites decreased and CS crystal plane d-spacing of CHF/CS composites became larger than that of pure CS rod. TG analysis showed that mixing a little amount of CHF could enhance thermal stability of CS rod, but when the content of CHF was higher than the optimum amount, its thermal stability decreased. When 0.5% CHF was added into CS matrix, the bending strength and bending modulus of the composite rods arrived at 114.2 MPa and 5.2 GPa, respectively, increased by 23.6% and 26.8% compared with pure CS rods, indicating that CHF/CS composite rods could be a better candidate for bone fracture internal fixation.

1. Introduction

Chitin, a natural polymer from marine resources [1], is found particularly in the shells of crustaceans such as crab and shrimp, the cuticles of insects, and the cell walls of fungi and is one of the most abundant biopolymers next to cellulose [2]. The shells contain 15%–40% chitin and its amount in the whole marine environment has been estimated at 1560 million tons [3, 4]. It has attracted more and more attention nowadays, due to its abundant resources, friendliness to the environment, and potential to substitute some petrochemicals [1]. Commercially, chitin is obtained at a relatively low cost from the wastes of the seafood processing industry. Briefly, the process consists of deproteinization of the raw shell material in a dilute NaOH solution and decalcification in a dilute HCl solution [5]. Chitosan (CS), a fully or partially deacetylated form of chitin, has become important materials in various fields, including medicine, biochemistry, analytical chemistry, and chemical engineering [6]. This derivative product with higher degree of deacetylation (D.D) results from the reaction of chitin with alkali (40%–45% NaOH solution) at elevated temperatures at prolonged exposures [5, 7].

Chitin and CS are polymers consisted of N-acetyl-glucosamine and N-glucosamine units randomly or block distributed throughout the biopolymer chain (Figure 1) [7, 8]. They are characterized by D.D; when D.D is lower than 50%, the biopolymer is named chitin. Conversely, when D.D is higher than 50%, the biopolymer is named CS [8]. The D.D is affected by both the source of the biopolymer and the preparation methods and may range from as low as 30% to almost 100% [9]. It is a key parameter that influences the physicochemical properties of chitin and CS, such as solubility, surface energy, chain conformation, and biological properties [9, 10]. Chitin is not soluble in common solvents because of the strong intermolecular hydrogen bonding, while it is soluble only in special solvents such as hexafluoroacetone and N, N-dimethylacetamide (DMAc) containing 5%–8% LiCl [3]. CS is insoluble in either organic solvents or water; however, it could be readily dissolved in weak acidic solutions, due to the presence of amino groups. The solubilization occurs by protonation of the $-NH_2$ on the C-2 position of the D-glucosamine repeat unit, whereby the polysaccharide is converted to a polyelectrolyte in acidic media [11]. To obtain a soluble product, the D.D of CS should reach 80%–85% or higher [5].

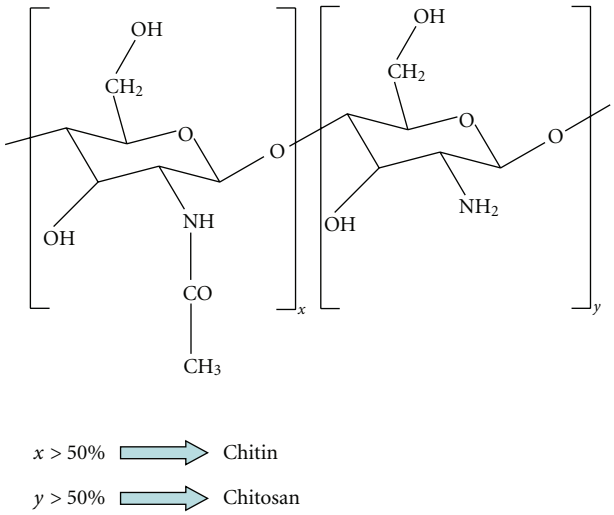

Figure 1: Molecular structures of chitin and CS.

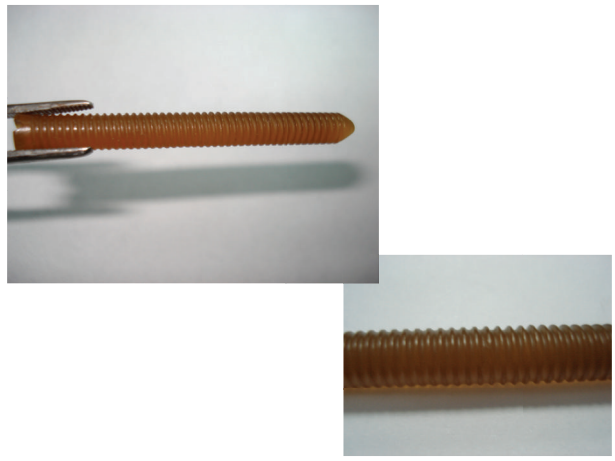

Figure 2: Photo of CS screws.

Both chitin and CS have excellent material properties such as biocompatibility, biodegradability, nontoxicity, as well as chemical and physical stability [12]. Chitin has been generally used in hemostasis and oral dosage excipient. It is also a competent biomaterial in wound healing, anti-inflammation, cholesterol modulation, and enzyme immobilization [13]. CS-based implants, the biocompatible materials with the host tissue, showed little fibrous encapsulation and chronic inflammation and have been tested for tissue engineering in a number of shapes and physical forms, including porous scaffolds and gels. Excellent porous structures, membranes, blocks, tubes, and beads have been obtained by lyophilization [5, 13]. α-Chitin whisker-reinforced CS nanocomposite films were prepared using solution-casting technique. The increase in the tensile strength of the nanocomposite films with increasing α-chitin whisker content could be attributed to the interaction between CS molecules and α-chitin whiskers via hydrogen bonding [14]. However it is difficult to prepare 3-dimensional chitosan rod by Twin Screw Extruder or Single Screw Extruder, because there are stronger intramolecular and intermolecular H-bonds in chitosan, which make the melting temperature of chitosan higher than its decomposing temperature. Novel 3-dimensional CS rod with layer-by-layer structure and its composite rod with multifunctional properties have been constructed via in situ precipitation method by our group (Figure 2) [15–18]. It can be used as bioabsorbable devices for internal fixation, which not only reduce stress shielding to the bone but also avoid a second operation for removal [19]. In this study, CHF/CS composite rods with layer-by-layer structure were prepared by in situ precipitation method. The forming mechanism, microstructure morphology and mechanical properties of CHF/CS composite rods were explored in the following sections.

2. Materials and Experiments

2.1. Materials. The materials are CS (Biomedical grade, $M_\eta = 5.63 \times 10^5$, D.D = 91%, Qingdao Haihui Bioengineering Co., Ltd), chitin fiber (CHF, denier: 2.3 ± 0.5 dtex, Weifang Youngdeok Chitosan Co., Ltd), acetic acid (HAc, CP, Yixing Niujia chemical reagent plant), and sodium hydroxide (NaOH, AR, Hangzhou Xiaoshan chemical reagent corporation). These materials are commercially available and used without further purification.

2.2. Preparation of CHF/CS Composite Rods. Different weight (0.05 g, 0.1 g, 0.2 g, and 0.3 g, resp.) of CHFs, which were cut into short fibers (~5 mm in length), were added into 400 ml acetic acid aqueous solution (2%, v/v) and stirred for 0.5 hour. Then 20 g of CS powder were added and stirred for 2 hours. Finally CHFs were suspended in the viscous CS solution. The resulting solution was statically placed for 24 hours to remove the air bubbles trapped in the viscous liquid. The mixture solution was poured into cylindrical mold and then immerged into sodium hydroxide aqueous solution with a concentration of 5% (wt/v) for 6 hours to form CHF/CS gel rod. The gel rod was washed with deionized water and air-dried in oven at 60°C.

2.3. SEM Observations. HITACHI S-4800 SEM produced by Japan was used to observe the microstructure of the samples which were sputter-coated by gold before observation.

2.4. X-Ray Diffraction Analysis. Crystallinity of the samples was studied with X-ray Diffraction (Rigaku D/max 2550PC) using a monochromatic Cu Kα radiation generated at 40 kV, 300 mA. The samples were scanned from 5° to 60° at 10°/min.

2.5. Thermal Analysis. The TGA of the samples was studied on Pyris-6 Thermo Analyses (TA) apparatus produced by PerkinElmer and measurements were recorded from 50°C to 600°C at a heating rate of 20°C/minute under flow N_2 atmosphere (flow rate: 40 ml/minute).

2.6. Testing of Mechanical Properties. All of the samples were air-dried in oven at 60°C for 2 hours to remove the moisture

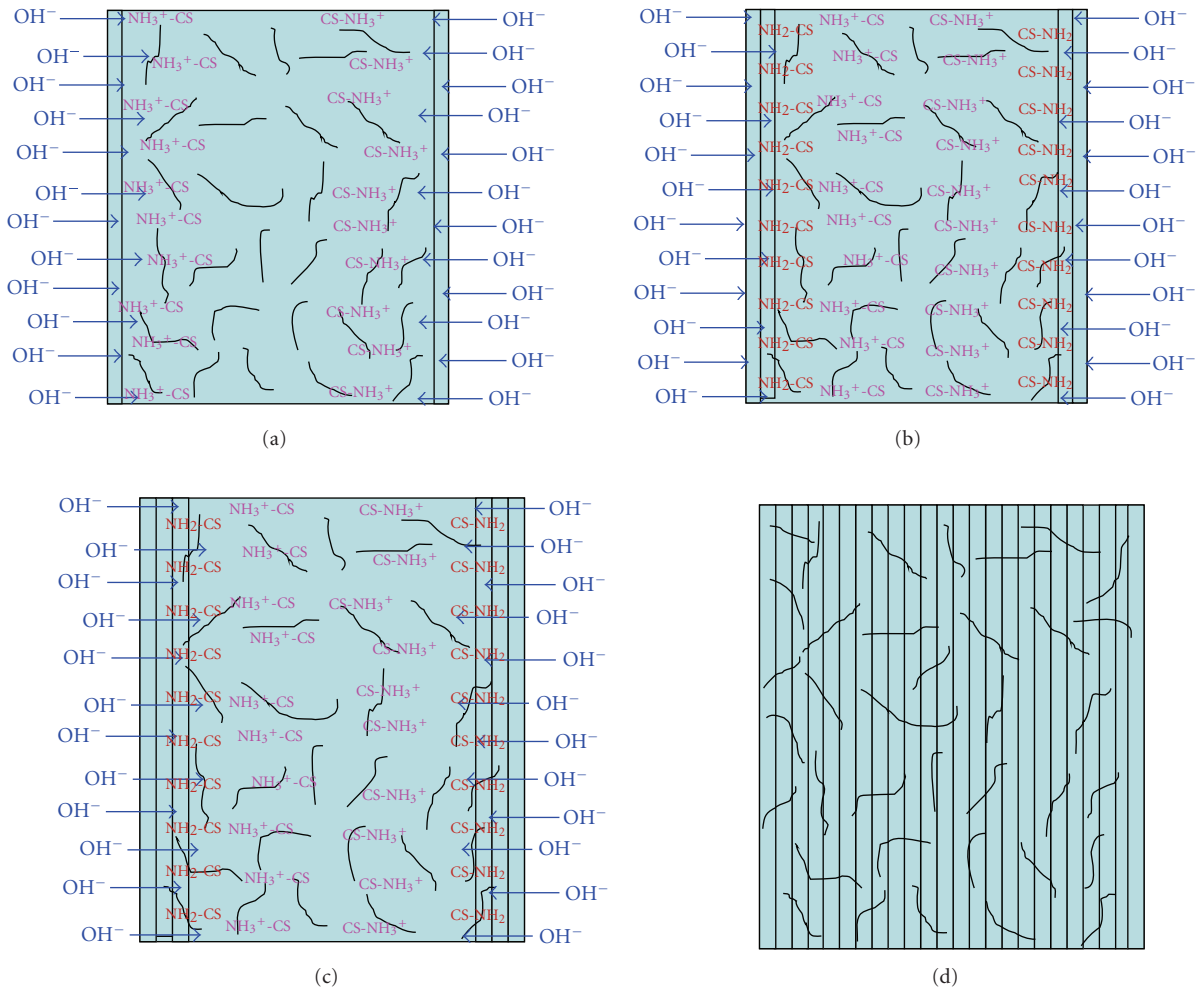

Figure 3: The schematic representation about forming process of CHF/CS gel rod with layer-by-layer structure (vertical section).

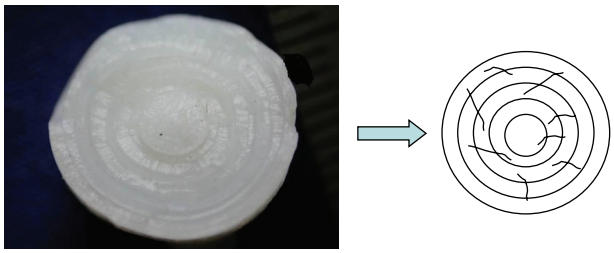

Figure 4: Layer-by-layer structure of CHF/CS gel rod (cross section).

before testing. Bending strength and bending modulus were determined by three-point bending tests (five rods per group), which were performed on the universal materials testing machine made by Shenzhen Reger Company (Shenzhen, China). The span length was 40 mm and loading rate was 2 mm/min.

3. Results and Discussion

3.1. Forming Mechanism of CHF/CS 3D Composite Rods. The forming process of CHF/CS gel rod with layer-by-layer structure was shown in Figure 3. The solubility of CS largely depends on the pH value of environments because of the existence of amino groups. The free amino group of CS was protonated to CS–NH_3^+ at pH = 4.2 [20, 21], but when CS–NH_3^+ encountered massive OH^-, CS would be precipitated, as shown in what follows:

$$\begin{aligned} &\text{CS–NH}_2 + \text{HAc} \longrightarrow \text{CS–NH}_3^+ + \text{Ac}^-, \\ &\text{CS–NH}_3^+ + \text{OH}^- \longrightarrow \text{CS–NH}_2(\downarrow) + \text{H}_2\text{O}. \end{aligned} \quad (1)$$

However CHFs could not be dissolved in acetic acid aqueous solution, so that they dispersed in the viscous CS solution. The mixture solution was charged into semipermeable template which could separate the CHF/CS solution from NaOH solution, so that small molecules and ions such as H_2O, Na^+, OH^-, and Ac^- could permeate except for CS macromolecules (Figure 3(a)). Due to the concentration gradient of alkali between inside and outside of the semipermeable template, OH^- could diffuse from outside into CHF/CS solution and react with CS–NH_3^+. As a result, protonated CS was precipitated in situ to form one layer adhering to semipermeable template closely (Figure 3(b)). As

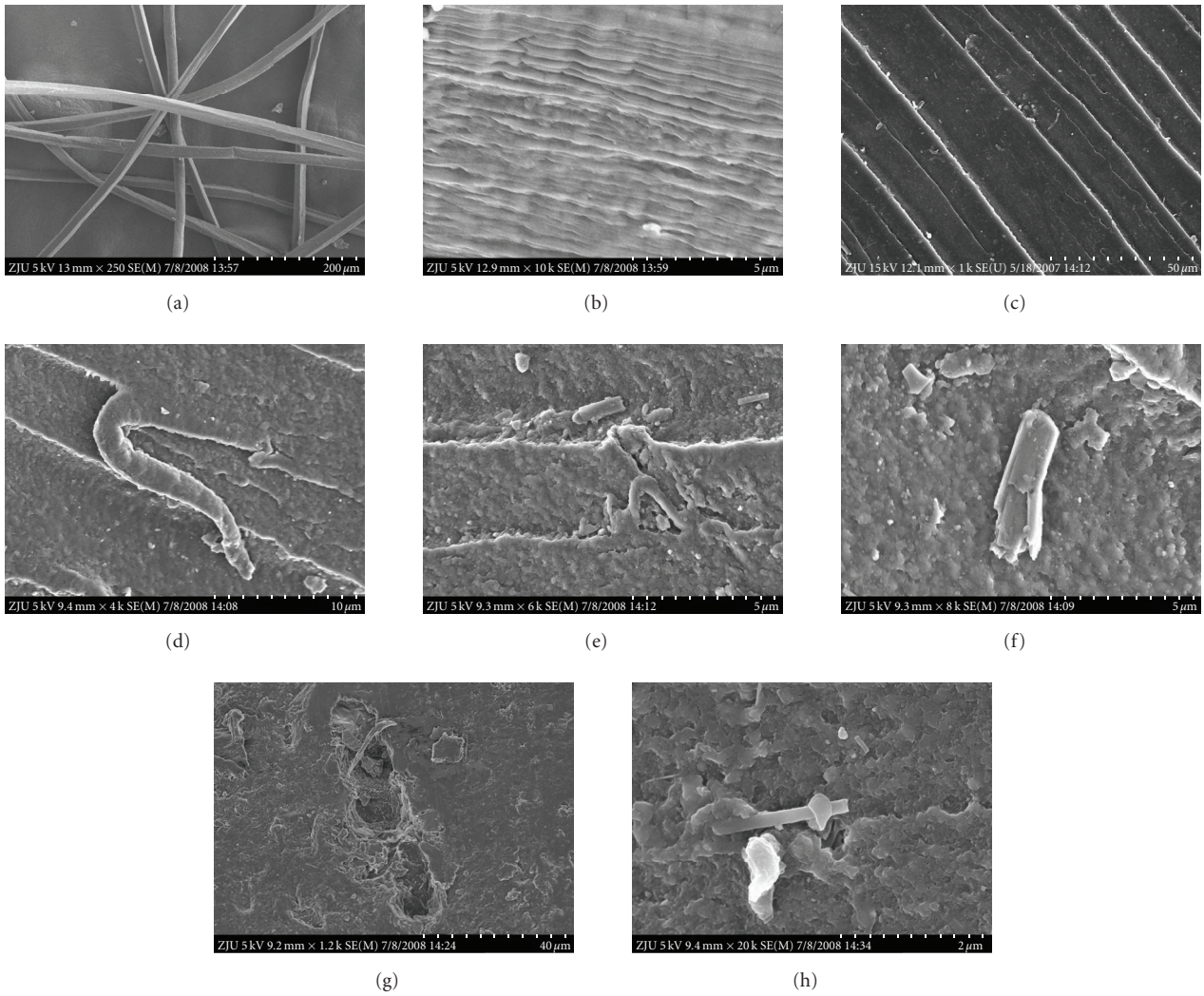

Figure 5: SEM micrographs of (a) CHF (×250), (b) CHF (×10,000), (c) CS rod (×1000), (d) CHF/CS (0.25/100, wt/wt) (×4000), (e) CHF/CS (0.5/100, wt/wt) (×6000), (f) CHF/CS (0.5/100, wt/wt) (×8000), (g) CHF/CS (1/100, wt/wt) (×1200), and (h) CHF/CS (1.5/100, wt/wt) (×2000).

the diffusion process continuing, CS precipitated layer-by-layer to from concentric circle structure (Figures 3(c), 3(d), and 4). At the same time, CHFs were embedded in the CS matrix. Then CHF/CS gel rods were dried and layers became much tighter due to the shrinkage stress.

3.2. Microstructure Morphology of CHF/CS 3D Composites. Microstructure morphology of the CHF, CS rod, CHF/CS (0.25/100, wt/wt), CHF/CS (0.5/100, wt/wt), CHF/CS (1/100, wt/wt), and CHF/CS (1.5/100, wt/wt) was shown in Figure 5. The size of CHF was ~10 μm in width. The fiber was not in column form but had several edges. And when it was magnified by 10,000 (Figure 5(b)), undulate surface could be seen, so that the sufficient rough surface and edges of the fiber could potentially enhance the mechanical combining stress between fiber and matrix. Layer-by-layer structure could be clearly seen on the cross-section of pure CS rod in Figure 5(c), which was in accordance with the schematic representation about forming process of CHF/CS gel rod. One fiber with CS adhered on the surface traversed several layers in Figure 5(d). And fiber embedded in CS matrix along with the layer could be seen in Figures 5(e) and 5(h). Fiber was pulled out from CS matrix and chipped facet edge could be observed in Figure 5(f), and holes with fiber fragments remained in CS matrix were very shallow (Figure 5(g)), indicating that interface between fiber and matrix was combined so tightly. CS was the continuous phase that could transfer stress, whereas CHF was randomly dispersed in CS matrix to connect layers of the rod and could endure outside stress.

3.3. Crystallization Property of Samples. XRD patterns of pure CS rod, CHF, and CHF/CS rod (0.5/100, wt/wt) were shown in Figure 6. The peaks at 2θ of 10.6° and 20.4° are characteristic diffraction peaks of CS (Figure 6(a)). Ratana Rujiravanit reported that α-chitin whiskers exhibited two major scattering peaks at 2θ of ~9° and ~19° [14]. At the same time, 2θ of CHF shown in Figure 6(b) were

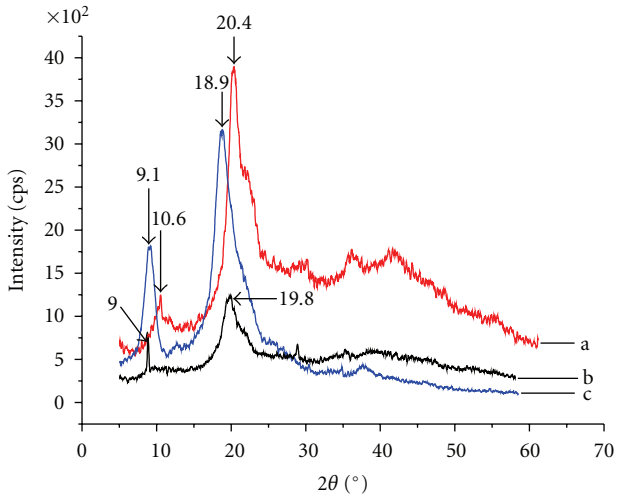

Figure 6: XRD patterns for (a) CS rod, (b) CHF, and (c) CHF/CS (0.5/100, wt/wt).

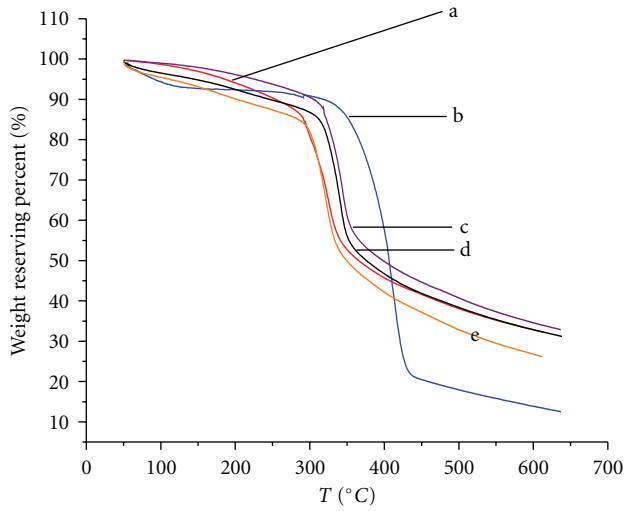

Figure 7: TG curves for (a) CS rod, (b) CHF, (c) CHF/CS (0.25/100, wt/wt), (d) CHF/CS (0.5/100, wt/wt), and (e) CHF/CS (1/100, wt/wt), in the 50–600°C temperature range under N_2 atmosphere.

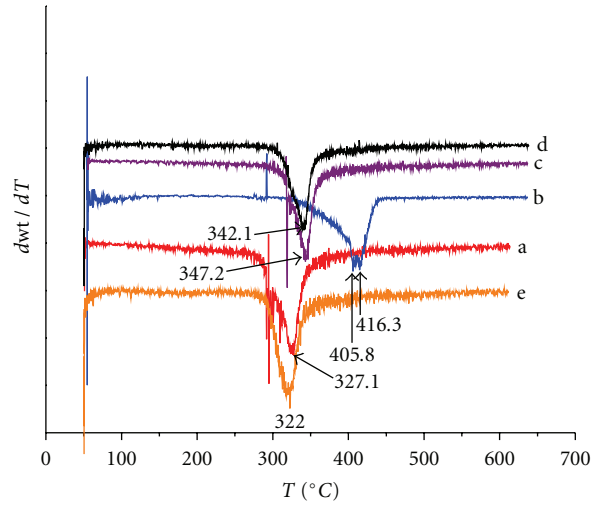

Figure 8: DTG curves for (a) CS rod, (b) CHF, (c) CHF/CS (0.25/100, wt/wt), (d) CHF/CS (0.5/100, wt/wt), and (e) CHF/CS (1/100, wt/wt), in the 50–600°C temperature range under N_2 atmosphere.

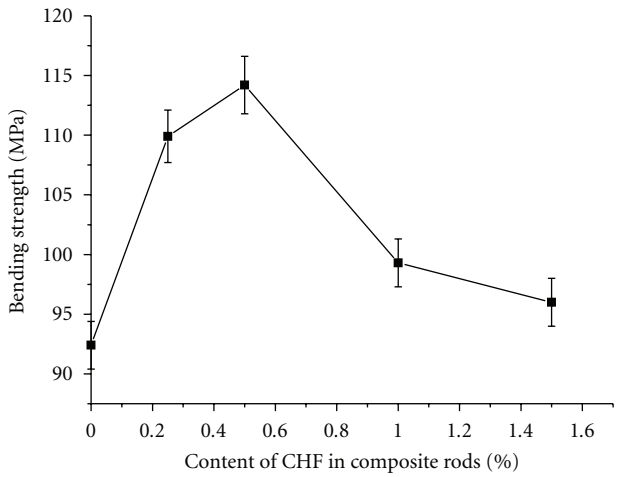

Figure 9: Bending strength of CHF/CS composites influenced by content of CHF.

9.1° and 18.9°, respectively, which were in accordance with previous research. While small amount of CHF was added into CS matrix, two diffraction peaks shifted to 9.0° and 19.8°, and intensity of the peaks decreased compared with pure CS rod and pure CHF (Figure 6(c)), indicating strong interactions between CS and CHF, resulting in the reduction of crystallinity of CHF/CS composites. According to the Bragg equation ($2d\,sin\theta = n\lambda$), CS crystal plane spacing (d) of CHF/CS composites has been become larger than that of pure CS rod.

3.4. Thermal Properties of CHF/CS Composites. The thermal gravimetric (TG) curves of CS rod, CHF, CHF/CS (0.25/100, wt/wt), CHF/CS (0.5/100, wt/wt), and CHF/CS (1/100, wt/wt) were shown in Figure 7, which were tested in the 50–600°C temperature range under N_2 atmosphere. The temperatures about different mass residual percentage (T_{mr}) of the samples were listed in Table 1. When a little CHF was added into CS matrix (CHF/CS = 0.25/100, wt/wt), T_{mr} of CHF/CS composite was higher than that of pure CS rod. Along with increasing content of CHF, T_{mr} of CHF/CS composites decreased. The thermal stability of CHF/CS (0.5/100, wt/wt) rod was weaker than that of CHF/CS (0.25/100, wt/wt) rod but slightly better than that of pure CS rod. When the ratio of CHF/CS arrived at 1/100 (wt/wt), its thermal stability was slightly weaker than that of pure CS rod. In all, thermal stability of CS rod could be enhanced by incorporating little CHF, but decreased at higher content of CHF.

Differential thermogravimetric (DTG) curves of the samples were shown in Figure 8. The temperatures of the fastest

Table 1: The temperatures about mass residual percentage of samples (/°C).

Mass residual percentage	CS rod	CHF	CHF/CS (0.25/100, wt/wt)	CHF/CS (0.5/100, wt/wt)	CHF/CS (1/100, wt/wt)
90%	253.9	318.2	305.4	245.8	202.2
70%	319.1	384.6	341.8	336.3	316.6
50%	365.7	406.4	398.2	375.9	349.6

weight loss rate (T_{fl}) of CHF were 405.8°C and 416.3°C. The T_{fl} of CS rod, CHF/CS (0.25/100, wt/wt), CHF/CS (0.5/100, wt/wt), and CHF/CS (1/100, wt/wt) were 327.1°C, 347.2°C, 342.1°C, and 322.0°C, respectively. Obviously, the T_{fl} of CHF/CS (0.25/100, wt/wt) and CHF/CS (0.5/100, wt/wt) was higher than pure CS rod, indicating that the thermal stability of CHF/CS is enhanced by adding little CHF. But the T_{fl} of CHF/CS (1/100, wt/wt) was lower than that of pure CS rod, so that the thermal stability of CHF/CS composite decreased.

3.5. Mechanical Properties of CHF/CS Composite Rods. Chitin whiskers were used to reinforce CS nanocomposite films successfully. When there were 2.96% (wt%) chitin whiskers in the composite films, the tensile strength of nanocomposite films could arrive at 83.8 ± 2.9 MPa, while the tensile strength of pure CS films was 64.9 ± 0.7 MPa [14]. The mechanical properties of CHF/CS composite rods were shown in Figure 9. The bending strength of CHF/CS composites was increased first and then reduced along with the increasing of the content of CHF. Bending strength and bending modulus of pure CS rods are 92.4 MPa and 4.1 GPa, respectively. When 0.5% CHF was added into CS matrix, the bending strength and bending modulus of composite rod maximized at 114.2 MPa and 5.2 GPa, respectively, increased by 23.6% and 26.8% compared with pure CS rods. When much more CHF was added into CS matrix, the mechanical properties of composite rods were reduced due to much more fiber tips as stress concentrators.

4. Conclusions

CHF and CS 3D composite rods with layer-by-layer structure were constructed by in situ precipitation method. CHF could be suspended in the viscous CS solution since CHF could not be dissolved in acetic acid aqueous solution, while CS could be dissolved due to the different D.D between CHF and CS. Undulate surface of CHF seen using SEM demonstrated that sufficient rough surfaces and edges of the fiber could enhance the mechanical combining stress between fiber and matrix. Microstructure morphology also indicated that interface between fiber and matrix was combined tightly. CS was the continuous phase that can transfer stress, whereas CHF was random dispersed in CS matrix to connect layers of the rod and could endure outside stress. While small amount of CHF was added into CS matrix, intensity of the peaks decreased compared with pure CS rod and pure CHF, showing that crystallinity of CHF/CS composites decreased. CS crystal plane spacing (d) of CHF/CS composites has become larger than that of pure CS rod. Mixed little CHF could enhance thermal stability of CS rod to an optimum and higher content of CHF would decrease its thermal stability. When 0.5% CHF was added into CS matrix, the bending strength and bending modulus of composite rods maximized at 114.2 MPa and 5.2 GPa, respectively, increased by 23.6% and 26.8% compared with pure CS rods. Thus, CHF/CS composite rods could be a novel biomedical device used for bone fracture internal fixation.

Acknowledgment

This work was funded by the National Natural Science Foundation of China (Grant No. 50773070), the Key Basic Research Development Plan (Project 973) of China (Grant No. 2005CB623902) and Grand Science and Technology Special Project of Zhejiang Province (Grant No. 2008C11087).

References

[1] L. Chen, Y. Du, H. Wu, and L. Xiao, "Relationship between molecular structure and moisture-retention ability of carboxymethyl chitin and chitosan," *Journal of Applied Polymer Science*, vol. 83, no. 6, pp. 1233–1241, 2002.

[2] D. Suzuki, M. Takahashi, M. Abe et al., "Comparison of various mixtures of β-chitin and chitosan as a scaffold for three-dimensional culture of rabbit chondrocytes," *Journal of Materials Science: Materials in Medicine*, vol. 19, no. 3, pp. 1307–1315, 2008.

[3] K. Kurita, "Chitin and chitosan: functional biopolymers from marine crustaceans," *Marine Biotechnology*, vol. 8, no. 3, pp. 203–226, 2006.

[4] E. Agulló, M. S. Rodríguez, V. Ramos, and L. Albertengo, "Present and future role of chitin and chitosan in food," *Macromolecular Bioscience*, vol. 3, no. 10, pp. 521–530, 2003.

[5] B. Krajewska, "Membrane-based processes performed with use of chitin/chitosan materials," *Separation and Purification Technology*, vol. 41, no. 3, pp. 305–312, 2005.

[6] T. Honma, T. Senda, and Y. Inoue, "Thermal properties and crystallization behaviour of blends of poly(ε-caprolactone) with chitin and chitosan," *Polymer International*, vol. 52, no. 12, pp. 1839–1846, 2003.

[7] K. Van De Velde and P. Kiekens, "Structure analysis and degree of substitution of chitin, chitosan and dibutyrylchitin by FT-IR spectroscopy and solid state13C NMR," *Carbohydrate Polymers*, vol. 58, no. 4, pp. 409–416, 2004.

[8] E. Khor and L. Y. Lim, "Implantable applications of chitin and chitosan," *Biomaterials*, vol. 24, no. 13, pp. 2339–2349, 2003.

[9] R. Jayakumar, N. Selvamurugan, S. V. Nair, S. Tokura, and H. Tamura, "Preparative methods of phosphorylated chitin and chitosan—an overview," *International Journal of Biological Macromolecules*, vol. 43, no. 3, pp. 221–225, 2008.

[10] T. Wu and S. Zivanovic, "Determination of the degree of acetylation (DA) of chitin and chitosan by an improved first

derivative UV method," *Carbohydrate Polymers*, vol. 73, no. 2, pp. 248–253, 2008.

[11] M. Rinaudo, "Chitin and chitosan: properties and applications," *Progress in Polymer Science*, vol. 31, no. 7, pp. 603–632, 2006.

[12] V. G. Mir, J. Heinämäki, O. Antikainen et al., "Direct compression properties of chitin and chitosan," *European Journal of Pharmaceutics and Biopharmaceutics*, vol. 69, no. 3, pp. 964–968, 2008.

[13] Y.-C. Kuo and I.-N. Ku, "Cartilage regeneration by novel polyethylene oxide/chitin/chitosan scaffolds," *Biomacromolecules*, vol. 9, no. 10, pp. 2662–2669, 2008.

[14] J. Sriupayo, P. Supaphol, J. Blackwell, and R. Rujiravanit, "Preparation and characterization of α-chitin whisker-reinforced chitosan nanocomposite films with or without heat treatment," *Carbohydrate Polymers*, vol. 62, no. 2, pp. 130–136, 2005.

[15] Q. L. Hu, X. Z. Qian, B. Q. Li, and J. C. Shen, "Studies on chitosan rods prepared by in situ precipitation method," *Chemical Journal of Chinese Universities-Chinese*, vol. 24, no. 3, pp. 528–531, 2003.

[16] Z. K. Wang, Q. L. Hu, X. G. Dai, H. Wu, Y. X. Wang, and J. C. Shen, "Preparation and characterization of cellulose fiber/chitosan composites," *Polymer Composites*, vol. 30, no. 10, pp. 1517–1522, 2009.

[17] Z. K. Wang, Q. L. Hu, and L. Cai, "Chitosan and multi-walled carbon nanotube composite rods," *Chinese Journal of Polymer Science*. In press.

[18] Z. K. Wang and Q. L. Hu, "Chitosan rods reinforced by N-carboxyl propionyl chitosan sodium," *Acta Physico-Chimica Sinica*. In press.

[19] A. Yang and R. Wu, "Mechanical properties and interfacial interaction of a novel bioabsorbable chitin fiber reinforced poly (ε-caprolactone) composite," *Journal of Materials Science Letters*, vol. 20, no. 11, pp. 977–979, 2001.

[20] Q. Hu, B. Li, M. Wang, and J. Shen, "Preparation and characterization of biodegradable chitosan/hydroxyapatite nanocomposite rods via in situ hybridization: a potential material as internal fixation of bone fracture," *Biomaterials*, vol. 25, no. 5, pp. 779–785, 2004.

[21] B. Q. Li, D. C. Jia, Y. Zhou, Q. L. Hu, and W. Cai, "In situ hybridization to chitosan/magnetite nanocomposite induced by the magnetic field," *Journal of Magnetism and Magnetic Materials*, vol. 306, no. 2, pp. 223–227, 2006.

Hindawi Publishing Corporation
International Journal of Polymer Science
Volume 2010, Article ID 175264, 12 pages
doi:10.1155/2010/175264

Research Article

In Situ Degradation of Chitosan-Polygalacturonic Acid/Hydroxyapatite Nanocomposites in Cell Culture Media

Rohit Khanna, Kalpana S. Katti, and Dinesh R. Katti

Department of Civil Engineering, North Dakota State University, Fargo, ND 58105, USA

Correspondence should be addressed to Kalpana S. Katti, kalpana.katti@ndsu.edu

Received 12 February 2010; Revised 22 March 2010; Accepted 22 March 2010

Academic Editor: Shanfeng Wang

The molecular and mechanical characteristics of in situ degradation behavior of chitosan-polygalacturonic acid/hydroxyapatite (Chi-PgA-HAP) nanocomposite films is investigated using Fourier Transform Infrared spectroscopy (FTIR), Atomic Force Microscopy (AFM), and modulus mapping techniques for up to 48 days of soaking in cell culture media. The surface molecular structure of media-soaked samples changes over the course of 48 days of soaking, as indicated by significant changes in phosphate vibrations (1200–900 cm^{-1}) indicating apatite formation. Chitosan-Polygalacturonic acid polyelectrolyte complexes (PECs) govern structural integrity of Chi-PgA-HAP nanocomposites and FTIR spectra indicate that PECs remain intact until 48 days of soaking. In situ AFM experiments on media-soaked samples indicate that soaking results in a change in topography and swelling proceeds differently at the initial soaking periods of about 8 days than for longer soaking. In situ modulus mapping experiments are done on soaked samples by probing ~1–3 nm of surface indicating elastic moduli of ~4 GPa resulting from proteins adsorbed on Chi-PgA-HAP nanocomposites. The elastic modulus decreases by ~2 GPa over a long exposure to cell culture media (48 days). Thus, as water enters the Chi-PgA-HAP sample, surface molecular interactions in Chi-PgA-HAP structure occur that result in swelling, causing small changes in nanoscale mechanical properties.

1. Introduction

Recent developments in design of novel polymeric biomaterials have allowed researchers to confront many of the challenges dealing with the design of novel biomaterials. The tremendous potential of biodegradable polymers for tissue engineering and medical devices results from their biocompatibility, ease in processing, and capability of controlled degradation in response to biological environment. Candidate materials for bone tissue engineering include natural polymers (chitosan, collagen, hyaluronan, fibrin), synthetic polymers (polycaprolactone, polylactic acid, polyglycolic acid, and their copolymers) and inorganic materials (tricalcium phosphate, hydroxyapatite). Also, the natural biodegradable and biofunctional biopolymer, chitosan, has been considered as a potential candidate material for numerous biomedical applications including controlled drug release [1, 2], wound dressing [3], and more recently, for tissue engineering application [4–13]. Chitosan [β(1,4)-linked 2-amino-2-deoxy-D glucan] is a cationic polysaccharide obtained by N-acetylation of chitin. Chitosan provides improved cell attachment, since the polysaccharide backbone of chitosan is structurally similar to glycoaminoglycans, the major component of ECM of cartilage and bone [14]. Due to cationic character of chitosan, it interacts with a number of polyanions and has been used in preparation of various polyelectrolyte complexes with natural polyanions such as alginic acid, dextran sulphate, heparin, pectin, and xanthan [15, 16]. Another natural biodegradable biopolymer, polygalacturonic acid (PgA), is a water-soluble polyanionic polysaccharide, consisting of a linear chain of D-galacturonic acid units with α(1-4) glycosidic linkages. This is a principal component of pectin that exists in cellular walls of plants. Pectin is extensively used in food industry as a gelling agent and widely used in the production of jams and jellies, confectionary products and for stabilization of yogurts [17] and drug production such as for antidiarrheic, detoxicants and as protectors of gastrointestinal tract [18, 19].

Appropriate mechanical property of bone tissue engineering scaffold is one of the key factors in selection and

design of biomaterials, which may limit the independent use of natural chitosan/pectin-based materials. Chitosan, has been reported to possess improved biocompatibility, mechanical strength, hard tissue regeneration and tailored degradation kinetics by incorporation of hydroxyapatite (HAP) [20, 21] and gelatin [20, 22, 23], alginate [24], and so forth. By employing electrostatically complementary nature of chitosan and PgA and by adopting a biomimetic synthesis route, we designed and developed novel chitosan-PgA-hydroxyapatite (Chi-PgA-HAP) nanocomposites [25–27] which exhibited a substantial improvement in mechanical properties. Our FTIR results demonstrated that strong interfacial interactions in Chi-PgA-HAP structures are believed to be the key factors in mechanical property improvement [25–27]. Biocompatibility results demonstrated that human osteoblasts (CRL 11732) generated mineralized bone nodules on Chi-PgA-HAP fibrous nanocomposites without using any differentiating media suggesting that Chi-PgA-HAP substrates are osteoinductive and provide an appropriate microenvironment for cell organization and tissue regeneration [27].

For suitability of Chi-PgA-HAP nanocomposites for bone tissue engineering, their degradation behavior needs to be evaluated. Ideally, material degradation rate should match the rate of tissue regeneration, while generating nontoxic degradation products. Both chitosan and pectin are well known to be enzymatically degradable and water resistant [18, 19, 28, 29]. Several investigations on enzymatic degradation of chitosan (with varying degree of deacetylation) for human use have been carried out in lysozyme [30–34], since it is found in human body fluid, including serum (concentration 4–13 mg/L) and tears (450–1230 mg/L) [35]. Chitosan-pectin membranes have been reported to swell considerably in water and their swelling characteristics depend on pH, temperature, ionic strength, and degree of polyelectrolyte complex formation [18, 29, 36]. Swelling behavior of chitosan-pectin membranes is an attractive property for drug delivery systems [37, 38]. In situ swelling behavior of Chitosan-PgA-HAP nanocomposites in terms of change in surface properties has not been investigated. Here, we present the in situ swelling behavior of Chi-PgA-HAP nanocomposite films over the soaking period of 48-day in cell culture media. In situ swelling experiments include the evaluation of topography, chemistry and nanomechanical properties of soaked 2D substrates in a fully hydrated state. 2D substrates have been utilized due to their relative ease as compared to 3D scaffolds. In situ AFM experiments were performed in cell culture media at a temperature of 37°C, to obtain the topography of soaked samples. Modulus mapping technique has been recently used to obtain the surface elastic properties of dentin-enamel junction [39] and biomimetic nanohydroxyapatite particles [40]. However, this technique has not been used till now to evaluate the purely elastic properties of constituents of soaked samples under fully immersed conditions. In the present work, in situ modulus mapping experiments were designed and elastic properties of soaked samples were obtained in fully submerged conditions (cell culture media; 37°C) by applying extremely shallow displacements (~2-3 nm). Molecular structure of both dry and soaked specimen was investigated by Fourier Transform Infrared spectroscopy.

2. Materials and Methods

2.1. Film Preparation. HAP nanoparticles were prepared by wet precipitation route from sodium phosphate (Na_2HPO_4; J. T. Baker), and calcium chloride ($CaCl_2$; EM Sciences) by maintaining pH at 7.44. The detailed processing procedures have been discussed elsewhere [41]. Chitosan (MW 190,000, >85% deacetylation) and polygalacturonic acid (MW 25000) were obtained from Sigma-Aldrich chemicals. Chitosan and PgA solutions were prepared in deionized water at a concentration of 1 g/100 mL. The pH of chitosan solution was adjusted by adding acetic acid and that of PgA solution was adjusted by adding NaOH. The pH of resulting solutions was adjusted to 4.5. Chitosan-PgA solution was prepared by adding chitosan solution dropwise to PgA solution followed by sonication for 3 minutes. For synthesis of Chi-PgA-HAP nanocomposite, HAP nanoparticles (1 g) were suspended in 100 mL of deionized water and sonicated for 1 hour to obtain a uniform dispersion of nanoparticles. Subsequently, sonicated HAP nanoparticles were mixed with sonicated Chitosan-PgA solution and further sonicated for 90 seconds to obtain a homogeneous solution. Films of two compositions were prepared (Chi-PgA-10% HAP and Chi-PgA-20% HAP) on TCPS (Tissue Culture Polystyrene) petridishes by solvent evaporation at room temperature under clear-air laboratory environment. For making films, Chi-PgA-HAP solution was diluted to 1 : 10 ratio with deionized water and 3 mL of resulting solution was air-dried on tissue culture polystyrene petridishes. Both the nanocomposite substrates were found to be biocompatible and Chi-PgA-20% HAP composition was selected for soaking study.

2.2. Soaking Experiments. All the samples were UV sterilized and subsequently soaked in 5 mL of cell culture media for 1, 2, 8, 24, and 48-day, respectively, under standard incubator conditions (37°C, 5% CO_2). Cell culture media was prepared by adding DMEM (Dulbecco's modified eagle medium; Hyclone), supplemented with 2.5 mM l-glutamine (without phenol red), 10% FBS (fetal bovine serum; ATCC) and 1% antibiotic (G418; J R Scientific Inc.). At the end of predetermined time, films samples were taken out of incubator, and washed twice with PBS and immediately taken for the AFM/FTIR/nanoindentation analyses. Culture media were replaced after every 3 days.

2.3. FTIR Experiments. FTIR experiments were carried out using a Nicolet 850 FT-IR spectrometer with a KBr beam splitter using reflectance accessory (45° angle of incidence). Spectra were collected in the range of 4000–500 cm^{-1} at a spectral resolution of 4 cm^{-1}. Film samples of chitosan, PgA and Chi-PgA-HAP nanocomposites were prepared on the clean gold substrates and allowed to dry overnight. FTIR spectra were obtained on soaked samples which were air-dried before data acquisition. A gold-coated metal plate was used to collect the background spectrum.

2.4. In Situ AFM Experiments Using Multimode Heater. Topography of dry and soaked samples was characterized by Atomic Force Microscope (multimode AFM: Veeco Metrology Group, Santa Barbara, CA), equipped with a Nanoscope IIIa controller and J-type piezo scanner. The equipment has z-axis resolution of around 0.5 A°. Silicon nitride cantilever probes (Model: NP-S20) with pyramidal tips of ~20 nm radius of curvature and a nominal stiffness of 0.06 N/m were used for imaging under contact mode in clean-air laboratory environment with 40%–50% relative humidity. For performing in situ AFM experiments in fully immersed conditions, Multimode low temperate heater from Veeco Metrology (Santa Barbara, CA) was used. It enabled in situ AFM analyses of soaked samples in a controlled liquid environment. Major components of the system include a fluid cell, a heating element, Thermal Applications Controller (TAC), and spacer block. For a detailed description of components available for Multimode Scanning Probe Microscopes, AFM technical support note 392 can be referred. The sample temperature was set and maintained at 37°C by regulating the heating element and tip heater voltage with the help of Thermal Applications Controller (TAC). The whole sample-fluid-tip was thermally equilibrated for at least 20 minutes to enable the tests to be performed in a stable and controlled environment (cell culture media; 37°C).

2.5. In Situ Modulus Mapping Technique. A Hysitron triboscope nanomechanical instrument (Minneapolis, MN) equipped with nanoscope IIIa controller (Veeco Metrology, Santa Barbara, CA) was used to test the dry and soaked samples with a Berkovich (three-sided pyramid; a 100–200 nm tip radius) diamond indenter fluid tip. The fluid tip with a longer steel shaft allows a liquid level up to 3-4 mm to be maintained above the sample surface and also ensures the machine calibration in the liquid. In order to avoid any meniscus forces, the tip was fully submerged in the liquid prior to testing. In situ modulus mapping experiments were performed on soaked samples in cell culture fluid and at a temperature of 37°C to simulate incubator conditions. Modulus mapping is a surface nanomechanical characterization technique that enables the measurement of purely elastic properties of material surface by applying extremely shallow displacements (~2-3 nm). Detailed description of principles of modulus mapping technique, its formulation, and application can be found elsewhere [39, 42]. In force modulation mode, a quasistatic force of 3 μN was superimposed by a 2 μN sinusoidal force at a frequency of 200 Hz. A total of 256 × 256 tests were done to obtain a modulus map in only 10–15 minutes.

For testing in liquid environment, a special fluid cell was designed by using O-rings (9/16″ O.D. × 3/8″ × 3/32″) glued onto 15 mm steel discs. Samples (0.5 cm × 0.5 cm) were glued and kept inside the fluid cell and then, flushed with liquid level up to 3-4 mm for testing in fully submerged conditions. The whole tip-sample-fluid assembly was then heated and maintained to 37°C using Multimode heater as described in Section 2.4. Before data acquisition, the entire setup was allowed to equilibrate for at least 20 minutes. Before starting modulus mapping experiment, the tip was wiped with acetone soaked tissue wipes to remove any ions/salts which may have adsorbed from the previous measurements. Tip calibration was done using a standard quartz sample with known elastic modulus. Extreme care was taken to keep the samples under the wet conditions before the in situ testing to avoid the effect of drying on nanomechanical measurements.

All the AFM, modulus mapping and FTIR experiments were performed using on least 3 samples for each set of test conditions. All the tests were repeated at least twice to account for repeatability and reproducibility of test measurements.

3. Results and Discussion

3.1. Molecular Nature of Surfaces of Soaked Chi-PgA-HAP Nanocomposite Samples. FTIR spectroscopy was used in a reflection mode to characterize the surface molecular structure of soaked samples. Figure 1 shows the FTIR spectra of dry and soaked Chi-PgA-HAP samples within the range 4000–500 cm^{-1}. The band positions and their assignments have been summarized in Tables 1, 2, and 3. The band at 1666 cm^{-1}, as seen in Figure 1, is a characteristic vibration of N-acetylated chitin and is assigned to Amide I band. It can also overlap with Amide I band from carbonyl stretching in protein structure, as proteins from cell culture media can get adsorbed onto surface of Chi-PgA-HAP samples. The band at 1622 cm^{-1} is attributed to asymmetric stretching vibration of dissociated carboxylate (COO^-) [26, 43]. This band shifts slightly to lower wavenumber, to 1605 cm^{-1} in soaked samples, which indicates that the change in environment of Chi-PgA-HAP structure through its interaction with water, possibly through hydrogen bonds with Chi-PgA-HAP structure. As water enters the Chi-PgA-HAP sample which contains polyelectrolyte complexes with $-NH_3^+$, $-COO^-$ ions, surface structure of Chi-PgA-HAP structure can get modified. In such a case, swelling can occur due to mutual repulsion between positively/negatively charged species along with interactions of these charges species with water. Swelling characteristics of chitosan-pectin have been reported to be modified by preparing the samples at varying pH [44].

PgA-HAP interactions were also affected as a result of soaking, as revealed in 1100–1000 cm^{-1} region of FTIR spectra of soaked samples (Figure 2). PgA interacts with HAP through dissociated carboxylate groups. As carboxylate groups carry negative charge, calcium ions in HAP can act as binding sites for PgA-HAP complexes [26]. To investigate PgA-HAP interactions, phosphate regions were carefully observed for both dry and soaked samples, as shown in Figure 2(a–h). Figure 2(a, b) shows the FTIR spectrum obtained from dry chitosan and dry PgA film, respectively. Bands observed at 1086 cm^{-1}, 1055 cm^{-1}, and 1032 cm^{-1} in PgA (Figure 2(b)), originate from skeletal vibrations involving C–O stretching, which are characteristic of saccharide structure of PgA [18]. Comparing FTIR spectrum of PgA (Figure 2(b)) with that of dry Chi-PgA-HAP (Figure 2(c)),

Table 1: Band assignment of dry and soaked Chi-PgA-HAP films for 3380–2860 cm^{-1} regions.

Band assignment	Band position as per the testing conditions					
	Dry	1 day	2 days	8 days	24-day	48-day
Asymmetric N–H stretching	3386	3377	3365	3365	3368	3360
symmetric N–H stretching	3290	3284	3292	3288	not observed	not observed
Asymmetric C–H stretching	2931	2936	2933	2932	2934	2933
Symmetric C–H stretching	2878	2878	2874	2878	2866	2869

Table 2: Band assignment of dry and soaked Chi-PgA-HAP films for 1660–1240 cm^{-1} regions.

Band assignment	Band position as per the soaking conditions					
	Dry	1 day	2 days	8 days	24-day	48-day
Amide I	1666	1665		1666	1665	1665
Asymmetric COO^- stretching	1622	1605	1624	1604	1605	1603
NH_3^+ deformation	1534	1532	1534	1533	1534	1539
symmetric COO^- stretching	1414	1417	1418	1420	1416	1421
C–H bending vibration of ring	1330	1331	1329	1328	1332	1336
	1242	1245	1237	1244	1243	1246

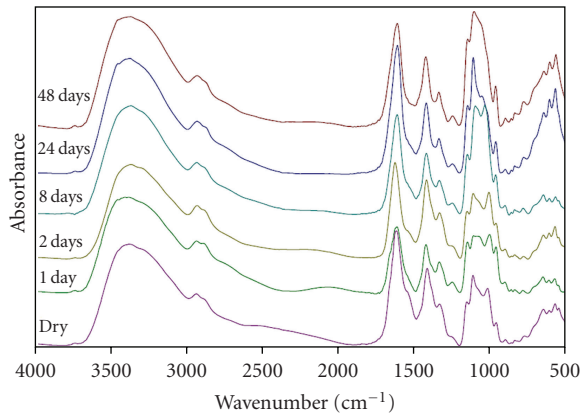

Figure 1: FTIR spectra obtained on dry and soaked Chi-PgA-HAP nanocomposite film samples after 1, 2, 8, 24 and 48-day, respectively in the regions 4000–500 cm^{-1}.

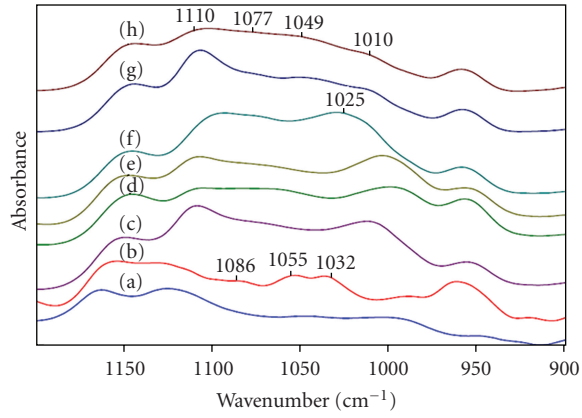

Figure 2: FTIR spectra of dry chitosan (a), dry PgA (b), dry Chi-PgA-HAP nanocomposites (c) and soaked Chi-PgA-HAP nanocomposite film samples over 1, 2, 8, 24 and 48-day (d–h), respectively in the regions 1200–900 cm^{-1}.

bands originating from –C–O–C– glycosidic linkages overlap with bands from phosphate regions and occur as a broad band (1100–1000 cm^{-1}) in Figure 2(c). Some of the characteristic bands of HAP structure, that is, asymmetric PO stretching vibrations in HAP structure occur at 1113 cm^{-1}, 1070 cm^{-1}, and 1009 cm^{-1} regions can be clearly observed in dry Chi-PgA-HAP samples. Significant changes in band positions in phosphate regions (1200–900 cm^{-1}) were not observed throughout the soaking duration. However, significant changes in shape of bands in phosphate regions (1200–900 cm^{-1}) in soaked samples, over a soaking duration of 48-day indicate that interactions in PgA-HAP structure changes as a result of soaking. Comparing spectrum of PgA (Figure 2(b)), dry Chi-PgA-HAP (Figure 2(c)), and pure HAP [45] with that of 48-day soaked sample (Figure 2(h)), characteristic shape of phosphate regions observed on 48 soaked sample matched with that observed in HAP structure. It appears, that as soaking proceeds, more HAP nanoparticles may get exposed onto the surface of soaked samples. Similar observations of exposed HAP particles were made in AFM topography image of 48-day soaked samples, as discussed in the next section. There can be another possibility of apatitic growth on soaked film samples, which accounted for the visibility of characteristic bands of HAP structure on 48-day soaked Chi-PgA-HAP sample.

Overall, FTIR spectroscopy results on soaked samples indicate that the degradation of Chi-PgA-HAP nanocomposite films was not severe in cell culture medium until 48-day of soaking. There were apparent changes in surface chemistry of soaked Chi-PgA-HAP substrates as compared to dry substrates. Severe degradation can be expected on dissociation of Chi-PgA polyelectrolyte complexes (PECs) and can also be due to breaking of –C–O–C– glycosidic linkages in Chitosan/PgA structure. Spectral changes in both Chi-PgA-HAP complexes and –C–O–C– glycosidic linkages were not observed in soaked samples. It can be due to the fact that both chitosan and PgA have been reported

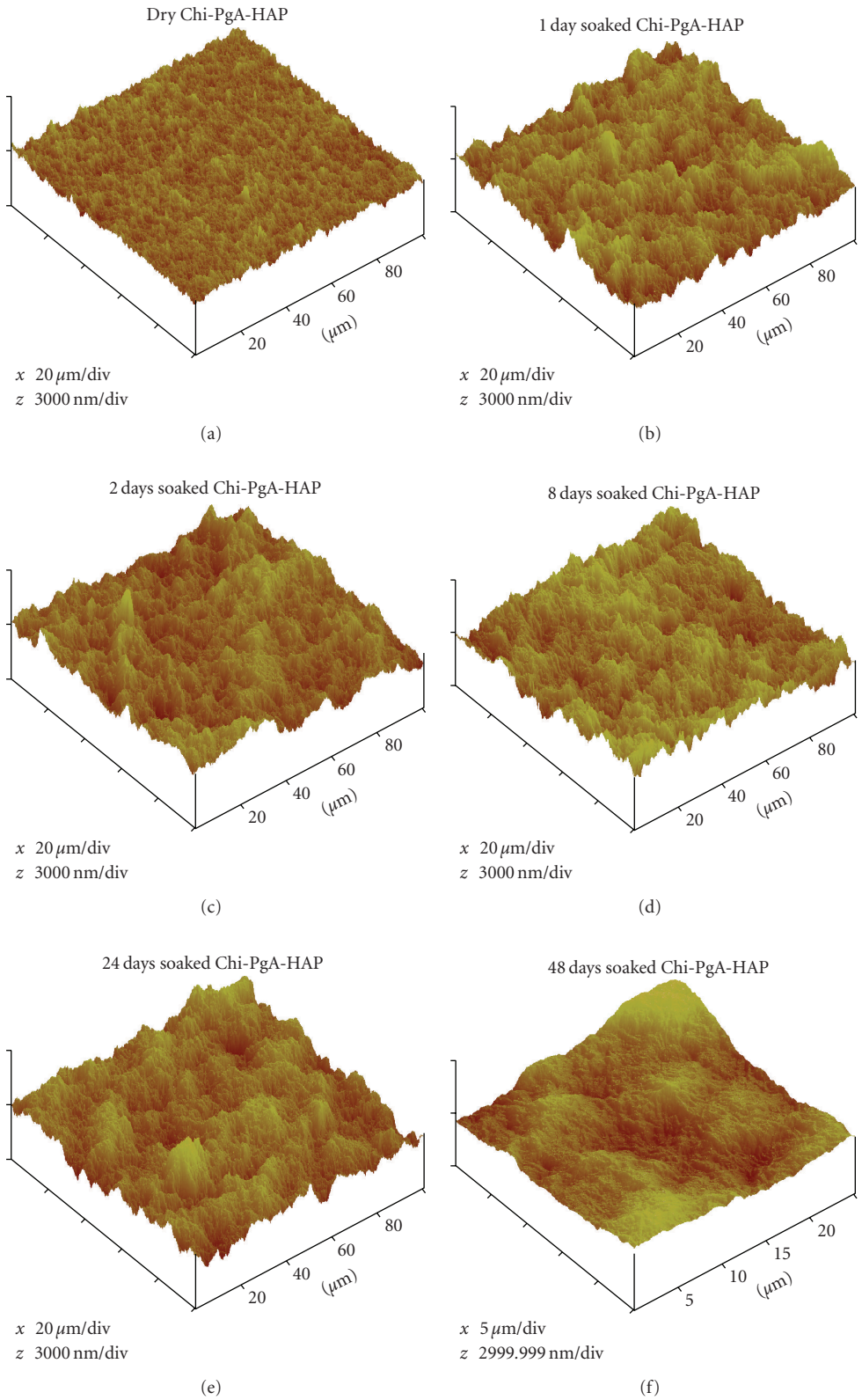

Figure 3: AFM 3D topographic images of dry (a) and soaked Chi-PgA-HAP samples for 1, 2, 8, 24, and 48-day, respectively (b)–(f). Topographic changes are evident after soaking in cell culture media. Topographic features (ridges, valleys, and pits) appear in a random fashion during the initial soaking duration up to 8 days, and then, more gradual changes are observed during the longer soaking period up to 48-day, as seen in topographic images (e, f).

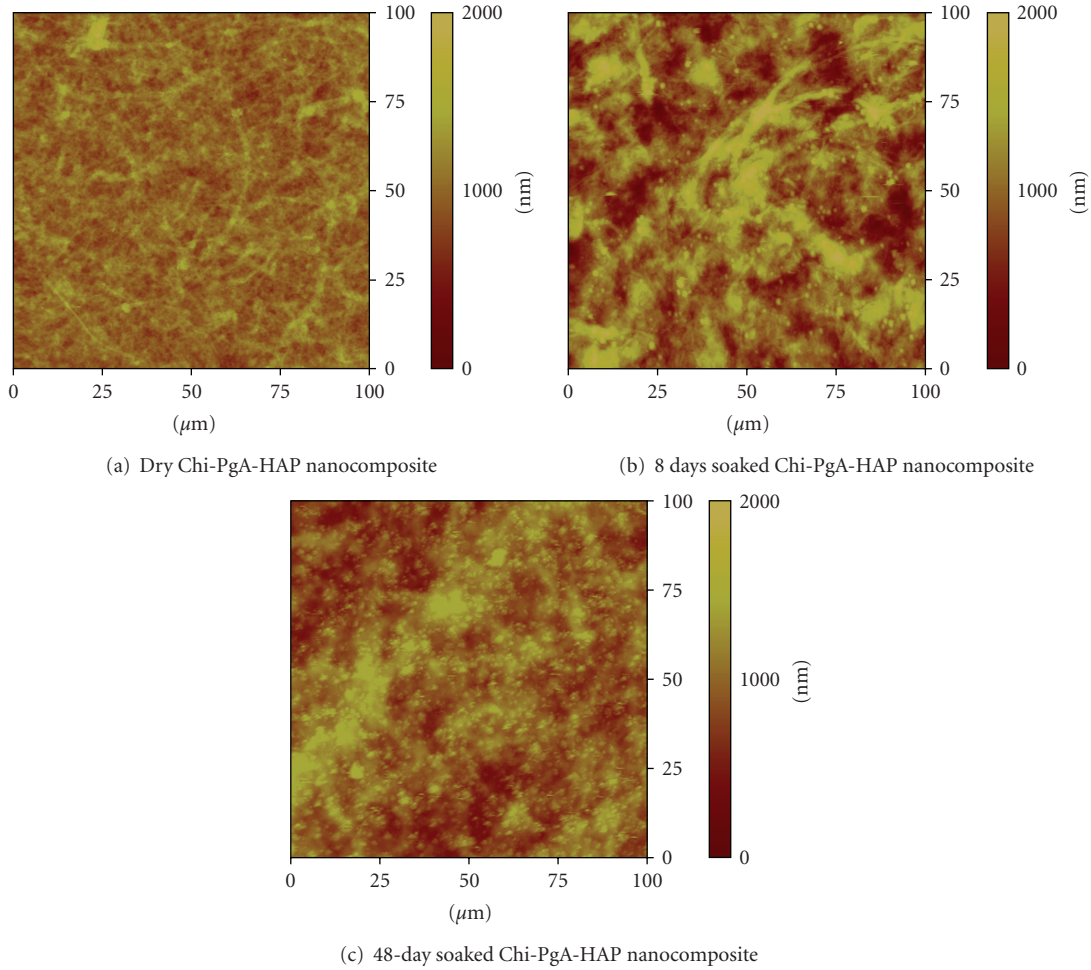

(a) Dry Chi-PgA-HAP nanocomposite

(b) 8 days soaked Chi-PgA-HAP nanocomposite

(c) 48-day soaked Chi-PgA-HAP nanocomposite

Figure 4: AFM topography image indicating the distribution of bundles of Chi-PgA fibers in the Chi-PgA-HAP nanocomposite; HAP nanoparticles are barely discernible in AFM topography image of dry sample. (a) Topographic variations and HAP nanoparticles are more commonly observed in AFM topography image of sample after 8 days of soaking. (b) ~80% of scan area appears to be covered with HAP nanoparticles in the AFM topographic image obtained on 48-day soaked sample (c).

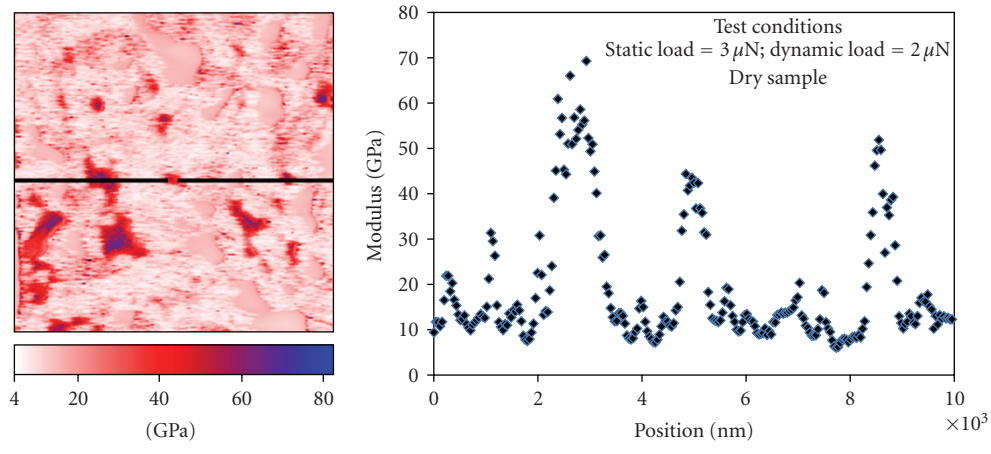

(a)

(b)

Figure 5: Modulus map of dry Chi-PgA-HAP nanocomposite (10 μm × 10 μm) (a) and modulus data along the line of 10 μm length (b). High modulus values are due to stiffer HAP phase and lower modulus values are due to soft polymer phases.

Table 3: Band assignment of dry and soaked Chi-PgA-HAP films for 1150–500 cm^{-1} regions.

Band assignment	Band position as per the soaking conditions (cm^{-1})					
	Dry	1 day	2 days	8 days	24-day	48-day
C–O stretching in ν(C–O–C)	1155	1150	1154	1151	1149	1152
ν_3 asymmetric PO stretching	1113, 1070	1107, 1061	1110, 1067	1102	1107, 1072, 1043	1110, 1077, 1049
ν_1 symmetric PO stretching	1009, 954	996, 953	1001, 952	1021, 956	1009, 956	1010, 960
P–O(H) stretching	894	895	894	895	896	896
O–H bending in HAP structure	645	645	645	644	643	645
ν_4 O–P–O bending	569	569	568	566	563	564

to be enzymatically degradable [19, 30, 31] and degrade primarily through lysozyme-mediated hydrolysis. Moreover, fully deacetylated chitosan has low degradation rates due to inability of hydrolytic enzymes to penetrate the crystalline microstructures. Slow degradation characteristics in our study can be due to high deacetylation degree of chitosan (>85%) and maintenance of structural integrity of PECs in cell culture media.

3.2. AFM Topographic Characterization. Topographical signatures of swelling/degradation were investigated by carrying out systematic in situ AFM experiments in hydrated environment using the Multimode heater, as described in Section 2.4. Representative AFM topographic images of dry and soaked film samples are shown in Figure 3. Topography of soaked samples was investigated for 1, 2, 8, 24 and 48-day, respectively. For investigating the major changes in substrate topography at the microscale, large scan sizes ($100\,\mu m \times 100\,\mu m$) were obtained on both dry and soaked regions. Figure 3(a) shows a smooth 3D topography of dry Chi-PgA-HAP nanocomposite. Further, significant changes in topography were observed after soaking in cell culture medium, as indicated in Figures 3(b)–3(f). After 1 day of soaking, a rough corrugated appearance as indicated by the uneven distribution of sharp ridges and valleys in the microstructure (Figure 3(b)) is observed. Figure 3(c) shows the 3D topography after 2 days of soaking. Ridges appear to grow in height and were observed to have nonuniform distribution over the entire scan area. After 8 days of soaking, some of sharp ridges appear to decrease in height or flatten out and more valleys or grooves were observed (Figure 3(d)). The ridges appear to flatten out and take the shape of circular features (bright spots), were observed to be unevenly distributed over the microstructure.

Soaking experiments were carried out for longer periods to observe the topographical changes of Chi-PgA-HAP samples over a long term exposure. Figure 3(e) indicates the 3D topography of 24-day soaked substrate. As seen in AFM topographic image, deep grooves and pits appear to be present over the entire area. In the literature, swelling characteristics of chitosan and pectin based materials have been commonly reported in terms of the water absorption and water retention [18, 28, 30, 32, 46]. Our AFM results demonstrate that topography changes dramatically upon soaking in cell culture media (1 day) which can be due to swelling of Chi-PgA-HAP biodegradable polymer nanocomposite. Irregularities in topographic features indicate that swelling profiles are site-specific, depending on the access of water into the polymer structures. Due to hydrophilic nature of Chi-PgA-HAP nanocomposite, diffusion of water into the matrix of nanocomposite is faster than degradation, which can result in swelling of the Chi-PgA-HAP nanocomposite prior to degradation. Swelling appears to proceed in a nonuniform fashion during the initial soaking period up to 8 days as indicated by dramatic changes in ridges and valleys in AFM topography images. Sizes and shapes of circular features also appear to be distorted and the irregular shaped larger pits appear to be formed by the coalescence of smaller pits, as revealed by more diffused patterns of light and dark regions in the AFM topographic image of 48-day soaked sample (Figure 3(f)).

The topographic changes can occur due to change in molecular interactions as demonstrated in FTIR spectra of soaked samples (Figure 1). Selected 2D AFM topographic images ($100\,\mu m \times 100\,\mu m$) were taken for dry (Figure 4(a)), 8 days (Figure 4(b)) and 48-day (Figure 4(c)) soaked nanocomposite samples to correlate the topographic observations with the chemistry of soaked samples. As seen in Figure 4(a), bundles of Chi-PgA fibers were observed and HAP particles were barely visible on the surface of dry sample. After 8 days of soaking in cell culture media, HAP nanoparticles were observed on the surface of soaked sample, as seen in AFM topographic image (Figure 4(b)). Figure 4(c) indicates the AFM topography image of 48-day soaked Chi-PgA-HAP sample. It appears that ~80% of the scan area is covered with HAP nanoparticles and FTIR spectrum taken on this sample exhibited the characteristic shape of phosphate bands which match closely with that observed in case of pure HAP samples [45]. This suggests that as soaking proceeds, molecular interactions in Chi-PgA-HAP structures change (phosphate regions; Figure 2), thereby, exposing more HAP nanoparticles to surface of soaked samples and these observations were not made in dry Chi-PgA-HAP samples (both AFM images & FTIR results).

3.3. Nanoscale Elastic Properties by In Situ Modulus Mapping Technique. In situ elastic properties of soaked samples were obtained in presence of cell culture media and at a temperature of 37°C (using Multimode heater) using modulus mapping technique. The description of test procedures is

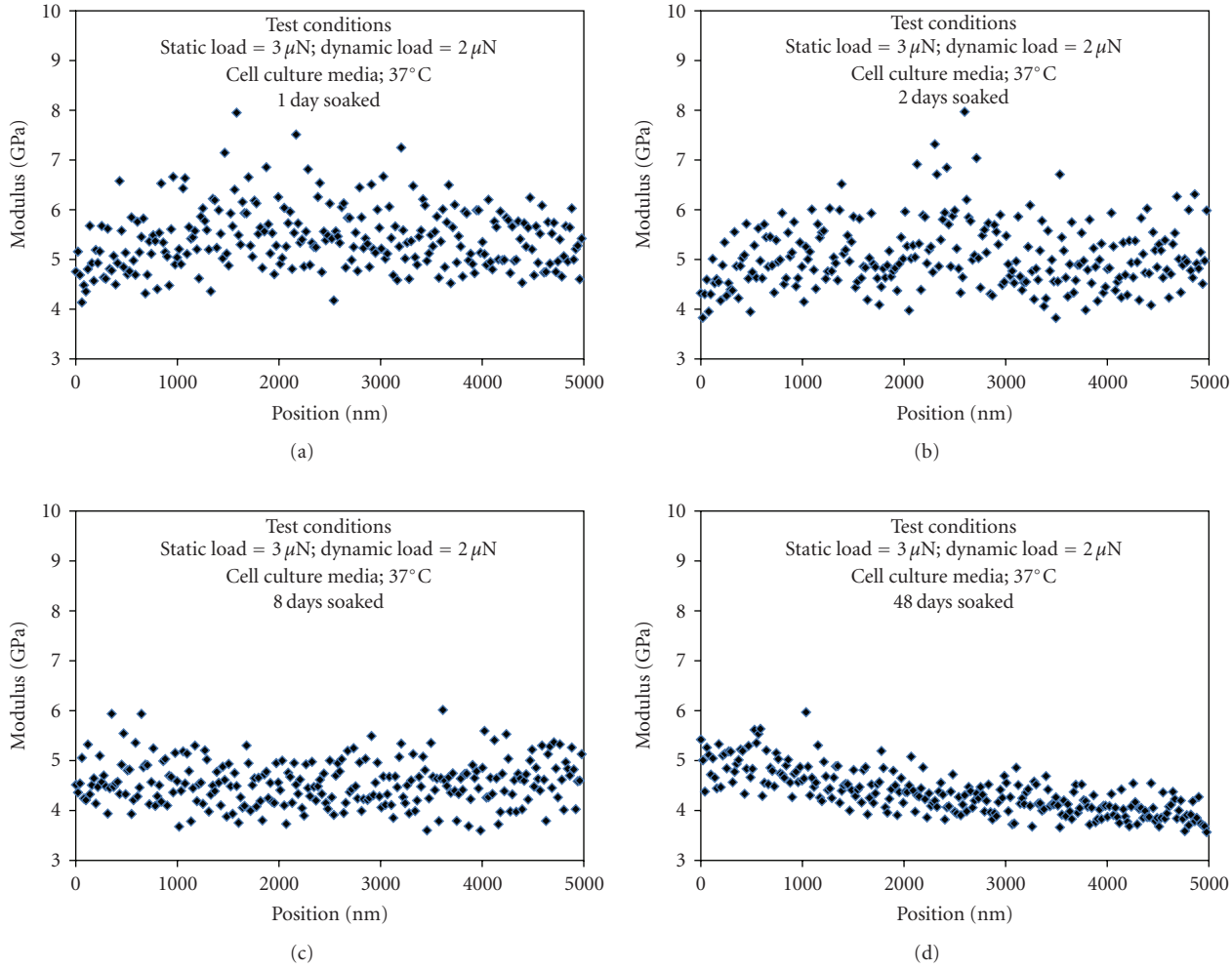

Figure 6: In situ modulus mapping results of 1-(a), 2-(b), 8-(c), and 48-(d) day soaked Chi-PgA-HAP samples. Moduli versus position plots indicate the nanoscale elastic responses of surfaces of soaked samples.

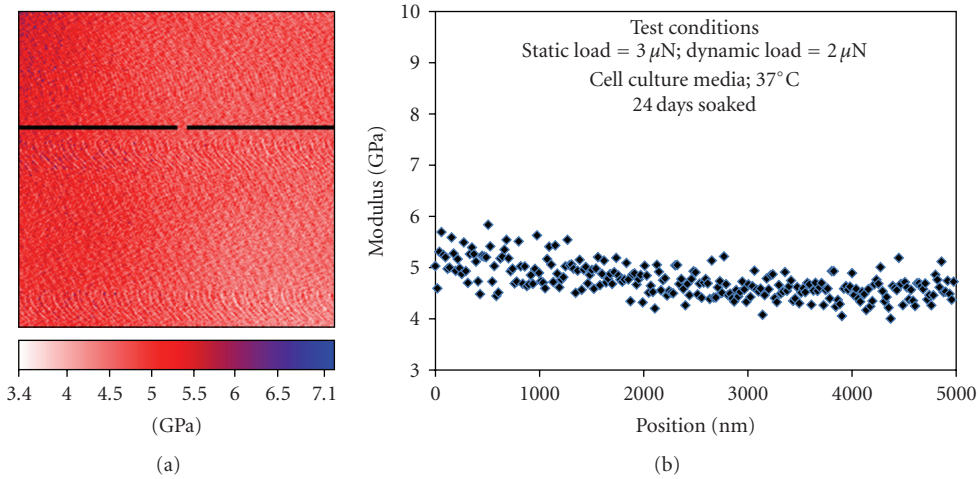

Figure 7: In situ modulus mapping results of 24-day soaked Chi-PgA-HAP samples. Modulus map indicates that there is not significant variation in surface elastic properties of soaked samples (a); modulus versus position plot indicates the mean modulus values of ~5 GPa (b).

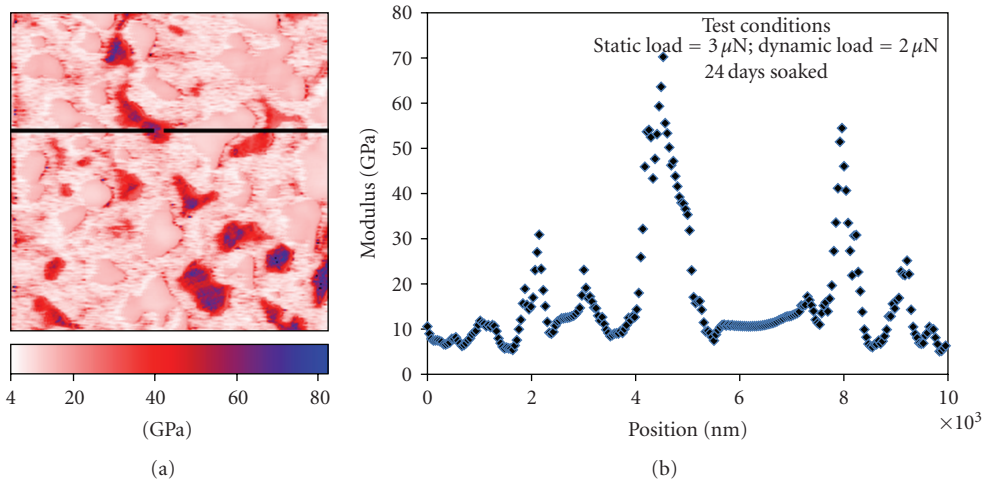

Figure 8: Modulus mapping results of 24-day soaked (but dried) Chi-PgA-HAP sample and tested in air. Chi-PgA-HAP samples. Modulus map indicates that high moduli in the range of 4–80 GPa are observed on surface of dried samples. (a) Modulus versus position plot indicates the elastic responses of the surfaces of 24-day soaked sample.

given in Section 2.4. Figure 5(a) shows the modulus map of a scan area of 10 μm × 10 μm on surface of dry Chi-PgA-HAP nanocomposite film. In modulus map image, lighter color corresponds to lower elastic moduli (~4 GPa) due to relatively softer polymer phase, that is, Chi-PgA phase. Darker color corresponds to higher elastic moduli (~80 GPa), which indicate the elastic responses from the stiffer hydroxyapatite phase or from the regions having a very thin polymer layer. A combined elastic response (~10–30 GPa) from both the polymer and HAP phase is indicated by mixed color patches observed in the modulus map image. The composite elastic modulus can be obtained from the surfaces of biomimetic nanohydroxyapatite, as reported in our prior work [40]. The variation in modulus values along the scan length of 10 μm indicates the local distribution of constituents in the microstructure (Figure 5(b)).

Figures 6(a)–6(d) show the modulus data of samples soaked in cell culture media for 1, 2, 8, and 48-day, respectively. Representative line scans were selected from modulus maps obtained as per each soaking experiment conditions, and modulus values were plotted as function of position. In situ elastic moduli of 3.5–8 GPa have been obtained from the surfaces of soaked substrates for upto 2 days of soaking. These are the nanoscale elastic responses of the swollen phases or constituents of Chi-PgA-HAP substrate. An observed scatter in modulus values within 4–8 GPa is consistently observed during the initial soaking duration (Figures 6(a) and 6(b)). Over the longer soaking duration (Figures 6(c) and 6(d)), less scatter in moduli was observed and moreover, nanoscale modulus is observed to decrease by ~2 GPa.

Elastic modulus in the range of 2–4 GPa [47] has been measured from the gold nanoparticles functionalized with bovine serum albumin and streptavidin using nanoindentation technique (load = 5 μN). The elastic modulus of ~3-4 GPa measured using modulus mapping technique (load = 5 μN) can result from the nanoscale elastic response from the proteins adsorbed on the surface of soaked samples, which also match closely with that reported in literature. Protein adsorption on Chi-PgA-HAP nanocomposites is more likely due to its hydrophilic nature. Specifically, chitosan's cationic nature allows various electrostatic interactions with negatively charged species such as proteins, anionic glycoaminoglycans [4]. Chi-PgA-HAP structure with mainly $-NH_2$, –COOH and $-(COO^{-}NH_3^{+})$ complexes can interact with proteins and modify the surfaces. Performing in situ elastic property measurement in cell culture fluid and at 37°C can give the nanoscale properties of proteins adsorbed on Chi-PgA-HAP substrates in their natural environment. However, in a modulus mapping technique, it is not easy to identify the elastic responses of individual sites, due to a potential overlap between the modulus values of proteins and sites of soaked substrate.

Further, additional experiments were done on soaked but air dried samples in clear air laboratory environment to see the effect of dehydration from the soaked polymer nanocomposite samples. Selected results are presented herein for modulus mapping experiments on 24-day soaked samples and tested in a fully hydrated state and unhydrated (dried) environment. Figure 7(a) indicates the modulus map obtained after 24-day of soaking and tested in a hydrated state (cell culture media; 37°C). Modulus values of 4–6 GPa were observed with a mean value of ~5 GPa (Figure 7(b)). Figure 8(a) indicates the modulus map obtained after 24-day of soaking, and completely dried in air, and then, tested in clean-air laboratory environment. Modulus data were plotted as a function of position over a length of 10 μm (Figure 8(b)). Modulus values in the range of ~4–80 GPa were observed. Significantly large difference in modulus values observed by testing under the hydrated and unhydrated environment can result from dehydration effects from the surface of the swollen polymer specimen which makes its surface more stiff. Effect of sample dehydration on nanomechanical properties is less important

for hard materials like metals, ceramics and some hard tissues. However, soft and spongy polymers (e.g., Chi-PgA-HAP biodegradable polymer nanocomposites) which exhibit swelling characteristics, have entrapped water in their structures. Hence, testing such samples in a dry environment can severely affect the mechanical properties, as seen in our modulus mapping results. It has been shown that even in case of hard tissue like bone, upon dehydration, hardness can be increased by 17%–30% and modulus by 15%–50% [48, 49]. Therefore, it is important that in situ nanomechanical mesurements are carried out in a liquid environment to get in situ elastic properties of water-swollen polymeric structures. Our results suggest that modulus mapping is a promising technique to evaluate the purely elastic properties of proteins and that of soaked substrates.

4. Conclusions

The in situ degradation/swelling behavior of novel Chi-PgA-HAP nanocomposites is characterized by FTIR, AFM and modulus mapping technique. FTIR results demonstrated that molecular structure of soaked samples changes over the course of 48-day of soaking in cell culture media, as indicated by significant variations in phosphate vibrations. As water enters the Chi-PgA-HAP sample, interactions in Chi-PgA-HAP structure are modified that can result in swelling. PECs govern the structural integrity in Chi-PgA-HAP nanocomposites and FTIR spectra indicated that PECs were still in-tact until 48-day of soaking. In situ AFM experiments on soaked samples indicate that soaking results in a change in topography due to swelling of Chi-PgA-HAP substrates. AFM topographic images indicate that swelling proceeds in an inhomogeneous fashion during the initial soaking period up to 8 days and then, occurs in a more gradual fashion during the longer soaking periods. In situ modulus mapping experiments on soaked samples represent the elastic properties of surface of soaked samples. Elastic moduli of ~4 GPa are observed, which may result from nanoscale elastic responses of proteins adsorbed on Chi-PgA-HAP nanocomposites. Modulus mapping results of soaked samples indicate that nanoscale elastic modulus decreases by ~2 GPa over a long exposure to cell culture media (48-day) and there were no major changes in surface mechanical properties over 48-day of soaking in cell culture media.

This work has important implications for tissue engineering. For instance, mostly biodegradable materials are used in the fabrication of tissue engineering scaffolds. Biodegradable materials can undergo physic chemical-mechanical changes under the wet conditions, as also indicated by our study. It is now understood that cells do respond to such physico-chemical changes which can also affect cell-biomaterial interactions. In order to correlate the changes in physical properties of degrading substrate to cellular responses (biochemical/biomechanical), a systematic evaluation of in situ material properties of biodegradable materials in nearly physiological environment is required, which merits scientific interest.

References

[1] S. Miyazaki, K. Ishii, and T. Nadai, "The use of chitin and chitosan as drug carriers," *Chemical & Pharmaceutical Bulletin*, vol. 29, no. 10, pp. 3067–3069, 1981.

[2] K. Aiedeh, E. Gianasi, I. Orienti, and V. Zecchi, "Chitosan microcapsules as controlled release systems for insulin," *Journal of Microencapsulation*, vol. 14, no. 5, pp. 567–576, 1997.

[3] G. Kratz, C. Arnander, J. Swedenborg, et al., "Heparin-chitosan complexes stimulate wound healing in human skin," *Scandinavian Journal of Plastic and Reconstructive Surgery and Hand Surgery*, vol. 31, no. 2, pp. 119–123, 1997.

[4] S. V. Madihally and H. W. T. Matthew, "Porous chitosan scaffolds for tissue engineering," *Biomaterials*, vol. 20, no. 12, pp. 1133–1142, 1999.

[5] W.-C. Hsieh, C.-P. Chang, and S.-M. Lin, "Morphology and characterization of 3D micro-porous structured chitosan scaffolds for tissue engineering," *Colloids and Surfaces B*, vol. 57, no. 2, pp. 250–255, 2007.

[6] Y. Wan, H. Wu, and D. Wen, "Porous-conductive chitosan scaffolds for tissue engineering, 1: preparation and characterization," *Macromolecular Bioscience*, vol. 4, no. 9, pp. 882–890, 2004.

[7] J. Nakamatsu, F. G. Torres, O. P. Troncoso, M. L. Yuan, and A. R. Boccaccini, "Processing and characterization of porous structures from chitosan and starch for tissue engineering scaffolds," *Biomacromolecules*, vol. 7, no. 12, pp. 3345–3355, 2006.

[8] A. Wang, Q. Ao, W. Cao, et al., "Porous chitosan tubular scaffolds with knitted outer wall and controllable inner structure for nerve tissue engineering," *Journal of Biomedical Materials Research Part A*, vol. 79, no. 1, pp. 36–46, 2006.

[9] L. Peng, X. R. Cheng, J. W. Wang, D. X. Xu, and G. Wang, "Preparation and evaluation of porous chitosan/collagen scaffolds for periodontal tissue engineering," *Journal of Bioactive and Compatible Polymers*, vol. 21, no. 3, pp. 207–220, 2006.

[10] Y. Wan, A. X. Yu, H. Wu, Z. X. Wang, and D. J. Wen, "Porous-conductive chitosan scaffolds for tissue engineering II. In vitro and in vivo degradation," *Journal of Materials Science: Materials in Medicine*, vol. 16, no. 11, pp. 1017–1028, 2005.

[11] H. F. Liu, F. L. Yao, Y. Zhou, et al., "Porous poly (DL-lactic acid) modified chitosan-gelatin scaffolds for tissue engineering," *Journal of Biomaterials Applications*, vol. 19, no. 4, pp. 303–322, 2005.

[12] L. Ma, C. Y. Gao, Z. W. Mao, et al., "Collagen/chitosan porous scaffolds with improved biostability for skin tissue engineering," *Biomaterials*, vol. 24, no. 26, pp. 4833–4841, 2003.

[13] J. Yang, T. W. Chung, M. Nagaoka, M. Goto, C.-S. Cho, and T. Akaike, "Hepatocyte-specific porous polymer-scaffolds of alginate/galactosylated chitosan sponge for liver-tissue engineering," *Biotechnology Letters*, vol. 23, no. 17, pp. 1385–1389, 2001.

[14] E. Khor and L. Y. Lim, "Implantable applications of chitin and chitosan," *Biomaterials*, vol. 24, no. 13, pp. 2339–2349, 2003.

[15] S. Dumitriu and E. Chornet, "Inclusion and release of proteins from polysaccharide-based polyion complexes," *Advanced Drug Delivery Reviews*, vol. 31, no. 3, pp. 223–246, 1998.

[16] C. Peniche and W. Arguelles-Monal, "Chitosan based polyelectrolyte complexes," *Macromolecular Symposia*, vol. 168, pp. 103–116, 2001.

[17] W. G. T. Willats, P. Knox, and J. D. Mikkelsen, "Pectin: new insights into an old polymer are starting to gel," *Trends in Food Science & Technology*, vol. 17, no. 3, pp. 97–104, 2006.

[18] P. Bernabé, C. Peniche, and W. Argüelles-Monal, "Swelling behavior of chitosan/pectin polyelectrolyte complex membranes. Effect of thermal cross-linking," *Polymer Bulletin*, vol. 55, no. 5, pp. 367–375, 2005.

[19] L. S. Liu, M. L. Fishman, J. Kost, and K. B. Hicks, "Pectin-based systems for colon-specific drug delivery via oral route," *Biomaterials*, vol. 24, no. 19, pp. 3333–3343, 2003.

[20] F. Zhao, W. L. Grayson, T. Ma, B. Bunnell, and W. W. Lu, "Effects of hydroxyapatite in 3-D chitosan-gelatin polymer network on human mesenchymal stem cell construct development," *Biomaterials*, vol. 27, no. 9, pp. 1859–1867, 2006.

[21] B. Q. Li, Q. L. Hu, X. Z. Qian, Z. P. Fang, and J. C. Shen, "Bioabsorbable chitosan/hydroxyapatite composite rod prepared by in-situ precipitation for internal fixation of bone fracture," *Acta Polymerica Sinica*, no. 6, pp. 828–833, 2002.

[22] W. Y. Xia, W. Liu, L. Cui, et al., "Tissue engineering of cartilage with the use of chitosan-gelatin complex scaffolds," *Journal of Biomedical Materials Research Part B*, vol. 71, no. 2, pp. 373–380, 2004.

[23] V. Chiono, E. Pulieri, G. Vozzi, G. Ciardelli, A. Ahluwalia, and P. Giusti, "Genipin-crosslinked chitosan/gelatin blends for biomedical applications," *Journal of Materials Science: Materials in Medicine*, vol. 19, no. 2, pp. 889–898, 2008.

[24] Z. S. Li, H. R. Ramay, K. D. Hauch, D. M. Xiao, and M. Q. Zhang, "Chitosan-alginate hybrid scaffolds for bone tissue engineering," *Biomaterials*, vol. 26, no. 18, pp. 3919–3928, 2005.

[25] D. Verma, K. S. Katti, D. R. Katti, and B. Mohanty, "Mechanical response and multilevel structure of biomimetic hydroxyapatite/polygalacturonic/chitosan nanocomposites," *Materials Science and Engineering C*, vol. 28, no. 3, pp. 399–405, 2008.

[26] D. Verma, K. S. Katti, and D. R. Katti, "Effect of biopolymers on structure of hydroxyapatite and interfacial interactions in biomimetically synthesized hydroxyapatite/biopolymer nanocomposites," *Annals of Biomedical Engineering*, vol. 36, no. 6, pp. 1024–1032, 2008.

[27] D. Verma, K. S. Katti, and D. R. Katti, "Osteoblast adhesion, proliferation and growth on polyelectrolyte-complex-hydroxyapatite nanocomposites," *Philosophical Transactions. Series A*, vol. 368, no. 1917, pp. 2083–2097, 2010.

[28] M.-W. Lee, C.-L. Hung, J.-C. Cheng, and Y.-J. Wang, "A new anti-adhesion film synthesized from polygalacturonic acid with 1-ethyl-3-(3-dimethylaminopropyl)carbodiimide crosslinker," *Biomaterials*, vol. 26, no. 18, pp. 3793–3799, 2005.

[29] W. Argüelles-Monal, O. L. Hechavarría, L. Rodríguez, and C. Peniche, "Swelling of membranes from the polyelectrolyte complex between chitosan and carboxymethyl cellulose," *Polymer Bulletin*, vol. 31, no. 4, pp. 471–478, 1993.

[30] S. M. Lim, D. K. Song, S. H. Oh, D. S. Lee-Yoon, E. H. Bae, and J. H. Lee, "In vitro and in vivo degradation behavior of acetylated chitosan porous beads," *Journal of Biomaterials Science, Polymer Edition*, vol. 19, no. 4, pp. 453–466, 2008.

[31] W. Tachaboonyakiat, T. Serizawa, and M. Akashi, "Inorganic-organic polymer hybrid scaffold for tissue engineering—II: partial enzymatic degradation of hydroxyapatite-chitosan hybrid," *Journal of Biomaterials Science, Polymer Edition*, vol. 13, no. 9, pp. 1021–1032, 2002.

[32] K. Tomihata and Y. Ikada, "In vitro and in vivo degradation of films of chitin and its deacetylated derivatives," *Biomaterials*, vol. 18, no. 7, pp. 567–575, 1997.

[33] S. Hirano, H. Tsuchida, and N. Nagao, "N-acetylation in chitosan and the rate of its enzymic hydrolysis," *Biomaterials*, vol. 10, no. 8, pp. 574–576, 1989.

[34] W. L. Cao, M. Y. Cheng, Q. Ao, Y. D. Gong, N. M. Zhao, and X. F. Zhang, "Physical, mechanical and degradation properties, and schwann cell affinity of cross-linked chitosan films," *Journal of Biomaterials Science, Polymer Edition*, vol. 16, no. 6, pp. 791–807, 2005.

[35] D. W. Ren, H. F. Yi, W. Wang, and X. J. Ma, "The enzymatic degradation and swelling properties of chitosan matrices with different degrees of N-acetylation," *Carbohydrate Research*, vol. 340, no. 15, pp. 2403–2410, 2005.

[36] A. Cárdenas, W. Argüelles-Monal, F. M. Goycoolea, I. Higuera-Ciapara, and C. Peniche, "Diffusion through membranes of the polyelectrolyte complex of chitosan and alginate," *Macromolecular Bioscience*, vol. 3, no. 10, pp. 535–539, 2003.

[37] J. R. R. de Souza, J. I. X. de Carvalho, M. T. S. Trevisan, R. C. M. de Paula, N. Ricardo, and J. P. A. Feitosa, "Chitosan-coated pectin beads: characterization and in vitro release of mangiferin," *Food Hydrocolloids*, vol. 23, no. 8, pp. 2278–2286, 2009.

[38] K. D. Yao, H. L. Tu, F. Cheng, J. W. Zhang, and J. Liu, "pH-sensitivity of the swelling of a chitosan-pectin polyelectrolyte complex," *Angewandte Makromolekulare Chemie*, vol. 245, pp. 63–72, 1997.

[39] G. Balooch, G. W. Marshall, S. J. Marshall, O. L. Warren, S. A. S. Asif, and M. Balooch, "Evaluation of a new modulus mapping technique to investigate microstructural features of human teeth," *Journal of Biomechanics*, vol. 37, no. 8, pp. 1223–1232, 2004.

[40] R. Khanna, K. S. Katti, and D. R. Katti, "Nanomechanics of surface modified nanohydroxyapatite particulates used in biomaterials," *Journal of Engineering Mechanics*, vol. 135, no. 5, pp. 468–478, 2009.

[41] K. S. Katti, P. Turlapati, D. Verma, R. Bhowmik, P. K. Gujjula, and D. R. Katti, "Static and dynamic mechanical behavior of hydroxyapatite-polyacrylic acid composites under simulated body fluid," *American Journal of Biochemistry and Biotechnology*, vol. 2, no. 2, pp. 73–79, 2006.

[42] S. A. S. Asif, K. J. Wahl, R. J. Colton, and O. L. Warren, "Quantitative imaging of nanoscale mechanical properties using hybrid nanoindentation and force modulation," *Journal of Applied Physics*, vol. 90, no. 3, pp. 1192–1200, 2001.

[43] K. Kato, Y. Eika, and Y. Ikada, "In situ hydroxyapatite crystallization for the formation of hydroxyapatite/polymer composites," *Journal of Materials Science*, vol. 32, no. 20, pp. 5533–5543, 1997.

[44] F. Bigucci, B. Luppi, T. Cerchiara, et al., "Chitosan/pectin polyelectrolyte complexes: selection of suitable preparative conditions for colon-specific delivery of vancomycin," *European Journal of Pharmaceutical Sciences*, vol. 35, no. 5, pp. 435–441, 2008.

[45] D. Verma, K. Katti, and D. Katti, "Experimental inves-tigation of interfaces in hydroxyapatite/polyacrylic acid/polycaprolactone composites using photoacoustic FTIR spectroscopy," *Journal of Biomedical Materials Research Part A*, vol. 77, no. 1, pp. 59–66, 2006.

[46] W. W. Thein-Han and R. D. K. Misra, "Biomimetic chitosan-nanohydroxyapatite composite scaffolds for bone tissue engineering," *Acta Biomaterialia*, vol. 5, no. 4, pp. 1182–1197, 2009.

[47] H. P. Wampler and A. Ivanisevic, "Nanoindentation of gold nanoparticles functionalized with proteins," *Micron*, vol. 40, no. 4, pp. 444–448, 2009.

[48] J.-Y. Rho and G. M. Pharr, "Effects of drying on the mechanical properties of bovine femur measured by nanoindentation," *Journal of Materials Science: Materials in Medicine*, vol. 10, no. 8, pp. 485–488, 1999.

[49] S. Hengsberger, A. Kulik, and Ph. Zysset, "Nanoindentation discriminates the elastic properties of individual human bone lamellae under dry and physiological conditions," *Bone*, vol. 30, no. 1, pp. 178–184, 2002.

Hindawi Publishing Corporation
International Journal of Polymer Science
Volume 2010, Article ID 436178, 9 pages
doi:10.1155/2010/436178

Research Article

Bimodal Porous Scaffolds by Sequential Electrospinning of Poly(glycolic acid) with Sucrose Particles

B. Wulkersdorfer,[1] K. K. Kao,[1,2] V. G. Agopian,[1,2] A. Ahn,[1] J. C. Dunn,[2,3] B. M. Wu,[2,3] and M. Stelzner[1,2]

[1] *Department of Surgery, VA Greater Los Angeles Health Care System, Los Angeles, CA 90073, USA*
[2] *Department of Surgery, University of California at Los Angeles, Los Angeles, CA 90095, USA*
[3] *Department of Bioengineering, University of California at Los Angeles, Los Angeles, CA 90095, USA*

Correspondence should be addressed to M. Stelzner, matthias.stelzner@med.va.gov

Received 20 November 2009; Revised 20 January 2010; Accepted 20 January 2010

Academic Editor: Shanfeng Wang

Electrospinning is a method to produce fine, biopolymer mesh with a three-dimensional architecture that mimics native extracellular matrix. Due to the small fiber diameter created in this process, conventional electrospun scaffolds have pore sizes smaller than the diameter of most cells. These scaffolds have limited application in tissue engineering due to poor cell penetration. We developed a hybrid electrospinning/particulate leaching technique to create scaffolds with increased porosity and improved cellular ingrowth. Poly(glycolic acid) (PGA) and a sucrose-ethanol suspension were electrospun in equal, alternating sequences at intervals of one, two, and ten minutes each. The scaffolds revealed fiber mesh with micropores of 10 μm and uniformly distributed sucrose particles. Particulate leaching of sucrose from the one- or two-minute scaffolds revealed honeycomb structures with interconnected macropores between 50 and 250 μm. Sucrose leaching from the ten-minute scaffolds resulted in laminated structures with isolated macropores between 200 and 350 μm. Macropore size was directly proportional to the duration of the sucrose spinning interval. After 24 hours of cell culture, conventionally spun scaffolds demonstrated no cellular penetration. Conversely, the PGA/sucrose scaffolds demonstrated deep cellular penetration. This hybrid technique represents a novel method of generating electrospun scaffolds with interconnected pores suitable for cellular ingrowth.

1. Introduction

Tissue engineering aims to develop "biological substitutes that restore, maintain, or improve tissue or organ function[1]". A commonly used approach has involved seeding cells harvested from donor tissue onto a three-dimensional matrix and ultimately implanting the device, such that the cells grow, organize, and function to augment or replace the damaged organ [2]. An ideal bioengineered matrix would be biocompatible and biodegradable yet have sufficient mechanical integrity to maintain its architecture until the seeded cells produced a new extracellular matrix (ECM) and replicate the donor organ [3].

Various biodegradable polymers have been used to create biomimetic scaffolds for tissue engineering, including poly(lactic acid) (PLA), poly(epsilon-caprolactone) (PCL), poly(lactic-co-glycolic acid) (PLGA), and poly(glycolic acid) (PGA) [4–7]. These poly(alpha-hydroxyesters) are commonly employed for clinical use in suture material and wound dressings, and have well known degradation characteristics. In vivo, these polyesters degrade by random hydrolysis and enzymatic action [8]. PGA and PLGA can be completely degraded from two to four weeks, whereas PCL and PLA may take up to 12 to 24 months for complete mass loss [9].

Porous scaffolds are particularly suited for use in tissue engineering because they have several properties that mimic the ECM, including a large surface area, pore size suitable for cellular ingrowth, and a three-dimensional environment conducive to promoting cell to cell contact [10]. Various techniques have been developed to fabricate porous scaffolds including solvent casting and particulate leaching [11], freeze

drying [12], phase separation [13], solid free-form fabrication [14], foaming [15, 16], sintering [17], electroblowing [18], and electrospinning [19].

Electrospinning, or electrostatic spinning, was first developed in the early 1930's by Formhals; however, it was not until the 1960's that Taylor elucidated the fundamentals of the jet forming process, sparking a renewed interest in the larger scientific community [19]. It was found that by spinning a polymer solution under a large electric potential, electrostatic forces overcome the weaker forces of surface tension in the liquid, and create a fine charged jet [20]. The jet is then carried in the direction of the electric field, all the while thinning and elongating. Due to inherent instabilities of the jet motion, a dense nonwoven randomly oriented mesh can be collected on the counter electrode [10]. The typical setup is simple and inexpensive; it consists of a collector, a syringe pump containing a polymer solution, and a high voltage power supply [21].

The fibers generated by electrospinning typically range from 10 nm to 10 μm in diameter, depending on the material, concentration, viscosity, electrical potential, working distance, and ambient conditions [9, 22, 23]. Eichhorn and Sampson have demonstrated that pore radius is proportional to fiber diameter [24]. Effective pore sizes of electrospun scaffolds would be anticipated to be between 0.5 and 5 μm. Kwon et al. have developed electrospun matrices with fiber diameters ranging from 0.3 μm to 7 μm and pore sizes of 0.2 to 30 μm using various biodegradable copolyesters [25]. In electrospun meshes, fiber diameters from 10 nm to 10 μm in diameter have been shown to promote cell attachment [22]. However, paradoxically the small pore sizes would restrict cellular infiltration and proliferation of cells which typically range from 5 to 20 μm [26]. In order to generate a scaffold with both fine fibers and larger pore sizes, an alternative technique had to be developed.

The purpose of this study is to generate electrospun PGA scaffolds with increased porosity by combining electrospinning with particulate leaching. We modified the conventional electrospinning technique by alternately spinning a polymer solution with a sucrose suspension and subsequently leaching the sucrose crystals.

2. Materials and Methods

2.1. Electrospinning. For the electrospinning process, a 10% weight/volume solution of poly(glycolic acid) (PGA; Lakeshore Biomaterials; Birmingham, AL) was dissolved in 1,1,1,3,3,3-hexafluoro-2-propanol (HFP; Sigma-Aldrich (Fluka, Milwaukee, WI) and mixed on an orbital shaker for at least 12 hours. The solution was dispensed through an 18-gauge blunt needle (Integrated Dispensing Solutions Inc., Agoura Hills, CA) attached to a 10 mL plastic syringe (Becton Dickenson and Company, Franklin Lakes, NJ) with a syringe pump (Harvard Apparatus, Holliston, MA) at a flow rate of 1 mL/h. A 5 mm thick copper rod collector (McMaster Carr Co, Atlanta, GA) covered by copper foil (Lyon Industries Chicago Inc., South Elgin, IL) was placed at a distance of 8 cm from the needle tip and rotated at 1,200 rpm. Electrospinning was performed by applying an electrical field of 28 kV from a high voltage power source (Series PS/EL, Glassman High Voltage Inc., High Bridge, NJ) between the needle tip and the collector electrode. Nanofibers were collected on the target electrode rotating at 2000 rpm to form a nonwoven tubular structure.

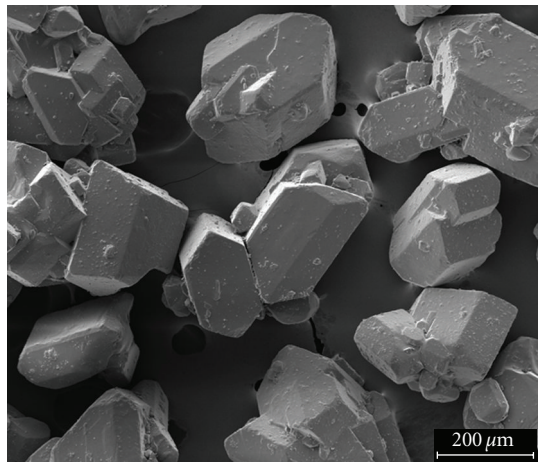

Figure 1: SEM image: sucrose particles.

Confectioner's sugar (Pure Cane Sugar C&H, C&H Sugar Company, Inc., Crockett, CA) was sieved to a particle size ranging 250–350 μm in diameter (Figure 1) and then a suspension of 70% weight/volume solution of sucrose with 70% ethanol (Fisher Scientific, Fairlawn, NJ) was prepared immediately prior to use.

Most sucrose crystals remained undissolved within the liquid phase, and the crystal suspension was of low viscosity. The sucrose-ethanol suspension was electrospun using the aforementioned apparatus at a distance of 15 cm to the same target collector used for the PGA.

To determine the effects of spin time, PGA and sucrose solutions were alternately spun in 1 : 1 ratios at time intervals of one, two, and ten minutes each (i.e., one minute of PGA spinning followed by one minute of sucrose spinning; two minutes of PGA spinning followed by two minutes of sucrose spinning; ten minutes of PGA spinning followed by ten minutes of sucrose spinning). Electrospinning using the PGA solution was alternated with the sucrose solution to create multi-layered scaffolds of 20 to 40 layers. PGA scaffolds spun without sucrose served as controls. After fabrication the electrospun tube was carefully removed from the target. The tube was leached twice in 37°C warm distilled water for ten minutes followed by dehydration in a hood under constant airflow.

2.2. Scanning Electron Microscopy (SEM). Before and after particulate leaching, 500 μm cross sections of the electrospun tubes were prepared, sputter-coated with gold (Hummer II, Technics, Alexandria, VA) and imaged by scanning electron microscope (SEM) (Dual Beam NOVA 600, FEI Company, Portland, OR). Images were acquired at an accelerating voltage of 20 kV. For each experimental group, five images from different areas of the scaffolds were randomly picked and evaluated by a blinded observer to measure pore sizes.

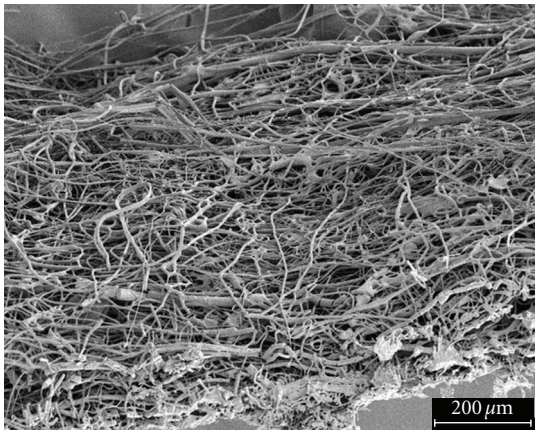

Figure 2: SEM image: cross-sectional view of control electrospun tube.

An average pore size was expressed as mean ± standard error of mean.

2.3. Cell Culture. NIH/3T3 fibroblasts (ATCC, Manassas, VA) were cultured in cell-specific complete growth media (ATCC, Manassas, VA) supplemented with 10% bovine calf serum (Colorado Serum Company, Denver, CO) and 1% antibiotic solution (20,000 U/mL penicillin and 20,000 μg/mL streptomycin) (Cambrex BioScience, Walkersville, MD). This medium was used for all subsequent experimental steps. Cell cultures were maintained in a humidified 37°C cell culture incubator with a 95% O_2/5% CO_2 environment. Culture media were replaced every three days. Fibroblasts were passaged three times, removed by 0.25% trypsin-EDTA treatment (Invitrogen-GIBCO, Carlsbad, CA), counted, and prepared for seeding onto the electrospun scaffolds.

2.4. Scaffold Preparation and Seeding. Electrospun tubes were cut into 1 cm^2 sheets and subjected to plasma etching (Plasma Cleaner and Sterilizer, PDC-32G, Harrick Scientific, NY) for three minutes. The tubes were disinfected in 80% ethanol for 30 minutes, serially hydrated through an alcohol series in distilled water (70%, 60%, 50% and 40% ethanol), subsequently rinsed with sterile phosphate buffered solution (PBS) (Fisher, Pittsburgh, PA) and dried under sterile conditions in a hood at room temperature for two hours. Prior to cell seeding, scaffolds were placed in a 24-well cell culture plate and prewetted with culture medium. For each scaffold 2×10^5 fibroblasts were then suspended in 20 μL complete growth media and placed as a drop in the center of the electrospun biopolymer mesh. To allow for cell attachment, the samples were incubated at 37°C for two hours before they were completely covered with media. Seeded scaffolds were harvested 24 hours after seeding. Scaffolds that received cell-free media served as negative controls.

2.5. Histological Evaluation. Samples were harvested and fixed in 10% neutral buffered formalin (Fisher Diagnostics, Middletown, VA), rinsed with PBS and embedded in OCT compound (Sakura Finetek, Torrance, CA). Embedded scaffolds were stored at −80°C until sectioning. Cryosections were cut at 10 μm thicknesses using a cryostat (Microm GmbH, Walldorf, Germany) and stored at −80°C until used. For fluorescent nuclear staining, frozen cryosections were taken from the −80°C freezer and allowed to thaw and dry at room temperature for 15 minutes. Fluorescent staining was performed by adding mounting medium with 4′, 6-diamidino-2-phenylindole (DAPI) (Vector Laboratories, Burlingame, CA) to the sections and incubating them in a dark environment for 5 minutes at room temperature. DAPI-stained sections were evaluated under a fluorescent microscope (ImageJ 1.42 software, National Institute of Health, http://rsbweb.nih.gov/ij/index.html; Carl Zeiss, Hallbergmoos, Germany) and evaluated at magnifications of 100× and 200×. Five sections per experimental group taken from different areas of the cell seeded scaffolds were randomly picked and analyzed for cell penetration depth within the scaffolds. Due to variations in scaffold thickness, exact micron measurements of cell penetration were not useful; instead, a blinded observer was asked to assign subjective penetration scores based on perceived cell depth with the following scores: no penetration (0), very poor penetration (+), moderate penetration (++), or deep penetration (+++).

3. Results

Representative SEM samples of control and sequential electrospun scaffolds are shown in Figures 2–5. The control scaffold, that is, PGA without sucrose particles, revealed the typical architecture and random fiber distribution of a conventional electrospun mesh (Figure 2). Fiber diameters varied between 1–5 μm and pores measured 10 μm on average; no macropores were found.

Our maximum electrospinning intervals for PGA and sucrose were ten minutes. Preliminary experiments with 15-minute spinning time intervals produced delaminated layers (data not shown). Minimum electrospinning intervals were one minute. Spinning intervals for PGA and sucrose less than one minute proved to be unreliable due to equipment limitations.

All sequentially electrospun scaffolds revealed randomly oriented PGA fibers with diameters between 1–5 μm. The average macropore size ranged from 50–300 μm with diameters correlating with spinning time intervals. Ten-minute intervals created the largest pores and one-minute intervals created the smallest pores (Figure 6).

Spinning for one minute resulted in macropore sizes ranging from 50 to 150 μm, spinning for two minutes created macropore sizes from 100 to 250 μm, and spinning for ten minutes revealed macropore sizes from 200 to 350 μm in diameter. Pore sizes within areas of PGA mesh without sucrose averaged 10 μm in diameter.

The density of sucrose distribution varied with time. With ten-minute sequential time intervals, the scaffolds revealed dense packing of incorporated sucrose crystals (Figure 3(a)). One- and two-minute alternating sequences

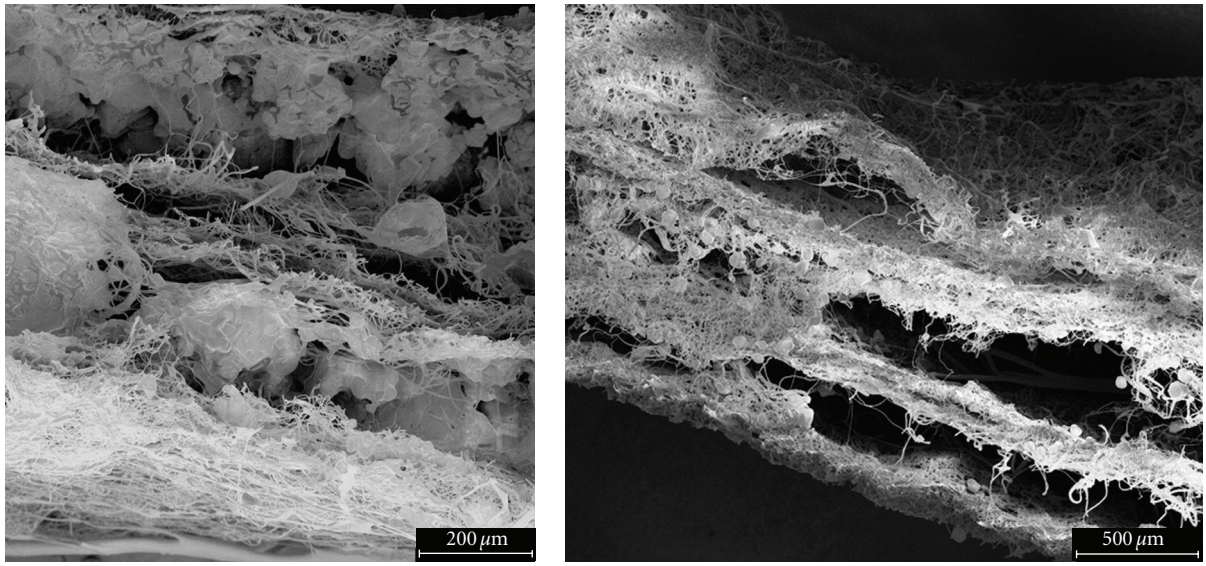

(a) Sugar particles embedded in the PGA scaffold (b) Scaffold after leaching of sugar crystals

Figure 3: SEM images: cross-sectional view of electrospun tubes; the electrospinning interval was 10 minutes.

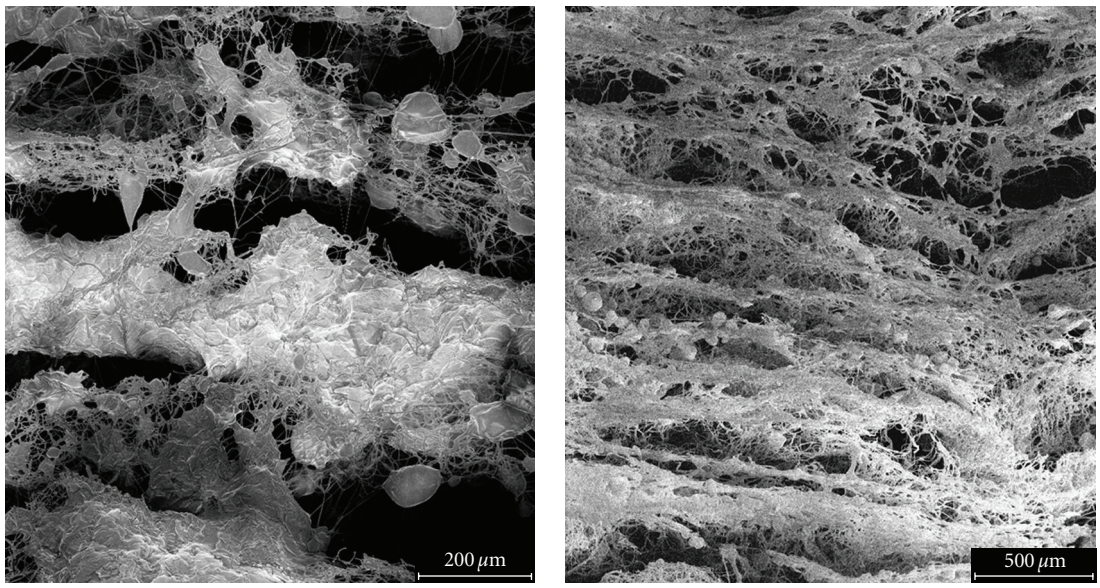

(a) Sugar particles embedded in the PGA scaffold (b) Scaffold after leaching of sugar crystals

Figure 4: SEM images: cross-sectional view of electrospun tubes; the electrospinning interval was 2 minutes.

resulted in crystals that were less densely packed (Figures 4(a) and 5(a)). All samples demonstrated homogenous distribution of sucrose crystals.

PGA matrix architecture also demonstrated variability that correlated with interval times. Ten-minute time intervals produced thick, dense mesh layers of PGA fibers that were clearly discernible from the PGA-embedded sucrose layers (Figure 3(a)). In contrast, one- or two-minute intervals created a more integrated honeycomb-like structure of PGA and sucrose layers (Figures 4(a) and 5(a)). Two-minute intervals resulted in a coarser honeycomb structure, while the one-minute spinning time formed a more delicate network. Fine fibers of 2–5 μm in diameter appeared suspended in the lumen of most pores.

Leaching of the scaffolds completely dissolved the embedded sucrose, leaving macroporous PGA structures in all cases (Figures 3(b), 4(b), and 5(b)). Sucrose "pockets" lined with PGA fibers may be seen. The tubular structures were form-stable and did not collapse. However, macropore sizes after leaching were reduced approximately 5–10%. Of note, sucrose particles averaged 250 to 350 μm (Figure 1), whereas average macropore diameter ranged between 50 to

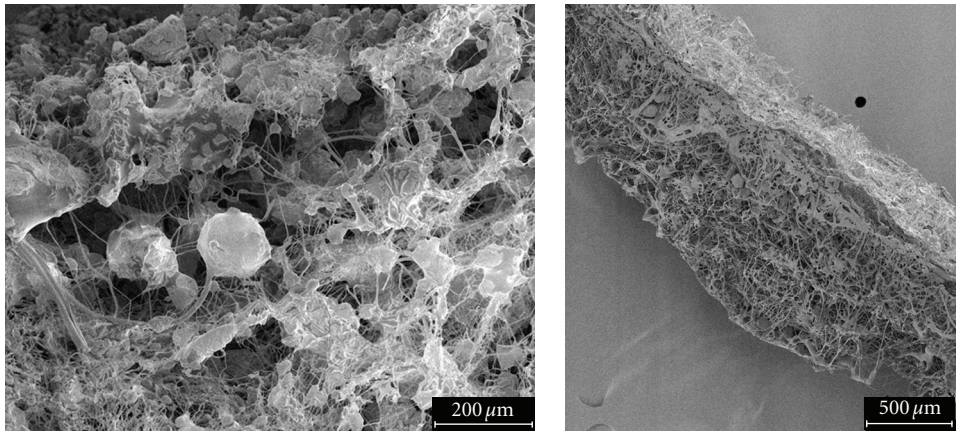

(a) Sugar particles embedded in the PGA scaffold (b) Scaffold after leaching of sugar crystals

Figure 5: SEM images: Cross-sectional view of electrospun tubes; the electrospinning interval was 1 minute.

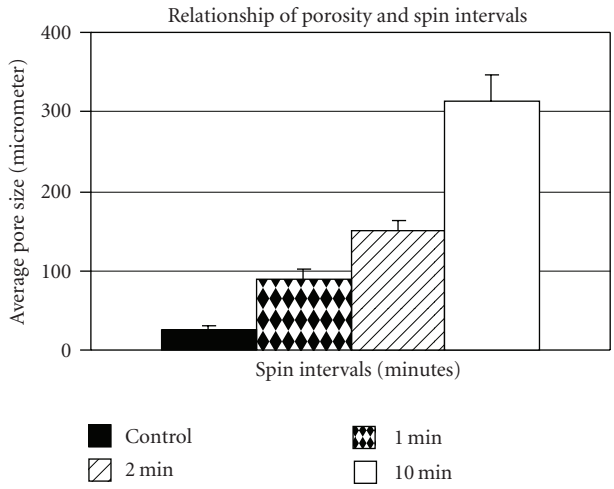

Figure 6: Relationship between porosity and spin intervals.

350 μm. Ten-minute intervals left alternating layers of void space and dense PGA mesh layers. Rare communication between macropores and periodic layer delamination was noted in the ten-minute interval scaffolds (Figure 3(b)). One- and two-minute time intervals revealed honeycomb-like structures after sucrose leaching. The PGA fiber pockets were seen to communicate through defects in the PGA mesh layers, thus creating macroporous interconnections (Figures 4(b) and 5(b)).

Interconnection of macropores in the one- and two-minute spun scaffolds was confirmed by our cell penetration assay (Figure 7).

After cell seeding, fibroblasts attached to the interior of the material. Nuclear staining with DAPI indicated that seeded cells were located on and within the electrospun scaffolds. Penetration into the deeper layers of the mesh was variable. Despite exhibiting larger macropores, ten-minute interval scaffolds (Figures 7(c) and 7(d)) and control scaffolds (Figures 7(a) and 7(b)) had cells attached to the surface with only minimal cell penetration into the matrix. Although the ten-minute scaffolds showed slightly more cell penetration than the control matrix, the denser PGA fibers surrounding the large macropores appeared to create a barrier that prevented the cells from reaching the deeper structures of the scaffold. More pronounced cell penetration occurred in one-minute scaffolds. The deepest penetration (to about 250 μm) was found in two-minute scaffolds (Figures 7(e) and 7(f)). In all samples with cell penetration, cells within the scaffolds appeared to be distributed along the fibers lining the "walls" of the pores. Data representing a synopsis of these results are shown in Table 1.

Table 1: Penetration scores for five randomly selected sections from each study group.

	Control	10 minutes	2 minutes	1 minute
Section 1	0	+	++	++
Section 2	+	+	++	++
Section 3	0	++	++	+
Section 4	+	+	+	+++
Section 5	O	+	+++	+

(0 denotes no penetration; +++ denotes deep penetration).

4. Discussion

The combination of electrospinning sucrose particles and poly(glycolic acid) represents a hybrid method that incorporates particulate leaching to create a nonwoven scaffold with uniform fiber diameter, macropores, and interconnected pores of fixed size. With the traditional method of simple electrospinning, porosity is limited due to high scaffold density resulting from small fiber diameters. Cells seeded onto control samples without sucrose were unable to penetrate the scaffold surface and were not seen within the scaffold interior; the high fiber density and smaller pore sizes (10 μm) inhibited cell penetration. In contrast, with our hybrid technique of electrospinning and particulate leaching

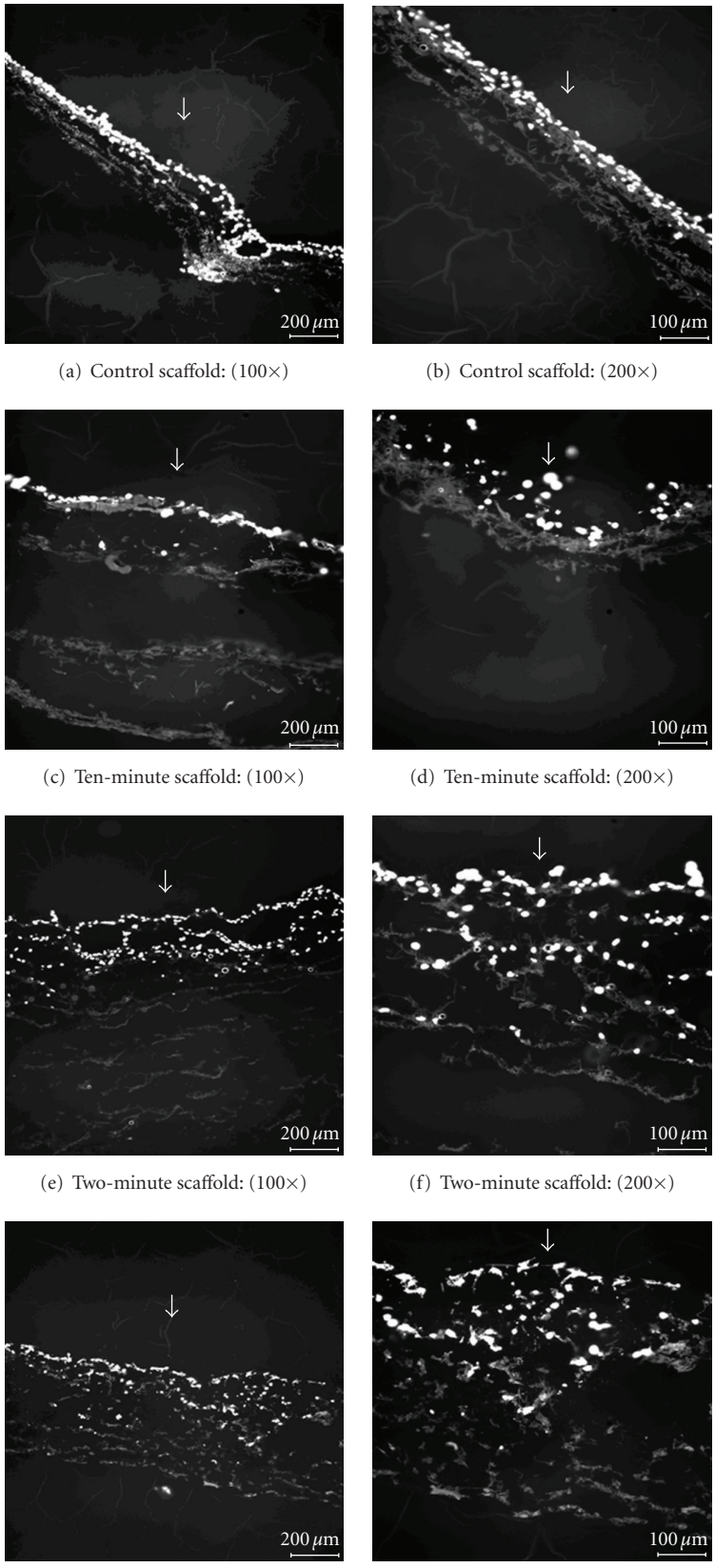

(a) Control scaffold: (100×)
(b) Control scaffold: (200×)
(c) Ten-minute scaffold: (100×)
(d) Ten-minute scaffold: (200×)
(e) Two-minute scaffold: (100×)
(f) Two-minute scaffold: (200×)
(g) One-minute scaffold: (100×)
(h) One-minute scaffold: (200×)

Figure 7: Cryosections of seeded scaffolds with DAPI nuclear stained cells at 24 hours. White arrows point towards the scaffold seeding surface.

we were able to fabricate a matrix with fiber diameters of 1–5 μm and a larger pore structure in the range of 50–350 μm. In addition, we were able to control the pore distribution and interconnectedness by varying the duration of both sucrose-ethanol and polymer spinning times. The result was a homogenous distribution of pores throughout the architecture that was unaffected by the evaporation of the solvents.

Macropore size was dictated by porogen diameter and spinning times. Though the average size of sucrose crystals was 250–350 μm, pore sizes as small as 50 μm were found. This was likely due to the sifting process which included smaller sucrose crystals within the sucrose-ethanol solution. In future studies, ultrasonic size sorting could be employed to more accurately separate out porogens of a desired size.

Spinning time was the fundamental variable in the creation of macroporous scaffolds. The upper and lower time limits of electrospinning during which the production of a form-stable, porous scaffolds may be fabricated were one and ten minutes, respectively. With shorter electrospinning times of one or two minutes, scaffolds suitable for cell infiltration and migration were generated with apparent honeycomb-like structures and interconnected pores of 50–250 μm. Conversely, with an electrospinning time interval of ten minutes, macroporous layers created by sucrose deposition alternated with denser layers of PGA fibers. Though the pore size was larger (200 to 350 μm) in these scaffolds due to increased sucrose deposition, the ten-minute time interval resulted in a laminated structure with decreased pore interconnection which limited cellular infiltration. In the manufacture of porous scaffolds, polymer and sucrose spinning times may be varied to determine macropore size and pore interconnectedness and to improve cellular penetration. In order to avoid laminated structures, future studies could involve co-spinning of the solutions using a double-spinneret technique. By cospinning PGA and sucrose solutions, a more uniform incorporation of sucrose particles within the fibers could potentially be obtained.

Other efforts to expand and control the pore sizes of electrospun scaffolds have been previously described [26–28]. Kidoaki et al. introduced a new multilayer electrospinning technique to create ordered structures of type I collagen, styrenated gelatin, and segmented polyurethane. By sequentially spinning different polymers, the authors engineered more complex, hierarchically designed scaffolds than could be made by simple electrospinning alone. By mixing PLLA and polyethylene glycol, Pantojas et al. could modify fiber morphology such that nanometric pores were created [29]. Zhu et al. utilized a novel rotating frame cylinder as a collection device, which resulted in varying porosity based on rotational speed [30]. Nam et al. introduced sodium chloride crystals with poly(E-caprolactone) (PCL) in the electrospinning process [26]. During fabrication, salt particles were deposited by gravity onto the electrospun PCL fibers. This resulted in a compact structure with multiple layers. The PCL scaffold structure described by these authors resembled our ten-minute interval sample, with dense polymer fiber layers alternating with void space. However, in contrast to our technique, their PCL scaffolds lacked a homogenous porous architecture. This difference may be attributable to our use of sucrose suspended in solution rather than the direct use of a dry crystalline powder.

Leong et al. utilized a cryogenic technique to incorporate ice crystals into a poly(D,L-lactide) electrospun scaffold [28]. By varying the humidity of the electrospinning environment, they attained pore sizes ranging from 900–5000 μm^2. However, they found cell infiltration into the scaffolds to be limited to 50 μm. In our study cell penetration was variable; however, cells were found up to 250 μm deep in the scaffold structure. This finding was in contrast to the results of Nam et al. As a consequence of using PCL, a polymer with significantly slower degradation kinetics, Nam's group could seed and culture cells on scaffolds for up to 3 weeks. This was significantly longer than our 24-hour incubation period. Consequently, they observed cell penetration and proliferation deep within the scaffold at 3000 to 6000 μm.

Though we successfully generated highly porous electrospun scaffolds, our study had several limitations. There is not a definitive explanation for the correlation between electrospinning time and pore size. We demonstrated that pore sizes ranged from 50 to 150 μm, 100 to 250 μm, and 200 to 350 μm in diameter with increasing spinning times. Most likely, increased sucrose deposition occurred with longer time intervals. In order to generate larger pores, crystal deposition would necessarily occur in areas immediately adjacent to one another, yet jet instability within the Taylor cone would dictate a more random distribution. Regardless, it has been noted that deposition of particles larger than 150 μm may result in clustering [26]. As we utilized sucrose crystals 250–300 μm in diameter, it is likely that clustered deposition occurred. Additional investigation utilizing different particle sizes is warranted to elucidate the relationship between electrospinning time, particle deposition, and pore size.

PGA is a linear aliphatic polyester with a high degree of crystallization (45–55%) which renders it insoluble in most organic solvents; exposure to ethanol during scaffold production does not cause any structural changes [31]. In addition, wetting during cellular seeding does not induce any scaffold shrinkage. However, as may be seen in our SEM images (Figures 2(a), 3(a), and 4(a)) the sucrose-laden scaffolds appear to have several areas of "fused" PGA fibers or a "beads-on-a-string" appearance. This architecture may be the result of using a PGA solution with insufficient viscosity. As Kumbar et al. have demonstrated, decreasing polymer concentration, which implies decreased viscosity, may result in breaking down of the jet formed in the electrospinning process. The result would be an electrospray of microdroplets rather than fibers [32]. Though the areas of beading were minimal, future studies warrant investigation into increased concentrations of PGA solutions.

Another limitation of our study lay in our histologic assessment of cell penetration. Our method of assigning penetration scores was necessarily subjective, without absolute depth criteria. This was a consequence of the heterogeneity of scaffold thickness, and we felt that absolute measurements would have been misleading. In addition, our method of

gravity-seeding may have limited cell adhesion and subsequent proliferation. Additional investigations of cell behavior on and in our scaffolds may be performed using new seeding methods, such as agitation [33], dynamic mixing [34], perfusion flow-seeding [35], or filtration seeding [36].

In our study, we investigated three electrospinning conditions to create porous scaffolds: (a) one minute of PGA spinning followed by one minute of sucrose spinning, (b) two minutes of PGA spinning followed by two minutes of sucrose spinning, and (c) ten minutes of PGA spinning followed by ten minutes of sucrose spinning. In each case, time intervals were kept constant throughout the entire sequence, with a 1 : 1 ratio of PGA and sugar spinning times. Further studies that focus on varying PGA or sugar solution spin times could be investigated. As discussed above, the ten-minute interval resulted in larger macropores, but reduced interconnectedness. Thus in order to increase pore size as well as interconnectedness, the ratio of PGA to sugar spinning times could be extended to a ratio of 1 : 2 or 1 : 3 in order to create a more honeycomb-like structure rather than a laminated structure.

5. Conclusion

We have identified a simple technique of sequential, alternating electrospinning of PGA and sucrose solutions. This method results in fine PGA fiber scaffolds with pores of 50–350 μm. Pore size can be controlled by varying the time intervals for each spinning sequence. Combination electrospinning represents an excellent modality to generate designer scaffolds with controllable pore sizes that promote cell attachment and penetration. Further studies will be needed to further refine this method.

Acknowledgments

The authors express their deepest thanks to Sergey V. Prikhodko, PhD, their SEM specialist, for his superb technical help as well as to Xu Yuhuan, PhD, and Min Lee, PhD, for their expert advice on electrospinning methods.

References

[1] R. Langer and J. P. Vacanti, "Tissue engineering," *Science*, vol. 260, no. 5110, pp. 920–926, 1993.

[2] T. C. Grikscheit and J. P. Vacanti, "The history and current status of tissue engineering: the future of pediatric surgery," *Journal of Pediatric Surgery*, vol. 37, no. 3, pp. 277–288, 2002.

[3] D. W. Hutmacher, "Scaffold design and fabrication technologies for engineering tissues—state of the art and future perspectives," *Journal of Biomaterials Science, Polymer Edition*, vol. 12, no. 1, pp. 107–124, 2001.

[4] B. Sharma and J. H. Elisseeff, "Engineering structurally organized cartilage and bone tissues," *Annals of Biomedical Engineering*, vol. 32, no. 1, pp. 148–159, 2004.

[5] F. Rosso, G. Marino, A. Giordano, M. Barbarisi, D. Parmeggiani, and A. Barbarisi, "Smart materials as scaffolds for tissue engineering," *Journal of Cellular Physiology*, vol. 203, no. 3, pp. 465–470, 2005.

[6] W. J. Li, K. G. Danielson, P. G. Alexander, and R. S. Tuan, "Biological response of chondrocytes cultured in three-dimensional nanofibrous poly(epsilon-caprolactone) scaffolds," *Journal of Biomedical Materials Research A*, vol. 67, no. 4, pp. 1105–1114, 2003.

[7] W. J. Li, C. T. Laurencin, E. J. Caterson, R. S. Tuan, and F. K. Ko, "Electrospun nanofibrous structure: a novel scaffold for tissue engineering," *Journal of Biomedical Materials Research*, vol. 60, no. 4, pp. 613–621, 2002.

[8] N. Ashammakhi and P. Rokkanen, "Absorbable polyglycolide devices in trauma and bone surgery," *Biomaterials*, vol. 18, no. 1, pp. 3–9, 1997.

[9] D. Liang, B. S. Hsiao, and B. Chu, "Functional electrospun nanofibrous scaffolds for biomedical applications," *Advanced Drug Delivery Reviews*, vol. 59, no. 14, pp. 1392–1412, 2007.

[10] S. Y. Chew, Y. Wen, Y. Dzenis, and K. W. Leong, "The role of electrospinning in the emerging field of nanomedicine," *Current Pharmaceutical Design*, vol. 12, no. 36, pp. 4751–4770, 2006.

[11] R. C. Thomson, M. J. Yaszemski, J. M. Powers, and A. G. Mikos, "Hydroxyapatite fiber reinforced poly(α-hydroxy ester) foams for bone regeneration," *Biomaterials*, vol. 19, no. 21, pp. 1935–1943, 1998.

[12] P. X. Ma and R. Zhang, "Synthetic nano-scale fibrous extracellular matrix," *Journal of Biomedical Materials Research*, vol. 46, no. 1, pp. 60–72, 1999.

[13] R. Zhang and P. X. Ma, "Poly(α-hydroxyl acids)/hydroxyapatite porous composites for bone- tissue engineering. I. Preparation and morphology," *Journal of Biomedical Materials Research*, vol. 44, no. 4, pp. 446–455, 1999.

[14] D. W. Hutmacher, "Scaffolds in tissue engineering bone and cartilage," *Biomaterials*, vol. 21, no. 24, pp. 2529–2543, 2000.

[15] M. H. Sheridan, L. D. Shea, M. C. Peters, and D. J. Mooney, "Bioabsorbable polymer scaffolds for tissue engineering capable of sustained growth factor delivery," *Journal of Controlled Release*, vol. 64, no. 1–3, pp. 91–102, 2000.

[16] L. Singh, V. Kumar, and B. D. Ratner, "Generation of porous microcellular 85/15 poly (DL-lactide-co-glycolide) foams for biomedical applications," *Biomaterials*, vol. 25, no. 13, pp. 2611–2617, 2004.

[17] Y. Kuboki, Q. Jin, and H. Takita, "Geometry of carriers controlling phenotypic expression in BMP-induced osteogenesis and chondrogenesis," *Journal of Bone and Joint Surgery. America*, vol. 83, supplement 1, part 2, pp. S105–115, 2001.

[18] I. C. Um, D. Fang, B. S. Hsiao, A. Okamoto, and B. Chu, "Electro-spinning and electro-blowing of hyaluronic acid," *Biomacromolecules*, vol. 5, no. 4, pp. 1428–1436, 2004.

[19] G. I. Taylor, "Electrically driven jets," *Proceedings of the Royal Society of London*, vol. 313, pp. 453–475, 1969.

[20] C. P. Barnes, S. A. Sell, E. D. Boland, D. G. Simpson, and G. L. Bowlin, "Nanofiber technology: designing the next generation of tissue engineering scaffolds," *Advanced Drug Delivery Reviews*, vol. 59, no. 14, pp. 1413–1433, 2007.

[21] Q. P. Pham, U. Sharma, and A. G. Mikos, "Electrospinning of polymeric nanofibers for tissue engineering applications: a review," *Tissue Engineering*, vol. 12, no. 5, pp. 1197–1211, 2006.

[22] S. V. Fridrikh, J. H. Yu, M. P. Brenner, and G. C. Rutledge, "Controlling the fiber diameter during electrospinning," *Physical Review Letters*, vol. 90, no. 14, Article ID 144502, 4 pages, 2003.

[23] S. G. Kumbar, R. James, S. P. Nukavarapu, and C. T. Laurencin, "Electrospun nanofiber scaffolds: engineering soft tissues," *Biomedical Materials*, vol. 3, no. 3, Article ID 034002, 2008.

[24] S. J. Eichhorn and W. W. Sampson, "Statistical geometry of pores and statistics of porous nanofibrous assemblies," *Journal of the Royal Society Interface*, vol. 2, no. 4, pp. 309–318, 2005.
[25] I. K. Kwon, S. Kidoaki, and T. Matsuda, "Electrospun nano- to microfiber fabrics made of biodegradable copolyesters: structural characteristics, mechanical properties and cell adhesion potential," *Biomaterials*, vol. 26, no. 18, pp. 3929–3939, 2005.
[26] J. Nam, Y. Huang, S. Agarwal, and J. Lannutti, "Improved cellular infiltration in electrospun fiber via engineered porosity," *Tissue Engineering*, vol. 13, no. 9, pp. 2249–2257, 2007.
[27] S. Kidoaki, I. K. Kwon, and T. Matsuda, "Mesoscopic spatial designs of nano- and microfiber meshes for tissue-engineering matrix and scaffold based on newly devised multilayering and mixing electrospinning techniques," *Biomaterials*, vol. 26, no. 1, pp. 37–46, 2005.
[28] M. F. Leong, M. Z. Rasheed, T. C. Lim, and K. S. Chian, "In vitro cell infiltration and in vivo cell infiltration and vascularization in a fibrous, highly porous poly(D,L-lactide) scaffold fabricated by cryogenic electrospinning technique," *Journal of Biomedical Materials Research*, vol. 91, no. 1, pp. 231–240, 2008.
[29] V. M. Pantojas, E. Velez, D. Hernandez, and W. Otano, "Initial study on fibers and coatings for the fabrication of bioscaffolds," *Puerto Rico Health Sciences Journal*, vol. 28, no. 3, pp. 258–265, 2009.
[30] X. Zhu, W. Cui, X. Li, and Y. Jin, "Electrospun fibrous mats with high porosity as potential scaffolds for skin tissue engineering," *Biomacromolecules*, vol. 9, no. 7, pp. 1795–1801, 2008.
[31] J. C. Middleton and A. J. Tipton, "Synthetic biodegradable polymers as orthopedic devices," *Biomaterials*, vol. 21, no. 23, pp. 2335–2346, 2000.
[32] S. G. Kumbar, S. Bhattacharyya, S. Sethuraman, and C. T. Laurencin, "A preliminary report on a novel electrospray technique for nanoparticle based biomedical implants coating: precision electrospraying," *Journal of Biomedical Materials Research B*, vol. 81, no. 1, pp. 91–103, 2007.
[33] K. J. L. Burg, W. D. Holder Jr., C. R. Culberson, et al., "Comparative study of seeding methods for three-dimensional polymeric scaffolds," *Journal of Biomedical Materials Research*, vol. 51, no. 4, pp. 642–649, 2000.
[34] G. Vunjak-Novakovic, B. Obradovic, I. Martin, P. M. Bursac, R. Langer, and L. E. Freed, "Dynamic cell seeding of polymer scaffolds for cartilage tissue engineering," *Biotechnology Progress*, vol. 14, no. 2, pp. 193–202, 1998.
[35] S. S. Kim, C. A. Sundback, S. Kaihara, et al., "Dynamic seeding and in vitro culture of hepatocytes in a flow perfusion system," *Tissue Engineering*, vol. 6, no. 1, pp. 39–44, 2000.
[36] Y. Li, T. Ma, D. A. Kniss, L. C. Lasky, and S. T. Yang, "Effects of filtration seeding on cell density, spatial distribution, and proliferation in nonwoven fibrous matrices," *Biotechnology Progress*, vol. 17, no. 5, pp. 935–944, 2001.

Hindawi Publishing Corporation
International Journal of Polymer Science
Volume 2010, Article ID 807935, 8 pages
doi:10.1155/2010/807935

Research Article

Hyaluronan Immobilized Polyurethane as a Blood Contacting Material

Feirong Gong, Yue Lu, Hui Guo, Shujun Cheng, and Yun Gao

Key Laboratory for Ultrafine Materials of Ministry of Education, School of Materials Science and Engineering, East China University of Science and Technology, Shanghai 200237, China

Correspondence should be addressed to Shujun Cheng, chshj2003@yahoo.cn

Received 1 March 2010; Accepted 16 March 2010

Academic Editor: Shanfeng Wang

Hyaluronan (hyaluronic acid, HA) was immobilized onto the surface of amino-functionalized polyurethane films with the goal of obtaining a novel kind of biomaterial which had the potential in blood-contacting applications. The amino-functionalized polyurethane was prepared by synthesized acidic polyurethane whose pendant carboxyl groups were treated with an excess amount of 1,3-diaminopropane in the presence of N,N-carbonyldiimidazole (CDI). Attenuated total reflection Fourier transform infrared spectroscopy (ATR-FTIR), Raman spectroscopy (RS), scanning electron microscopy (SEM), and water contact angle measurement were used to confirm the surface changes at each step of treatment, both in morphologies and chemical compositions. APTT and PT results showed that HA immobilization could prolong the blood coagulation time, thus HA-immobilized polyurethane (PU-HA) exhibited improved blood compatibility. Cytotoxicity analysis showed that the PU-HA films synthesized in this study were cytocompatible and could support human vein endothelial cells (HUVECs) adhesion and proliferation.

1. Introduction

Thermoplastic polyurethanes (PU) have been widely used for various biomedical applications due to their excellent mechanical properties and proper blood compatibility. Recently, much effort has been focused on polyurethanes as blood-contacting materials, such as cardiovascular biomaterials, hemodialysis blood line sets, central venous catheters (CVC), and IV bags [1, 2]. However, surface-induced thrombosis, protein fouling, and cytocompatibility have become the major drawbacks that hinder their further biomedical applications as blood-contacting materials. Surface modification is an effective approach to improve the blood compatibility, the size, shape, and mechanical properties of the original material maintained. Many studies have been performed on producing a blood-compatible surface by tailoring with poly(ethylene glycol) (PEG) [3, 4], heparin [5, 6], heparin-like [7–9], phospholipid polymer [10–13], hirudin [14], sulfobetaine [15, 16], and so on. Although many hydrogels or hydrophilized surfaces exhibit good blood compatibility, most of these are not truly antithrombogenic but only antithromboadhesive [17] as they curtail or inhibit platelets and blood cell adhesion rather than prolong the coagulation time.

Hyaluronan (HA), a linear biopolymer naturally abundant in mammalian tissues, is composed of repeating units of N-acetyl-D-glucosamine and D-glucuronic acid, linked by β-(1,4) and β-(1,3) glycosidic junctions [18]. HA has been identified as a nontoxic, biodegradable, biocompatible, and nonimmunogenic material, and its degradation products of hyaluronicdase digestion are non-toxic oligomeric sugars that are mitogenic for endothelial cells in vitro and are correlated with blood vessel growth in vitro and in vivo [19–21]. Thus, HA has been widely used in biomedical applications such as scaffolds for wound healing, ophthalmic surgery, arthritis treatment, drug delivery, and implantation [22–25].

In this paper, HA-immobilized polyurethane was synthesized and characterized. The main purpose of this study was to improve the blood compatibility of the PU films by surface immobilization of HA. The coagulation time and the culture of human vein endothelial cells (HUVEC) in vitro were used to evaluate the blood compatibility and cytotoxicity, respectively.

2. Materials and Methods

2.1. Materials. 1, 6-hexane diisocyanate (HDI) was purchased from Bayer with purity greater than 99.5%. Polycarbonate diols (PCDL) with a number average molecular weight of 2000 g·mol^{-1} was kindly provided by Asahi Kasei Corporation and dried in vacuum at 50°C for 24 hours prior to use. 2,2-bis(hydroxymethyl) propionic acid (bis-MPA) was purchased from Acros and used as received. Dimethylformamide (DMF) and tetrahydrofuran (THF) were refluxed over calcium hydride (CaH_2) for three days and distilled before use. 1,3-diaminepropane and 1-Ethyl-3-[3-(dimethylaminopropyl)] carbodiimide hydrochloride (EDC·HCl), and N,N-carbonyldiimidazole (CDI) were purchased from GL Biochem Ltd. (Shanghai, China) and used as received. Hyaluronan sodium salt (HA) with different molecular weights ($M_w = 10 \times 10^3$ and 40×10^3) was purchased from Shanghai Trustin Chemical Co., Ltd (China). Other reagents were commercially available and used as received.

2.2. Preparations of the PU Base Polymer. The acidic polyurethane used in this study was synthesized by the traditional two-step method under nitrogen protection. In an oven-dried four-neck flask equipped with a stir bar, reflux condenser, and nitrogen on command, 0.63 g (3.75 mmol) of HDI and three drops of dibutyltin dilaurate (DBTDL) were dissolved in 10 mL of DMF and maintained at 80°C with continuous stirring. 5 g (2.5 mmol) of PCDL dissolved in 20 mL of DMF was added dropwise to the reactor. The prepolymer synthesis was continued until the isocyanate (NCO) content reached the theoretical value determined by dibutyl amine titration. A 10 mL solution of chain extender bis-MPA (0.1675 g, 1.25 mmol) in DMF was added to the prepolymer solution and was stirred at 80°C to allow the chain extending reaction to take place. The mixture was stirred until the NCO peak at 2270 cm^{-1} in the IR spectrum disappeared. A small amount of methanol was added to the solution to quench the reaction. Subsequently, the polymer solution was poured into a large amount of water and the precipitate was collected after dried in vacuum at 50°C for 24 hours. The obtained polymer was then re-dissolved in dichloromethane and the solution was centrifuged at 13,000 rpm for 10 minutes to remove the heavy metal catalyst. Finally, the polymer solution was poured into a large amount of chilled methanol and the precipitate was collected.

2.3. Preparation of Amino-Functionalized Polyurethane (PU-NH_2). PU (2 g, n[COOH] = 0.5 mmol, determined by titration) and CDI (0.405 g, 2.5 mmol) were dissolved in 100 mL of THF and stirred at room temperature for 12 hours to activate the pendant carboxyl groups of the polymer. Then 0.185 g (2.5 mmol) of 1,3-diaminepropane dissolved in 10 mL of THF was added slowly within 0.5 hour. The mixture was allowed to stir at room temperature for additional 12 hours. Once the reaction was completed, the catalyst was filtered off and the solution was centrifuged at 13,000 rpm for 10 minutes, and finally precipitated into excess methanol. This process was repeated again to remove any residue of unreacted CDI. After dried in vacuum at room temperature for 24 hours, PU-NH_2 was obtained as a white solid.

2.4. Preparation of PU-NH_2 Films and Surface Immobilization of HA. The PU-NH_2 films were prepared via the solution casting method. A PU-NH_2 solution (10%, w/v) was prepared by dissolving the polymer into a glass container having tetrahydrofuran (THF) as solvent. The mixture was stirred continually at room temperature until a homogeneous solution was formed. Then, the solution was poured into leveled 5 mm PTFE casting plates and cast into films at room temperature for 24 hours. The films were removed from the casting plates and dried in a vacuum oven at 60°C for 12 hours to remove residual solvent. Each film was then cut into 2 cm × 2 cm and the average thickness of the film was about 100 μm.

Sodium citrate (22 g) was dissolved in distilled water (1000 mL) and the pH of this solution was adjusted to 4.75 by adding 0.1 M HCl solution. 1-Ethyl-3-[3- (dimethylamidopropyl)] carbodiimide·HCL (EDC·HCL, 10 mg) was then dissolved in the pH-adjusted solution (10 mL) to produce a 0.1 wt% EDC aqueous solution. A certain amount of HA was dissolved in the EDC solution to activate the carboxylic acid groups of HA with gentle stirring. Several pieces of PU-NH_2 films (2 cm × 2 cm) were immersed into the above solution for surface immobilization of HA. The immobilization reaction was carried out for 12 hours with gentle stirring. The molar ratio of EDC : HA was fixed as 4 : 1. After the immobilization reaction, the films were washed with PBS solutions five times and subsequently rinsed with distilled water in an ultrasonic cleaner for 5 minutes and finally vacuum dried. The HA immobilized PU were named as PU-HA_1 and PU-HA_4, in which the number indicate that the molecular weight of HA used in the reaction was 10×10^3 and 40×10^3, respectively.

2.5. Spectral Analysis. The ATR-FTIR spectra of the modified PU films were obtained using MAGNA spectrophotometer (Thermo Nicolet, MA, USA) equipped with a ZnSe reflection element. Raman spectra were measured on an inVia+Reflex dispersive Raman spectrometer equipped with a 785 nm laser. FT-IR measurements were performed on a Nicolet 5700 FTIR spectrophotometer.

2.6. Contact Angle Measurements and Equilibrium Water Content. The water contact angles of the modified and unmodified films were measured using a Ramhart 100 goniometry. For each film, the measurements were repeated in three different areas and at least 10 times for the same area. Finally, the average values were informed.

The equilibrium water content of samples and the effect of ionic strength on the equilibrium swelling ratio were determined according to the methods [26] with slight modification. Three quotients of dried polymer films (2 × 2 cm^2) were respectively immersed into phosphate buffered saline (PBS, pH = 7.4) and distilled water at 37°C for

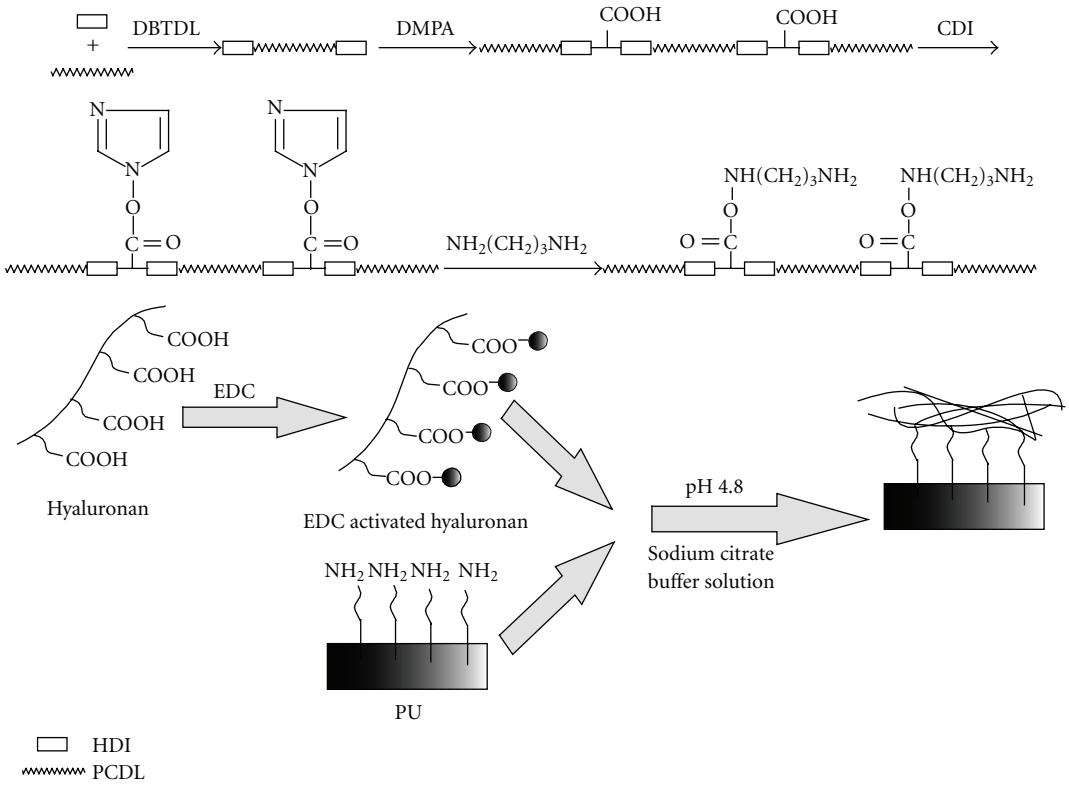

Figure 1: Synthesis of HA-immobilized PU films.

1, 2, 4, 12, 24, and 48 hours. At each time point, the samples were removed and blotted lightly with filter paper to remove excess water. The weight of the hydrated samples was then determined and the water adsorption was calculated.

2.7. Scanning Electron Microscope (SEM) Characterization. The surface morphologies of modified and unmodified surfaces of PU films were characterized by a scanning electron microscope (SEM, JSM-6360LV, JOEL). The samples were coated with a sputtered Au coating in order to prevent charge effects during the observations.

2.8. Coagulation Assays. Coagulation assays were performed to evaluate material-induced abnormalities in the intrinsic and extrinsic coagulation pathways. The end point for these assays was the duration for the onset of fibrin (clot) formation when platelet-poor plasma (PPP) was contacted with the test and control substrates. To obtain PPP, the human whole blood, which was treated with citric acid, was centrifuged at 3000 rpm for 15 minutes to separate the blood corpuscles. Activated partial thromboplastin time (APTT) and prothrombin time (PT) were used in this report.

APTT is a simple and highly reliable measurement of the capacity of blood to coagulate through the intrinsic coagulation mechanism and the effect of the biomaterial on possible delay of the process. The obtained PPP (0.1 mL), predetermined amounts of test samples and cephalin (0.1 mL; Actin, Sigma) were placed in a test tube kept at 37°C, followed by the addition of 0.025 M $CaCl_2$ solution (0.1 mL) after 5 minutes incubation. The plasma solution was monitored for clotting by manually dipping a stainless-steel wire hook coated with silicon into the solution to detect fibrin threads. Clotting times were recorded at the first signs of any fibrin formation on the hook. The experiment was repeated in quadruplicate and a mean value was calculated. PT was measured to assess HA-induced deferment or interdiction of extrinsic coagulation pathway. Platelet-poor plasma (0.1 mL) was layered atop the sample at 37°C, and supplemented with 0.9% NaCl-thromboplastin (Factor III, 0.1 mL Sigma) containing Ca^{2+} was added to the PPP. The clotting time of the plasma solution was observed as described in the APTT experiment. The experiment was repeated in quadruplicate and a mean value was calculated.

2.9. Cell Responses. Cell attachment and proliferation were evaluated by seeding human vein endothelial cells (HUVEC) (1×10^5 cells/mL) on the polymer films in the medium (Dulbecco's modified Eagle's medium, DMEM, Gibco) supplemented with 10% fetal bovine serum (FBS, Gibco) in 12-well tissue culture plates. Next, 3 mL of medium was added to the wells and mixed with the cells. The cells were then cultured in a humidified incubator equilibrated with 5% CO_2-95% air for 7 days. The cells attached onto the polymer surfaces were observed using a phase contrast microscope. The viability of cells was quantitatively measured by the MTT assay. Their counterparts with incubation with PU were used as a control.

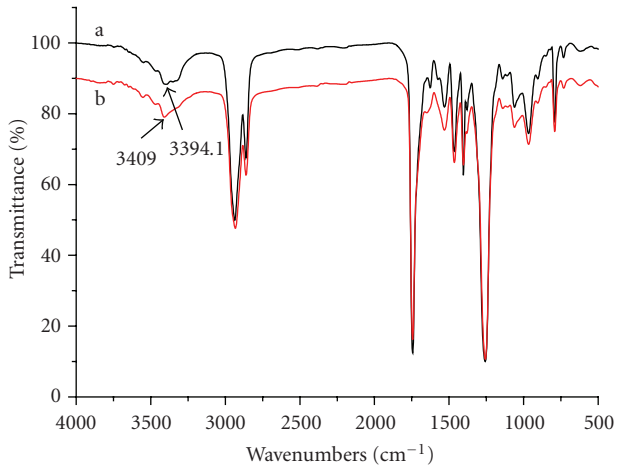

Figure 2: FT-IR spectra of PU (a) and PU-NH_2 (b).

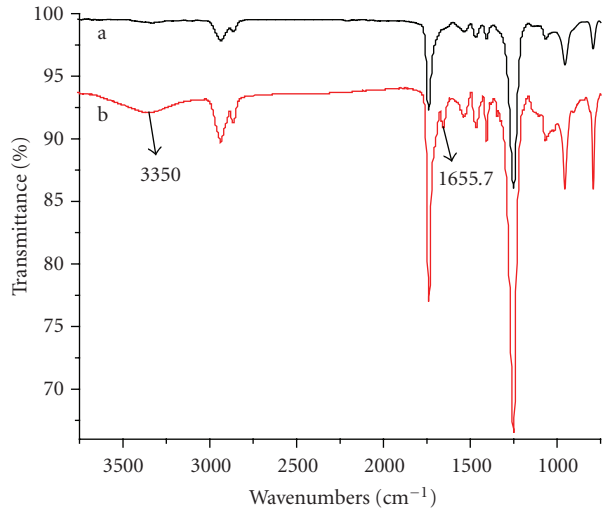

Figure 3: ATR-FTIR spectra of PU-NH_2 (a) and PU-HA films (b).

2.10. Statistical Analysis. Comparison between two groups was analyzed by the one-tailed Student's t-test using statistical software (SPSS). Data is presented as mean ± SD. A difference of $P < .05$ was considered statistically significant.

3. Results and Discussion

3.1. Synthesis. In this study, the PCDL soft segments were reacted with HDI to prepare the isocyanate terminated prepolymer, which further reacted with bis-MPA to form the base polyurethane with pendant carboxyl groups. The molar ratio of HDI : PCDL : bis-MPA was fixed as 3 : 2 : 1. In order to obtain HA-immobilized PU films, a water-soluble carbodiimide EDC is employed as cross-linking agent for its well known ability to link HA with amines. The cross-coupling reaction can be summarized as follows. EDC firstly reacts with carboxyl groups to form an unstable intermediate O-acylisourea, which, in the absence of nucleophiles, could be rearranged to be a stable N-acylurea via cyclic electronic displacement. In the presence of nucleophiles such as amines, the O-acylisourea formation is followed by a nucleophilic attack, forming an amide linkage between the amine and the acid. Moreover, the reaction of EDC with carboxyl groups is dependent on pH, and the optimal pH ranges from 4.0 to 5.0. Here, amine groups were introduced onto the PU chains by reacting with 1,3-diaminepropane. HA was then immobilized onto the surface of PU-NH_2 films by preactivating the carboxylic acid groups of HA with coupling agent EDC and they were subsequently reacted with the surface exposed free amine groups of the films. The purification of the products could be easily carried out by washing these films in PBS solutions several times and rinsing them with distilled water in an ultrasonic cleaner for 5 minutes. After that, noncovalently conjugated HA and urea byproduct can be removed. The synthetic route was illustrated in Figure 1.

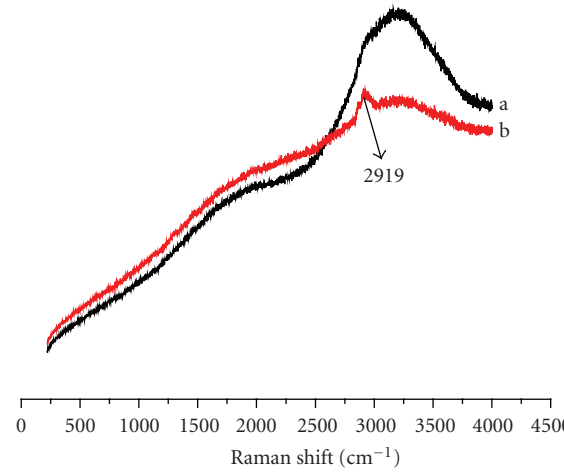

Figure 4: Raman spectra of PU-NH_2 (a) and PU-HA (b).

3.2. Spectral Analysis. To investigate the chemical structure, FT-IR, ATR-FTIR and Raman spectroscopy were performed on PU, PU-NH_2 and PU-HA. FT-IR spectra of PU (Figure 2) showed characteristic bands of urethane groups at 3394.4 cm^{-1} (N-H stretching), 1744 cm^{-1} (NHCOO stretching), and 1531 cm^{-1} (C-N stretching, combined with N-H stretching). All of these peaks provide convincing evidence for the formation of polyurethane. From a preliminary study of FT-IR, it was found that the spectra of PU-NH_2 were almost the same as that of the PU control. This is because the absorption based on the amide (N-H) of the amino groups in PU-NH_2 was overlapped by the amide bond in PU itself. A slight shift from 3394.4 cm^{-1} to 3409 cm^{-1} was observed, which was mainly caused by the formation of amino groups on PU chains. The existence of amino groups on PU films was further confirmed by ninhydrin as the film could display purple when amino reacted with ninhydrin at 80°C for 10 minutes.

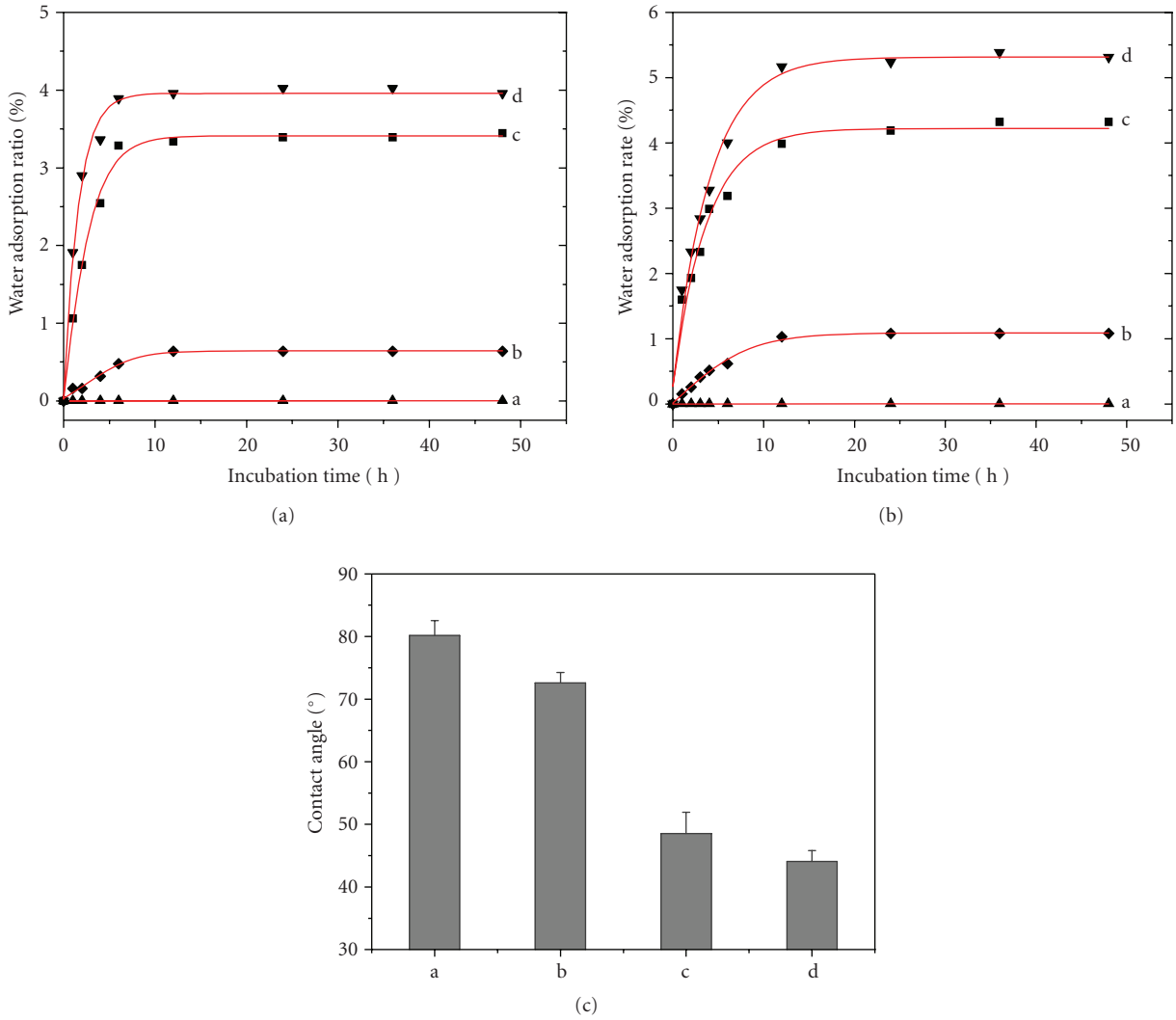

Figure 5: Water absorption of different PU films; a: PU, b: PU-NH_2, c: PU-HA_1, d: PU-HA_4 in PBS (a), deionized water (b), (c) contact angle results.

Figure 3 shows the ATR-FTIR spectra of PU surfaces immobilized with 1,3-diamine-propane (PU-NH_2) and HA (PU-HA). In the spectra of PU-HA, the peaks at 3350 cm^{-1} and 1657 cm^{-1} corresponding to the hydroxyl group (−OH) and the amide C=O stretching respectively, are related to the presence of HA. Raman spectroscopy (Figure 4) was also used to characterize the surface change before and after HA immobilization. A new peak was observed at 2919 cm^{-1} which was attributed to the hydroxyl group (−OH) stretching of alcohol chelate since the hydroxyl groups in HA could form a chelated structure.

3.3. Hydrophilicity. The water uptake for the samples in PBS (a) and deionized water (b) at 37°C as a function of time was shown in Figure 5. Water uptake was measured to determine the hydrophilicity of PU films before and after modification and this parameter was expected to have an important influence on cell responses. The chemical composition was the main factor controlling the amount of absorbed water. For PU almost no water could be absorbed into the polymer matrix within 48 hours. The hydrophilicity of PU-NH_2 was improved slightly due to the appearance of amino groups. A much more hydrophilic character, which increases as the molecular weight of HA increases, was observed when HA immobilized on the surface. This result was expected, given the highly hydrophilic nature of HA.

The water contact angle measurement of PU, PU-NH_2, and PU-HA was shown in Figure 5(c). The PU-NH_2 film showed a slight decrease in water contact angle of 72° in contrast to unmodified PU film (80°). This result is consistent with that of water uptake experiment. After immobilizing HA on PU-NH_2 surface, the water contact angle value further decreased, and decreased slightly with increasing the molecular weight of HA. The decrease of contact angle is an index of the chemical changes occurring on the film surfaces, which renders the surface more hydrophilic with respect to the virgin film. It was expected

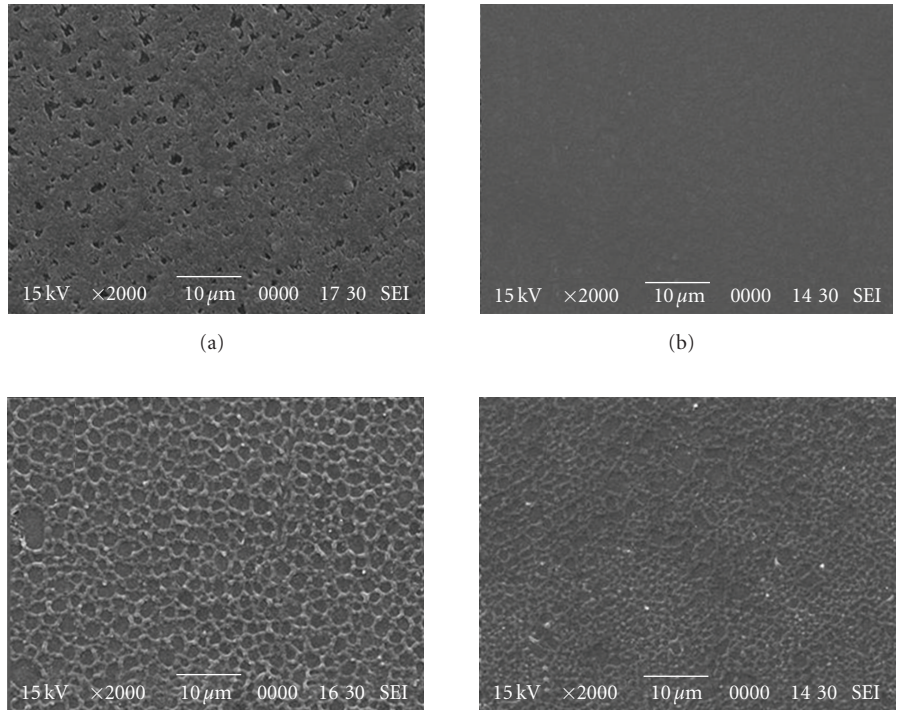

Figure 6: SEM images of the polymer surfaces made at 5000×. (a) PU shows a rough surface. (b) The surface of PU-NH_2 displays a relatively flat surface. (c) and (d) The surfaces of PU-HA_1 and PU-HA_4 show a semiporous structure.

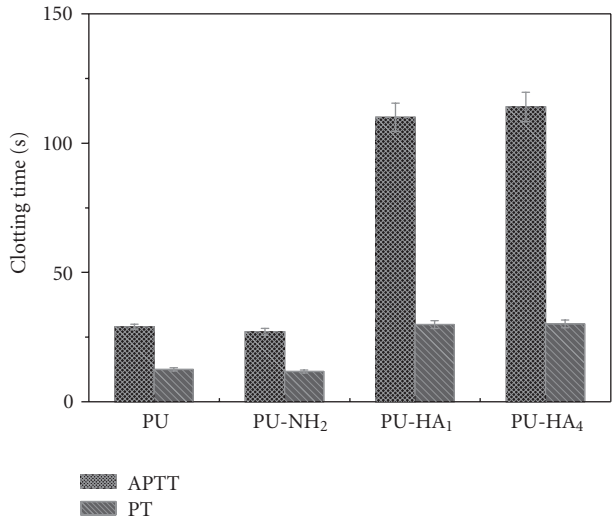

Figure 7: Comparison of anticoagulant properties of different films: APTT and PT ($n = 3$, mean ± S.D.).

that the higher hydrophilicity for PU-HA could be induced by a large amount of negatively charged carboxylic groups in HA backbone and rough surface with a large surface area.

3.4. Surface Morphology. SEM micrographs in Figure 6 illustrated the surface morphology changes of PU films before and after each step of treatment. As shown in Figure 6, the surface of PU base polymer was rough with irregular pores. After the first step of 1,3-diaminepropane conjugation, the polymer surface became relatively smooth, which could be interpreted by the improved compatibility of the hard and soft segments after extending the side chain. After the second step of immobilizing HA on the surface of PU-NH_2 film, a semi-porous structure was observed. The surface morphology certainly affected the related properties of the polymer including wettability, contact angle, and cell responses.

3.5. Coagulation Time. The blood coagulation system includes the intrinsic pathway, the extrinsic pathway, and the common pathway. APTT and PT are used to examine mainly the intrinsic and extrinsic pathway, respectively. Figure 7 shows the clotting time of modified and unmodified PU. PU-NH_2 shows essentially the same APTT and PT result as the native PU. The APTT and PT for PU, PU-NH_2, and PU-HA were 29s, 12.5s; 27s, 11.7s; 110s, 29.8s; 114s, 30.1s. HA-immobilized PU instead exhibits a strong increase in APTT and PT, thereby exerts an anti-coagulant effect. And the molecular weight of HA has little effect on the blood clotting time. The above results indicate that the anticoagulant activity of the PU films has been retained after HA immobilization. The prolonged APTT and PT of PU-HA films suggested that the coagulation mechanisms probably worked through two pathways: the intrinsic pathway and the extrinsic pathway.

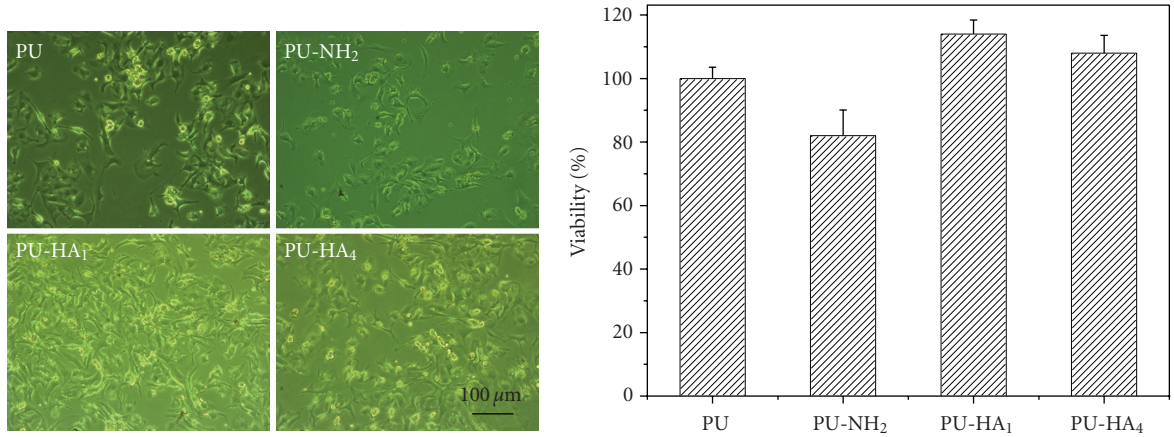

FIGURE 8: Phase contrast images of HUVECs attached on the surface of PU, PU-NH_2, PU-HA_1 and PU-HA_4 7 days postseeding. There is a significant difference ($P < .05$) between PU and PU-NH_2, PU-HA_1, PU-HA_2. No significant difference is between PU-HA_1 and PU-HA_2. The scale bar in the micrograph of PU-HA_4 stands for 100 μm and it is applicable for all micrographs in the panel.

3.6. Cell Attachment. Preliminary studies were performed to evaluate in vitro cell attachment and proliferation on the surfaces of the PU, PU-NH_2 and PU-HA films using HUVECs. Figure 8 shows the morphology of HUVECs adhered to and proliferated on the surface of these polymer films after 7 days post seeding. As shown in Figure 8, there are only a few cells that could adhere to and proliferate on the surface of PU. The number of attached HUVECs decreases while 1,3-diaminepropane was conjugated to PU probably due to the existence of amino groups which was known to be cytotoxic. In contrast, cells adhere to and proliferate better on PU-HA films. It was also found that the molecular weight of the conjugated HA has some influence on the attachment of the cells. There appeared to be fewer cells adherent on the PU-HA surface with higher molecular weight of HA. The cytotoxicity of the PU films before and after modification was qualitatively investigated by the MTT assay. The result indicated that the viability of cells incubated on the HA immobilized PU-NH_2 surface was significantly greater than that on the PU and PU-NH_2 ($P < .05$), suggesting that the HA immobilized PU in this study had a better cytocompatibility. No difference was found between PU-HA_1 and PU-HA_4.

There are many factors influence cell responses on biomaterials: mechanical property [27], electrical surface charge [28], hydrophilicity [29], and surface morphology [30], and so forth. Usually the cell response is a combination of all these different stimuli, so it is impossible to find a unique factor to explain these data. The obtained results can be explained as follows: (a) the difference of the cell number between PU and PU-NH_2 is mainly caused by the electrostatic factor since negatively charged surfaces show increase cells attachment; (b) cells prefer to adhere to PU-HA not only because of its rough surface and anionic surface charge, but also because HA is an extracellular matrix (ECM) component; (c) fewer cells adherent to PU-HA_4 with high molecular weight may be influenced by hydrophilicity.

4. Conclusions

In this paper, we have synthesized a novel kind of polyurethane with carboxyl groups at the side chain by two-step solution polymerization. In order to provide a convenient way to immobilize HA, free amino groups have been introduced into the PU base polymer. The variation of ATR-FTIR, RS, water contact angle and morphology showed that HA was successfully immobilized on the surface of PU. HA immobilization not only improved the hydrophilicity, but also greatly prolonged the coagulation time and improved the cell biocompatibility in comparison with base PU and PU-NH_2. Hence, it can be concluded that the HA immobilization is a promising way to enhance cell-material interaction, resulting in a blood-contacting material with high efficiency to accelerate the endothelium regeneration.

Acknowledgments

This paper was supported by the 863 Project of 2007AA02Z450 from the Ministry of Science and Technology of China. The authors thank Shanghai Aosi Biological Technology Service Co., Ltd. for the help in cell culture and coagulation time test.

References

[1] Y. Zhu, C. Gao, T. He, and J. Shen, "Endothelium regeneration on luminal surface of polyurethane vascular scaffold modified with diamine and covalently grafted with gelatin," *Biomaterials*, vol. 25, no. 3, pp. 423–430, 2004.

[2] D.-A. Wang, L.-X. Feng, J. Ji, Y.-H. Sun, X.-X. Zheng, and J. H. Elisseeff, "Novel human endothelial cell-engineered polyurethane biomaterials for cardiovascular biomedical applications," *Journal of Biomedical Materials Research A*, vol. 65, no. 4, pp. 498–510, 2003.

[3] H. W. Kim, C. W. Chung, and Y. H. Rhee, "UV-induced graft copolymerization of monoacrylate-poly(ethylene glycol) onto poly(3-hydroxyoctanoate) to reduce protein adsorption and platelet adhesion," *International Journal of Biological Macromolecules*, vol. 35, no. 1-2, pp. 47–53, 2005.

[4] B. Balakrishnan, D. S. Kumar, Y. Yoshida, and A. Jayakrishnan, "Chemical modification of poly(vinyl chloride) resin using poly(ethylene glycol) to improve blood compatibility," *Biomaterials*, vol. 26, no. 17, pp. 3495–3502, 2005.

[5] Y. J. Du, J. L. Brash, G. McClung, L. R. Berry, P. Klement, and A. K. C. Chan, "Protein adsorption on polyurethane catheters modified with a novel antithrombin-heparin covalent complex," *Journal of Biomedical Materials Research A*, vol. 80, no. 1, pp. 216–225, 2007.

[6] Q. Lu, S. Zhang, K. Hu, Q. Feng, C. Cao, and F. Cui, "Cytocompatibility and blood compatibility of multifunctional fibroin/collagen/heparin scaffolds," *Biomaterials*, vol. 28, no. 14, pp. 2306–2313, 2007.

[7] D. K. Han, N. Y. Lee, K. D. Park, Y. H. Kim, H. I. Cho, and B. G. Min, "Heparin-like anticoagulant activity of sulphonated poly(ethylene oxide) and sulphonated poly(ethylene oxide) grafted polyurethane," *Biomaterials*, vol. 16, no. 6, pp. 467–471, 1995.

[8] F. M. Kanmangne, D. Labarre, H. Serne, and M. Jozefowicz, "Heparin-like activity of insoluble sulphonated polystyrene resins. I. Influence of the surface density, nature and binding of substituted anionic groups," *Biomaterials*, vol. 6, no. 5, pp. 297–302, 1985.

[9] H. J. Lee, K. D. Park, H. D. Park, et al., "Platelet and bacterial repellence on sulfonated poly(ethylene glycol)-acrylate copolymer surfaces," *Colloids and Surfaces B*, vol. 18, no. 3-4, pp. 355–370, 2000.

[10] W. Feng, S. Zhu, K. Ishihara, and J. L. Brash, "Adsorption of fibrinogen and lysozyme on silicon grafted with poly(2-methacryloyloxyethyl phosphorylcholine) via surface-initiated atom transfer radical polymerization," *Langmuir*, vol. 21, no. 13, pp. 5980–5987, 2005.

[11] T. Nakaya and Y.-J. Li, "Phospholipid polymers," *Progress in Polymer Science*, vol. 24, no. 1, pp. 143–181, 1999.

[12] A. Korematsu, Y. Takemoto, T. Nakaya, and H. Inoue, "Synthesis, characterization and platelet adhesion of segmented polyurethanes grafted phospholipid analogous vinyl monomer on surface," *Biomaterials*, vol. 23, no. 1, pp. 263–271, 2002.

[13] J. Yuan, S. Lin, and J. Shen, "Enhanced blood compatibility of polyurethane functionalized with sulfobetaine," *Colloids and Surfaces B*, vol. 66, no. 1, pp. 90–95, 2008.

[14] T. Furuzono, K. Ishihara, N. Nakabayashi, and Y. Tamada, "Chemical modification of silk fibroin with 2-methacryloyloxyethyl phosphorylcholine. II. Graft-polymerization onto fabric through 2-methacryloyloxyethyl isocyanate and interaction between fabric and platelets," *Biomaterials*, vol. 21, no. 4, pp. 327–333, 2000.

[15] J.-C. Lin and S.-M. Tseng, "Surface characterization and platelet adhesion studies on polyethylene surface with hirudin immobilization," *Journal of Materials Science: Materials in Medicine*, vol. 12, no. 9, pp. 827–832, 2001.

[16] J. Yuan, L. Chen, X. Jiang, J. Shen, and S. Lin, "Chemical graft polymerization of sulfobetaine monomer on polyurethane surface for reduction in platelet adhesion," *Colloids and Surfaces B*, vol. 39, no. 1-2, pp. 87–94, 2004.

[17] B. D. Ratner, "Blood compatibility—a perspective," *Journal of Biomaterials Science, Polymer Edition*, vol. 11, no. 11, pp. 1107–1119, 2000.

[18] K. Surendrakumar, G. P. Martyn, E. C. M. Hodgers, M. Jansen, and J. A. Blair, "Sustained release of insulin from sodium hyaluronate based dry powder formulations after pulmonary delivery to beagle dogs," *Journal of Controlled Release*, vol. 91, no. 3, pp. 385–394, 2003.

[19] D. C. West, I. N. Hampson, F. Arnold, and S. Kumar, "Angiogenesis induced by degradation products of hyaluronic acid," *Science*, vol. 228, no. 4705, pp. 1324–1336, 1985.

[20] R. C. Savani, G. Cao, P. M. Pooler, A. Zaman, Z. Zhou, and H. M. DeLisser, "Differential involvement of the hyaluronan(HA) receptors CD44 and receptor for HA-mediated motility in endothelial cell function and angiogenesis," *Journal of Biological Chemistry*, vol. 276, no. 39, pp. 36770–36778, 2001.

[21] A. Sattar, P. Rooney, S. Kumar, et al., "Application of angiogenic oligosaccharides of hyaluronan increases blood vessel numbers in rat skin," *Journal of Investigative Dermatology*, vol. 103, no. 4, pp. 576–579, 1994.

[22] S. Y. Lee, J. H. Oh, J. C. Kim, Y. H. Kim, S. H. Kim, and J. W. Choi, "In vivo conjunctival reconstruction using modified PLGA grafts for decreased scar formation and contraction," *Biomaterials*, vol. 24, no. 27, pp. 5049–5059, 2003.

[23] S. A. Zawko, S. Suri, Q. Truong, and C. E. Schmidt, "Photopatterned anisotropic swelling of dual-crosslinked hyaluronic acid hydrogels," *Acta Biomaterialia*, vol. 5, no. 1, pp. 14–22, 2009.

[24] H. S. Yoo, E. A. Lee, J. J. Yoon, and T. G. Park, "Hyaluronic acid modified biodegradable scaffolds for cartilage tissue engineering," *Biomaterials*, vol. 26, no. 14, pp. 1925–1933, 2005.

[25] E. Esposito, E. Menegatti, and R. Cortesi, "Hyaluronan-based microspheres as tools for drug delivery: a comparative study," *International Journal of Pharmaceutics*, vol. 288, no. 1, pp. 35–49, 2005.

[26] T. Segura, B. C. Anderson, P. H. Chung, R. E. Webber, K. R. Shull, and L. D. Shea, "Crosslinked hyaluronic acid hydrogels: a strategy to functionalize and pattern," *Biomaterials*, vol. 26, no. 4, pp. 359–371, 2005.

[27] C.-M. Lo, H.-B. Wang, M. Dembo, and Y.-L. Wang, "Cell movement is guided by the rigidity of the substrate," *Biophysical Journal*, vol. 79, no. 1, pp. 144–152, 2000.

[28] M. T. Khorasani, S. MoemenBellah, H. Mirzadeh, and B. Sadatnia, "Effect of surface charge and hydrophobicity of polyurethanes and silicone rubbers on L929 cells response," *Colloids and Surfaces B*, vol. 51, no. 2, pp. 112–119, 2006.

[29] J. H. Lee, S. J. Lee, G. Khang, and H. B. Lee, "The effect of fluid shear stress on endothelial cell adhesiveness to polymer surfaces with wettability gradient," *Journal of Colloid and Interface Science*, vol. 230, no. 1, pp. 84–90, 2000.

[30] D.-T. Lin, T.-H. Young, and Y. Fang, "Studies on the effect of surface properties on the biocompatibility of polyurethane membranes," *Biomaterials*, vol. 22, no. 12, pp. 1521–1529, 2001.

Hindawi Publishing Corporation
International Journal of Polymer Science
Volume 2010, Article ID 985137, 10 pages
doi:10.1155/2010/985137

Research Article

Investigation of Genipin Cross-Linked Microcapsule for Oral Delivery of Live Bacterial Cells and Other Biotherapeutics: Preparation and In Vitro Analysis in Simulated Human Gastrointestinal Model

Hongmei Chen, Wei Ouyang, Christopher Martoni, Fatemeh Afkhami, Bisi Lawuyi, Trisna Lim, and Satya Prakash

Department of Biomedical Engineering and Physiology, Biomedical Technology and Cell Therapy Research Laboratory, Artificial Cells and Organs Research Centre, Faculty of Medicine, McGill University, Montreal, Qc, Canada H3A 2B4

Correspondence should be addressed to Satya Prakash, satya.prakash@mcgill.ca

Received 15 March 2010; Accepted 31 May 2010

Academic Editor: Shanfeng Wang

Oral therapy utilizing engineered microorganisms has shown promise in the treatment of many diseases. By microencapsulation, viable cells can overcome the harsh gastrointestinal (GI) environment and secrete needed therapeutics into the gut. These engineered cells should be encased without escaping into the GI tract for safety concerns, thus robust microcapsule membrane is requisite. This paper examined the GI performance of a novel microcapsule membrane using a dynamic simulated human GI model. Results showed that the genipin cross-linked alginate-chitosan (GCAC) microcapsules possessed strong resistance to structural disintegration in the simulated GI environment. Leakage of encapsulated high molecular weight dextran, a model material to be protected during the simulated GI transit, was negligible over 72 h of exposure, in contrast to considerable leakage of dextran from the non-cross-linked counterparts. These microcapsules did not alter the microflora and enzymatic activities in the simulated human colonic media. This study suggested the potential of the GCAC microcapsules for oral delivery of live microorganisms and other biotherapeutics.

1. Introduction

Advances in molecular biology research have introduced a wide range of genetically engineered (GE) microorganisms with a superior capacity to produce disease-modifying substrates, such as cytokines, enzymes, vaccines, hormones, antibodies, growth factors, and other therapeutic products [1, 2]. The use of these microorganisms opens up new hopes of treating a wide array of human diseases. Because the secreted biologics are generally fragile and easily degraded or denatured [3], encapsulation technology may offer significant advantages over the conventional biotechnological production methods. Being protected against external stresses, encapsulated bacteria remain viable and functional. They can be delivered proximally to the target site *in vivo* and continuously secrete therapeutic products to the host at a more effective concentration [4]. Recent research on the microencapsulation of GE cells has demonstrated great potential in the treatment of kidney failure, cancers, hypercholesteraemia, and many other diseases [5–13].

Oral ingestion is usually a preferred route of administration for therapy; however, microcapsules containing bacterial cells and other biotherapeutic molecules can be disrupted in the harsh gastrointestinal (GI) system by a number of means such as low pH, antimicrobial substances and mechanical stress [14]. Furthermore, the eruption of microcapsules and the subsequent release of engineered bacteria could induce many adverse effects on the body [2]. It was previously shown that oral administration of repeated doses of bacteria may stimulate a host immune response [15, 16]. Propagation of foreign bacteria in the GI tract may cause uncontrolled and persistent production of harmful substances, and may

detrimentally disrupt and/or replace the natural microflora [2, 17]. There are also risks of immunomodulation and gene transfer associated with the use of novel microorganisms [18]. Therefore, it is essential that GE bacteria be encased in the microcapsules, perform the therapeutic functions during the GI transit, and be excreted along with the intact microcapsules in feces without being retained in the body, even though these GE cells are classified as nonpathogenic [7]. To fulfill these requirements, it is important to maintain the structural integrity of microcapsules and thus prevent cell leakage during the GI transit. Current literature reports on oral delivery systems mainly focus on the controlled release of encapsulated contents, for example, probiotics and drugs [4, 19–23]. Scanty research is available on microcapsules intended to retain cells throughout the GI transit.

Alginate and chitosan are biomaterials widely studied for cell encapsulation because of their excellent biocompatibility, status as FDA approved food additives, and mild process conditions [24–28]. It was reported that the ionically linked alginate-chitosan (AC) membrane improved gastric survival of probiotics, but some limitations such as inadequate stability, susceptibility to degradation and cell leakage persist [29–33]. Genipin and its derivatives, extracted from gardenia fruits [34], have traditionally been used as a herbal medicine and a natural colorant in the food industry [35]. Previous research has demonstrated its low cytotoxicity and potential in protein and live cell delivery [36–38]. We have previously developed a novel covalently cross-linked microcapsule system composed of a calcium alginate core with a genipin cross-linked chitosan membrane [36, 39]. Our recent data showed that this microcapsule membrane possessed strong membrane stability and resistance to enzymatic degradation [40]. The purpose of this study is to further evaluate the potential of this genipin cross-linked alginate-chitosan (GCAC) microcapsule system for GI applications by using a dynamic human GI model. For comparison, the frequently used AC microcapsules were also tested.

2. Materials and Methods

2.1. Chemicals. Sodium alginate (low viscosity), and fluorescein isothiocyanate (FITC) labeled dextran (*Mw* 2,000 KD) were supplied by Sigma-Aldrich, USA. Chitosan (low viscosity, $Mv = 7.2 \times 10^4$, degree of deacetylation or DDA = 73.5%) and genipin were purchased from Wako BioProducts, USA. 4-nitrophenyl-α-D galactopyranoside, 4-nitrophenyl-α-D glucopyranoside, and 4-nitrophenyl-β-D galactopyranoside were obtained from Acros Organics, USA. 4-nitrophenol, 4-nitrophenyl-β-D glucopyranoside, and 4-nitrophenyl-β-D glucuronide were purchased from Sigma-Aldrich, USA. All other reagents and solvents were of reagent grade and used as received without further purification.

2.2. Preparation of Microcapsules. The AC and GCAC microcapsules were prepared as per previously reported protocol [39]. Unless otherwise specified, the cross-linking reaction was performed by suspending the AC microcapsules in a genipin solution (2.5 mg/mL) at room temperature (RT). Sterile microcapsules were prepared similarly except that the entire encapsulation procedure was carried out in a biological containment hood and all solutions used were either 0.22 μm filtered or autoclaved to ensure sterility. Microcapsules containing high molecular weight FITC-labeled dextran were prepared by mixing FITC-dextran with an alginate solution, making the final concentrations of alginate and FITC-dextran at 15 mg/mL and 2 mg/mL, respectively. The subsequent processes, including the formation of alginate beads, coating and cross-linking were performed using the aforementioned procedures.

2.3. Simulation of the Human Gastrointestinal (GI) Environment. The human GI conditions used in this study were simulated *in vitro* by means of five sequential bioreactors (Figure 1). Each compartment simulates a different part of the human GI tract: the stomach, the small intestine, the ascending colon, the transverse colon, and the descending colon [41, 44]. Human fecal slurries containing normal human GI bacterial cells were inoculated into the simulated colon (the last three vessels). Food content of human western diet suspension, composed of (per liter) 1 g arabinogalactan, 2 g pectin, 1 g xylan, 3 g potato starch, 0.4 g glucose, 3 g yeast extract, 1 g peptone, 4 g mucin, and 0.5 g cystein, was fed to the first vessel three times a day. After feeding, acidification of the stomach (pH $\leq$ 2) occurred, followed by neutralization (pH $\geq$ 6.8) in the second vessel and addition of simulated pancreatic juice (0.9 g pancreatin, 6 g bile salts, and 12 g $NaHCO_3$ per liter) to the simulated small intestine. Afterwards, the suspension was transferred to the simulated ascending colon, the transverse colon, and the descending colon, and finally excreted as effluent. The first two reactors were of the fill-and-draw principle with programmed periods of residence and stirring, and the last three were continuously agitated (approximately 250 rpm). The whole system was maintained under anaerobic conditions by flushing the headspace of each vessel with N2 for 15 minutes every day and the temperature of each vessel was kept constant at 37°C by a thermostat. The pH conditions, fluid volume, retention time at each stage, as well as the entire transit were simulated under computer control. This *in vitro* human GI model was validated against *in vivo* data by earlier studies [41].

2.4. Resistance of Microcapsules to the Simulated Human GI Transit. To study the microcapsule resistance to the simulated human GI transit, microcapsules (0.80 g) were exposed to the simulated human GI fluids for the estimated maximum period of time for the human GI transit (Table 1) [42]. Microcapsule samples were withdrawn at varied stages for morphological examination under an inverted microscope (LOMO, PC), and microphotographs taken as records using a digital camera (Canon Power shot G2, Japan). Percent defective microcapsules were estimated in three randomly picked observation fields.

To assess the recovery of microcapsules after the simulated human GI transit, microcapsules of known weight were placed in a sealed teabag-like container and exposed to the simulated GI media according to the timetable described in Table 1. At the final stage, the retrieved microcapsules were washed, dried using filter paper for approximately 10 min

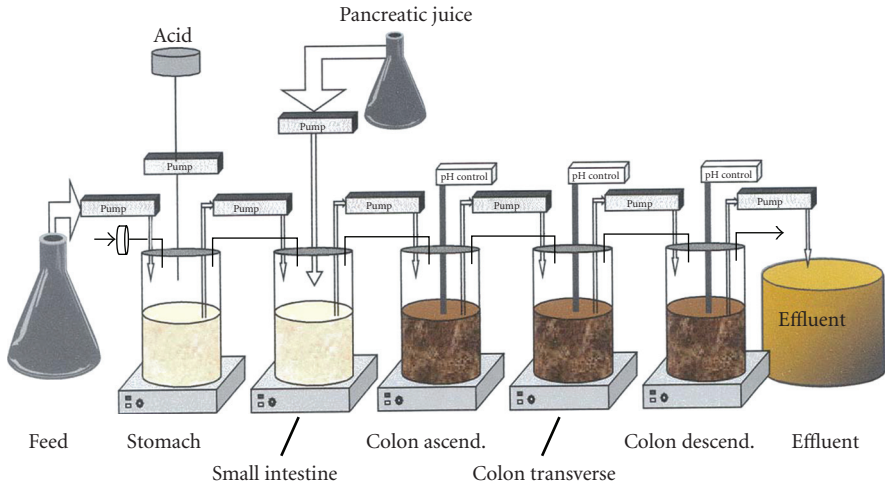

(a)

(b)

(c)

Figure 1: Computer controlled dynamic *in vitro* human GI model. (a) schematic; (b) 5-bioreactors set-up; and (c) online computer control.

and weighed. Percent recovery was defined as: % recovery = $(W_0 - W)/W_0 * 100$, where W_0 and W are the weights of the microcapsules before and after being exposed to the simulated GI transit, respectively.

2.5. Retention of Encapsulated Macromolecules against Leaching to the Simulated Human GI Fluids. To evaluate the capacity of the GCAC microcapsules to retain enclosed large-sized materials, high molecular weight FITC-dextran was encapsulated as a model macromolecule. These FITC-dextran-containing microcapsules (0.60 ± 0.01 g) were exposed to 2 mL of the simulated human gastric fluid taken from the GI model and incubated in an Environ shaker at 37°C, 100 rpm for 1 hour, followed by a 72 hours incubation in 2 mL of the simulated human intestinal fluid from the GI model (37°C, 100 rpm). Samples of the incubation media were withdrawn periodically and leaking of the encapsulated FITC-dextran was assessed spectrofluorometrically using a Microplate Fluorescence Reader (FLx800, Bio-Tek Instruments, Inc.) at absorption and emission wavelengths of 485 nm and 528 nm, respectively. Volume of the incubation medium was kept constant by adding fresh simulated fluid after sampling. Data are presented as mean ± s.d. from triplicate experiments.

2.6. Effect of Microcapsules on the Simulated Gut Microflora. To investigate the influence of oral administered microcapsules on gut microflora, sterile microcapsules (1.0 g) were mixed with the suspension of the simulated transverse colon (10 mL). After 0, 6, 12, and 24 hours of anaerobic incubation at 37°C, samples of the incubation medium were aseptically withdrawn and serially diluted with physiological saline. Bacterial enumeration for specific fecal marker microorganisms, *Escherichia coli, Staphylococcus* sp., *Lactobacillus sp.* as well as total aerobes and total anaerobes, was performed using an agar-plate-count assay. The plating media and incubation conditions used in the experiments are listed in Table 2. The simulated colonic suspension without microcapsules was used as control.

Table 1: Exposure of microcapsules to the simulated human GI transit (72 h in total) and the corresponding morphological changes.

Compartment in GI model	Stomach (V1[a])	Small intestine (V2[a])	Ascend. Colon (V3[a])	Transverse colon (V4[a])	Descend. Colon (V5[a])
pH	≤2	7.2–7.4	5.6–5.8	6.2–6.4	6.6–6.8
Exposure time (h)	2	4	18	24	24
Microcapsule morphology[b]	Intact	Swelled, ~15% deformed	Collapsed	Collapsed or dissolved	Adhesive, ~30% ruptured
Microcapsule morphology[c]	Intact	Slightly swelled,<1% burst	Spherical, <2% broken	Spherical intact	Spherical intact

[a]Vessel (V) of bioreactors in the GI model representing the human GI tract.
[b]Microcapsules cross-linked by genipin at 4°C.
[c]Microcapsules cross-linked by genipin at RT.

Table 2: Media and incubation conditions used for enumeration of representative microbes in the simulated human colon.

Microbial group	Medium	Incubation conditions and time	Colonies formed
Total aerobes	Brain heart infusion agar	Aerobic, 37°C, 24 hours	White
Total anaerobes	Brain heart infusion agar	Anaerobic, 37°C, 72 hours	White
Escherichia coli	Mc Conkey agar	Aerobic, 43°C, 24 hours	Red-purple
Staphylococcus sp.	Mannitol Salt agar	Aerobic, 37°C, 48 hours	White with yellow/purple zone
Lactobacillus sp.	Rogosa agar	Anaerobic, 37°C, 72 hours	White

2.7. Effect of Microcapsules on the Microbial Enzyme Activities in the Simulated Colonic Media. To assess the effect of oral administered microcapsules on the GI microbial enzyme activities, the suspension from the simulated transverse colon (20 mL) was incubated anaerobically at 37°C in the presence of sterile microcapsules (2.0 g) for up to 24 hours. At different time points of 0, 12, and 24 hours, the enzymatic activities of β-galactosidase, β-glucosidase, β-glucuronidase, α-galactosidase, and α-glucosidase in the incubation medium were analyzed spectrometrically using the method described earlier [43, 44]. The absorbance at 405 nm was recorded by a μQuant multiplate reader (Bio-Tek Instruments). The simulated colonic fluid free of microcapsules was used as control. Results are expressed as percentage of enzymatic activities relative to the control at each time point. Data of the control samples at each time point were normalized to 100%.

Numerical values are shown as mean ± standard deviation. Statistical analyses used the two-tailed Student's t-test with $P < .05$ considered significantly different.

3. Results

3.1. Resistance of Microcapsule to the Simulated Human GI Transit. To assess the resistance to the GI environment, the GCAC microcapsules were exposed to the simulated GI media representing different phases of digestion for a length of time based on the estimated maximum retention in the human GI tract (Table 1). Figure 2 depicts the photomicrographs of the microcapsules after exposure to the simulated human GI fluids. The tested microcapsules remained morphologically stable during the simulated gastric incubation (2 hours, pH ≤ 2.0) (Figures 2(a), 2(d)), but behaved differently in the subsequent simulated intestinal transit depending on the extent of cross-linking. The GCAC microcapsules cross-linked at 4°C swelled appreciably in the simulated small intestine (pH 7.2–7.4) (Figure 2(b)). They became fragile and adhesive in the simulated descending colon where shriveled or partially dissolved beads were observed. When leaving the simulated descending colon, 30–40% of the microcapsules lost their structural integrity (Figure 2(c)). In contrast, the majority of the GCAC microcapsules cross-linked at higher temperature (RT) maintained their physical stability during the entire simulated human GI transit (Figures 2(e) and 2(f)), with more than 80% recovery after 72 hours exposure (Figure 3). In comparison, the recovery of the GCAC microcapsules with less cross-link (cross-linked at 4°C) was lower (61.4%) (Figure 3).

3.2. Retention of Encapsulated HMW Dextran during the Simulated GI Transit. To examine the capacity of the GCAC microcapsules to encase large-sized materials in the GI environment, encapsulated high molecular weight FITC-labeled dextran was exposed to the simulated human GI media. Being a large polymer of 2,000 KD, this fluorescent probe was indefinitely withheld inside the intact microcapsules and could not leak out unless the microcapsule membranes became defective or damaged [45]. During the first hour of exposure to the simulated gastric fluid, no FITC-dextran was detected in the incubation medium (data not shown). In the subsequent exposure to the simulated intestinal medium, the leakage of the encapsulated FITC-dextran from the non-cross-linked AC microcapsules increased gradually with the incubation time, attaining the fluorescence intensity of 70, 100 and 115 at 24, 48 and 72 hours, respectively. In contrast,

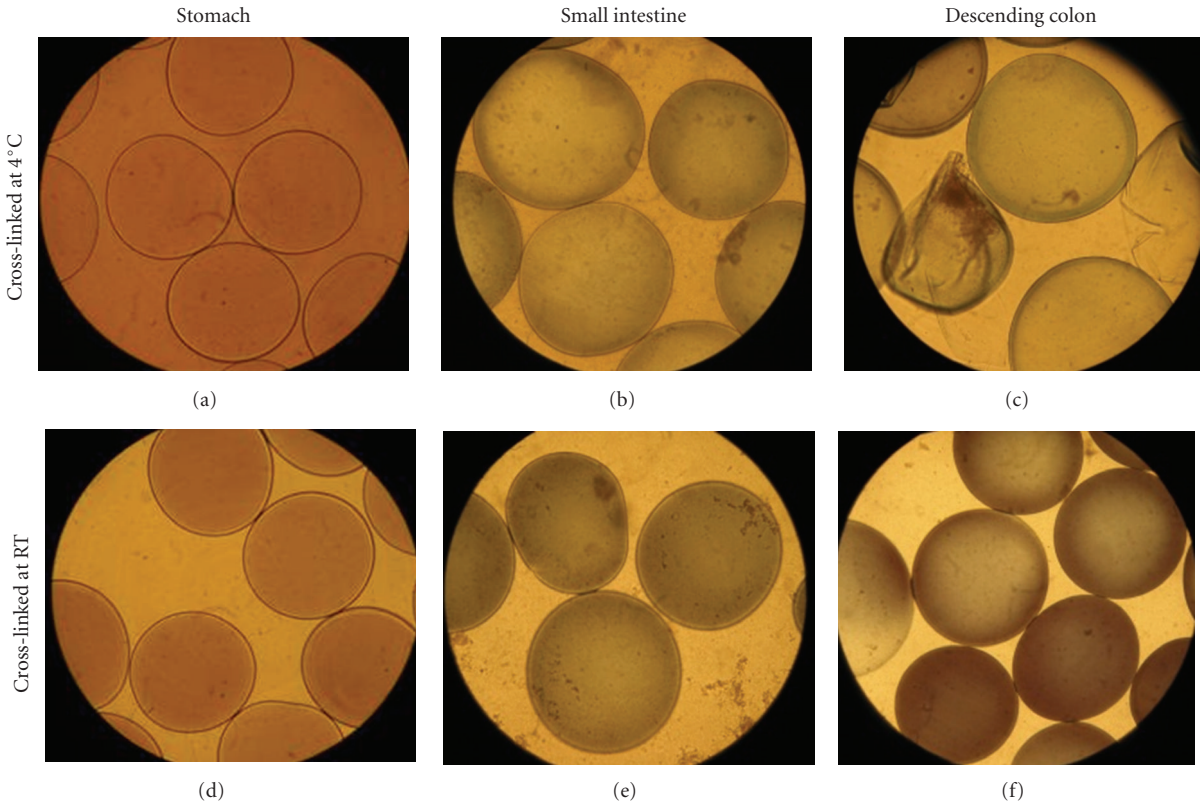

Figure 2: Microphotographs of the GCAC microcapsules cross-linked at 4°C (a)–(c) and RT (d)–(f) during the simulated human GI transit in the simulated stomach, small intestine, and descending colons. Original magnification at 90x.

negligible amounts of FITC-dextran escaped from the GCAC microcapsules, with very low fluorescence intensity of the medium detected (not exceeding 50) throughout the experiment (Figure 4), which significantly outran those of the AC microcapsules.

3.3. Oral Administration of Microcapsules on Gut Microflora and Enzymatic Activities. The effect of microcapsules on human GI microflora was assessed by investigating the population of fecal marker microorganisms and the activity of 5 representative GI microbial enzymes in the simulated colonic media containing sterile microcapsules. Since the simulated GI model is a dynamic system, static experiments were performed in this study to maximize the effects. We found no marked differences in the tested microbial population including total aerobes, total anaerobes, *Escherichia coli, Staphylococcus sp.,* and *Lactobacillus sp.* in the stimulated colonic media containing tested microcapsules of either AC or GCAC formulation when compared to the control media in the absence of tested microcapsules (Table 3, all $P > .05$).

Figure 5 shows the effect of the microcapsules on the activities of microbial enzymes in the simulated transverse colon suspension. As time elapsed, a slight decline in the tested enzymatic activities was found in the simulated colonic fluids in the presence of microcapsules. As an exception, a decrease of more than 20% in the activity of β-glucuronidase was detected after 12 hours of contact with microcapsules, yet the loss remained at a similar level with extended incubation for up to 24 hours (Figure 5(c)). No significant differences in the alteration of enzymatic activities were found when the GCAC microcapsules were compared with the AC microcapsules ($P > .05$).

4. Discussion

For successful exploitation of microcapsules as an oral delivery device, understanding of their performance under physiologically pertinent conditions that represent the human GI tract is essential. Although *in vivo* research using specific techniques such as histological sectioning [46], radiography [47] and gamma scintigraphy [48, 49] can progressively track the microcapsules in the GI tract, it remains difficult to follow the orally administered microcapsule at every stage of digestion on either animals or humans due to tedious processing, small size of the microcapsules, limited detection resolution and ethical constraints. *In vitro* simulation offers a number of advantages, for example, well-controlled experimental conditions and easy sampling, especially preferable for screening and examining a variety of samples. Buffered solutions, for example, with pH at 1-2 or 6.5-7.5, are frequently reported in literature as the simulated GI fluids [31, 50, 51]; however they only represent the pH in the stomach and in the intestine, and do not mimic the complex human GI microbial ecosystem. While other *ex vivo* and *in vitro* simulated models including USP apparatus were also reported [52], most of them were static systems, where

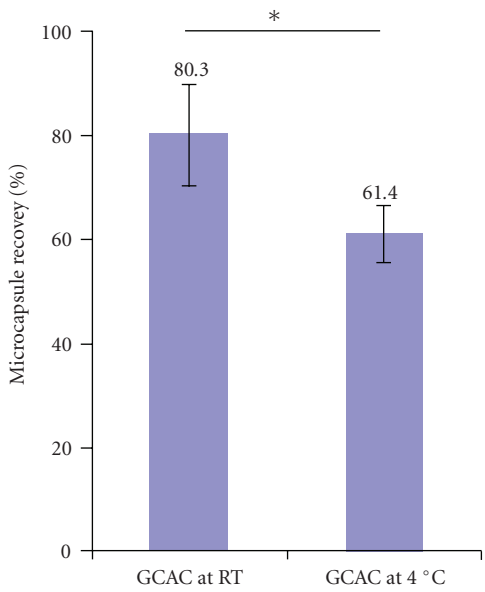

Figure 3: Recovery of microcapsules after 72 hours of the simulated human GI transit. * indicates significant difference at $P < .05$.

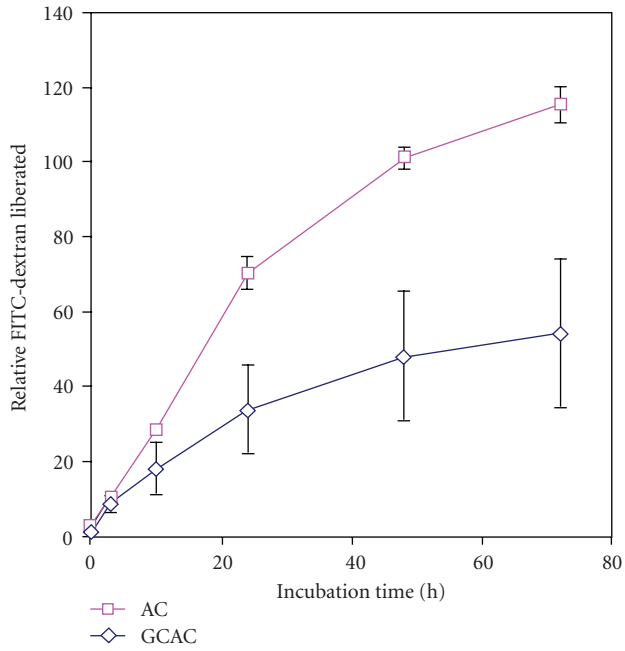

Figure 4: Leaching of the encapsulated FITC-dextran into the simulated intestinal medium following 1 hour simulated gastric exposure. Error bars indicate standard deviation of the mean ($n = 3$).

fluids cannot be continuously transferred into the sequential GI compartments. Our present study used a dynamic computer-controlled human simulated GI model, which mimics the gradual transit of ingested materials through the simulated GI tract from feeding to discharge. It also maintains the microbial community actually presented in the human intestinal system, which allows for assessing the behavior of the microcapsules under more physiologically pertinent conditions.

As has been noted earlier, it is imperative that microcapsules maintain physical integrity during the GI transit to prevent the leaking of genetically engineered cells, which is strongly dependent on the microcapsule's robustness and stability. So far few studies were reported to address this matter [44]. The present study investigated the behaviour of the GCAC microcapsules in the simulated human GI environment. When exposed to the simulated GI media, the microcapsules experienced the simulated transit through the GI tract including pH fluctuation, enzymatic degradation, microorganism actions, mechanical stresses, as well as other related chemical and physiological constraints. The exposure time was chosen according to the maximum period retention in the human GI tract that represents the most challenging case for the tested microcapsules. The better-preserved morphology and higher retrieval rate associated with the GCAC microcapsules cross-linked at RT (Figures 2 and 3) indicated improved membrane stability by higher degree of cross-linking. Moreover, negligible amounts of encapsulated fluorescent probe were released into the incubation GI media from the GCAC microcapsules (Figure 4), suggesting that the integrity of the microcapsule membrane was withheld. In contrast, the non-cross-linked AC microcapsules were found vulnerable to structural disruption in the harsh GI condition, likely due to the relatively weak polyelectrolyte complexation of membrane materials that are prone to gastric and proteolytic degradation. These findings corroborated the results reported previously [44, 53–55]. The present study demonstrated that covalent cross-linking of microcapsule membranes by genipin substantially improved the resistance to membrane degradation in the simulated human GI environment.

Another important prerequisite of oral therapy utilizing microencapsulation is that the administration of microcapsules should not disturb the natural colonic flora, particularly when prolonged and repeated oral intake of a rather large quantity of microcapsules is required for therapy. Microcapsules are made of various materials and chemicals through complexation and cross-linking reactions, all of which may have an effect on the biocompatibility of the final microcapsules. In particular, the well-balanced gut microbiota are important in maintaining human health [56, 57] and should not be altered by the intake of microcapsules. When taken into account the static nature and a rather large dosage (1.0 g of microcapsules in 10 mL of intestinal fluid) of the experiments in this *in vitro* study, our results suggested that the materials used to construct the microcapsules did not evoke appreciable adverse effects on the human intestinal flora and that genipin cross-linked chitosan membranes did not compromise the biocompatibility of the microcapsules when compared to the non-cross-linked subjects. Decrease in the activities of the tested microbial enzymes in the simulated colonic media containing microcapsules was detected. It could possibly be attributed to the binding effect or diffusion of the enzymes to the microcapsules, though further research may continue to elucidate the consequence.

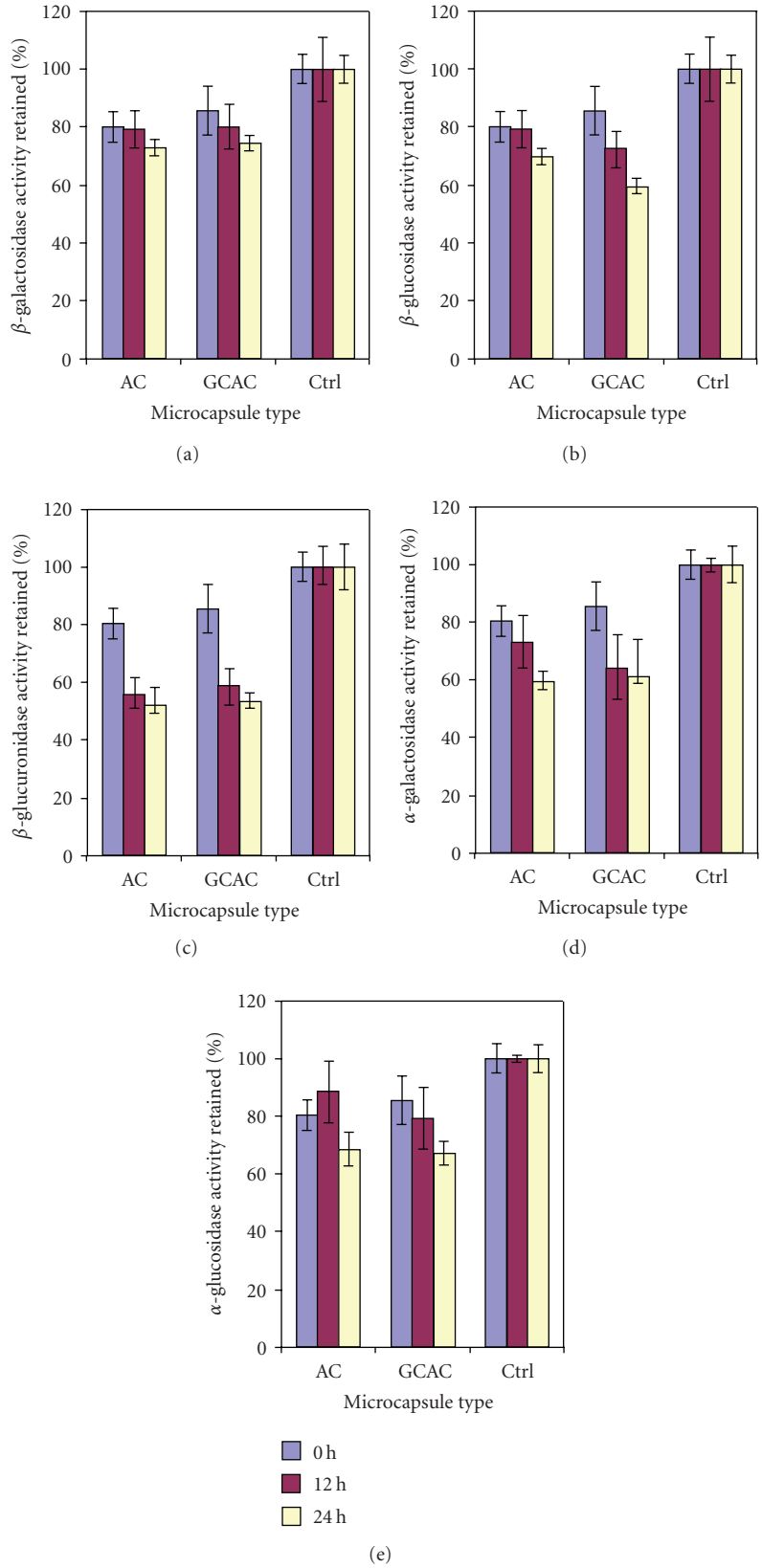

Figure 5: Percent microbial enzyme activities retained in the suspension of the simulated human transverse colon in the presence of microcapsules relative to that in the absence of microcapsules (control). Values for the controls at each time point were normalized to 100 % and were used to calculate the percent enzyme activities retained in the microcapsule-containing media at corresponding time points. (a) β-galactosidase; (b) β-glucosidase; (c) β-glucuronidase; (d) α-galactosidase; and (e) α-glucosidase.

Table 3: Effects of microcapsules on fecal marker microbes in the simulated transverse colon.

Microbes	Incubation time (h)	Log CFU/mL medium[a]		
		GCAC[b]	AC[b]	Control[c]
Total aerobes	0	8.41	8.41	8.41
	6	8.37	8.32	8.36
	12	8.36	8.37	8.39
	24	8.22	8.17	8.04
Total anaerobes	0	8.44	8.44	8.44
	6	8.37	8.33	8.41
	12	8.37	8.43	8.40
	24	8.41	8.30	8.03
Escherichia coli	0	8.31	8.31	8.31
	6	8.18	7.97	8.18
	12	8.20	8.02	8.41
	24	8.10	8.03	8.68
Staphylococcus sp.	0	6.96	6.96	6.96
	6	6.52	6.60	6.81
	12	6.61	6.72	6.77
	24	6.57	6.62	6.54
Lactobacillus sp.	0	5.48	5.48	5.48
	6	5.45	5.52	5.51
	12	5.35	5.40	5.32
	24	5.50	5.46	5.37

[a] $n = 3$, standard deviation <0.20.
[b] Colonic suspension in the presence of microcapsules.
[c] Colonic suspension in the absence of microcapsules.

5. Conclusions

This study examined the performance of the genipin cross-linked alginate-chitosan microcapsules under physiologically pertinent GI conditions using a dynamic simulated human GI model. Results showed that these GCAC microcapsules possessed superior resistance against disintegration in the simulated GI environment and did not appreciably alter the normal gut flora. This novel microcapsule formulation is promising for oral delivery of genetically engineered bacteria; however, further studies on encapsulated cell viability in the gut lumen are needed before its full potential can be realized.

Acknowledgments

This paper was supported by the Canadian Institutes of Health Research (CIHR) MOP 64308. Postgraduate fellowships from the Natural Sciences and Engineering Research Council of Canada (to H. Chen and C. Martoni) and Fonds Québécois de la Recherche sur la Nature et les Technologies (to H. Chen and W. Ouyang) are greatly acknowledged. The authors also thank M. L. Jones for his help with the GI model set-up, T. Haque, M. Shafiei, and H. Wightman for assistance in the experiments.

References

[1] S. Prakash and J. Bhathena, "Live bacterial cells as orally delivered therapeutics," *Expert Opinion on Biological Therapy*, vol. 5, no. 10, pp. 1281–1301, 2005.

[2] L. Steidler, "Genetically engineered probiotics," *Bailliere's Best Practice and Research in Clinical Gastroenterology*, vol. 17, no. 5, pp. 861–876, 2003.

[3] M. Goldberg and I. Gomez-Orellana, "Challenges for the oral delivery of macromolecules," *Nature Reviews Drug Discovery*, vol. 2, no. 4, pp. 289–295, 2003.

[4] G. Orive, R. M. Hernández, A. Rodríguez Gascón et al., "History, challenges and perspectives of cell microencapsulation," *Trends in Biotechnology*, vol. 22, no. 2, pp. 87–92, 2004.

[5] G. Bergers and D. Hanahan, "Cell factories for fighting cancer," *Nature Biotechnology*, vol. 19, no. 1, pp. 20–21, 2001.

[6] J. Bloch, A. C. Bachoud-Lévi, N. Déglon et al., "Neuroprotective gene therapy for Huntington's disease, using polymer-encapsulated cells engineered to secrete human ciliary neurotrophic factor: results of a phase I study," *Human Gene Therapy*, vol. 15, no. 10, pp. 968–975, 2004.

[7] T. M. S. Chang, "Therapeutic applications of polymeric artificial cells," *Nature Reviews Drug Discovery*, vol. 4, no. 3, pp. 221–235, 2005.

[8] M. L. Jones, H. Chen, W. Ouyang, T. Metz, and S. Prakash, "Microencapsulated genetically engineered *Lactobacillus plantarum 80* (pCBH1) for bile acid deconjugation and its implication in lowering cholesterol," *Journal of Biomedicine and Biotechnology*, vol. 2004, no. 1, pp. 61–69, 2004.

[9] S. Prakash and T. M. S. Chang, "Microencapsulated genetically engineered live E. coli DH5 cells administered orally to maintain normal plasma urea level in uremic rats," *Nature Medicine*, vol. 2, no. 8, pp. 883–887, 1996.

[10] T.-A. Read, D. R. Sorensen, R. Mahesparan et al., "Local endostatin treatment of gliomas administered by microencapsulated producer cells," *Nature Biotechnology*, vol. 19, no. 1, pp. 29–34, 2001.

[11] C. J. D. Ross, L. Bastedo, S. A. Maier, M. S. Sands, and P. L. Chang, "Treatment of a lysosomal storage disease, mucopolysaccharidosis VII, with microencapsulated recombinant cells," *Human Gene Therapy*, vol. 11, no. 15, pp. 2117–2127, 2000.

[12] A. D. Tagalakis, I. A. Diakonov, I. R. Graham et al., "Apolipoprotein E delivery by peritoneal implantation of encapsulated recombinant cells improves the hyperlipidaemic profile in apoE-deficient mice," *Biochimica et Biophysica Acta*, vol. 1686, no. 3, pp. 190–199, 2005.

[13] J. M. Van Raamsdonk, C. J. D. Ross, M. A. Potter et al., "Treatment of hemophilia B in mice with nonautologous somatic gene therapeutics," *Journal of Laboratory and Clinical Medicine*, vol. 139, no. 1, pp. 35–42, 2002.

[14] L. R. Johnson, *Physiology of the Gastrointestinal Tract*, Elsevier Academic Press, Burlington, Mass, USA, 2006.

[15] J. Chin, B. Turner, I. Barchia, and A. Mullbacher, "Immune response to orally consumed antigens and probiotic bacteria," *Immunology and Cell Biology*, vol. 78, no. 1, pp. 55–66, 2000.

[16] N. Ishibashi and S. Yamazaki, "Probiotics and safety," *American Journal of Clinical Nutrition*, vol. 73, no. 2, pp. 465S–470S, 2001.

[17] C. P. Champagne, N. J. Gardner, and D. Roy, "Challenges in the addition of probiotic cultures to foods," *Critical Reviews in Food Science and Nutrition*, vol. 45, no. 1, pp. 61–84, 2005.

[18] S. Salminen, A. von Wright, L. Morelli et al., "Demonstration of safety of probiotics—a review," *International Journal of Food Microbiology*, vol. 44, no. 1-2, pp. 93–106, 1998.

[19] S. Freiberg and X. X. Zhu, "Polymer microspheres for controlled drug release," *International Journal of Pharmaceutics*, vol. 282, no. 1-2, pp. 1–18, 2004.

[20] L. R. Moses, K. J. Dileep, and C. P. Sharma, "Beta cyclodextrin-insulin-encapsulated chitosan/alginate matrix: oral delivery system," *Journal of Applied Polymer Science*, vol. 75, no. 9, pp. 1089–1096, 2000.

[21] E. Nechaeva, "Development of oral microencapsulated forms for delivering viral vaccines," *Expert Review of Vaccines*, vol. 1, no. 3, pp. 385–397, 2002.

[22] G. Orive, A. R. Gascón, R. M. Hernández, A. Domínguez-Gil, and J. L. Pedraz, "Techniques: new approaches to the delivery of biopharmaceuticals," *Trends in Pharmacological Sciences*, vol. 25, no. 7, pp. 382–387, 2004.

[23] V. R. Sinha and A. Trehan, "Biodegradable microspheres for protein delivery," *Journal of Controlled Release*, vol. 90, no. 3, pp. 261–280, 2003.

[24] A. Bartkowiak, "Optimal conditions of transplantable binary polyelectrolyte microcapsules," *Annals of the New York Academy of Sciences*, vol. 944, pp. 120–134, 2001.

[25] D. W. Green, I. Leveque, D. Walsh et al., "Biomineralized polysaccharide capsules for encapsulation, organization, and delivery of human cell types and growth factors," *Advanced Functional Materials*, vol. 15, no. 6, pp. 917–923, 2005.

[26] T. Haque, H. Chen, W. Ouyang et al., "In vitro study of alginate-chitosan microcapsules: an alternative to liver cell transplants for the treatment of liver failure," *Biotechnology Letters*, vol. 27, no. 5, pp. 317–322, 2005.

[27] D. Maysinger, O. Berezovskaya, and S. Fedoroff, "The hematopoietic cytokine colony stimulating factor 1 is also a growth factor in the CNS.2. Microencapsulated CSF-1 and LM-10 cells as delivery systems," *Experimental Neurology*, vol. 141, no. 1, pp. 47–56, 1996.

[28] D. Maysinger, K. Krieglstein, J. Filipovic-Grcic, M. Sendtner, K. Unsicker, and P. Richardson, "Microencapsulated ciliary neurotrophic factor: physical properties and biological activities," *Experimental Neurology*, vol. 138, no. 2, pp. 177–188, 1996.

[29] T. Chandy, D. L. Mooradian, and G. H. R. Rao, "Evaluation of modified alginate-chitosan-polyethylene glycol microcapsules for cell encapsulation," *Artificial Organs*, vol. 23, no. 10, pp. 894–903, 1999.

[30] G. Klinkenberg, K. Q. Lystad, D. W. Levine, and N. Dyrset, "Cell release from alginate immobilized Lactococcus lactis ssp. lactis in chitosan and alginate coated beads," *Journal of Dairy Science*, vol. 84, no. 5, pp. 1118–1127, 2001.

[31] W. Krasaekoopt, B. Bhandari, and H. Deeth, "The influence of coating materials on some properties of alginate beads and survivability of microencapsulated probiotic bacteria," *International Dairy Journal*, vol. 14, no. 8, pp. 737–743, 2004.

[32] G. Orive, A. Bartkowiak, S. Lisiecki et al., "Biocompatible oligochitosans as cationic modifiers of alginate/Ca microcapsules," *Journal of Biomedical Materials Research—Part B*, vol. 74, no. 1, pp. 429–439, 2005.

[33] A. Zanina, A. Vilesov, and T. Budtova, "Shear-induced solvent release from gel particles: application to drug-delivery systems," *International Journal of Pharmaceutics*, vol. 242, no. 1-2, pp. 137–146, 2002.

[34] C. Djerassi, J. D. Gray, and F. A. Kincl, "Naturally occurring oxygen heterocyclics. 9. Isolation and characterization of genipin," *Journal of Organic Chemistry*, vol. 25, no. 12, pp. 2174–2177, 1960.

[35] J.-E. Park, J.-Y. Lee, H.-G. Kim, T.-R. Hahn, and Y.-S. Paik, "Isolation and characterization of water-soluble intermediates of blue pigments transformed from geniposide of Gardenia jasminoides," *Journal of Agricultural and Food Chemistry*, vol. 50, no. 22, pp. 6511–6514, 2002.

[36] H. Chen, W. Ouyang, M. Jones et al., "Preparation and characterization of novel polymeric microcapsules for live cell encapsulation and therapy," *Cell Biochemistry and Biophysics*, vol. 47, no. 1, pp. 159–167, 2007.

[37] J. Jin, M. Song, and D. J. Hourston, "Novel chitosan-based films cross-linked by genipin with improved physical properties," *Biomacromolecules*, vol. 5, no. 1, pp. 162–168, 2004.

[38] F.-L. Mi, Y.-C. Tan, H.-F. Liang, and H.-W. Sung, "In vivo biocompatibility and degradability of a novel injectable-chitosan-based implant," *Biomaterials*, vol. 23, no. 1, pp. 181–191, 2002.

[39] H. Chen, W. Ouyang, B. Lawuyi, and S. Prakash, "Genipin cross-linked alginate-chitosan microcapsules: membrane characterization and optimization of cross-linking reaction," *Biomacromolecules*, vol. 7, no. 7, pp. 2091–2098, 2006.

[40] H. Chen, W. Ouyang, C. Martoni, and S. Prakash, "Genipin cross-linked polymeric alginate-chitosan microcapsules for oral delivery: in-vitro analysis," *International Journal of Polymer Science*, vol. 2009, Article ID 617184, 16 pages, 2009.

[41] K. Molly, M. V. Woestyne, and W. Verstraete, "Development of a 5-step multi-chamber reactor as a simulation of the human intestinal microbial ecosystem," *Applied Microbiology and Biotechnology*, vol. 39, no. 2, pp. 254–258, 1993.

[42] N. Berrada, J. F. Lemeland, G. Laroche, P. Thouvenot, and M. Piaia, "Bifidobacterium from fermented milks: survival during gastric transit," *Journal of Dairy Science*, vol. 74, no. 2, pp. 409–413, 1991.

[43] J. O. Berg, C. E. Nord, and T. Wadstrom, "Formation of glycosidases in batch and continuous culture of Bacteroides fragilis," *Applied and Environmental Microbiology*, vol. 35, no. 2, pp. 269–273, 1978.

[44] H. Chen, W. Ouyang, M. Jones, T. Haque, B. Lawuyi, and S. Prakash, "In-vitro analysis of APA microcapsules for oral delivery of live bacterial cells," *Journal of Microencapsulation*, vol. 22, no. 5, pp. 539–547, 2005.

[45] F. A. Leblond, J. Tessier, and J.-P. Hallé, "Quantitative method for the evaluation of biomicrocapsule resistance to mechanical stress," *Biomaterials*, vol. 17, no. 21, pp. 2097–2102, 1996.

[46] J. Kovacs-Nolan and Y. Mine, "Microencapsulation for the gastric passage and controlled intestinal release of immunoglobulin Y," *Journal of Immunological Methods*, vol. 296, no. 1-2, pp. 199–209, 2005.

[47] R. Narayani and K. P. Rao, "Polymer-coated gelatin capsules as oral delivery devices and their gastrointestinal tract behaviour in humans," *Journal of Biomaterials Science. Polymer Edition*, vol. 7, no. 1, pp. 39–48, 1995.

[48] Y. Sato, Y. Kawashima, H. Takeuchi, H. Yamamoto, and Y. Fujibayashi, "Pharmacoscintigraphic evaluation of riboflavin-containing microballoons for a floating controlled drug delivery system in healthy humans," *Journal of Controlled Release*, vol. 98, no. 1, pp. 75–85, 2004.

[49] I. R. Wilding, D. Clark, H. Wray, J. Alderman, N. Muirhead, and C. R. Sikes, "In vivo disintegration profile of encapsulated and nonencapsulated sumatriptan: gamma scintigraphy in healthy volunteers," *Journal of Clinical Pharmacology*, vol. 45, no. 1, pp. 101–105, 2005.

[50] A. Lamprecht, H. Yamamoto, H. Takeuchi, and Y. Kawashima, "Design of pH-sensitive microspheres for the colonic delivery of the immunosuppressive drug tacrolimus," *European Journal of Pharmaceutics and Biopharmaceutics*, vol. 58, no. 1, pp. 37–43, 2004.

[51] T. Reddy and S. Tammishetti, "Gastric resistant microbeads of metal ion cross-linked carboxymethyl guar gum for oral drug delivery," *Journal of Microencapsulation*, vol. 19, no. 3, pp. 311–318, 2002.

[52] F. Delie, "Evaluation of nano- and microparticle uptake by the gastrointestinal tract," *Advanced Drug Delivery Reviews*, vol. 34, no. 2-3, pp. 221–233, 1998.

[53] S. R. Bhatia, S. F. Khattak, and S. C. Roberts, "Polyelectrolytes for cell encapsulation," *Current Opinion in Colloid and Interface Science*, vol. 10, no. 1-2, pp. 45–51, 2005.

[54] B. R. S. Hsu, S. H. Fu, J. S. Tsai, Y. Y. Huang, H. S. Huang, and K. S. S. Chang, "The plasminogen-plasmin fibrinolytic system accelerates degradation of alginate-poly-L-lysine-alginate microcapsules in vitro," *Transplantation Proceedings*, vol. 29, no. 3, pp. 1877–1880, 1997.

[55] H. Zimmermann, D. Zimmermann, R. Reuss et al., "Towards a medically approved technology for alginate-based microcapsules allowing long-term immunoisolated transplantation," *Journal of Materials Science*, vol. 16, no. 6, pp. 491–501, 2005.

[56] K. Hirayama and J. Rafter, "The role of lactic acid bacteria in colon cancer prevention: mechanistic considerations," *Antonie Van Leeuwenhoek, International Journal of General and Molecular Microbiology*, vol. 76, no. 1–4, pp. 391–394, 1999.

[57] G. L. Simon and S. L. Gorbach, "Intestinal flora in health and disease," *Gastroenterology*, vol. 86, no. 1, pp. 174–193, 1984.

Hindawi Publishing Corporation
International Journal of Polymer Science
Volume 2010, Article ID 423460, 8 pages
doi:10.1155/2010/423460

Review Article

Amphiphilic Poly(3-hydroxy alkanoate)s: Potential Candidates for Medical Applications

Baki Hazer

Department of Chemistry, Zonguldak Karaelmas University, 67100 Zonguldak, Turkey

Correspondence should be addressed to Baki Hazer, bhazer2@yahoo.com

Received 3 December 2009; Accepted 31 December 2009

Academic Editor: Shanfeng Wang

Poly(3-hydroxy alkanoate)s, PHAs, have been very attractive as biomaterials due to their biodegradability and biocompatibility. These hydrophobic natural polyesters, PHAs, need to have hydrophilic character particularly for drug delivery systems. In this manner, poly(ethylene glycol) (PEG) and hydrophilic functional groups such as amine, hydroxyl, carboxyl, and sulfonic acid have been introduced into the PHAs in order to obtain amphiphilic polymers. This review involves in the synthesis and characterization of the amphiphilic PHAs.

1. Introduction

Biomaterials have been widely used in medical applications, such as drug delivery, tissue engineering, device-based therapies, and medical imaging [1, 2]. Synthetic and naturally occurring polymers have played important role in the treatment of disease and the improvement of health care. Among them, PHAs are promising materials for biomedical applications in tissue engineering and drug delivery system because they are natural, renewable, biodegradable, and biocompatible thermoplastics. PHAs have been used to develop devices, including sutures, nerve repair devices, repair patches, slings, cardiovascular patches, orthopedic pins, adhesion barriers, stents, guided tissue repair/regeneration devices, articular cartilage repair devices, nerve guides, tendon repair devices, bone-marrow scaffolds, tissue engineered cardiovascular devices, and wound dressing. However the direct use of these polyesters has been hampered by their hydrophobic character and some physical shortcomings [3]. The key to biocompatibility of biomedical implantable materials is to render their surface in a way that minimizes hydrophobic interaction with the surrounding tissue. Therefore, hydrophilic groups have been introduced into the PHAs in order to obtain amphiphilic polymer. This review has been focused on the chemically modified PHAs with enhanced hydrophilic character as biomaterials for medical applications.

2. PHAs

PHAs are accumulated as intracellular granules as a result of a metabolic stress upon imbalanced growth due to a limited supply of an essential nutrient and the presence of an excess of a carbon source. These novel biopolymers have material properties ranging from rigid and highly crystalline to flexible, rather amorphous and elastomeric. There have been many studies reported on the modification reactions to enhance mechanical and thermal properties to prepare new biomaterials for the medical applications [4–13]. PHAs can be classified into three groups based on the number of carbon atoms in the monomer units: short-chain-length (*scl*PHA) containing 3–5 carbon atoms that are produced by *Ralstonia eutropha* (also referred *Watersia eutropha, A. Eutrophus*), medium-chain-length (*mcl*PHA) containing 6–14 carbon atoms, and long-chain-length (*lcl*PHAs), with more than 14 carbon atoms [14, 15]. *Pseudomonas oleovorans* is a very versatile microrgnism for PHA production because it can produce medium chain length polyesters (*mcl*PHA) and long chain length polyesters (*lcl*PHA) from a wide variety of carbon substrates. These

Table 1: Classification of the bacterial polyesters.

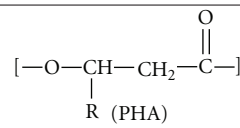

Carbon source	Poly(3-hydroxy alkanoate) (PHA)			Thermal and mechanical properties		
	Type	Side chain (R)	Name*	T_g (°C)	T_m (°C)	Elongation (%)
Sugar, glucose, acetic acid	Short chain length	Methyl, ethyl	PHB PHV	15	170	5
Alkanoic acids, alkanes, and alkanols	Medium chain length	propyl, butyl, pentyl, hexyl, heptyl	PHHx PHHp PHO PHN PHD	−40	60	800
Plant oily acids	Long chain length	More than 14 carbon per repeating unit		−50	40	Soft, sticky

*B: butyrate, V: valerate, Hx: hexanoate, Hp: heptanoate, O: octanoate, N: nonanoate, D: decanoate, T_g and T_m are glass transition and melting temperatures, respectively.

types of the bacterial polyesters have been summarized in Table 1.

3. Amphiphilic PHAs

Amphiphilic polymers can be synthesized by introducing hydrophilic groups such as hydroxyl, carboxyl, amine, glycol, and hydrophilic polymers such as PEG, poly(vinyl alcohol), polyacryl amide, poly acrylic acids, hydroxy ethyl methacrylate, poly vinyl pyridine, and poly vinyl pyrrolidone to a hydrophobic moiety. Because of their ability to form micelles, amphiphilic block copolymers are strong candidates for potential applications as emulsifiers, dispersants, foamers, thickeners, rinse aids, and compatibilizers [16, 17]. Similarly, amphiphilic PHAs can also be synthesized by introducing hydrophilic groups such as hydroxyl, carboxyl, amine, sulfonic acid, ethylene glycol, and PEG. PEG is a polyether that is known for its exceptional blood and tissue compatibility. It is used extensively as biomaterial in a variety of drug delivery vehicles and is also under investigation as surface coating for biomedical implants. PEG, when dissolved in water, has a low interfacial free energy and exhibits rapid chain motion, and its large excluded volume leads to steric repulsion of approaching molecules [18]. These properties make PEG excellent biocompatible material. Hydroxylation of the PHAs can be carried out by using both biosynthetic and chemical modification. The biosynthetic hydroxylation of the PHAs has successfully been reviewed by Foster, recently [19]. Chemical modifications of the PHAs have been extensively studied [6, 9, 15, 20–24]. In this review, selective chemical modification reactions in order to obtain amphiphilic PHAs will be discussed.

4. Synthesis of Amphiphilic PHAs

Selective chemical modification of the PHAs involves functionalization and grafting reactions of the PHAs. Hydrophilic groups such as hydroxyl, carboxyl, amine, glycol and sulfonic acid can be introduced into the PHAs by means of functionalization. In grafting reactions, some hydrophilic groups have been attached in the PHA chain to obtain amphiphilic polymer.

4.1. Transesterification. Some ester group(s) of the PHA is exchanged with an alcohol in transesterification process. Transesterification is carried out in melt or in solution. Hydroxylation of the PHBs via chemical modification is usually achieved by the transesterification reactions to obtain diol ended PHB. Transesterification reactions in the melt between poly(ethylene glycol), mPEG, and PHB yield diblock amphiphilic copolymer with a dramatic decrease in molecular weight [25]. Catalyzed transesterification in the melt is used to produce diblock copolymers of poly([*R*]-3-hydroxybutyric acid), PHB, and monomethoxy poly(ethylene glycol), mPEG, in the presence of a catalyst, in a one-step process. The formation of diblocks is accomplished by the nucleophilic attack from the hydroxyl endgroup of the mPEG catalyzed by bis(2-ethylhexanoate) tin.

When the transesterification reaction between PHB and ethylene glycol in diglyme as a solvent is carried out, the telechelic PHB with MW at around 2000 Dalton is obtained [26]. Stannous octanoate as a transesterification catalyst causes the reaction of carboxylic end group and diol, quantitatively. Basically, short chain diol or polyol moiety can rarely renders a hydrophilic character to the longer hydrophobic PHA. Therefore amphiphilic character of the telechelic PHAs and PEGylated PHAs have been stood poor.

Telecehelic PHB obtained by this way can be used in the preparation of the polyester urethanes via diisocyanate chain extension reaction with synthetic aliphatic polyester as soft segment [27, 28]. PHB-g-Poly(ε-caprolactone) (PCL) graft copolyester urethane samples exhibited the elongation at break up to 900%.

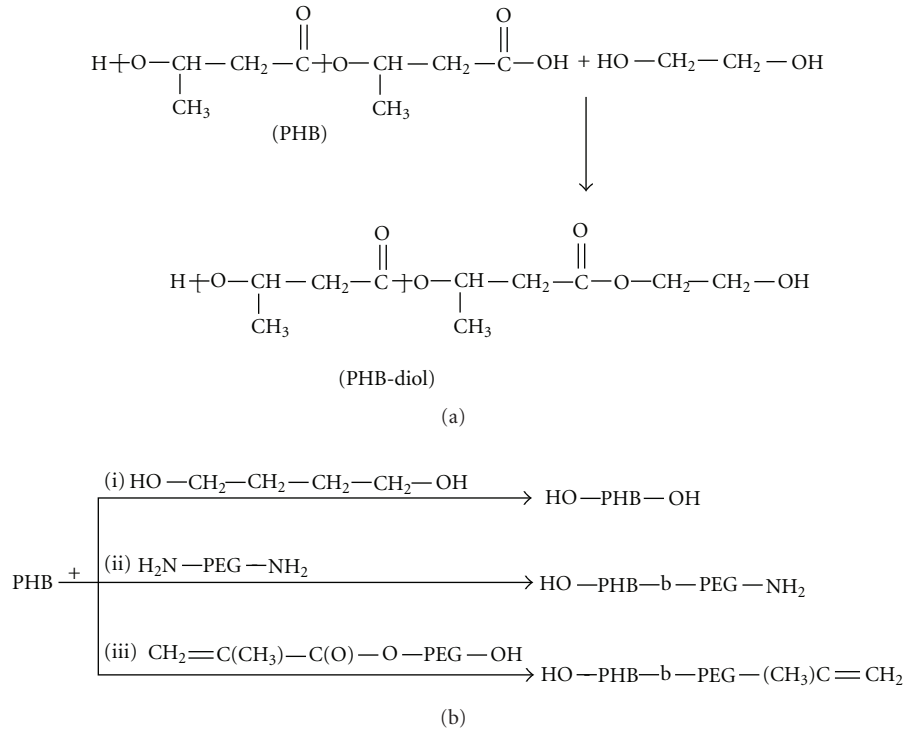

Figure 1: (a) Formation of the diol ended PHB via transesterification in the presence of ethylene glycol. (b) Transesterification reactions of PHB with (i) butane diol, (ii) transamidation with bisaminopropyl ended PEG, and (iii) transesterification reactions of PHB with methacryloyl oxy ethylene glycol in solution.

Two segmented biodegradable poly(ester-urethane) series, based on bacterial PHB as the hard segments, and either PCL or PBA as the soft segments, were easily synthesized by one-step solution polymerizations. Transesterification reaction of PHB with methacryloyl oxy poly(ethylene glycol) (MW: 526), poly(ethylene glycol) bis (2-aminopropyl ether) with MW 1000 and 2000 was achieved to obtain PHB-b-PEG telechelic diblock copolymers [29]. Similarly, telechelic PHB can also be obtained by transesterification with 1,4-butane diol in 1,2-dichloro benzene under reflux conditions. The transesterification reactions can be designed in Figure 1.

4.2. Carboxylation and Hydroxylation of the Pendant Double Bonds. Most used unsaturated PHAs are mclPHAs obtained from unsaturated edible oils and synthetic olefinic substrates. When Pseudomonas oleovorans is grown on unsaturated carbon source such as soybean oily acids, 7-octenoic acid and 10-undecenoic acid, unsaturated PHAs are obtained [30–33]. Figure 2 shows the synthesis of the unsaturated PHAs.

Microbial polyesters containing unsaturated side chains are open the way for chemical modification reactions to prepare PHA derivatives. Pendent double bonds of the poly(3-hydroxy octanoate-co-10-undecenoate), PHOU, can be oxidized to the diol (PHOU-diol) and carboxylic acid (PHOU-COOH). $KMnO_4$ is used as an oxidizing agent. In mild conditions PHOU-diol is obtained [34]. While PHOU was insoluble in a polar solvent, PHOU-diol was soluble in methanol, acetone/water (80/20, v/v), and DMSO, even with 40%–60% of double bonds unconverted, but it was insoluble in nonpolar solvents such as chloroform, THF, acetone. Figure 3 shows the PHOU-diol. The use of $NaHCO_3$ even in hot solution (55°C) resulted mainly in diol groups, not carboxylic groups, while the same reaction at room temperature using $KHCO_3$, led to the conversion of the pendant unsaturated groups to the carboxyl groups [35]. Figure 4 shows the PHOU with pendant carboxyl groups.

Carboxylation of PHOU using OsO_4 as oxidant can be performed with the small decrease in MW after the reaction [36]. The quantitative hydroxylation of pendant vinyl groups of poly(3-hydroxy-10-undecenoate) (PHU) with the use of either the borobicyclononane or the borane–tetrahydrofuran complex is also achieved in high yield [37, 38]. After hydroxylation, the thermal stability and the molecular weight of the hydroxylated PHU showed small decreases; however, full solubility in methanol and almost full solubility in water are achieved [37, 38].

Water wettability of saturated PHAs, poly(3-hydroxy butyrate) (PHB) and poly(3-hydroxy butyrate-co-3-hydroxy hexanoate) (PHBHHx) can also be improved by carboxyl ion implantation. Ion implantation is performed at energy of 150 keV with fluences ranging from 5×10^{12} to 1×10^{15} ions/cm^2. Contact angle measurements are confirmed that the ion implantation improves the water wettability [39].

Epoxidation of the unsaturated polyester with m-chloroperbenzoic acid, as a chemical reagent, yields to

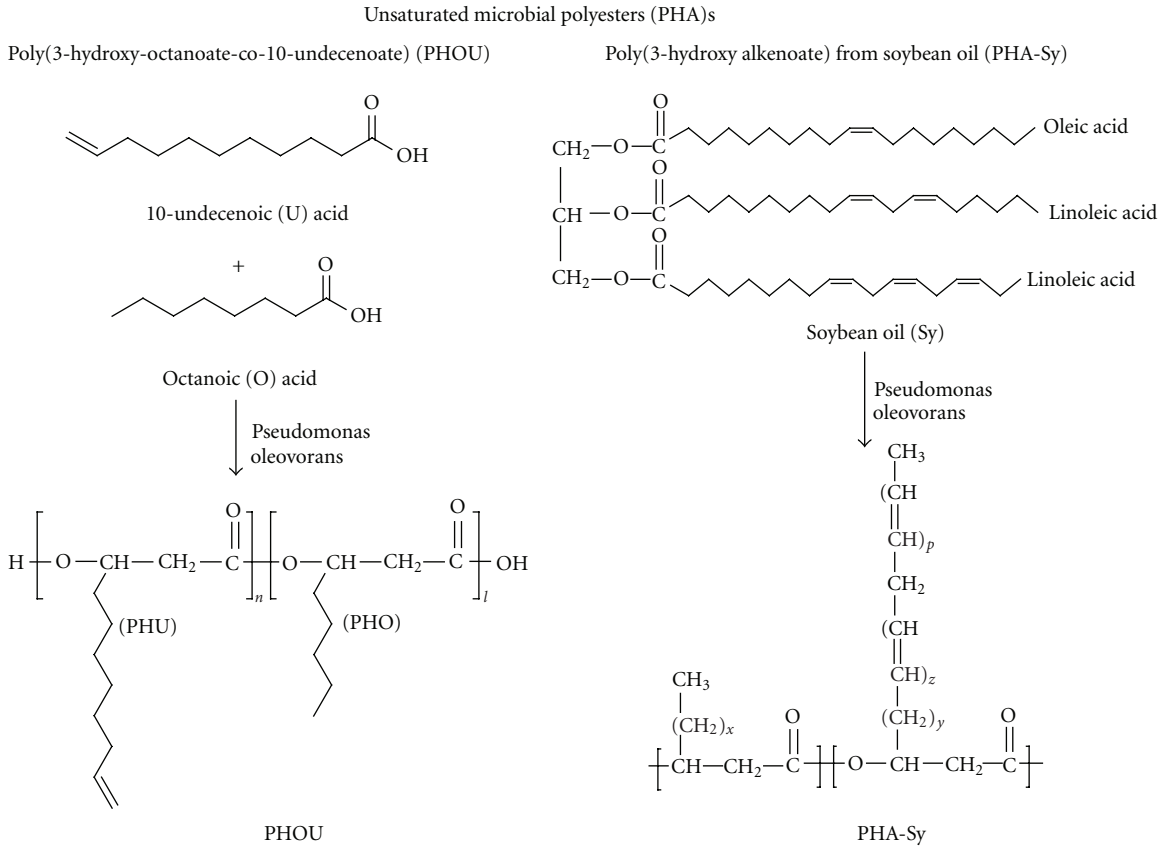

Figure 2: Synthesis of two types of unsaturated PHAs from *Pseudomonas oleovorans* (i) grown on soybean (PHA-Sy) and (ii) 10-undecenoic acid and octanoic acid (PHOU).

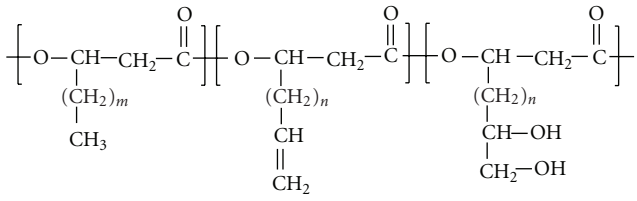

Figure 3: PHOU with pendant hydroxyl groups (PHOU-OH).

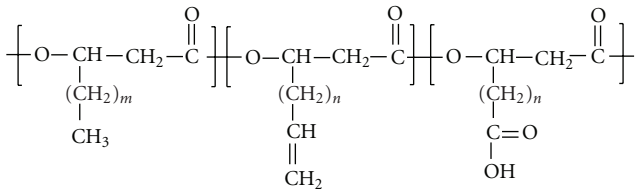

Figure 4: PHOU with pendant carboxylic acids (PHOU-COOH).

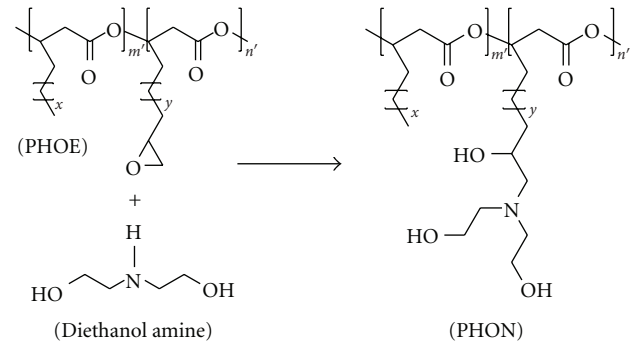

Figure 5: The conversion reaction of epoxidized-PHOU (PHOE) to hydroxylated PHOU in the presence of diethanol amine (PHON).

quantitative conversions of the unsaturated groups into epoxy groups [40]. Primary and secondary amines can be reacted with epoxide groups to yield hydrophilic compounds. Reaction between hexamethylene diamine with epoxidized PHOU provides cross-linked polyester [41].

Enhenced hydrophilicity of the PHOU has recently been achieved by the reaction between epoxidized PHOU and diethanol amine to give highly hydrophilic polyester, PHON [42]. The first reaction involved the transformation of the vinyl-terminated side chains of PHOU to epoxide groups (PHOE). Figure 5 shows the conversion reaction of epoxidized PHOU (PHOE) to hydroxylated PHOU in the presence of diethanol amine.

The successful side chain conversion was further substantiated by the change in solubility when converting PHOU to PHOE to PHON. As the functionalized side chains became more polar, the polymer became soluble in more polar solvents. In this aspect, PHON was soluble in water.

4.3. Quarternization and Sulfonation of the PHAs. Halogenation of the polymers is a versatile method to open the way for further functionalization [29, 43, 44]. Addition of the chlorine and bromine into the double bond is quantitative and halogenated PHAs can be easily obtained by this way [29]. Chlorination is performed by either the addition to double bonds of the unsaturated PHA obtained from soybean oil (PHA-Sy) or substitution reactions with saturated hydrocarbon groups [43, 44]. Chlorination of the sticky, soft PHA-Sy with double bond provides polyester with hard, brittle, and crystalline physical properties depending on the chlorine content. By this way, it is possible to introduce 35 wt% chlorine to the PHA. In case of the chlorinated PHO, glass transition temperature has been shifted to +2°C from −40°C [44]. For further functionalization, quaternization reactions of the chlorinated PHA with triethylamine (or triethanol amine) can be performed. Additionally, aqueous solution of $Na_2S_2O_3 \cdot 5H_2O$ can be reacted with solution of chlorinated PHA (PHA-Cl) in acetone to give sulfonate derivative of the PHO [44].

4.4. Grafting Reactions of the PHAs

4.4.1. Chitosan Grafting. Chemical modifications of chitosan by grafting method are important to prepare multifunctional materials in different fields of application and to improve its chemical, physical, and mechanical properties [45, 46]. Chitosan-g-Poly(3-hydroxy butyrate-co-3-hydroxy valerate) (PHBV) graft copolymer was synthesized and grafting of linoleic acid on chitosan were performed by condensation reaction under vacuum at 90–95°C. Chitosan-g-PHBV graft copolymers exhibit different solubility behavior such as solubility, insolubility, or swelling in 2 wt% acetic acid and in water as a function of degree of substitution of NH_2 while pure chitosan does not swell in water. Chitosan-g-PHBV graft copolymer is shown in Figure 6.

4.4.2. Sugar Grafting. Glycopolymers are emerging as a novel class of neoglycoconjugates useful for biological studies and they are prepared either by copolymerization or grafting methods [47]. Since it has been shown that thiosugars are potent tools in glycobiology, 1-thiomaltose derivatives has been grafted onto PHAs in two ways [48]; the thiol sugar is added to the double bond and the reaction between thiol sugar and bromo end groups of polyester biosynthesized from 11-bromoundecanoic acid [49]. These new grafted polymers are insoluble in dichloromethane and chloroform, but very soluble in *N*,*N*-dimethylformamide and dimethyl sulfoxide, as opposed to their parent PHAs. As expected, modified PHAs are more hydrophilic than their parent compounds.

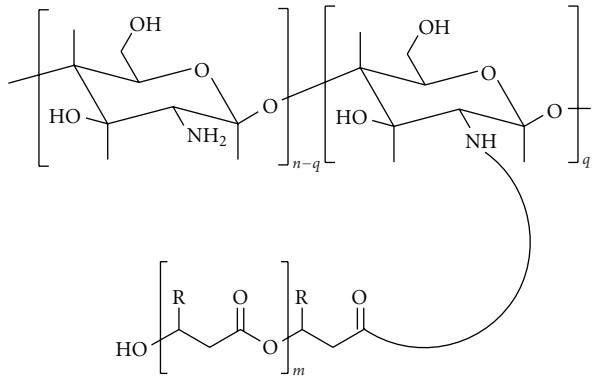

R: - CH_2CH_3
- CH_3 for PHBV
R: - $(CH_2)_2CH_3$
- $(CH_2)_4CH_3$
- $(CH_2)_6CH_3$ for PHO

Figure 6: Chitosan-g-PHBV graft copolymer.

4.4.3. PEG Grafting. Diazo linkaged PEG, a polyazoester synthesized by the reaction of PEG and 4,4′-azobis(4-cyanopentanoyl chloride) creates PEG macroradicals which is easily attack to the double bonds of the unsaturated PHA to obtain the PHA-*g*-PEG cross-linked graft copolymers [50]. PHAs containing double bonds in the side chain (PHA-DB) were obtained by cofeeding *Pseudomonas oleovorans* with a mixture of nonanoic acid and anchovy (hamci) oily acid (in weight ratios of 50/50 and 70/30). PHA-DB was thermally grafted with a [50].

Graft copolymers of the saturated mclPHAs can be synthesized by using macroradicals via H-abstraction from the tertiary carbon of the polyester [51, 52]. Similarily, macroradicals onto the PHAs are induced by the UV irradiation via H-abstraction in the presence of a PEG-macromonomer to prepare PEG-g-PHO graft copolymers [53, 54]. Homogeneous solutions of poly(3-hydroxyoctanoate) (PHO) and the monoacrylate-poly(ethylene glycol) (PEGMA) monomer in chloroform were irradiated with UV light to obtain PEGMA-grafted PHO (PEGMA-*g*-PHO) copolymers. The results of the protein adsorption and platelet adhesion tests show that the blood compatibility was also enhanced by grafting the PEGMA chains. The adsorption of proteins and platelets was increasingly suppressed, as the grafting degree of PEGMA onto PHO increased. Glycerol 1,3-diglycerol diacrylate-grafted poly(3-hydroxyoctanoate) copolymers are also prepared by heating homogeneous solutions of PHO, diacrylate monomer, and benzoyl peroxide initiator [55]. The resulting copolymers have enhanced thermal properties and mechanical strengths. The surfaces and the bulk of the graft copolymers became more hydrophilic as the diglycerol-diacrylate grafting density in the copolymer increased. Many studies have reported that hydrophilic surfaces, such as those of hydro gels and PEG-grafted polymers, suppress protein adsorption and platelet adhesion. The surfaces of this graft copolymers become more hydrophilic with grafted

Table 2: Methods for the synthesis of the amphiphilic PHAs.

PHA	Synthesis	Product	Reference
PHB	Transesterification with mPEG2000 (in melt)	PHB-b-PEG	[25]
PHB	Transesterification with PEG2000 (in solution)	PHB-g-PEG	[29]
PHB	Transesterification with Diethylene glycol (in melt)	PHB-diol	[26]
PHO	UV-irradiation with methacrylated-PEG	PHO-g-PEG	[53]
PHU	UV-irradiation with methacrylated-PEG	PHO-g-PEG	[54]
PHO	Free radical polymerization with acrylate	PHO-g-Poly-glycerol diacrylate	[55]
PHA-un-	Free radical polymerization with saturated polyazoester based on PEG	PHA-g-PEG	[50]
PHOU	Epoxidation and reaction with diethanol amine	PHA with pendant amine side groups	[42]
PHOU	Epoxidation and reaction with hexamethylene diamine	Cross-linked PHOU	[41]
PHB	Condensation with chitosan	PHB-g-chitosan	[45]
PHO	Condensation with chitosan	PHO-chitosan	[46]
PHOU	Hydroxylation of the double bonds	PHOU with pendant-OH	[34, 37, 38]
PHOU	Carboxylation of the double bonds	PHOU with pendant-COOH	[35, 36]
PHB	Urethane formation of PHB and PCL containing dihydroxyl ends	PHB-g-PCL	[27, 28]
PHOU	Thiol addition of thio-maltose to double bonds	PHOU-g-sugar	[48]
PHOU	Esterification of carboxylated PHOU with PEG	PHOU-g- PEG	[56]

diglycerol groups. These surface characteristics make this graft copolymer to prevent protein adsorption and platelet adhesion very effectively. Domenek et al. achieved the amphiphilic copolymer based on PHOU and PEG [56]. Carboxylic acid terminal groups in the side chains are reacted with PEG in the presence of dicyclohexyl carbamate at room temperature. Amphiphilic graft copolymer obtained is soluble in the mixture of H_2O/acetone (80/20) whereas precursor PHOU is not soluble.

As a summary, Table 2 indicates the sum of the chemical modification reactions to obtain amphiphilic PHAs.

5. Conclusion

Microbial polyesters are biocompatible and biodegradable hydrophobic natural thermoplastics. Amphiphilic PHAs from swollen in water to soluble in water are much more desirable in the drug delivery system and tissue engineering. In most attempts to synthesize amphiphilic PHAs, degradation of the polyester chain has been unavoidable. To obtain new amphiphilic PHAs with high molecular weight and their medical applications have been attractive for scientists.

Acronyms

PHA: Poly(3-hydroxy alkanoate)
PEG: Poly(ethylene glycol)
*scl*PHA: Short-chain-length PHA
*mcl*PHA: Medium-chain-length PHA
*lcl*PHA: long-chain-length PHA
PHB: Poly([*R*]-3-hydroxybutyric acid)
mPEG: Monomethoxy poly(ethylene glycol)
PHOU: Poly(3-hydroxy octanoate-co-10-undecenoate)
PHU: Poly(3-hydroxy-10-undecenoate)
PHBHx: Poly(3-hydroxy butyrate-co-3-hydroxy hexanoate)
PHON: Diethanol amin derivative of PHOU
PHOE: Epoxide derivative of PHOU
PHA-Sy: PHA obtained from soybean oil
PHA-Cl: Chlorinated PHA
PHA-DB: Poly(3-hydroxyalkanoate)s containing double bonds in the side chain
PEGMA: Monoacrylate-poly(ethylene glycol)
PHBV: Poly(3-hydroxy butyrate-co-3-hydroxy valerate)

Acknowledgment

This work was financially supported by TUBITAK (Grant no. 108T423) and ZKU Research Fund.

References

[1] R. Langer and D. A. Tirrell, "Designing materials for biology and medicine," *Nature*, vol. 428, no. 6982, pp. 487–492, 2004.

[2] S. Mitragotri and J. Lahann, "Physical approaches to biomaterial design," *Nature Materials*, vol. 8, no. 1, pp. 15–23, 2009.

[3] S. P. Valappil, S. K. Misra, A. Boccaccini, and I. Roy, "Biomedical applications of polyhydroxyalkanoates, an overview of animal testing and in vivo responses," *Expert Review of Medical Devices*, vol. 3, no. 6, pp. 853–868, 2006.

[4] A. J. Anderson and E. A. Dawes, "Occurrence, metabolism, metabolic role, and industrial uses of bacterial polyhydroxyalkanoates," *Microbiological Reviews*, vol. 54, no. 4, pp. 450–472, 1990.

[5] R. W. Lenz and R. H. Marchessault, "Bacterial polyesters: biosynthesis, biodegradable plastics and biotechnology," *Biomacromolecules*, vol. 6, no. 1, pp. 1–8, 2005.

[6] B. Hazer and A. Steinbüchel, "Increased diversification of polyhydroxyalkanoates by modification reactions for industrial and medical applications," *Applied Microbiology and Biotechnology*, vol. 74, no. 1, pp. 1–12, 2007.

[7] K. Sudesh, H. Abe, and Y. Doi, "Synthesis, structure and properties of polyhydroxy alkanoates: biological polyesters," *Progress in Polymer Science*, vol. 25, pp. 1503–1555, 2000.

[8] A. Steinbüchel and B. Füchtenbusch, "Bacterial and other biological systems for polyester production," *Trends in Biotechnology*, vol. 16, no. 10, pp. 419–427, 1998.

[9] D. Y. Kim, W. K. Kim, M. G. Chung, and Y. H. Rhee, "Biosynthesis, modification, and biodegradation of bacterial medium-chain-length polyhydroxyalkanoates," *Journal of Microbiology*, vol. 45, no. 2, pp. 87–97, 2007.

[10] R. H. Marchessault, "Polyhydroxyalkanoate (PHA) History at Syracuse University and Beyond," *Cellulose*, vol. 16, pp. 357–359, 2009.

[11] W. J. Orts, G. A. R. Nobes, J. Kawada, S. Nguyen, G.-E. Yu, and F. Ravenelle, "Poly(hydroxyalkanoates): biorefinery polymers with a whole range of applications. The work of Robert H. Marchessault," *Canadian Journal of Chemistry*, vol. 86, no. 6, pp. 628–640, 2008.

[12] M. Zinn, B. Witholt, and T. Egli, "Occurrence, synthesis and medical application of bacterial polyhydroxyalkanoate," *Advanced Drug Delivery Reviews*, vol. 53, no. 1, pp. 5–21, 2001.

[13] Q. Wu, Y. Wang, and G.-Q. Chen, "Medical application of microbial biopolyesters polyhydroxyalkanoates," *Artificial Cells, Blood Substitutes, and Biotechnology*, vol. 37, no. 1, pp. 1–12, 2009.

[14] K. Ruth, G. de Roo, T. Egli, and Q. Ren, "Identification of two acyl-CoA synthetases from Pseudomonas putida GPo1: one is located at the surface of polyhydroxyalkanoates granules," *Biomacromolecules*, vol. 9, no. 6, pp. 1652–1659, 2008.

[15] A. Steinbuchel and H. E. Valentin, "Diversity of bacterial polyhydroxyalkanoic acids," *FEMS Microbiology Letters*, vol. 128, no. 3, pp. 219–228, 1995.

[16] S. Förster and M. Antonietti, "Amphiphilic block copolymers in structure-controlled nanomaterial hybrids," *Advanced Materials*, vol. 10, no. 3, pp. 195–217, 1998.

[17] N. Hadjichristidis, M. Pitsikalis, S. Pispas, and H. Iatrou, "Polymers with complex architecture by living anionic polymerization," *Chemical Reviews*, vol. 101, no. 12, pp. 3747–3792, 2001.

[18] K. J. Townsend, K. Busse, J. Kressler, and C. Scholz, "Contact angle, WAXS, and SAXS analysis of poly(β-hydroxybutyrate) and poly(ethylene glycol) block copolymers obtained via *Azotobacter vinelandii* UWD," *Biotechnology Progress*, vol. 21, no. 3, pp. 959–964, 2005.

[19] L. J. R. Foster, "Biosynthesis, properties and potential of natural-synthetic hybrids of polyhydroxyalkanoates and polyethylene glycols," *Applied Microbiology and Biotechnology*, vol. 75, no. 6, pp. 1241–1247, 2007.

[20] B. Hazer, "Chemical modification of synthetic and biosynthetic polyesters," in *Biopolymers*, A. Steinbuchel, Ed., vol. 10, chapter 6, pp. 181–208, John Wiley & Sons, Weinheim, Germany, 2003.

[21] S. Ilter, B. Hazer, M. Borcakli, and O. Atici, "Graft copolymerisation of methyl methacrylate onto a bacterial polyester containing unsaturated side chains," *Macromolecular Chemistry and Physics*, vol. 202, no. 11, pp. 2281–2286, 2001.

[22] B. Hazer, "Chemical modification of bacterial polyester," *Current Trends in Polymer Science*, vol. 7, pp. 131–138, 2002.

[23] B. Cakmakli, B. Hazer, and M. Borcakli, "Poly(styrene peroxide) and poly(methyl methacrylate peroxide) for grafting on unsaturated bacterial polyesters," *Macromolecular Bioscience*, vol. 1, no. 8, pp. 348–354, 2001.

[24] B. Hazer, "Poly(β-hydroxynonanoate) and polystyrene or poly(methyl methacrylate) graft copolymers: microstructure characteristics and mechanical and thermal behavior," *Macromolecular Chemistry and Physics*, vol. 197, no. 2, pp. 431–441, 1996.

[25] F. Ravenelle and R. H. Marchessault, "One-step synthesis of amphiphilic diblock copolymers from bacterial poly([R]-3-hydroxybutyric acid)," *Biomacromolecules*, vol. 3, no. 5, pp. 1057–1064, 2002.

[26] T. D. Hirt, P. Neuenschwander, and U. W. Suter, "Telechelic diols from poly[(R)-3-hydroxybutyric acid] and poly[(R)-3-hydroxy butyric acid]-co-[(R)-3-hydroxyvaleric acid]," *Macromolecular Chemistry and Physics*, vol. 197, no. 5, pp. 1609–1614, 1996.

[27] G. R. Saad, "Calorimetric and dielectric study of the segmented biodegradable poly(ester-urethane)s based on bacterial poly[(R)-3-hydroxybutyrate]," *Macromolecular Bioscience*, vol. 1, no. 9, pp. 387–396, 2001.

[28] G. R. Saad, Y. J. Lee, and H. Seliger, "Synthesis and characterization of biodegradable poly(ester-urethanes) based on bacterial poly(R-3-hydroxybutyrate)," *Journal of Applied Polymer Science*, vol. 83, no. 4, pp. 703–718, 2001.

[29] H. Erduranlı, B. Hazer, and M. Borcakli, "Post polymerization of saturated and unsaturated poly(3-hydroxy alkanoate)s," *Macromolecular Symposia*, vol. 269, no. 1, pp. 161–169, 2008.

[30] B. Hazer, O. Torul, M. Borcakli, R. W. Lenz, R. C. Fuller, and S. D. Goodwin, "Bacterial production of polyesters from free fatty acids obtained from natural oils by *Pseudomonas oleovorans*," *Journal of Environmental Polymer Degradation*, vol. 6, no. 2, pp. 109–113, 1998.

[31] R. D. Ashby and T. A. Foglia, "Poly(hydroxyalkanoate) biosynthesis from triglyceride substrates," *Applied Microbiology and Biotechnology*, vol. 49, no. 4, pp. 431–437, 1998.

[32] K. Fritzsche and R. W. Lenz, "Production of unsaturated polyesters by *Pseudomonas oleovorans*," *International Journal of Biological Macromolecules*, vol. 12, no. 2, pp. 85–91, 1990.

[33] Y. B. Kim, R. W. Lenz, and R. C. Fuller, "Poly-3-hydroxyalkanoates containing unsaturated repeating units produced by *Pseudomonas oleovorans*," *Journal of Polymer Science Part A*, vol. 33, pp. 1367–1374, 1995.

[34] M. Y. Lee, W. H. Park, and R. W. Lenz, "Hydrophilic bacterial polyesters modified with pendant hydroxyl groups," *Polymer*, vol. 41, no. 5, pp. 1703–1709, 2000.

[35] M. Y. Lee and W. H. Park, "Preparation of bacterial copolyesters with improved hydrophilicity by carboxylation," *Macromolecular Chemistry and Physics*, vol. 201, no. 18, pp. 2771–2774, 2000.

[36] D. J. Stigers and G. N. Tew, "Poly(3-hydroxyalkanoate)s functionalized with carboxylic acid groups in the side chain," *Biomacromolecules*, vol. 4, no. 2, pp. 193–195, 2003.

[37] M. S. Eroglu, B. Hazer, T. Ozturk, and T. Caykara, "Hydroxylation of pendant vinyl groups of poly(3-hydroxy undec-10-enoate) in high yield," *Journal of Applied Polymer Science*, vol. 97, no. 5, pp. 2132–2139, 2005.

[38] E. Renard, A. Poux, L. Timbart, V. Langlois, and P. Guérin, "Preparation of a novel artificial bacterial polyester modified with pendant hydroxyl groups," *Biomacromolecules*, vol. 6, no. 2, pp. 891–896, 2005.

[39] D. M. Zhang, F. Z. Cui, Z. S. Luo, Y. B. Lin, K. Zhao, and G. Q. Chen, "Wettability improvement of bacterial polyhydroxyalkanoates via ion implantation," *Surface and Coatings Technology*, vol. 131, pp. 350–354, 2000.

[40] M.-M. Bear, M.-A. Leboucher-Durand, V. Langlois, R. W. Lenz, S. Goodwin, and P. Guerin, "Bacterial poly-3-hydroxyalkenoates with epoxy groups in the side chains," *Reactive and Functional Polymers*, vol. 34, no. 1, pp. 65–77, 1997.

[41] M. Y. Lee, S. Y. Cha, and W. H. Park, "Crosslinking of microbial copolyesters with pendant epoxide groups by diamine," *Polymer*, vol. 40, no. 13, pp. 3787–3793, 1999.

[42] J. Sparks and C. Scholz, "Synthesis and characterization of a cationic Poly(β-hydroxyalkanoate)," *Biomacromolecules*, vol. 9, no. 8, pp. 2091–2096, 2008.

[43] A. H. Arkin, B. Hazer, and M. Borcakli, "Chlorination of poly(3-hydroxy alkanoates) containing unsaturated side chains," *Macromolecules*, vol. 33, no. 9, pp. 3219–3223, 2000.

[44] A. H. Arkin and B. Hazer, "Chemical modification of chlorinated microbial polyesters," *Biomacromolecules*, vol. 3, no. 6, pp. 1327–1335, 2002.

[45] G. Yu, F. G. Morin, G. A. R. Nobes, and R. H. Marchessault, "Degree of acetylation of chitin and extent of grafting PHB on chitosan determined by solid state 15N NMR," *Macromolecules*, vol. 32, no. 2, pp. 518–520, 1999.

[46] H. Arslan, B. Hazer, and S. C. Yoon, "Grafting of poly(3-hydroxyalkanoate) and linoleic acid onto chitosan," *Journal of Applied Polymer Science*, vol. 103, no. 1, pp. 81–89, 2007.

[47] S. Muthukrishnan, G. Jutz, X. André, H. Mori, and A. H. E. Müller, "Synthesis of hyperbranched glycopolymers via self-condensing atom transfer radical copolymerization of a sugar-carrying acrylate," *Macromolecules*, vol. 38, no. 1, pp. 9–18, 2005.

[48] M. Constantin, C. I. Simionescu, A. Carpov, E. Samain, and H. Driguez, "Chemical modification of poly(hydroxyalkanoates). Copolymers bearing pendant sugars," *Macromolecular Rapid Communications*, vol. 20, no. 2, pp. 91–94, 1999.

[49] Y. B. Kim, R. W. Lenz, and R. C. Fuller, "Poly(β-hydroxyalkanoate) copolymers containing brominated repeating units produced by *Pseudomonas oleovorans*," *Macromolecules*, vol. 25, no. 7, pp. 1852–1857, 1992.

[50] B. Hazer, R. W. Lenz, B. Çakmaklı, M. Borcaklı, and H. Koçer, "Preparation of poly(ethylene glycol) grafted poly(3-hydroxyalkanoate) networks," *Macromolecular Chemistry and Physics*, vol. 200, no. 8, pp. 1903–1907, 1999.

[51] B. Hazer, "Poly(β-hydroxynonanoate) and polystyrene or poly(methyl methacrylate) graft copolymers: microstructure characteristics and mechanical and thermal behavior," *Macromolecular Chemistry and Physics*, vol. 197, no. 2, pp. 431–441, 1996.

[52] S. Ilter, B. Hazer, M. Borcakli, and O. Atici, "Graft copolymerisation of methyl methacrylate onto a bacterial polyester containing unsaturated side chains," *Macromolecular Chemistry and Physics*, vol. 202, no. 11, pp. 2281–2286, 2001.

[53] H. W. Kim, C. W. Chung, and Y. H. Rhee, "UV-induced graft copolymerization of monoacrylate-poly(ethylene glycol) onto poly(3-hydroxyoctanoate) to reduce protein adsorption and platelet adhesion," *International Journal of Biological Macromolecules*, vol. 35, no. 1-2, pp. 47–53, 2005.

[54] C. W. Chung, H. W. Kim, Y. B. Kim, and Y. H. Rhee, "Poly(ethylene glycol)-grafted poly(3-hydroxyundecenoate) networks for enhanced blood compatibility," *International Journal of Biological Macromolecules*, vol. 32, no. 1-2, pp. 17–22, 2003.

[55] H. W. Kim, M. G. Chung, Y. B. Kim, and Y. H. Rhee, "Graft copolymerization of glycerol 1,3-diglycerolate diacrylate onto poly(3-hydroxyoctanoate) to improve physical properties and biocompatibility," *International Journal of Biological Macromolecules*, vol. 43, no. 3, pp. 307–313, 2008.

[56] S. Domenek, V. Langlois, and E. Renard, "Bacterial polyesters grafted with poly(ethylene glycol): behaviour in aqueous media," *Polymer Degradation and Stability*, vol. 92, no. 7, pp. 1384–1392, 2007.

Hindawi Publishing Corporation
International Journal of Polymer Science
Volume 2010, Article ID 296094, 22 pages
doi:10.1155/2010/296094

Review Article

Surface Engineered Polymeric Biomaterials with Improved Biocontact Properties

Todorka G. Vladkova

Laboratory for Advanced Materials, Department of Polymer Engineering, University of Chemical Technology and Metallurgy, 8 Kl. Ohridski Boulevard., 1756 Sofia, Bulgaria

Correspondence should be addressed to Todorka G. Vladkova, tgv@uctm.edu

Received 4 August 2009; Revised 24 November 2009; Accepted 31 March 2010

Academic Editor: Shanfeng Wang

We present many examples of surface engineered polymeric biomaterials with nanosize modified layers, controlled protein adsorption, and cellular interactions potentially applicable for tissue and/or blood contacting devices, scaffolds for cell culture and tissue engineering, biosensors, biological microchips as well as approaches to their preparation.

1. Introduction

On many parameters, polymeric materials satisfy the requirements of biomedical applications. However, the last ones are limited in most cases by the nonsufficient biocontact properties of the polymer. Surface engineering creating nanosize layers with controlled chemical composition, topography and roughness, and hydrophilic/hydrophobic balance emerged as a simple, useful, and versatile approach to solve the problem.

From the mid-1900s to the end of the last century, biomaterials were petroleum-derived synthetic polymers designed to be inert in vivo, that is, to perform their function without interacting with the organism [1]. These biomaterials are characterized with exclusively low protein adsorption and weak interactions with blood, living tissues, and cells. Over the past decades, many new synthetic and biologically derived polymers have been studied and applied, altering this paradigm [2, 3]. Now material scientists have shifted toward the design of bioactive materials that integrate with biological molecules or cells and regenerate tissue [4–6]. Biomaterials for regenerative medicine and tissue engineering gain special interests. Tissue engineering is based on cell seeding on a substrate followed by culturing in bioreactor or directly in the human body. The substrate is often a polymeric biomaterial that should stimulate not only the cell attachment and differentiation but also the extra cellular matrix formation and tissue regeneration. Advanced biospecific and biomimetic materials consisting of bioinert environment enriched of ligands for adhesive receptors, usually short amino acid sequences, like Arg-Gly-Asp or carbohydrates and/or functional parts of hormones, enzymes or growth factors, are currently under intense investigation [7, 8].

Limited knowledge about the interface phenomena on the border of the living and nonliving matter, such as protein adsorption and bioadhesion, are the theoretical base for the development of bioinert or bioactive surface engineered biomaterials. The mechanisms of protein adsorption and bioadhesion are a key question in many studies but despite the enormous efforts, they remain not fully understood.

The biological cascade of all nondesirable reactions against biomaterials begins with deposition of proteins. Protein adsorption is the primary event in the biofouling. Secreted by cells, adhesive proteins mediate their interaction with the biomaterial surface. Therefore, many investigations are devoted to studying the adsorption mechanism of single, well-defined proteins or of concurrent adsorption from double and multicomponent systems on different surfaces [9–12]. Because of their versatile nature many proteins can

be adsorbed via many mechanisms when they are in front of complementary surfaces [13], which makes it difficult to control protein adsorption.

Knowing the mechanism of cell/surface interaction is very important for the design of biomaterial surfaces with improved biocontact properties. General theory of bioadhesion does not exist up to now despite the fundamental understanding of its molecular mechanisms can lead to the creation of material surfaces that can reduce or support the cell/biomaterial interface interaction [12, 14]. It is known that different cell types use different mechanisms when attaching to different surfaces and as a rule, cells do not interact with the surface directly but via proteins secreted by them and adsorbed on the surface adhesive, forming their own nonorganized layer [15]. According to a "classical scheme", adhesive factors, like fibronectin and vitronectin are present in the serum adsorbed on the substrate and the adhesion is in fact an interaction with them. This interaction is ligand-receptor because the cells have specialized receptors (integrins) through which they identify the adsorbed adhesive proteins-ligands [16, 17]. Guided by the substrate surface properties, conformational alterations of the adsorbed proteins possibly change their biological behavior [16]. In this context, the initial cellular interactions depend on the surface physicochemical properties such as the surface wettability, charges, heterogeneity, topography, roughness and presence of functional groups [15]. It is not clear why, but it is well-known that some materials with hydrophobic surface adsorb proteins in a way decreasing their native bioactivity [16]. Evidently, the adequate adhesive proteins adsorption is essential for the initial cell adhesion. In addition, it is known that the initial interface interaction between the cells and the contacting biomaterial mimics to some extent the natural adhesive interaction of cells and the extra cellular matrix. However, the cells not only interact with the adsorbed soluble matrix proteins, such as fibronectin and fibrinogen, they also tend to reorganize them in fibrils. This cellular activity depends significantly on different biomaterial surface parameters, such as hydrophilicity, chemical composition and charges [15]. Although the protein adsorption and cell/biomaterial surface interaction mechanisms are not fully understood, the surface physicochemical parameters known to influence these two phenomena could be summarized as follows [9, 12, 14, 15]:

(i) surface free energy and related parameters, hydrophilic/hydrophobic balance, polarity, water contact angle and its hysteresis,

(ii) surface charge and related electrostatic interactions,

(iii) type and mobility of the surface functional groups,

(iv) micro and nanotopography features and surface roughness [14, 18],

(v) thickness, density and adhesion of the modifying layer,

(vi) crystallinity [19].

The shape and size of the biomaterial particles also influence the cell recognition ability and interaction [20].

The effect of surface topography and chemistry on cellular response is of fundamental importance, especially where living systems encounter device surfaces in medical implants, tissue engineering and cell-based sensors. To understand these biological processes on the surfaces, there is a widespread interest in tailored surface-active materials produced by surface chemistry coupled with advanced patterning processes [21].

Most biomolecules have immense recognition power (specific binding) and at the same time demonstrate a tendency to physically adsorb onto solid substrate without specific receptor recognition (nonspecific adsorption). Therefore, to create useful materials for many biotechnology applications, interfaces are required that have both enhanced specific binding and reduced nonspecific binding. Thus, in applications such as sensors, the tailoring of surface chemistry and the use of micro and nanofabrication techniques became an important direction for the production of surfaces with specific binding properties and minimal background interference. Both self-assembled monolayers and polymer brushes have attracted considerable attention as surface-active materials [22].

Different surface engineering approaches to create biomaterials with improved biocontact properties are based on the relationship between the tissues, blood and other living matter contacting material surface properties and the interactions on the interface.

A variety of surface engineering methods is divided by Hoffman [21] into two main groups: physicochemical and biological. Examples of physicochemical methods are the acid etching/oxidation, ionizing irradiation treatments (various cold plasmas, ion or electron beams, and laser), photo-lithography, surface grafting of functional groups [23], based on well-known wet chemistry reactions. Plasma treatment is usually accompanied by so-called "surface reconstruction" tending to turn the surface back in its initial state. Therefore the plasma treatment is usually followed by chemical grafting or/and immobilization of biomolecules [22, 24–29].

Matrix proteins such as collagen and fibronectin, peptides or short peptide sequences such as RGD and GRGD as well as different growth factors are immobilized on the biomaterial surface besides chemical functional groups grafting and topographic features creation, to design a support mimicking the natural extra cellular matrix-specific features or functions [30–35]. This is the essence of the biological methods group including also simple physical preadsorption of proteins, peptides and/or growth factors, enzymes immobilization, and cell preseeding.

For a long time our research group has been developing polymer surfaces with controlled protein adsorption and initial cellular interactions potentially applicable in blood and/or tissue contacting devices, scaffolds for cell culture, and patterning of proteins. We present here examples of such biomaterials as well as their preparation approaches including some results from our investigations.

2. Bioinert Biomaterials

The early stage of surface engineering is devoted mainly to bioinert material surfaces design, that is, such that do not cause any undesirable reactions, (foreign-body or inflammatory reaction, encapsulation, thrombi formation and blood coagulation) when in contact with living matter (tissue, cells, blood) inside or outside the human body. Such surfaces are still of interest for a variety of blood and/or tissue contacting devices, intraocular lenses, patterned supports for tissue engineering, micro fluidic devices, and biosensors. Most of them have been designed on the concept of creatinng low-adhesion and protein-repellent surfaces that have weak interactions with cells.

Long ago, Ykada et al. [36] theoretically predicted that there are two possibilities for the work of adhesion of polymer surface in aqueous media to approach to zero, that is, to be nonadhesive: one is to be super hydrophilic, that is water-like with water contact angle, θ approaching to 0 and the other is to be strong hydrophobic with surface tension, γ approaching to 0. This is the starting point in the development of strong hydrophilic or strong hydrophobic low-adhesion, protein-repellent biomaterials and biofouling release surfaces.

The creation of hydrophilic low-adhesive surfaces is relatively easy and the water-soluble (biocompatible) polymers immobilization on the surface is one of the possibilities. Such polymers could strongly adsorb water and the presence of high water content on the surface have been accepted as potential advance of the biomaterial regarding its similarity to the living matter and especially for providing minimal interface tension in contact with blood that can reduce the protein adsorption and cells adhesion [25, 37–39]. A variety of polymer surfaces: hydrophilic poly(ether urethane), sulphated polyethylene (PE), hydroxyethyl methacrylate and other hydrogel-coated surfaces [9, 40, 41] have been designed to reduce protein, cell and bacterial adsorption at interfaces with biological tissues. Among them, PEG-coated surfaces confers protein and cell resistance with considerable success [42, 43]. A comparative ESCA study of the protein adsorption on different strong hydrophilic surfaces: positively charged (*N*-vinyl-pyrrolidone, NVP), negatively charged (Acrylic Acid, AA) and neutral (polyethylene glycol, PEG) clearly demonstrate the advantages of the neutral, strongly hydrophilic surfaces [44]. As it is seen from Table 1, the nitrogen content, originating from adsorbed BSA, is one order (and even more) lower on all PEG coated surfaces as compared to NVP- or AA- coated hydrophilic surfaces or to noncoated sulphated PE (PE-SO_3H) and polyvinylchloride (PVC) surfaces. The results of ellipsometry measurements of the protein adsorption [45, 46] are similar. Therefore, attempts to PEG immobilized surfaces preparation have been made later by many researchers using different chemical and plasma chemical methods including hydrogel formation on the surface.

Photo-polymerized or photo-crosslinked coatings are one of the most popular. Such can be prepared by polymerization in situ of deposited on a substrate photo-reactive PEG resin. PEG acrylates or methacrylates are suitable for free radical polymerization, initiated by photo-initiators like benzophenones and thioxanthones [9, 45]. A pioneer work [43, 45] describes a brush-like surface coating using monofunctional PEG-acrylates and a two-step UV polymerization to concentrate PEG chains on different polymer surfaces. The principle sketch of the two-step procedure for the photo-curing of a PEG-acrylate layer for enhancement of surface EO groups' density is presented in Figure 1. The two-step procedure includes precuring at low UV dosage to obtain a gel-like low cross-linked PEG coating with high mobility and yet low water solubility. The following exposure in water leads to migration of polar EO groups to the water interface. Finally, the layer is subjected to a high UV dosage. The structural features of these PEG hydrogel coatings are presented in Figure 2. The two-step procedure enhances the EO content at the interface of about twice. Strong hydrophilic (water contact angle $<10^\circ$) protein repellent surfaces (protein adsorption below 0.05 mg/m^2) could be prepared in this way on different polymers: PE, polyvinyl chloride, polystyrene, natural rubber, and polydimethyl siloxane [47–52]. R. Bischoff and G. Bischoff represent PEG hydrogel covering of polysiloxane tubing and tracheal prostheses preceded by plasma treatment [53]. Thin hydrogel formation by inferter-based photo-polymerization of dithiocarbamylated PEGs under UV irradiation or photo-polymerization has been reported by Lee et al. [54], Known and Matsuda [55] and Hahn et al. [56] aimed at photo-litographic patterning. Sequential formation of covalently bonded hydrogel multilayers thorough surface initiated photo-polymerization by using polymerizable PEG monoacrylates is described by Kizilel et al. [57].

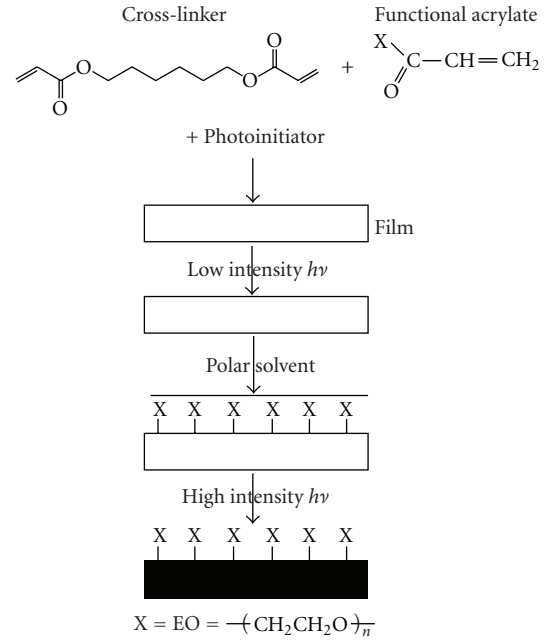

Figure 1: Two-step procedure for the photo-curing of a PEG-acrylate layer for enhancement of the surface density of EO groups [50].

Table 1: Cross-section corrected intensities of characteristic functional groups for various hydrophilic photo-polymeric films: N-vinylpyrrolidone (NVP), acrylic acid (AA) or polyethylene glycol mono-acrylates (PEG) on PE-OSO_3H and PVC after adsorption of bovine serum albumin (BSA).

C−O−/−CH_2−		−COO−/−CH_2−	O(1s)/−CH_2−	N/−CH_2−	N^+/−CH_2−	Cl(2p)/−CH_2−	I-$_{CH2}$- ($cs^{-1}eV^{-1}$)
PE-OSO_3H	0.57	0.27	0.45	0.15	0.04		2706
NVP	0.84	0.29	1.13	0.17	0.11		1040
AA	1.29	0.38	1.18	0.15	0.15		1062
PEG550	1.08	0.28	1.39	0.04	0.02		1402
PEG1900	2.06	0.46	1.47	0.03	0.01		1145
PEG5000	1.81	0.30	1.23	0.03	>0.01		1226
TMP$(EO)_{20}$	2.32	0.25	1.55	0.06	>0.01		1086
PVC	0.72	0.21	0.41	0.13	0.04	0.23	1693
PEG550	0.80	0.20	0.64	0.09	0.02	0.18	1600
PEG1900	1.32	0.24	0.80	0.04	0.02	0.18	1332
PEG5000	2.20	0.30	1.35		0.03	0.11	1051
TMP$(EO)_{20}$	0.76	0.19	0.55	0.11	0.04	0.11	1694

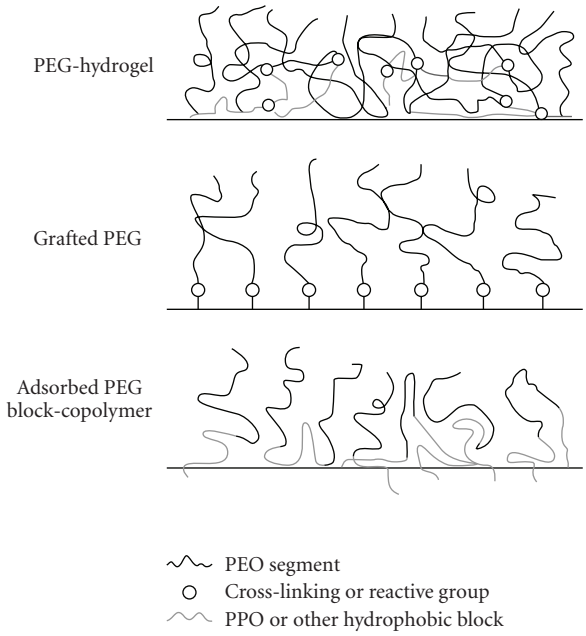

Figure 2: Schematic drawing that shows the structural features of PEG layers obtained by different coating: photo-polymerization, grafting and adsorption [50].

Ito et al. [58] performs photo-crosslinking immobilization of PEG on different surfaces and study subsequent interactions with proteins and cells, expecting that the hydrated nonionic surface would reduce the interaction with them. Photo-crosslinking immobilization is generally useful for the preparation of micropatterned surfaces because it uses a dry process. These researchers prepare photo-reactive PEG and carry out surface modification in the absence or in presence of a micropatterned mask. To assess nonspecific protein adsorption on the micro patterned surface, they adsorb horse radish peroxidase (HRP)-conjugated proteins and confirm a reduced protein adsorption by vanishingly small staining of HRP substrates on the immobilized regions. COS-7 cells have been cultured on the micropatterned surface. The cells do not adhere to the PEG-coated regions. In conclusion, photo-reactive PEG immobilized on various surfaces tends to reduce interaction with proteins and cells.

Chemical immobilization or grafting is another approach to create bioinert polymeric surfaces using suitable chemically reactive monomers such as hexaethylmetacrylate (HEMA), acrylic acid (AA), and PEG, among which PEG is most widely used. If the substrate surface is chemically reactive, the chemical immobilization or grafting can be performed directly. Otherwise, surface preactivation is necessary prior to the chemical immobilization or grafting, employing some wet chemistry methods to oxidize the surface or to introduce surface amino- or other functional groups, or ionizing irradiation using plasma, laser, and ion-beam.

A number of methods for covalent attachment of PEG to different polymer surfaces are known, requiring the employment of functionalized PEG (with derivative terminal OH groups), able to interact with a functionalized substrate surface. In case of strong hydrophobic and/or chemically inert polymers, surface preactivation is necessary by ionizing irradiation (plasma treatment, ion beam, laser, and HUV) or wet chemistry prior to the grafting the functionalized PEG. Figure 3 shows schematically the coupling procedure of PEG-aldehyde by Schiff base reaction with surface -NH_2 groups as an example and Figure 2 shows the structural model of the PEG surface. This reaction is convenient for use in aqueous media where it could be driven to completion by addition of $NaCNBH_3$, acting as a selective reducing agent for the imine product –CH=N– in presence of aldehyde. In order to increase the surface density of PEG chains, the immobilization reaction can be performed under solution conditions close to the cloud point when the repulsion between the PEG chains is small. To induce clouding at lower reaction temperatures, "salting out" with potassium sulfate can be performed. PEG-aldehyde and PEG-epoxide grafting at optimal reaction conditions leads to

the formation of surfaces with very low protein adsorption—below 0.05 mg/m^2 (by ellipsometry) [45, 50, 59].

Feng et al. [60] and Schlapak et al. [61] utilize PEG-amines for coupling with poly(N-hydroxysuccinimidil methacrylate) and Patel et al. [62] for coupling with silanized glass slides bearing aldehyde groups. Li et al. [63] graft living poly(ethylene oxide) to chloromethylated and crosslinked polystyrene and polypropylene substrates through the reaction of alkoxide with chloromethyl group.

Aldehyde groups bearing silanised surfaces could be grafted by NH_2-terminated PEG and on the other hand OH-containing surfaces can be immobilized with PEG-silanes. The second approach is used by Popat et al. [64], Piehler et al. [65] and Xu et al. [66] to improve the biocompatibility of nanoporous materials, biosensors and poly(acrylonitrile-*co*-maleic acid) asymmetric membranes, respectively. Groll et al. [67] prepare and characterize ultrathin coatings from isocyanate-terminated star PEG prepolymers. To interrupt platelet adhesion, Choi et al. [68] and Xu et al. [69] immobilize PEG derivatives on poly(acrylonitrile-*co*-maleic acid) and polyurethane respectively.

Ko et al. [70], Sebra et al. [71] and Beyer et al. [72] immobilize PEG or its sulphonate onto preoxidized in ozone polymer surfaces. Acrylamide-coated surfaces have been created also by radical graft copolymerization on preoxidized in UV ozone plasma generator [73].

Goda et al. [74] prepare biofouling poly(dimethyl siloxane) (PDMS) with excellent surface hydrophilicity and good oxygen permeability by surface initiated radical graft photo polymerization of 2-metacryloil-oxiethyl-phosphatydil cholin (MPC)—biomimetic synthetic phospholipid polymer, containing phosphatydilcholin groups.

Quasi-irreversible adsorption opens another way to PEG and other molecules of interest, immobilization on different surfaces. High-molecular-weight copolymers of PEG or other molecules can be adsorbed irreversibly, attaching at multiple adsorption sites. Although the free energy of adsorption for each side may be relatively small, the attachment of a molecule to several sides leads to a multiplication effect, so that the total free energy of adsorption of a polymer becomes quite large. For this reason, polymers tend to be adsorbed very strongly in many cases. One approach to achieving firmly attached PEG coatings at negatively charged surfaces is to physically adsorb a graft copolymer of PEG and polycation such as polyethylene imine (PEI), for example. Their structural features are shown in Figure 3 and they also demonstrate very low protein adsorption (below 0.05 mg/m^2) [75].

Dextran has recently been investigated as an alternative to PEG for low protein-binding, cell-resistant coatings on biomaterial surfaces [76]. Although antifouling properties of surface-grafted dextran and PEG are quite similar, the multivalent properties of dextran are advantageous when high-density surface immobilization of biologically active molecules to low protein-binding surface coatings is desired. The preferred methods of dextran immobilization for biomaterial applications should be simple with minimal toxicity. In this report, a method is described for covalent immobilization of dextran to material surfaces, which involves low residual toxicity reagents in mild aqueous conditions. With dextran-based surface coatings, it will be possible to develop well-defined surface modifications for better performance of long-term biomaterial implants.

Thanawala and Chaudhury [77] use acrylamid perfluoroether to create high hydrophobicity and antiadhesive properties of polymeric biomaterials.

The existing surface engineering strategies often require the presence of specific surface functional groups and extensive optimization, and they have limited capacity to be used for modification of variety materials. Thus, there is an ongoing need for versatile immobilization strategies that are capable of robustly anchoring not only PEG but also other antifouling polymers onto variety of medically relevant material surfaces or to create other types bioinert surfaces. Ober et al. [78–82] investigate different possibilities for creating low-energy low-adhesive nonbiofouling surfaces using mainly fluorine containing co-polymers.

Various irradiation methods, and especially both cold plasma treatment and coating are widely used for preactivation of different polymer surfaces with a creation of desired for following chemical coupling surface functionality as well as for creation of thin layers with altered hydrophilic/hydrophobic balance, chemical composition or topography and structuring. Using plasma of different gases and optimizing the operation conditions it is possible to input different functional groups on the surface or to create thin surface coating with varied properties. Figure 4 shows a simple sketch of the chemical composition of different radio frequency (RF) plasma discharge deposited films, based on the results from X-ray photoelectron spectroscopy (XPS). Comparative study of such plasma deposited films [83–85] indicate that both, strong hydrophobic silicon and strong hydrophilic PEG surfaces is characterized by very low protein adsorption, weak complement system activation and low cell and platelet adhesion that is in a compliance with the prediction of Ykada et al. [36].

Sioshansi et al. [86, 87] find that the argon ion implantation of the polymer surface reduces significantly the friction and biofouling of the catheters. The thrombogenicity and endothelial cells adhesion onto artificial vascular grafts could be also controlled by argon ion implantation [88].

Husein et al. [89, 90] establish that the ion implantation on polysiloxane surface from plasma source leads to an increase of the surface silanol groups similar to that when the same polymer is plasma or argon ion beam treated. Uncustomary differences in the cell sensitivity to similar on chemical composition polysiloxane surfaces, obtained by different irradiation methods are observed by some researchers [91] attributed to differences in the surface energy, especial electron structure and the corresponding electrical properties of the surface layer.

Bhushan et al. [92] prepare (by gas-phase deposition) ultra thin fluorosilane films to control the biomaterial surface hydrophobicity and to reduce or prevent the protein adsorption and cell interactions, the last ones of critical importance for the work of some biomedical nanodevices.

Surface topography is accepted now as a parameter influencing the wettability and hence the protein adsorption

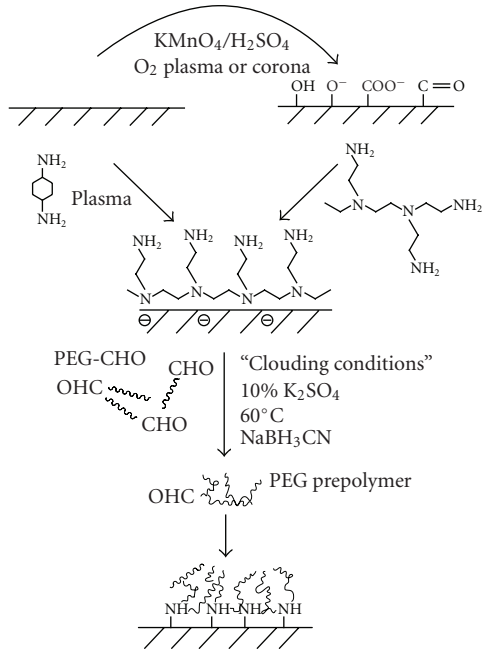

Figure 3: Grafting of PEG by the Schiff base reaction between PEG-CHO and surface-NH2 on polymer surfaces aminated in various ways, for example by treatment in di-amino-cyclohexane (DACH) plasma or by deposition of polyethyleneimine (PEI) on preoxidated polymer surface [50].

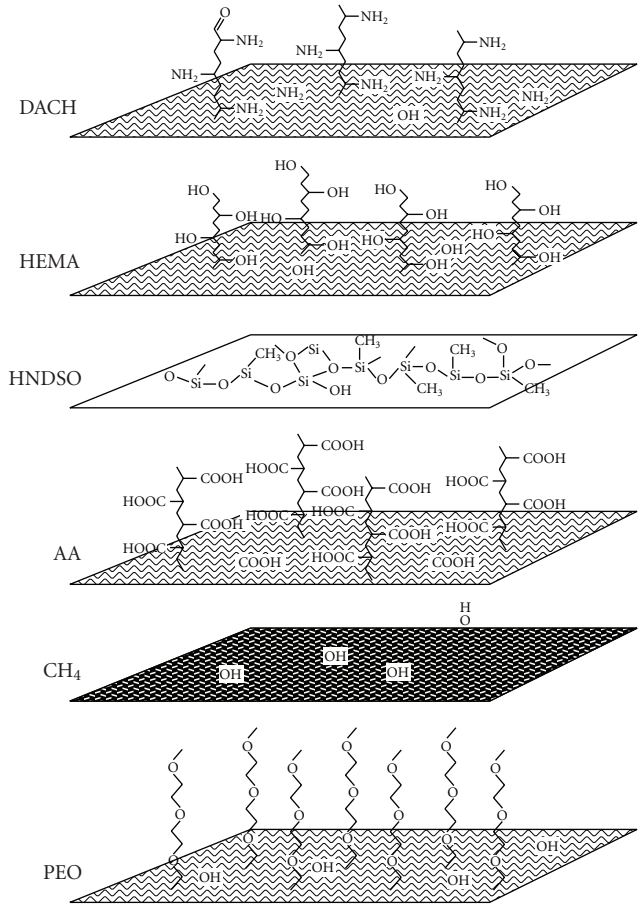

Figure 4: Chemical composition of plasma deposited polymer films: diaminocyclohexane (DACH), hydroxyethylmetacrylate (HEMA), hexamethyldisiloxane (HMDS), acrylic acid (AA), methane (CH_4) and polyethylene oxide (PEO) [50].

and biocontact properties of the biomaterials. Sear et al. [93] study surface texturing and collagen coating of biomaterials in respect to fibrosis inhibition and demonstrate that the biomaterial surface texturing is as important as the matrix proteins in the reduction of fibrosis and inflammatory reactions. Some types of surface texture almost eliminate the fibrous capsules formation whereas other inhibits their collaps [94].

3. Surface Engineered Biomaterials for Blood-Contacting Devices

The surface design of biomaterials for blood-contacting devices is of special interest and different approaches to creation of such with improved thrombo-resistance are described in a number of reviews [95, 96]. Different concepts are employed in the creation of biomaterials with improved blood contacting properties: physicochemical (zero critical surface tension or interfacial-free energy), micro heterogeneous surfaces (polymers with micro phase separated structure and segmented polyurethanes), simulation of blood vessel properties (surfaces with hydrophilic nature and high mobility, negatively charged surfaces), utilization of biologically active molecules (sustained release of heparin; heparinized surfaces), and biomembrane-like surfaces composed of polymer and phospholipids. However, the regulation of blood-biomaterial surface interaction is difficult and the many researches based on the abovementioned concepts have partial success.

It is experimentally established that an increase in the surface hydrophilicity decreases the cell adhesion. However, low cell adhesion does not certainly mean prevention of the biological activation. Some researchers [9, 97, 98] have established low platelet adhesion to strong polar surfaces and high thrombin activation and coagulation.

Most cells have negatively charged surfaces and therefore their electrostatic attraction or repulsion is of importance [9, 99–101]. Cell proliferation is also influenced by the biomaterial surface charge and hydrophilic/hydrophobic balance [102].

Biomaterials with micro-domain surfaces on which adsorbed proteins are able to self-organize accordingly the surface micro heterogeneity are another group bioinert biomaterials. It is demonstrated that the low-trombogeneity of block co-polymers of the type ABA with hydrophilic/hydrophobic micro-domain structure is due to a significant oppress of adhering platelets activation [103–106]. Typical representative of this group are the segmented poly(ether urethanes) [107].

Low platelet adhesion has been found on acrylamid or other hydrogel coatings as well as on collagen coatings

onto corona preactivated polymer surfaces, reducing fibrosis around the biomaterial implants as proved at experiments with animals in vivo [108–111].

Mirzadeh et al. [112–118] create super-hydrophobic polymer surfaces by laser treatment and turn them into hydrophilic ones grafting hexamethylacrylate (HEMA) after their preactivation by CO_2-pulse laser treatment. The data from in vitro investigations demonstrate significantly reduced platelet adhesion and aggregation on the two type modified surfaces but the best regarding the blood compatibility appears to be the super-hydrophobic one.

Regarding blood compatible materials, heparinized surfaces seem to be one of the most promising approaches and a number of ways to surface immobilization of heparin have been described [9, 119]. Heparin, which together with other sulphated gluco-amino-clucans naturally exists on the intra vascular endothelial cells, is a potent anticoagulant. Although graphitic carbon has been known and used as a biomaterial for a long time, the excellent biocompatibility of diamond-like carbon (DLC) films has been addressed only in a few cases. Steffen et al. [120] anticipate the combination of bioinert DLC films and surface immobilized bioactive biomolecules with antithrombogenic properties, such as the polysaccharide heparin, as a straightforward concept to optimize haemocompatibility of a wide variety of materials (vascular grafts, etc.), this strategy has been applied at polytetrafluorethylene (PTFE), poly(dimethyl siloxane) (PDMS), and polystyrene (PS). The DLC films were deposited on polymer surface by an energetic acetylene plasma beam and subsequently exposed to ammonia plasma before heparin was covalently coupled to such functionalized surfaces by an end-point attachment method. Ion-beam radiation of siloxane rubber at relatively high energy (50–150 keV) alters its surface chemical composition and wettability, leading to lower thrombus formation on the ion implanted haemodialysis catheters, proved in vivo experiments with animals [121–124]. Many basic concepts for development of blood compatible surface engineered polymeric biomaterials are described in the literature but the perfect nonthrombogenic material has never been obtained. The future trend is toward a combination of these concepts and hybridization of artificial materials and biological molecules.

4. Bioactive Biomaterials

Bioactivity is a necessary attribute of the current biomaterials for in growing implants, some biosensors, tissue engineering and regenerative medicine. The bioactive biomaterials establish specific interactions in contact with living matter (tissue, blood, cells) and mimic some human functions. They are actively interacting and integrating with their biological environment [125].

The principal goal of the regenerative medicine is to promote tissue regeneration and healing after injury or disease, that can be achieved through a delivery of cells and/or factors in tissue engineered scaffolds designed to provide a biomimetic microenvironment conductive to cell adhesion, proliferation, differentiation, and host tissue integration [126, 127].

Currently, most scaffolds provide a three-dimensional environment in which tissue can grow and develop, so that to be able to reproduce the functions of the tissue that it is intended to replace [128, 129]. Now scaffolds are being developed that either mimic the extra cellular matrix or the complete hierarchical structure of the tissue [130]. A variety of natural and synthetic biodegradable or biocompatible polymeric scaffolds is fabricated in a form of solid foam, nanofibrous matrix, microspheres, or hydrogel to provide an optimal microenvironment for cell proliferation, migration, and differentiation and guidance for cellular in-growth from host tissue. The scaffolds are further surface engineered to provide an extracellular matrix mimicking environment for better cell adhesion and tissue in-growth and in addition, to release bioactive molecules, such as growth factors, DNA, or drugs, in a sustained manner to facilitate tissue regeneration [131].

Evidently, the cell/biomaterial interaction is of key importance for all bioactive biomaterials and the knowledge about its mechanism can guide the surface engineering in the development of biomaterials with an optimal bioactivity.

5. Cell/Biomaterial Surface Interaction

The cell/biomaterial interaction is a complicated phenomenon and despite the enormous efforts of many researchers, its mechanism remains not fully understood [12, 15]. It is well-known, that different cell types use different attachment mechanisms to different surfaces but any way the cell attachment is mediated by deposition of adhesive proteins secreted by themselves. The initial interface interaction when cells contact biomaterial surface resemble to some extent the natural adhesive interaction of the cells with their extra cellular matrix. In addition, the cells not only interact with the adsorbed soluble matrix proteins, such as fibronectin and fibrinogen, they also tend to reorganize them in fibrils. This cellular activity depends strongly on the physicochemical properties of the biomaterial surface, such as hydrophylicity [9, 15], steric hindrance, the existence of a "conditioning layer", surface chemical composition and charge, surface topography and roughness [132]. Many chemical functional groups, such as hydroxyl, carbonyl, carboxyl, and amine, are important for the fate modulation of the attached cells [133]. For example, the macrophages ability to form giant multinuclear cells (granular reaction) on some hydrogel surfaces correlates with the presence of some functional groups. The macrophages joining probability decreases in the following row [134]:

$$\begin{aligned} &-\mathrm{N(CH_3)_2} > -\mathrm{OH} > -\mathrm{CONH\text{-}} > -\mathrm{SO_3H} \\ &> -\mathrm{COOH}\,(-\mathrm{COONa}). \end{aligned} \tag{1}$$

Similar interaction hierarchy is observed at cell incubation onto functionalized surfaces at which the cell attachment and growth decrease in the following row [135]

$$-\mathrm{CH_2NH_2} > -\mathrm{CH_2OH} > -\mathrm{CONH_2} > -\mathrm{COOH}. \tag{2}$$

Studying a number of model surfaces Altancov [15] concludes that the hydrophilic surfaces support the cell adhesion and proliferation, cell growth and the organization of the focal adhesion complex delivering the signal via integrin receptors. An optimum interaction with cells usually appears at moderate hydrophilicity (water contact angle of ~50°–65°). The synthesis and organization of fibronectin matrix by cells is better on surfaces bonding weakly fibronectin and other matrix proteins. The conformation of the adsorbed adhesive proteins plays also an important role in the adhesive interaction on strong hydrophilic noncharged surfaces [15, 75]. The shape and size of biomaterial surface structure can to control the cell proliferation and orientation [136].

6. Surface Engineered Biomaterials via Physicochemical Modification

In general, surface properties of implantable biomaterials dictate protein adsorption and behaviors with concomitantly determining of the cellular interactions. In most cases, specific cellular interactions are required for the formation of a desired tissue. A way to promote implant, scaffold and engineered tissue integration is to design the surface chemical composition and topography of the biomaterials to specifically enhance tissue integration [137–142]. The scaffold surface can be functionalized either by physical adsorption or chemical modification [143]. The surface chemical modification employs different organic chemistry reactions, ionizing radiation treatments (plasmas, ion-beams, and laser) and coatings, immobilization of biomolecules or the combinations of different approaches to control the surface characteristics of the biomaterial.

As mentioned above, despite that the reason is not fully understood, the moderate hydrophilic surfaces are preferred by the cells. Therefore, simple hydrophilization of hydrophobic surfaces is one the main approaches to improve their interaction with cells. The adsorbed adhesive proteins conformation, together with the possibility for easy detachment from the hydrophilic substrates [16] seems to be other important factors, because the cells "try" to organise their own matrix on the biomaterial surface [144–146]. The most physicochemical treatments lead in fact to some surface hydrophilization. PS treated with sulphuric acid or in glow discharge plasma, characterises with increased number of charged groups on the surface that improves the attachment and growth of many types of cells [147]. The naturally nonadhesive polymer poly(2-hydroxyethyl metacrylate) (PHEMA) demonstrates improved adhesion and proliferation of endothelial cells after sulphuric acid treatment [148]. RF cold plasma treated poly(ethylene terephthalate) (PET) surface demonstrate an improved attachment and spreading of fibroblasts and mioblasts [149]. PEG-coated surfaces are usually prepared to be protein repellent, antifouling and bioinert. But surprisingly, PEG coatings prepared by quasi-irreversible adsorption of a graft copolymer of poly(ethylene imine) (PEI) and PEG (PEI-PEG) demonstrate an unusually good cellular interaction: cell spreading, proliferation, adhesion, "early" and "late" matrix formation [75, 144]. The PEG coatings prepared in this way are strong hydrophilic (equilibrium water contact angle <10°) and characterize with very low adsorption of HSA, IgG, Fng, Fn, C3 and Cq1 (<0.05 mg/m^2 by ellipsometry) as shown in Table 2. In general, for such surfaces good biocompatibility is expected, in the sense of bioinertness but low cellular interactions. The observed unexpected good interaction with fibroblasts despite the strong hydrophilicity and very low protein adsorption is thought to be due to a specific PEG layer structuring providing an optimal conformational freedom for the protein reorganization [144].

Cold plasma obtained in low-pressure glow discharge has been often used to activate polymer surface, including siloxane membranes [25, 27, 29, 150] for further grafting of suitable monomers like acrylic acid (AA), hydroxyethyl-metacrylate (HEMA), and so forth. aimed at improvement of its interaction with living cells. On the other hand, ion-beam without following grafting [151, 152] is known as other possible way to improve biocontact properties of polysiloxanes [153, 154]. Plasma based Ar^+ beam performed in RF (13, 56 MHz) low-pressure with a serial capacitance can be employed for surface modification of PDMS to combine some advantages of both: ion-beam and plasma treatment, namely the durability of the modifying effect of the ion-beam with the simplicity of the plasma as compared to ion-beam equipment [155]. The presence of a serial capacitance ensures arise of an ion-flow inside the plasma volume directed toward the treated sample and the discharge power vary ensures varied ion-flow density. A partially mineralized surface layer, similar to that obtained after a conventional ion-beam is the result of plasma based Ar^+ beam treatment of PDMS surface as proven by XPS analysis and contact angle measurements [156, 157]. Plasma based Ar^+ beam treatment transforms the initially strong hydrophobic PDMS surface into a durably hydrophilic one, mainly due to raising of the polar component of the surface tension, this effect being most probably due to an enrichment of the modified surface layer with permanent dipoles of a [SiOx]-based network and elimination of the original methyl groups [156]. Such modification is accompanied also with altering of the surface topography and roughness [157] and leads to significant improvement of the initial cell adhesion not only in presence but also in absence of precoated fibronectin [156, 157].

Bearing radicals and hence activating PDMS surface, Ar^+ beam treatment opens a way to further grafting of suitable monomers. The acrylic acid (AA) grafted, in this way preactivated PDMS surface, is moderate hydrophilic (water contact angle of 62–73°, depending on the AA grafting density). The initial adhesion of human fibroblasts to AA grafted surfaces is significantly higher as compared to that on nonmodified PDMS surface but only in presence of precoated fibronectin [156, 157].

Oliveira et al. [158] have developed a new methodology to obtain bioactive coatings on bioinert and biodegradable polymers that are not intrinsically bioactive. Three types of materials have been used as a substrate: high molecular weight PE and two starch-based blends: starch/ethylene vinyl alcohol and starch/cellulose acetate. Blowing agent has been

Table 2: Protein adsorption (mg/m^2) as measured by ellipsometry.

Surface	A_{HSA}	A_{IgG}	A_{Fgn}	A_{Fn}	A_{C3}	A_{C1q}
Silika	0.35	1.10	2.9	1.90	3.10	1.90
PEI/PEG1500	—	<0.05	<0.05	—	—	—
PEI/PEG6000	<0.05	<0.05	<0.05	<0.05	<.05	<0.05
PEI/PEG12500	—	<0.05	<0.05	—	—	—

HAS: human serum albumin; IgG: immunogammaglobulin; Fgn: fibrinogen; Fn: fibronectin; C3: complement component; C1q: complement component.

used to prepare 3D porous architectures. Three type baths have been developed in order to produce the newly proposed auto-catalytic Ca-P coatings.

If the scaffold is bioactive gel-glass or an inorganic/organic nanocomposite, surface OH group will be present because of Si-OH (silanol) bonds, and many polymers also have high surface OH content (e.g., COOH-) that can be functionalized with APTS. Materials with OH groups will therefore attract proteins when implanted in vivo [159].

7. Surface Engineered Biomaterials via Biomolecules Immobilization

Surface modification of implant devices by immobilization of biological molecules is discussed in a number of reviews, for example [160]. In natural environment, cells grow onto substrate consisting different proteins and polysaccharides—extra cellular matrix (ECM). The last one not only provides mechanical support for the cells but also interacts directly with them and influences their growth, migration, morphology and differentiation. Surface modification of synthetic polymers that have suitable mechanical parameters and processability with biofunctional species providing similar to the natural ECM interaction allows combining advances of the synthetic and natural materials and resembling the interactions with specific ECM ligands [161]. To provide a support more closely resembling the natural ECM, in addition to the chemical functional groups, matrix proteins like collagen, fibronectin, and so forth could be immobilized on the synthetic polymeric material surfaces [162, 163]. This is the nature of biomimetic approach, that is, of the group of the biological methods aiming at resembling of some specific structural or functions features of the natural extra cellular micro environment [164]. This group of methods includes simple protein preadsorption, enzymes immobilization, and cell preseeding. However, it is not yet clear which proteins and how they affect the cell response. Interactions between peptides and scaffolds can result in completely different surface chemistry, topography, surface energy and charge. They can also lead to conformational changes in the peptide structure, which is usually undesirable. Proteins are usually adsorbed or bonded onto material surfaces in solution by immersing the material in phosphate buffer saline (PBS) containing proteins [165].

Various strategies have been attempted to immobilize biomolecules or small biological motives onto the surfaces of synthetic biomaterials devoid of active functional groups [166]. Physical adsorption is one of the methods for preparation of surfaces with well-defined properties that do not rely on chemical processing. It utilizes weak nonspecific intermolecular interactions between the surface and peptide species involved such as hydrogen bonding, hydrophobic interactions, Van der Waals forces, and weak valence electron interactions. To obtain biomimetic materials, surfaces can be simply coated with biomimetic peptides or another material possessing active functional groups, for example, poly-L-lysine (PLL) that can be subsequently used to chemically react with oligopeptides. Materials can also be coated with hybrid molecules such as PLL-RGD polymer-peptide molecules, which can be physically adsorbed to material surfaces. While physical adsorption is an effective way to immobilize biomimetic peptides to the surface of materials, coating only provide a transient modification of the material surface. The inability to control the peptide conformation and orientation upon the adsorbing substrate, peptide desorption or wash-off, diffusion kinetics, and inaccessibility to large molecules on the material surfaces are deficiencies of this method. Substances including PLL, collagen and cell adhesive proteins such as fibronectin, laminin or vitronectin have been adsorbed onto the surface of polymeric matrix to promote cell attachment [167, 168].

In order to fabricate biomimetic materials that can withstand long-term survival, a stable immobilization of such biomolecular motives to the substrate surface is critical to maintain the bioactivity and ultimately proper functioning. Substrate-immobilized biomimetic oligopeptides should be able to withstand the contractile forces extended by adhered cells upon the biomaterial surface during initial cellular attachment and resist the internalization by cells [166]. Covalent binding of functional biomolecules is necessary to provide a more stable cell adhesive stratum that can be achieved by direct or indirect chemical immobilization of collagen, gelatin, heparin, hyaluronic acid, short peptide sequences, originating from cell adhesive proteins such as the arginine-glycine-aspartic acid (RGD) or YIGSR, and sugar moieties such as galactose or lactose, have been grafted onto polymer surfaces to modulate cell-matrix interactions [169, 170].

Direct immobilization via chemical methods; however, can be accomplished when surface reactive groups are presented, which is not always the case with certain materials. Plasma-treated surfaces have been used to introduce active functional groups to biomaterial surfaces for direct covalent immobilization of biomolecules. Plasma treatments under a wide range of reacting gas types (ammonia, nitrogen, hydrogen, oxygen, and ozone) have been employed to be introduced various functional groups (e.g., carboxyl,

hydroxyl, carbonyl, ether, peroxide, and amine) of material surface. Karkhaneh et al. [171] modify the chemically inert PDMS simultaneously with acrylic acid (AA) and 2-hydroxyethyl methacrylate (HEMA) employing so-called "two-step plasma treatment", followed by collagen immobilization and study the cellular response to the modified surfaces. Such surface design significantly increases the number of the adhered and proliferated cells.

In plasma-induced graft polymerization, material surface is bombarded with energetic gaseous species (ions, electrons, free radicals, and low-energy photons) whose energy is transferred and dissipated thorough the solid by a variety of chemical and physical processes. The result is surface functionalization with amine, peroxide, carboxyl, and so forth. groups that can be utilized in a further chemical immobilization of biomolecules via graft polymerization [172–174]. Graft polymerization can result in producing specific surface properties for use in various applications to improve cell adhesion and spreading, to enhance the surface wettability and improve material biocompatibility. Graft polymerization can also be used to treat defined surface areas by using photo-masks or resists [175].

Plasma polymerization can be used to produce surfaces that are either nonadherent or keratinocyte adherent for tissue engineering of skin [176]. This technique is used to produce a background surface coated with octadiene, which is nonadhesive for the majority of cells. Onto this is placed a template of the letters "TONY" coated with acrylic acid. The placed on this surface cells adhere to the acrylic acid-coated surface but failed to adhere to the octadiene-coated surface. Thus, biomaterials can assist the transport and delivery of keratinocytes to a wound bed [177].

The covalent attachment of biologically recognizing molecules to the surface of some biomaterials is hampered by the lack of surface chemical reactivity. To overcome this problem, researchers utilize many different approaches to create functional groups on the surface of biomaterials to support covalent bonding of biological recognition motives, that is, they preactivate biomaterial surface employing different organic chemistry methods or ionizing radiation treatment (cold plasmas of different gases, ion-, laser beams, etc.). For example, Li et al. [178] immobilize RGD peptide fragments on the PDMS surfaces for cell culture indirectly. The immobilization procedure includes preliminary photochemical grafting of NHS-groups on the PDMS surface, followed by RGD bonding to the NHS groups via coupling reaction in presence of bi-functional photo-cross-linker. As compared to other methods for peptides bonding to PDMS, this one is relatively easy, effective and free of organic fouling of the PDMS surface. This approach could be employed for coupling other peptides or proteins to most polymeric materials. Such surface-engineered materials are stable during autoclaving and UV treatment, which make them suitable for repeat use at cell culture.

A liquid phase modification of PDMS micro fluidic channels includes an acid H_2O_2 solution oxidation and following silanation reaction, using pure silane reagents. Two different functional groups, PEG- and amino- have been included in this way on the PDMS surface for the protein adsorption passivation and biomolecules coupling, irrespectively. Biomolecules immobilized biomaterials could be used for cell seeding and incubation [179].

Carbodiimide chemistry is high effective and widely used method to covalently immobilized biomimetic peptides onto various carboxylated biomaterial surfaces via stable amide bonds [180–183]. Carbodiimides are widely used for carboxyl group activation via formation of mediating high reactive O-acylisocarbamide compounds. These active species interact with amine nucleophyls forming stable amide bonds [184]. Unfortunately, this method is not high enough selective. The biomimetic peptides often contain reactive functional groups presenting within the constituent amino acid side chain (e.g., carboxyl and guanidine groups) that leads to unwanted side reactions. *N*-hydroxysuccinimide (NHS) is often used to assist the carbodiimide coupling by forming an active ester intermediate via condensation of surface carboxylic acid groups and NHS. The ester derivative is less prone to hydrolyses, it can be prepared in advance and stored and used as an activated species in situ (e.g., in the presence of the amine nucleophile) without the risks of the unwonted reactions. The NHS-reactive ester intermediate is susceptible to nucleophilic attack by primary amines and results in the formation of stable amide bonds between the biomaterial surface and the N-terminus of the biomimetic peptide.

The immobilization of biomolecules to hydroxyl groups presenting on various biomaterial surfaces can be easily and directly accomplished with the use of highly reactive sulphonyle chlorides. Hydroxyl-containing surfaces can also be preactivated with tresyl chloride [185–187] to yield sulfonated surfaces that can readily undergo nucleophylic attack by primary ammines, thiols and imidasole groups [188–190]. Aminated surfaces can be effectively immobilized with bioactive peptides by reacting the solid surface with homobifunctional linkers, such as glutaraldehyde, disuccinimidil glutarate, or phenylene diisothiocyanate [191–193] via the N-terminus of the peptide. Carboxyl-terminus immobilization can also occur via carbodiimide-mediated immobilization of aminated surfaces. PE covered with cellular matrix proteins and cell-membrane antigens characterises with improved human endothelial cells adhesion and proliferation [194]. Surface functionalized micelles and shell cross-linked nanoparticles are research objective of Wooley group [195–198].

Collagen is a major structural component forming the natural ECM of connective tissue and organs [199]. Surface immobilization of collagen is one of the most established methods for endowing cell adhesive properties to the scaffolds. Poly(lactic acid) (PLA) and PLGA scaffolds chemically grafted with collagen after plasma treatment [200] and PLA scaffolds collagen immobilized by conjugation reaction via grafted poly(methacrylic acid) [201] show enhanced cell adhesion, spreading and growth. Collagen can be deposited on some surfaces from aqueous solution, for example, by using dip-pen nanolithography, to form nanoscale patterns with some control on the assembly for bone tissue growth [202, 203].

The direct covalent bonding of biomolecules to chemically inert polymer surfaces such as PE, PTFE, PDMS, is difficult and surface preactivation, followed by a multistep bonding procedure is necessary. For example, preactivation of PTFE by plasma treatment opens a way to a multistep procedure for peptide immobilization on its surface [204]. Plasma based Ar^+ beam treatment of PDMS also opens a way to its biofunctionalization by a multistep procedure including acrylic acid (AA) grafting and flexible PEG-spacer coupling prior to a collagen immobilization by peptide synthesis reaction. AA grafted PDMS surfaces are reacted with PEG bearing two terminal NH_2-groups. A known peptide synthesis reaction is used for the immobilization of collagen, type I on the AA grafted and PEG spacer coupled samples. Surface chemical composition, wettability, topography and roughness are controlled on every stage of the multistep procedure by XPS analysis, contact angle measurements and atom force microscopy (AFM) observations. Collagen immobilization via flexible spacer improves significantly the cellular interaction on the scarcely adhesive PDMS surface, this effect depending on the length of the PEG chain. This multistep procedure to biofunctionalization of strong hydrophobic chemically inert polymers has a potential to be used whenever need arises to control cellular interaction with the surface, for example cell culture, tissue engineering, biointegrating biomaterials.

Collagen's immunogenicity, due to its various biological functions, limits some applications. Gelatin is a good alternative for collagen because of absence of antigenity and easy of handling at high concentrations. Gelatin immobilized porous scaffolds (by physical entrapment and chemical cross-linking of the gelatin) show significantly enhanced surface properties for attachment, proliferation and osteoblasts ECM deposition [205].

Controlled deposition of ultra thin layers of silk and collagen by exploiting self-assembly can be performed using modified layer-by-layer techniques. Collagen has been deposited in ultra thin film format from aqueous solution based on hydrophobic interactions [206]. In addition, spray coated and deposited collagen films with entrapped drugs or cell growth factors have been reported [207]. An all-aqueous, stepwise deposition process, where control of silk structure locks in the formation of physical cross-links (β-sheets) determining the coating stability is the approach of Chen et al. [208] for silk layer deposition. Layer-by-layer techniques are widely used to form polymer-layered surfaces/structures of biologically functionalized coatings. Usually, the primary driving force in more traditional layer-by-layer assembly is the electrostatic interactions between oppositely charged polyelectrolytes that form interpenetrated layers when the substrate is immersed in an alternating fashion in two solutions. For collagen and silk, the driving force is primarily hydrophobic. The nanoscale silk-layered biomaterials are stable under physiological conditions and support human bone marrow stem cell adhesion, growth, and differentiation, and the incorporation of small or large molecules [209]. Since the ultrathin layers are stabilized by β-sheet physical cross-links, no post processing chemical cross-linking is required to stabilize the materials and the thin films. Silk proteins coating onto different biomaterial substrates for cell culture and tissue engineering applications have been reported, including poly(D,L-lactic acid) films, two- and three-dimensional polyurethane scaffolds, and two-dimensional poly(carbonate-urethane). Methanol treatment of the silk coatings induces the structural transition to the β-sheet and stabilizes the coatings [210–213]. Silk fiber composites have been optimized for surface chemistry and architecture, seeded with human adult bone marrow derived mesenhymal stem cells or fibroblasts, and cultivated in vitro under static or complex mechanical forces in specialized bioreactors to simulate a knee-like environment [214, 215].

Hyaluronic acid (HA) is nonsulfated glycosoaminoglycan that is a major substance of the gel-like component in the extra-cellular matrix of connective tissues. HA is capable of specific cell interaction via the CD44 receptor, which promotes wound healing and induces chondrogenesis. Therefore, HA has been chemically and physically incorporated into various tissue engineering scaffold matrices. HA modified chitosan-gelatin composite scaffolds increase the adhesion of fibroblasts [216] and HA modified PLGA scaffolds support the growth of chondrocytes with maintenance of its original phenotype, showing great potential for cartilage tissue engineering [217].

The sugar galactose has been utilized in scaffolds for liver tissue engineering. Porous scaffolds immobilized with galactose demonstrate improved hepatocyte attachment, viability and metabolic functions such as release of lactate dehydrogenase (LDH), albumin secretion and urea synthesis. Perfusion culture of hepatocytes with galactose-derivatized PLGA scaffolds further improves viability and functional activity of the cells [218, 219].

Immobilization of short chain peptide derivatives from the cell adhesive proteins onto the polymer surface can be a much more effective strategy rather than immobilization of whole protein. The surface immobilization of short peptides has several advantages: higher stability against conformational change, easy controllability of surface density and orientation, more favorable for ligand-receptor interaction and cell adhesion [220–222]. A blend mixture of PLGA and amine-end-functionalized PLGA has been used to fabricate scaffolds allowing surface immobilization of the peptide. Porous PGLA scaffolds exposing functional end groups toward the aqueous medium have been prepared by a gas foaming/salt leaching method, followed by immobilization of GRGDY onto the surface oriented functional groups via a bi-functional cross-linking agent. It has been demonstrated that seeding and cultivation of bone marrow steam cells within GRGDY modified scaffolds lead to enhanced cell adhesion and differentiation into osteoblast-like cells. The same immobilization method has been applied in electrospinning process to fabricate RGD modified PLGA nanofibers [223].

Peptides can also be attached to the surface of silica-based scaffolds by adsorption (hydrogen bonding) or by covalent bonding to create functionalized nanoporous surfaces. Protein attachment is assisted by the large concentration of OH groups (Si-OH) on the surface of sol-gel derived inorganic materials. Certain proteins may not be attached to simple

OH-groups; however the OH-group-covered glass surface can be functionalized with other organic groups that are tailored for specific protein attachment, such as amines (via amine propylthriethoxy silane, APTS) [224, 225].

Many peptide sequences involved in cellular interactions by receptor binding have been identified, including RGD, IKVAV and YIGSR [226]. Among these, the RGD sequence, which was first discovered in fibronectin, is probably one of the best known for use in tissue engineering applications. Immobilization of RGD onto 3D matrices improves their cell adhesive properties. RGD, along with other short peptide sequences such as IKVAV, YIGSR, RNAIAEIIKDI from laminin and HAV from N-cadherin, have been enzymatically incorporated into fibrin matrices to enhance neuritis extension [227, 228].

Smaller biologically active molecules, for example peptides, containing recognizable by cell receptors amino-acid sequences, can be also employed in the design of surfaces with improved cell attachment [229]. Arg-Gly-Asp (RGD) sequence, that is a peptide fragment presented in many cell adhesive proteins and bonding to the integrin receptors of different type cells, is the most intensively studied [230]. Similar peptide fragments have been immobilized onto the PTFE [231], poly(acrylamide) [232], poly(urethanes) [233, 234], poly(carbonate urethane), PEG [235], and other substrates. RGD-sequences adding induce cell adhesion and assists cell spreading and focal adhesion contacts formation on the otherwise nonadhesive polymers [236–238]. RGD coupling and plasma treatment have a significant influence on the mechanical strength of the yarns as well as cell responses in terms of adherence, proliferation, and differentiation [239]. To improve the endothelial cells adhesion and growth onto the surface of PEG modified poly(urethane), Lin et al. [240] graft the cell adhesive peptide Gly-Arg-Gly-Asp (GRGD) photo chemically. The improvement of cell growth appears to be depending on the density of GRGD grafting.

Be Bartolo et al. [241] modify the surface of poly(etherimid sulphone) membrane to mimic the outside cell environment, that is able to cause specific interactions with hepatocytes and hence the cell adhesion and organisation. They perform plasma deposition of acrylic acid followed by covalent immobilisation of RGD peptide via hydrophilic flexible spacer (linear diamino-PEG). The last one bonds covalently with one of its amino-groups to carboxyl group on the surface and with the other amino-group forms peptide bond with carboxyl group of the RGD peptide.

Human tissues such as connective, bone, and cardiac are working under mechanical loading and stress in vivo. Lateef et al. have aimed at an increase of the different cell types adhesion to poly(siloxane) surface at in vitro dynamic bending. Therefore they have developed surface modification method, based on a polysiloxane membrane water plasma treatment for 3-aminopropyl-three-ethoxy silane bonding and the aminosilane to be utilized for covalent GRGDSP-peptide sequence immobilization to the amino-groups by maleinimid cross-linker. Cardiac myoblasts demonstrate improved adhesion to such peptide-coupled membranes [242]. RGD immobilized plasma pretreated PLA scaffolds have demonstrated not only improved adhesion of osteoblast cells but also supported growth and differentiation and enhanced mineralization and formation of bone-like tissues [243, 244].

The natural environment for most cells is tissue extra cellular matrix, which is generally a type of hydrogel. Hydrogels are therefore potential materials for tissue engineering. The surface of hydrogels can be modified to tailor them to specific cell types. For example, the attachment of two extra cellular matrix protein sequences (Arg-Cly-Asp and Pro-His-Ser-Arg-Asn) to PEG hydrogel has been shown to increase osteoblasts cell function and also to decrease extracellular matrix production [245]. The immobilization of other biological molecules, like poly- and oligosaccharides or glycolipids also influences not only the cell attachment but also their function [246].

Chemo-selective legation is a more recent approach to chemical modification of biomaterial surfaces that involves a selective covalent coupling of unique and mutually reactive functional groups under mild conditions. Selected pears of groups are used to couple biomimetic peptides and other bioactive molecules to material surfaces via stable bonds without the needs of activating agent or interfering with other functional groups [247]. These reactions are highly chemoselective and behave like molecular "Velcro" [248]. The high efficiency and selectivity of the amino-oxy-aldehyde coupling reaction has been successfully demonstrated by attaching a variety of substances to proteins and immobilizing amino-oxy terminated RGD cyclopeptides to substrate surfaces [249, 250]. The oxime ligatation is compatible with most standard amino acid residues and the oxime bond is known to be reasonably stable both in vitro and in vivo.

Another approach to generate biomimetically-enhanced environment is to recreate the topographical context of native ECM through engineered three-dimensional nanofibrous matrices. The well-established, polymer-based processing method of electro-spinning and thermally induced phase separation, and protein self-assembly are all used to generate nanofibrous metrices [251–253]. Surface functional groups can be introduced in this case also by chemical treatments, such as alkaline hydrolysis, aminolysis, and oxidation/reduction reactions, silanation, chlorination, acylation, and quaternisation reactions.

Mata et al. [254] prepare micro textured PDMS surfaces to study the behavior of human bone connective tissue progenitor cells. Nanostructured poly(hydroxy-methyl siloxane) surfaces have been prepared by plasma treatment or low-energy ion beam to study the adhesion and proliferation of both, peritrocites and endothelial cells. It is supposed that the biomaterial surface properties can mediate and modulate the cell/surface adhesion via stereo-specific chemical interactions and/or electrostatic repulsion that can explain the different behavior of the peritrocites and the epithelial cells [255].

Polymeric scaffolds could be designed to function more actively in tissue remodeling and regeneration by growth factors incorporation. Heparin modification has been intensively studied for growth factor releasing matrices in tissue

engineering. Heparin is a highly sulfated glycosoaminoglycan (GAG) constituting the extracellular matrix known for its specific interaction with various angiogenic growth factors [256]. Heparin binding preserve the stability and biological activity of the growth factors. A wide variety of scaffold matrices, including nanofibers, prepared from collagen, fibrin, chitosan, alginate, PLA and PLGA, have been immobilized with heparin to achieve sustained release of growth factors [257–262]. Growth factors can be incorporated into the scaffold matrix either by bulk encapsulation, specific or nonspecific surface adsorption and adding microspheres encapsulating them.

The formation of blood vessels, providing facile transport of oxygen and nutrients is essential for the survival of growing tissue or organ in the tissue engineering [263]. Various angiogenetic growth factors, such as vascular endothelial growth factor (VEGF), acidic or basic fibroblast growth factor (aFGF, bFGF), angiopoietin, and platelet-derived growth factor (PDGF), have been incorporated into 3D matrices. However, serious problems reside in maintaining structural integrity and bioactivity of the protein at the direct encapsulation [264]. Simple physical adsorption of growth factors on the surface of scaffolds could partially solve this problem [265]. Porous poly(lactic acid) (PLA) sponges have been surface coated with bFGF. Engraftment of hepatocytes followed by implantation has resulted in improved blood vessel in-growth with increasing the extent of cell survival. However, the physical adsorption method failed to induce angiogenesis when implanted, due to lack of long-term sustained release effects at the local tissue side. To achieve sustained release of angiogenic growth factors from the scaffold, heparin immobilized scaffolds have been prepared which can interact with heparin-binding angiogenic growth factors, including VEGF and bFGF with specific binding affinity [266–268].

Yoon et al. [269] fabricated macroporous PLGA scaffolds using blending mixture of PLGA and NH_2-PEG-PLGA to generate surface amine groups for heparin immobilization. bFGF binding and release studies showed that bFGF sustained release while retaining its bioactivity as determined by proliferation of endothelial cells in vitro. When bFGF loaded heparin modified scaffolds have been implanted in vivo, significantly enhanced neovascularization has been observed. Heparin immobilized microspheres also release out bioactive bFGF in a sustained manner and exhibit pronounced angiogenic effect in an animal model [270, 271].

Porous scaffolds for bone and cartilage regeneration can be further enhanced by altering the surface properties through covalent coupling of cell growth factors. Covalently couplet protein gradients within three-dimensional fibrous scaffolds are crucial for generation of the gradient futures required in the formation of more complex skeletal tissues, such as osteohondral systems [272]. The majority of currently used implant materials in orthopedics lacks osteoconductivity. A number of surface modification techniques (hydrothermal-electrochemical deposition, plasma spraying, ion beam assisted deposition, and biomimetic deposition) have been employed to solve this problem. Furthermore, biomimetic processes have been also employed to render nonbioactive polymer tissue engineering scaffolds osteoconductive [273].

Stimuli (physical-, chemical- or biological)-responsive biomaterials creation is one of the latest directions. For example, the polymer hydrogels may be induced to swell or shrink in response to a variety of environmental stimuli, such as changes in pH or temperature, or the presence of a specific chemical substrate. When hydrogels swell or shrink, complex patterns may be generated on their surface. The character of gel surface can be modified by selectively depositing another material using a mask, for example, deposition of small areas of N-isopropylacrylamide (NIPA) gels on the surface of an acrylamide gel [274]. Ebara et al. [275] create PDMS micro channel system with stimuli responsive surface grafting poly(N-isopropylacryl amide) (PNIPA) onto the photoinitiator preadsorbed channel walls. The grafting density and the corresponding reversible hydrophilic/hydrophobic properties (water contact angle of about 35° below the critical solution temperature and of 82° above it) are controlled by varying the UV irradiation time and the photoinitiator amount. Stoica et al. [276] present new synthetic rout to couple selectively a modified octa-peptide, that is able to gel at low temperature, to the prototypical thermoresponsive poly(N-isopropylacryl amide) to give bioconjugate that exhibits double thermoresponsiveness.

8. Summary and Future Outlook

Polymeric biomaterials with controlled protein adsorption and cellular interactions are currently of extremely increasing interest, mainly because of their potential for applications in the regenerative medicine and tissue engineering. Repairing or replacing of damaged tissues or organs requires biocompatible materials that emulate living tissues. A future challenge is to modify biomaterials used for this purpose in a way that they imitate in their composition and/or structure the native physiological conditions for the tissue specific cells. Surface engineering plays an important role in the development of such biomaterials. Enormous research activity is focused now on the delivering of new and improved biomimetic biomaterials.

The level of biological complexity that needs to be recapitulated within a synthetic three-dimensional environment is still uncertain and further understanding of the interactions occurring at cell surface/substrate interface requires. It is likely that biofunctionalization strategies will continue to play a key role because they integrate micron- and nanoscale features into designed scaffolds better.

Development of stimuli-responsive polymeric biomaterials is expected to enable feedback-controlled scaffold structures for tissue engineering. Having a built-in adaptation of physical properties, such as elasticity or permeability, for example, similar synthetic polymer architectures will come closer to dynamic nature of the living matter.

The development of new strategies to creation of surface engineered biomaterials with improved biocontact properties (providing a biomimetic microenvironment conductive to cell adhesion, proliferation, differentiation, and host tissue

integration) requires a more in-depth investigation on the mechanisms of protein adsorption and reorganization, as well as of the bioadhesion and cell/biomaterial and cell/extra cellular matrix interactions, cell signaling and cell growth biology.

References

[1] N. Minoura, S. Aiba, Y. Fujiwara, N. Koshizaki, and Y. Imai, "The interaction of cultured cells with membranes composed of random and block copolypeptides," *Journal of Biomedical Materials Research*, vol. 23, no. 2, pp. 267–279, 1989.

[2] R. Large, *MRS Bulletin*, vol. 31, p. 447, 2004.

[3] B.-S. Kim and D. J. Mooney, "Development of biocompatible synthetic extracellular matrices for tissue engineering," *Trends in Biotechnology*, vol. 16, no. 5, pp. 224–229, 1998.

[4] R. Langer and J. P. Vacanti, "Tissue engineering," *Science*, vol. 260, no. 5110, pp. 920–926, 1993.

[5] L. L. Hench and J. M. Polak, "Third-generation biomedical materials," *Science*, vol. 295, no. 5557, pp. 1014–1017, 2002.

[6] J. Anderson, "A forecast of the future for biomaterials," in *Proceedings of the Future of Biomedical Materials (key note), Symposium*, Imperial Colleage London, September 2005.

[7] S. E. Sakiyama-Elbert and J. A. Hubbell, "Functional biomaterials: design of novel biomaterials," *Annual Review of Materials Science*, vol. 31, pp. 183–201, 2001.

[8] L. Bachakova, *Physiological Research*, vol. 53, pp. 35–45, 2004.

[9] C.-G. Gölander, *Preparation and properties of functionalized polymer surfaces*, Ph.D. thesis, The Royal Institute of Technology, Stockholm, Sweden, 1986.

[10] M. Malmsten, Ed., *Biopolymers at Interfaces*, Marcel Dekker, New York, NY, USA, 1998.

[11] S. Pasche, *Mechanisms of protein resistance of adsorbed PEG-Graft copolymers*, D.Sc. thesis, Swiss Federal Institute of Technology, Zurich, Switzerland, 2004.

[12] S. Drotleff, *Polymers and protein-conjugates for tissue engineering*, Ph.D. thesis, University of Regensburg, Regensburg, Germany, 2006.

[13] V. Hlady, R. A. VanWagenen, and J. D. Andrade, in *Surface and Interfacial Aspects of Biomedical Polymers*, J. D. Andrade, Ed., vol. 2, p. 81, Plenum Press, New York, NY, USA, 1985.

[14] M. Jager, C. Zilkens, K. Zanger, and R. Krauspe, "Significance of nano- and microtopography for cell-suraface interactions in orthopedic implants," *Journal of Biomedicine and Biotechnology*, vol. 2007, Article ID 69036, 2007.

[15] G. Altankov, *Cell/biomaterial surfaces interaction*, D.Sc. thesis, Institute of Biophysics, BAS, Sofia, Bulgaria, 2003.

[16] F. Grinnell and M. K. Feld, "Adsorption characteristics of plasma fibronectin in relationship to biological activity," *Journal of Biomedical Materials Research*, vol. 15, no. 3, pp. 363–381, 1981.

[17] J. D. Andrade and V. Hlady, "Protein adsorption and materials biocompatibility. A tutorial review and suggested hypothesis," *Progress in Surface Science*, vol. 79, pp. 1–63, 1986.

[18] V. Prasad, "Strategies for de novo engineering of tissues," in *Proceedings of the NATO ARW Nano-Engineered Systems for Regenerative Medicine*, Varna, Bulgaria, September 2007.

[19] J. Panell, "Material surface effects on biological interactions," in *Proceedings of the NATO ARW Nano-Engineered Systems for Regenerative Medicine*, Varna, Bulgaria, September 2007.

[20] J. Champion, "UROs, tacos, worms and surfboards: what they teach about material-cell interactions," in *Proceedings of the NATO ARW Nano-Engineered Systems for Regenerative Medicine*, Varna, Bulgaria, September 2007.

[21] W. Senaratne, P. Sengupta, V. Jakubek, D. Holowka, C. K. Ober, and B. Baird, "Functionalized surface arrays for spatial targeting of immune cell signaling," *Journal of the American Chemical Society*, vol. 128, no. 17, pp. 5594–5595, 2006.

[22] W. Senaratne, L. Andruzzi, and C. K. Ober, "Self-assembled monolayers and polymer brushes in biotechnology: current applications and future perspectives," *Biomacromolecules*, vol. 6, no. 5, pp. 2427–2448, 2005.

[23] S. Sano, K. Kato, and Y. Ikada, "Introduction of functional groups onto the surface of polyethylene for protein immobilization," *Biomaterials*, vol. 14, no. 11, pp. 817–822, 1993.

[24] A. Hoffman, *Annals of the New York Academy of Sciences*, pp. 97–101, 1988.

[25] P. K. Chu, J. Y. Chen, L. P. Wang, and N. Huang, "Plasma-surface modification of biomaterials," *Materials Science and Engineering*, vol. 36, no. 5-6, pp. 143–206, 2002.

[26] C. M. Chan, *Polymer Surface Modification and Characterization*, chapters 5–7, Hanser, Brookfield, Wis, USA, 1993.

[27] F. Abbasi, H. Mirzadeh, and A.-A. Katbab, "Modification of polysiloxane polymers for biomedical applications: a review," *Polymer International*, vol. 50, no. 12, pp. 1279–1287, 2001.

[28] U. Vohrer, "Interfacial engineering of functional textiles for biomedical applications," in *Plasma Technologies for Textiles*, R. Shishoo, Ed., p. 202, CRC Press; Boca Raton, Fla, USA, Woodhead, Cambridge, UK, 2007.

[29] C.-M. Chan, T.-M. Ko, and H. Hiraoka, "Polymer surface modification by plasmas and photons," *Surface Science Reports*, vol. 24, no. 1-2, pp. 1–54, 1996.

[30] K. R. Rau, *Surface modification of biomaterials by pulsed laser ablasion deposition and plasma/gamma polymerization*, Ph.D. thesis, University of Florida, Gainesville, Fla, USA, 2001.

[31] R. Shishoo, Ed., *Plasma Technologies for Textiles*, CRC Press; Boca Raton, Fla, USA, Woodhead, Cambridge, UK, 2007.

[32] A. Denizli, E. Piskin, V. Dixit, M. Arthur, and G. Gitnick, "Collagen and fibronectin immobilization of PHEMA microcarriers for hepatocyte attachment," *International Journal of Artificial Organs*, vol. 18, no. 2, pp. 90–95, 1995.

[33] S. Jaumotte-Thelen, I. Dozot-Dupont, J. Marchand-Brynaert, and Y.-J. Schneider, "Covalent grafting of fibronectin and asialofetuin at surface of poly(ethylene terephthalate) track-etched membranes improves adhesion but not differentiation of rat hepatocytes," *Journal of Biomedical Materials Research*, vol. 32, no. 4, pp. 569–582, 1996.

[34] R. Chen and J. A. Hunt, "Biomimetic materials processing for tissue-engineering processes," *Journal of Materials Chemistry*, vol. 17, no. 38, pp. 3974–3979, 2007.

[35] S. P. Massia and J. A. Hubbell, "Human endothelial cell interactions with surface-coupled adhesion peptides on a nonadhesive glass substrate and two polymeric biomaterials," *Journal of Biomedical Materials Research*, vol. 25, no. 2, pp. 223–242, 1991.

[36] Y. Ykada, M. Suzuki, and Y. Tamada, "Polymer surfaces possessing minimal interaction with blood components," in *Polymers as Biomaterials*, Plenum Press, New York, NY, USA, 1984.

[37] S. E. Sakiyama-Elbert and J. A. Hubbell, "Functional biomaterials: design of novel biomaterials," *Annual Review of Materials Science*, vol. 31, pp. 183–201, 2001.

[38] B. D. Ratner, *Biocompatibility of Clinical Implant Materials*, vol. 2 of *D. W. Williams, Eds.*, CRC Press, Boca Raton, Fla, USA, 1981.

[39] A. S. Hoffman, T. A. Horbett, and B. D. Ratner, "Interactions of blood and blood components at hydrogel interfaces," *Annals of the New York Academy of Sciences*, vol. 283, pp. 372–382, 1977.

[40] W. Kim and J. Feijen, " Surface modification of polymers for improved blood compatibility," *CRC Critical Reviews in Biocompatibility*, vol. 1, p. 229, 1985.

[41] K. Ishihara, *Biocompatible Polymers*, CRC Press, London, UK, 1994.

[42] B. D. Ratner and A. S. Hoffman, "Non-fouling surfaces," in *Biomaterials Science*, B. D. Ratner, A. S. Hoffman, F. J. Schoen, and J. E. Lemons, Eds., pp. 197–201, Elsevier, San Diego, Calif, USA, 2nd edition, 2004.

[43] J. M. Harries, Ed., *Poly(Ethylene Glycol) Chemistry. Biomedical and Biotechnical Applications*, Plenum Press, New York, NY, USA, 1992.

[44] C.-G. Gölander, S. Jönsson, T. Vladkova, P. Stenius, and J. C. Eriksson, "Preparation and protein adsorption properties of photopolymerized hydrophilic films containing N-vinylpyrrolidone (NVP), acrylic acid (AA) or ethyleneoxide (EO) units as studied by ESCA," *Colloids & Surfaces*, vol. 21, pp. 149–165, 1986.

[45] C.-G. Gölander, E.-S. Jönsson, T. Vladkova, et al., "Protein adsorption on some photo-polymerized hydrophilic films," in *Proceedings of the 8th International Symposium on Plasma Chemistry (IUPAC '87)*, vol. 8.27, Sofia, Bulgaria, July 1987.

[46] M. Malmsten and J. M. Van Alstine, "Adsorption of poly(ethylene glycol) amphiphiles to form coatings which inhibit protein adsorption," *Journal of Colloid and Interface Science*, vol. 177, no. 2, pp. 502–512, 1996.

[47] C.-G. Gölander, E.-S. Jönsson, and T. G. Vladkova, "EP022966 (B1); WO8602087 (A1); US4840851 (A); SU1729284 (A3); SE8404866 (L); SE444950 (B); NO861998 (A); JP62500307 (T); DK248986 (A); AU4965185 (A)".

[48] T. Vladkova, "Modification of polymer surfaces for medical application," in *Proceedings of the 13th Science Conference "Modification of Polymers"*, Kudowa Zdroj, Poland, September 1995.

[49] T. G. Vladkova, C.-G. Gölander, S. C. Christoskova, and E.-S. Jönsson, "Mechanically stable hydrophilic films based on oxialkylated macromers polymerizable by UV irradiation," *Polymers for Advanced Technologies*, vol. 8, no. 6, pp. 347–350, 1997.

[50] T. Vladkova, *Some Possibilities to Polymer Surface Modification*, UCTM Ed. Centre, Sofia, Bulgaria, 2001.

[51] T. Vladkova, E.-S. Jönsson, and C.-G. Gölander, "Surface modification of natural rubber latex films by peg hydrogel coating," *Journal of University of Chemical Technology and Metallurgy*, vol. 38, p. 131, 2003.

[52] T. Vladkova, "Surface modification of silicone rubber with poly(ethylene glycol) hydrogel coatings," *Journal of Applied Polymer Science*, vol. 92, no. 3, pp. 1486–1492, 2004.

[53] R. Bischoff and G. Bischoff, in *Proceedings of the 11th Conference of the European Society of Biomechanics*, Touluse, France, July 1998.

[54] B. P. Lee, K. Huang, F. N. Nunalee, K. Shull, and P. B. Messersmith, "Synthesis of 3,4-dihydroxyphenylalanine (DOPA) containing monomers and their co-polymerization with PEG-diacrylate to form hydrogels," *Journal of Biomaterials Science, Polymer Edition*, vol. 15, no. 4, pp. 449–464, 2004.

[55] I. K. Kwon and T. Matsuda, "Photo-iniferter-based thermoresponsive block copolymers composed of poly(ethylene glycol) and poly(N-isopropylacrylamide) and chondrocyte immobilization," *Biomaterials*, vol. 27, no. 7, pp. 986–995, 2006.

[56] M. S. Hahn, L. J. Taite, J. J. Moon, M. C. Rowland, K. A. Ruffino, and J. L. West, "Photolithographic patterning of polyethylene glycol hydrogels," *Biomaterials*, vol. 27, no. 12, pp. 2519–2524, 2006.

[57] S. Kizilel, E. Sawardecker, F. Teymour, and V. H. Pérez-Luna, "Sequential formation of covalently bonded hydrogel multilayers through surface initiated photopolymerization," *Biomaterials*, vol. 27, no. 8, pp. 1209–1215, 2006.

[58] Y. Ito, H. Hasuda, M. Sakuragi, and S. Tsuzuki, "Surface modification of plastic, glass and titanium by photoimmobilization of polyethylene glycol for antibiofouling," *Acta Biomaterialia*, vol. 3, no. 6, pp. 1024–1032, 2007.

[59] E. Kiss, C.-G. Gölander, and J. C. Eriksson, "Surface grafting of polyethyleneoxide optimized by means of ESCA," *Progress in Colloid & Polymer Science*, vol. 74, no. 1, pp. 113–119, 1987.

[60] C. L. Feng, Z. Zhang, R. Förch, W. Knoll, G. J. Vancso, and H. Schönherr, "Reactive thin polymer films as platforms for the immobilization of biomolecules," *Biomacromolecules*, vol. 6, no. 6, pp. 3243–3251, 2005.

[61] R. Schlapak, P. Pammer, D. Armitage, et al., "Glass surfaces grafted with high-density poly(ethylene glycol) as substrates for DNA oligonucleotide microarrays," *Langmuir*, vol. 22, no. 1, pp. 277–285, 2006.

[62] S. Patel, R. G. Thakar, J. Wong, S. D. McLeod, and S. Li, "Control of cell adhesion on poly(methyl methacrylate)," *Biomaterials*, vol. 27, no. 14, pp. 2890–2897, 2006.

[63] Y. Li, C. G. Worley, R. W. Linton, J. M. DeSimone, and E. T. Samulski, "Grafting of poly(ethylene oxide) to crosslinked polystyrene and polypropylene substrates with well-controlled chain length and functionalities," *Division of Polymer Chemistry—American Chemical Society*, vol. 37, no. 2, pp. 737–738, 1996.

[64] K.C. Popat, G. Mor, C. A. Grimes, and T. A. Desai, "Surface modification of nanoporous alumina surfaces with poly(ethylene glycol)," *Langmuir*, vol. 20, no. 19, pp. 8035–8041, 2004.

[65] J. Piehler, A. Brecht, R. Valiokas, B. Liedberg, and G. Gauglitz, "A high-density poly(ethylene glycol) polymer brush for immobilization on glass-type surfaces," *Biosensors and Bioelectronics*, vol. 15, no. 9-10, pp. 473–481, 2000.

[66] Z.-K. Xu, F.-Q. Nie, C. Qu, L.-S. Wan, J. Wu, and K. Yao, "Tethering poly(ethylene glycol)s to improve the surface biocompatibility of poly(acrylonitrile-co-maleic acid) asymmetric membranes," *Biomaterials*, vol. 26, no. 6, pp. 589–598, 2005.

[67] J. Groll, T. Ameringer, J. P. Spatz, and M. Moeller, "Ultrathin coatings from isocyanate-terminated star PEG prepolymers: layer formation and characterization," *Langmuir*, vol. 21, no. 5, pp. 1991–1999, 2005.

[68] I. Choi, S. K. Kang, J. Lee, Y. Kim, and J. Yi, "In situ observation of biomolecules patterned on a PEG-modified Si surface by scanning probe lithography," *Biomaterials*, vol. 27, no. 26, pp. 4655–4660, 2006.

[69] H. Xu, J. L. Kaar, A. J. Russell, and W. R. Wagner, "Characterizing the modification of surface proteins with poly(ethylene glycol) to interrupt platelet adhesion," *Biomaterials*, vol. 27, no. 16, pp. 3125–3135, 2006.

[70] Y. G. Ko, Y. H. Kim, K. D. Park, et al., "Immobilization of poly(ethylene glycol) or its sulfonate onto polymer surfaces by ozone oxidation," *Biomaterials*, vol. 22, no. 15, pp. 2115–2123, 2001.

[71] R. P. Sebra, K. S. Masters, C. Y. Cheung, C. N. Bowman, and K. S. Anseth, "Detection of antigens in biologically complex fluids with photografted whole antibodies," *Analytical Chemistry*, vol. 78, no. 9, pp. 3144–3151, 2006.

[72] M. Beyer, T. Felgenhauer, F. R. Bischoff, F. Breitling, and V. Stadler, "A novel glass slide-based peptide array support with high functionality resisting non-specific protein adsorption," *Biomaterials*, vol. 27, no. 18, pp. 3505–3514, 2006.

[73] D. Xiao, H. Zhang, and M. Wirth, "Chemical modification of the surface of poly(dimethylsiloxane) by atom-transfer radical polymerization of acrylamide," *Langmuir*, vol. 18, no. 25, pp. 9971–9976, 2002.

[74] T. Goda, T. Konno, M. Takai, T. Moro, and K. Ishihara, "Biomimetic phosphorylcholine polymer grafting from polydimethylsiloxane surface using photo-induced polymerization," *Biomaterials*, vol. 27, no. 30, pp. 5151–5160, 2006.

[75] T. Vladkova, N. Krasteva, A. Kostadinova, and G. Altankov, "Preparation of PEG-coated surfaces and a study for their interaction with living cells," *Journal of Biomaterials Science, Polymer Edition*, vol. 10, no. 6, pp. 609–620, 1999.

[76] S. P. Massia, J. Stark, and D. S. Letbetter, "Surface-immobilized dextran limits cell adhesion and spreading," *Biomaterials*, vol. 21, no. 22, pp. 2253–2261, 2000.

[77] S. K. Thanawala and M. K. Chaudhury, "Surface modification of silicone elastomer using perfluorinated ether," *Langmuir*, vol. 16, no. 3, pp. 1256–1260, 2000.

[78] S. Yang, J. Wang, K. Ogino, S. Valiyaveettil, and C. K. Ober, "Low-surface-energy fluoromethacrylate block copolymers with patternable elements," *Chemistry of Materials*, vol. 12, no. 1, pp. 33–40, 2000.

[79] L. Andruzzi, W. Senaratne, A. Hexemer, et al., "Oligo(ethylene glycol) containing polymer brushes as bioselective surfaces," *Langmuir*, vol. 21, no. 6, pp. 2495–2504, 2005.

[80] S. S. Hwang, C. K. Ober, S. Perutz, D. R. Iyengar, L. A. Schneggenburger, and E. J. Kramer, "Block copolymers with low surface energy segments: siloxane- and perfluoroalkane-modified blocks," *Polymer*, vol. 36, no. 6, pp. 1321–1325, 1995.

[81] S. Krishnan, R. Ayothi, A. Hexemer, et al., "Anti-biofouling properties of comblike block copolymers with amphiphilic side chains," *Langmuir*, vol. 22, no. 11, pp. 5075–5086, 2006.

[82] S. Krishnan, N. Wang, C. Ober, C. Finlay, J. Callow, and M. Callow, *Biomacromolecules*, vol. 117, pp. 2775–2783, 2009.

[83] T. Vladkova, "Modification of polymer surfaces for medical application," in *Proceedings of the 13th International Science Conference "Modification of Polymers"*, Kudowa Zdroj, Poland, September 1995.

[84] Y. Kicheva, T. Vladkova, V. Kostov, and C.-G. Gölander, "Preparation of surface modified PVC drain tubing and in vivo study of their biocompatibility," *Journal of the University of Chemical Technology and Metallurgy*, vol. 37, pp. 77–84, 2002.

[85] Y. Kicheva, V. Kostov, M. Mateev, and T. Vladkova, "In vitro and in vivo evaluation of biocompatibility of PVC materials with modified surfaces," in *Proceedings of the 6th Colloquium on Biomaterials*, Aahen, Germany, September 2002.

[86] P. Sioshansi and E. J. Tobin, "Surface treatment of biomaterials by ion beam processes," *Surface and Coatings Technology*, vol. 83, no. 1–3, pp. 175–182, 1996.

[87] M. Szicher, P. Sioshansi, and E. Frish, *Biomaterials for the 1990s:Polyurethanes, Silicones, and Ion Beam Modification Techniques, Part 2*, Spire, Bedford, Mass, USA, 1990.

[88] M. Inoue, Y. Suzuki, and T. Takagi, "Review of Ion Engineering Center and related projects in Ion Engineering Research Institute," *Nuclear Instruments and Methods in Physics Research B*, vol. 121, no. 1–4, pp. 1–6, 1997.

[89] I. F. Husein, C. Chan, and P. K. Chu, "Chemical structure modification of silicone surfaces by plasma immersion ion implantation," *Journal of Materials Science Letters*, vol. 19, no. 21, pp. 1883–1885, 2000.

[90] I. F. Husein, C. Chan, S. Qin, and P. K. Chu, "The effect of high-dose nitrogen plasma immersion ion implantation on silicone surfaces," *Journal of Physics D*, vol. 33, no. 22, pp. 2869–2874, 2000.

[91] C. Satriano, S. Carnazza, S. Guglielmino, and G. Marletta, "Differential cultured fibroblast behavior on plasma and ion-beam-modified polysiloxane surfaces," *Langmuir*, vol. 18, no. 24, pp. 9469–9475, 2002.

[92] B. Bhushan, D. Hansford, and K. K. Lee, "Surface modification of silicon and polydimethylsiloxane surfaces with vapor-phase-deposited ultrathin fluorosilane films for biomedical nanodevices," *Journal of Vacuum Science and Technology A*, vol. 24, no. 4, pp. 1197–1202, 2006.

[93] W. J. Sear, P. P. Capek, and F. J. Clubb, in *Proceedings of the 40th Annual Conference on ADAIO*, New York, NY, USA, April 1998.

[94] L. Hakelius and L. Ohlsen, "A clinical comparison of the tendency to capsular contracture between smooth and textured gel-filled silicone mammary implants," *Plastic and Reconstructive Surgery*, vol. 90, no. 2, pp. 247–254, 1992.

[95] K. Ishihara, "Blood compatible polymers," in *Biomedical Applications of Polymeric Materials*, T. Tsuruta, T. Hyashi, K. Kataoka, K. Ishihara, and Y. Kimura, Eds., CRC Press, Boca Raton, Fla, USA, 1993.

[96] D.-C. Sin, H.-L. Kei, and X. Miao, "Surface coatings for ventricular assist devices," *Expert Review of Medical Devices*, vol. 6, no. 1, pp. 51–60, 2009.

[97] P. Claesson and C.-G. Gölander, *Colloids and Surfaces*, vol. 20, p. 186, 1995.

[98] D. L. Coleman, D. E. Gregonis, and J. D. Andrade, "Blood-materials interactions: the minimum interfacial free energy and the optimum polar/apolar ratio hypotheses," *Journal of Biomedical Materials Research*, vol. 16, no. 4, pp. 381–398, 1982.

[99] M. D. Lelah, J. A. Pierce, L. K. Lambrecht, and S. L. Cooper, "Polyether-urethane ionomers: surface property/ex vivo blood compatibility relationships," *Journal of Colloid and Interface Science*, vol. 104, no. 2, pp. 422–439, 1985.

[100] S. Nagaoka, Y. Mory, and S. Nishiumi, "Interaction between blood components and hydrogels with polyoxyethylene chains," *Polymer Preprints*, vol. 34, no. 1, p. 67, 1983.

[101] H. Tanzawa, "Biomedical polymers: current status and overview," in *Biomedical Applications of Polymeric Materials*, T. Tsuruta, T. Hayashi, K. Kataoka, K. Ishihara, and Y. Kimura, Eds., p. 12, CRC Press, Boca Raton, Fla, USA, 1993.

[102] S. Hattori, J. D. Andrade, J. B. Hibbs Jr., D. E. Gregonis, and R. N. King, "Fibroblast cell proliferation on charged hydroxyethyl methacrylate copolymers," *Journal of Colloid and Interface Science*, vol. 104, no. 1, pp. 72–78, 1985.

[103] N. Minoura, S. Aiba, Y. Fujiwara, N. Koshizaki, and Y. Imai, "The interaction of cultured cells with membranes composed of random and block copolypeptides," *Journal of Biomedical Materials Research*, vol. 23, no. 2, pp. 267–279, 1989.

[104] H. Sato, A. Nakajima, T. Hayashi, G. W. Chen, and Y. Noishiki, "Microheterophase structure, permeability, and

biocompatibility of A-B-A triblock copolymer membranes composed of poly(gamma-ethyl L-glutamate) as the A component and polybutadiene as the B component," *Journal of Biomedical Materials Research*, vol. 19, no. 9, pp. 1135–1155, 1985.

[105] T. Okano, T. Aoyagi, K. Kataoka, et al., "Hydrophilic-hydrophobic microdomain surfaces having an ability to suppress platelet aggregation and their in vitro antithrombogenicity," *Journal of Biomedical Materials Research*, vol. 20, no. 7, pp. 919–927, 1986.

[106] T. Okano, M. Uruno, N. Sugiyama, et al., "Suppression of platelet activity on microdomain surfaces of 2-hydroxyethyl methacrylate-polyether block copolymers," *Journal of Biomedical Materials Research*, vol. 20, no. 7, pp. 1035–1047, 1986.

[107] K. D. Park, T. Okano, C. Nojiri, and S. W. Kim, "Heparin immobilization onto segmented polyurethaneurea surfaces—effect of hydrophilic spacers," *Journal of Biomedical Materials Research*, vol. 22, no. 11, pp. 977–992, 1988.

[108] T. Okada and Y. Ikada, *Makromolekulare Chemie*, vol. 192, p. 1705, 1991.

[109] S. M. Kirkham and M. E. Dangel, "The keratoprosthesis: improved biocompatability through design and surface modification," *Ophthalmic Surgery*, vol. 22, no. 8, pp. 455–461, 1991.

[110] T. Okada and Y. Ikada, "Tissue reactions to subcutaneously implanted, surface-modified silicones," *Journal of Biomedical Materials Research*, vol. 27, no. 12, pp. 1509–1518, 1993.

[111] Y. Kinoshita, T. Kuzuhara, M. Kirigakubo, M. Kobayashi, K. Shimura, and Y. Ikada, "Soft tissue reaction to collagen-immobilized porous polyethylene: subcutaneous implantation in rats for 20 wk," *Biomaterials*, vol. 14, no. 3, pp. 209–215, 1993.

[112] H. Mirzadeh, A. A. Katbab, and R. P. Burford, "CO2-pulsed laser induced surface grafting of acrylamide onto ethylene-propylene-rubber (EPR)—I," *Radiation Physics and Chemistry*, vol. 41, no. 3, pp. 507–519, 1993.

[113] H. Mirzadeh, M. T. Khorasani, A. A. Katbab, et al., "Biocompatibility evaluation of laser-induced AAm and HEMA grafted EPR—part 1: in-vitro study," *Clinical Materials*, vol. 16, no. 4, pp. 177–187, 1994.

[114] H. Mirzadeh, A. A. Katbab, M. T. Khorasani, R. P. Burford, E. Gorgin, and A. Golestani, "Cell attachment to laser-induced AAm- and HEMA-grafted ethylene-propylene rubber as biomaterial: in vivo study," *Biomaterials*, vol. 16, no. 8, pp. 641–648, 1995.

[115] M. T. Khorasani, H. Mirzadeh, and P. G. Sammes, "Laser induced surface modification of polydimethylsiloxane as a super-hydrophobic material," *Radiation Physics and Chemistry*, vol. 47, no. 6, pp. 881–888, 1996.

[116] H. Mirzadeh, M. Khorasani, and P. G. Sammes, "Laser surface modification of polymers. A novel technique for the preparation of blood compatible materials (II): in vitro assay," *Iranian Polymer Journal*, vol. 7, no. 1, pp. 5–13, 1998.

[117] M. T. Korasani, H. Mirzadeh, and P. G. Sammes, in *Surface Modification Technologies*, T. Sudarshan, A. Khor, and M. Eandin, Eds., p. 499, Institute of Materials, London, UK, 1996.

[118] M. T. Khorasani, H. Mirzadeh, and P. G. Sammes, "Laser surface modification of polymers to improve biocompatibility: HEMA grafted PDMS, in vitro assay—III," *Radiation Physics and Chemistry*, vol. 55, no. 5-6, pp. 685–689, 1999.

[119] R. Lasson, *Chemical constitution and biological properties of heparinized surface*, Ph.D. thesis, Karolinska Institute, Stockholm, Sweden, 1980.

[120] H. J. Steffen, J. Schmidt, and A. Gonzalez-Elipe, "Biocompatible surfaces by immobilization of heparin on diamond-like carbon films deposited on various substrates," *Surface and Interface Analysis*, vol. 29, no. 6, pp. 386–391, 2000.

[121] Y. Susuki, M. Kasakabe, M. Iwaki, and M. Suzuki, *Nuclear Instruments and Methods in Physics Research*, vol. B32, p. 120, 1998.

[122] Y. Susuki, C. Swapp, M. Kasakabe, and M. Iwaki, *Nuclear Instruments and Methods in Physics Research*, vol. B46, p. 354, 1990.

[123] Y. Suzuki, M. Kusakabe, M. Iwaki, H. Akiba, K. Kusakabe, and S. Sato, "In vivo evaluation of antithrombogenicity for ion implanted silicone usineg in -111-tropolone-platelets," *Japanese Journal of Artificial Organs*, vol. 19, no. 3, pp. 1092–1095, 1990.

[124] P. R. Udall, in *Dialysis Therapy*, A. R. Nilsen and R. N. Fine, Eds., Hanley & Belfus, Philadelphia, Pa, USA, 2nd edition, 1993.

[125] J. Anderson, "The future of biomedical materials (key note)," in *Proceedings of a Forecast of the Future for Biomaterials*, Imperial Colleage, September 2005.

[126] A. R. Boccaccini and J. J. Blaker, "Bioactive composite materials for tissue engineering scaffolds," *Expert Review of Medical Devices*, vol. 2, no. 3, pp. 303–317, 2005.

[127] E. Eisenbarth, "Biomaterials for tissue engineering," *Advanced Engineering Materials*, vol. 9, no. 12, pp. 1051–1060, 2007.

[128] M. M. Stevens, R. P. Marini, D. Schaefer, J. Aronson, R. Langer, and V. P. Shastri, "In vivo engineering of organs: the bone bioreactor," *Proceedings of the National Academy of Sciences of the United States of America*, vol. 102, no. 32, pp. 11450–11455, 2005.

[129] C. Weinand, I. Pomerantseva, C. M. Neville, et al., "Hydrogel-β-TCP scaffolds and stem cells for tissue engineering bone," *Bone*, vol. 38, no. 4, pp. 555–563, 2006.

[130] J. Jones, *Materials Today*, vol. 9, no. 12, p. 35, 2006.

[131] H. J. Chung and T. G. Park, "Surface engineered and drug releasing pre-fabricated scaffolds for tissue engineering," *Advanced Drug Delivery Reviews*, vol. 59, no. 4-5, pp. 249–262, 2007.

[132] G. Altankov, "Development of provisional extracellular matrix on the biomaterial interface: lessons from in vitro cell culture," in *Proceedings of the NATO Advanced Research Workshop on Nanoengineered Systems for Regenerative Medicine*, Varna, Bulgaria, September 2007.

[133] M. J. Lydon, T. W. Minett, and B. J. Tighe, "Cellular interactions with synthetic polymer surfaces in culture," *Biomaterials*, vol. 6, no. 6, pp. 396–402, 1985.

[134] K. Smetana Jr., "Cell biology of hydrogels," *Biomaterials*, vol. 14, no. 14, pp. 1046–1050, 1993.

[135] H.-B. Lin, W. Sun, D. F. Mosher, et al., "Synthesis, surface, and cell-adhesion properties of polyurethanes containing covalently grafted RGD-peptides," *Journal of Biomedical Materials Research*, vol. 28, no. 3, pp. 329–342, 1994.

[136] R. G. Flemming, C. J. Murphy, G. A. Abrams, S. L. Goodman, and P. F. Nealey, "Effects of synthetic micro- and nano-structured surfaces on cell behavior," *Biomaterials*, vol. 20, no. 6, pp. 573–588, 1999.

[137] K. Saha, J. F. Pollock, D. V. Schaffer, and K. E. Healy, "Designing synthetic materials to control stem cell phenotype,"

Current Opinion in Chemical Biology, vol. 11, no. 4, pp. 381–387, 2007.

[138] L. Moroni, J. A. A. Hendriks, R. Schotel, J. R. de Wijn, and C. A. van Blitterswijk, "Design of biphasic polymeric 3-dimensional fiber deposited scaffolds for cartilage tissue engineering applications," *Tissue Engineering*, vol. 13, no. 2, pp. 361–371, 2007.

[139] D.-A. Wang, S. Varghese, B. Sharma, et al., "Multifunctional chondroitin sulphate for cartilage tissue-biomaterial integration," *Nature Materials*, vol. 6, no. 5, pp. 385–392, 2007.

[140] H. Lee, S. M. Dellatore, W. M. Miller, and P. B. Messersmith, "Mussel-inspired surface chemistry for multifunctional coatings," *Science*, vol. 318, no. 5849, pp. 426–430, 2007.

[141] D. S. W. Benoit, A. R. Durney, and K. S. Anseth, "The effect of heparin-functionalized PEG hydrogels on three-dimensional human mesenchymal stem cell osteogenic differentiation," *Biomaterials*, vol. 28, no. 1, pp. 66–77, 2007.

[142] M. P. Ludolf and J. A. Hubbel, "Synthetic biomaterials as instructive extracellular microenvironments for morphogenesis in tissue engineering," *Nature Biotechnology*, vol. 25, pp. 47–55, 2007.

[143] H. J. Chung and T. G. Park, "Surface engineered and drug releasing pre-fabricated scaffolds for tissue engineering," *Advanced Drug Delivery Reviews*, vol. 59, no. 4-5, pp. 249–262, 2007.

[144] G. Altankov, T. Vladkova, N. Krasteva, A. Kostadinova, and I. Keranov, "Preparation of protein repellent PEI/PEG coatings and fibronectin reorganization study on the coated surfaces," *Journal of the University of Chemical Technology and Metallurgy*, vol. 44, no. 4, pp. 333–340, 2009.

[145] G. Altankov and T. Groth, "Reorganization of substratum-bound fibronectin on hydrophilic and hydrophobic materials is related to biocompatibility," *Journal of Materials Science*, vol. 5, no. 9-10, pp. 732–737, 1994.

[146] G. Altankov and T. Groth, "Fibronectin matrix formation by human fibroblasts on surfaces varying in wettability," *Journal of Biomaterials Science, Polymer Edition*, vol. 8, no. 4, pp. 299–310, 1996.

[147] C. F. Amstein and P. A. Hartman, "Adaptation of plastic surfaces for tissue culture by glow discharge," *Journal of Clinical Microbiology*, vol. 2, no. 1, pp. 46–54, 1975.

[148] G. N. Hannan and B. R. McAuslan, "Immobilized serotonin: a novel substrate for cell culture," *Experimental Cell Research*, vol. 171, no. 1, pp. 153–163, 1987.

[149] J. A. Chinn, T. A. Horbett, B. D. Ratner, M. B. Schway, Y. Haque, and S. D. Hauschka, "Enhancement of serum fibronectin adsorption and the clonal plating efficiencies of Swiss mouse 3T3 fibroblast and MM14 mouse myoblast cells on polymer substrates modified by radiofrequency plasma deposition," *Journal of Colloid and Interface Science*, vol. 127, no. 1, pp. 67–87, 1989.

[150] S.-D. Lee, G.-H. Hsiue, and C.-Y. Kao, "Preparation and characterization of a homobifunctional silicone rubber membrane grafted with acrylic acid via plasma-induced graft copolymerization," *Journal of Polymer Science A*, vol. 34, no. 1, pp. 141–148, 1996.

[151] C. Satriano, E. Conte, and G. Marletta, "Surface chemical structure and cell adhesion onto ion beam modified polysiloxane," *Langmuir*, vol. 17, no. 7, pp. 2243–2250, 2001.

[152] C. Satriano, S. Carnazza, S. Guglielmino, and G. Marletta, "Differential cultured fibroblast behavior on plasma and ion-beam-modified polysiloxane surfaces," *Langmuir*, vol. 18, no. 24, pp. 9469–9475, 2002.

[153] T. Vladkova, I. Keranov, and G. Altankov, "Preparation and properties of PDMS surfaces grafted with acrylic acid via plasma pretment or ion-beam induced graft copolymerization," in *Proceedings of the 4th International Conference on Chemical Societies of the South-Eastern European Countries (ICOSECS '04)*, Belgrad, Serbia, July 2004, A-P 26.

[154] T. Vladkova, I. Keranov, P. Dineff, and G. Altankov, "Ion-beam assisted surface modification of PDMS," in *Proceedings of the 18th Congres of Chemists and Technologiest of Macedonia*, Ohrid, Macedonia, September 2004, PPM-16.

[155] R. Hippler, S. Pfau, M. Schmidt, and K. Schönbach, Eds., *Low Temperature Plasma Physics. Fundamental Aspects and Applications*, Willey-VCH, Berlin, Germany, 2000.

[156] T. G. Vladkova, I. L. Keranov, P. D. Dineff, et al., "Plasma based Ar+ beam assisted poly(dimethylsiloxane) surface modification," *Nuclear Instruments and Methods in Physics Research B*, vol. 236, no. 1–4, pp. 552–562, 2005.

[157] I. Keranov, T. G. Vladkova, M. Minchev, A. Kostadinova, G. Altankov, and P. Dineff, "Topography characterization and initial cellular interaction of plasma-based ar1 beam-treated PDMS surfaces," *Journal of Applied Polymer Science*, vol. 111, no. 5, pp. 2637–2646, 2009.

[158] J. M. Oliveira, I. B. Leonor, and R. L. Reis, "Preparation of bioactive coatings on the surface of bioinert polymers through an innovative auto-catalytic electroless route," *Key Engineering Materials*, vol. 284–286, pp. 203–206, 2005.

[159] T. Kawai, C. Ohtsuki, M. Kamitakahara, et al., "A comparative study of apatite deposition on polyamide films containing different functional groups under a biomimetic condition," *Journal of the Ceramic Society of Japan*, vol. 113, no. 1321, pp. 588–592, 2005.

[160] M. Morra, "Biomolecular modification of implant surfaces," *Expert Review of Medical Devices*, vol. 4, no. 3, pp. 361–372, 2007.

[161] J. L. West, "Biofunctional polymers," in *Encyclopedia of Biomaterials and Biomedical Engineering*, pp. 89–95, 2007.

[162] A. Denizli, E. Piskin, V. Dixit, M. Arthur, and G. Gitnick, "Collagen and fibronectin immobilization of PHEMA microcarriers for hepatocyte attachment," *International Journal of Artificial Organs*, vol. 18, no. 2, pp. 90–95, 1995.

[163] S. Jaumotte-Thelen, I. Dozot-Dupont, J. Marchand-Brynaert, and Y.-J. Schneider, "Covalent grafting of fibronectin and asialofetuin at surface of poly(ethylene terephthalate) track-etched membranes improves adhesion but not differentiation of rat hepatocytes," *Journal of Biomedical Materials Research*, vol. 32, no. 4, pp. 569–582, 1996.

[164] R. Chen and J. A. Hunt, "Biomimetic materials processing for tissue-engineering processes," *Journal of Materials Chemistry*, vol. 17, no. 38, pp. 3974–3979, 2007.

[165] B. B. Hole, J. A. Schwarz, J. L. Gilbert, and B. L. Atkinson, "A study of biologically active peptide sequences (P-15) on the surface of an ABM scaffold (PepGen P-15) using AFM and FTIR," *Journal of Biomedical Materials Research A*, vol. 74, no. 4, pp. 712–721, 2005.

[166] C. T. Laurencin and L. S. Nain, Eds., *Nanotechnology and Tissue Engineering: The Scaffold*, CRC Press, Boca Raton, Fla, USA, 2009.

[167] C. R. Nuttelman, D. J. Mortisen, S. M. Henry, and K. S. Anseth, "Attachment of fibronectin to poly(vinyl alcohol) hydrogels promotes NIH3T3 cell adhesion, proliferation, and migration," *Journal of Biomedical Materials Research*, vol. 57, no. 2, pp. 217–223, 2001.

[168] R. S. Braty, J. Crean, D. Lappin, and C. Godson, *Journal of Biomedical Materials Research*, vol. 56, pp. 78–82, 2001.

[169] M. P. Lutolf and J. A. Hubbell, "Synthetic biomaterials as instructive extracellular microenvironments for morphogenesis in tissue engineering," *Nature Biotechnology*, vol. 23, no. 1, pp. 47–55, 2005.

[170] U. Hersel, C. Dahmen, and H. Kessler, "RGD modified polymers: biomaterials for stimulated cell adhesion and beyond," *Biomaterials*, vol. 24, no. 24, pp. 4385–4415, 2003.

[171] A. Karkhaneh, H. Mirzadeh, and A. R. Ghaffariyeh, "Two-step plasma surface modification of PDMS with mixture of HEMA and AAC: collagen immobilization and in vitro assays," in *Proceedings of the 5th IASTED International Conference on Biomedical Engineering*, pp. 433–438, Innsbruck, Austria, February 2007.

[172] V. B. Ivanov, J. Behnisch, A. Hollander, F. Mehdorn, and H. Zimmermann, "Determination of functional groups on polymer surfaces using fluorescence labelling," *Surface and Interface Analysis*, vol. 24, no. 4, pp. 257–262, 1996.

[173] J. Davies, C. S. Nunnerley, A. C. Brisley, et al., "Argon plasma treatment of polystyrene microtiter wells. Chemical and physical characterisation by contact angle, ToF-SIMS, XPS and STM," *Colloids and Surfaces A*, vol. 174, no. 3, pp. 287–295, 2000.

[174] F. Poncin-Epaillard and G. Legeay, "Surface engineering of biomaterials with plasma techniques," *Journal of Biomaterials Science, Polymer Edition*, vol. 14, no. 10, pp. 1005–1028, 2003.

[175] U. König, M. Nitschke, M. Pilz, F. Simon, C. Arnhold, and C. Werner, "Stability and ageing of plasma treated poly(tetrafluoroethylene) surfaces," *Colloids and Surfaces B*, vol. 25, no. 4, pp. 313–324, 2002.

[176] J. Johns, *Materials Today*, vol. 11, no. 5, p. 29, 2008.

[177] D. B. Haddow, D. A. Steele, R. D. Short, R. A. Dawson, and S. MacNeil, "Plasma-polymerized surfaces for culture of human keratinocytes and transfer of cells to an in vitro wound-bed model," *Journal of Biomedical Materials Research A*, vol. 64, no. 1, pp. 80–87, 2003.

[178] B. Li, J. Chen, and J. H.-C. Wang, "RGD peptide-conjugated poly(dimethylsiloxane) promotes adhesion, proliferation, and collagen secretion of human fibroblasts," *Journal of Biomedical Materials Research A*, vol. 79, no. 4, pp. 989–998, 2006.

[179] G. Sui, J. Wang, C.-C. Lee, et al., "Solution-phase surface modification in intact poly(dimethylsiloxane) microfluidic channels," *Analytical Chemistry*, vol. 78, no. 15, pp. 5543–5551, 2006.

[180] Ch. Baquey, F. Palumbo, M. C. Porte-Durrieu, G. Legeay, A. Tressaud, and R. D'Agostino, "Plasma treatment of expanded PTFE offers a way to a biofunctionalization of its surface," *Nuclear Instruments and Methods in Physics Research B*, vol. 151, no. 1–4, pp. 255–262, 1999.

[181] S. Sano and S. Wong, *Chemistry of Protein Conjugation and Cross-Linking*, CRC Press, Boca Raton, Fla, USA, 1991.

[182] N. Shangguan, S. Katukojvala, R. Greenberg, and L. J. Williams, "The reaction of thio acids with azides: a new mechanism and new synthetic applications," *Journal of the American Chemical Society*, vol. 125, no. 26, pp. 7754–7755, 2003.

[183] S. Drotleff, *Polymers and protein-conjugates for tissue engineering*, Ph.D. thesis, University of Regensburg, Regensburg, Germany, 2006.

[184] T. Hermanson, *Bioconjugate Techniques*, Academic Press, San Diego, Calif, USA, 1996.

[185] Y. W. Tong and M. S. Shoichet, "Peptide surface modification of poly(tetrafluoroethylene-co-hexafluoropropylene) enhances its interaction with central nervous system neurons," *Journal of Biomedical Materials Research*, vol. 42, no. 1, pp. 85–95, 1998.

[186] S. P. Massia and J. A. Hubbell, "Human endothelial cell interactions with surface-coupled adhesion peptides on a nonadhesive glass substrate and two polymeric biomaterials," *Journal of Biomedical Materials Research*, vol. 25, no. 2, pp. 223–242, 1991.

[187] S. P. Massia and J. A. Hubbell, "Covalently attached GRGD on polymer surfaces promotes biospecific adhesion of mammalian cells," *Annals of the New York Academy of Sciences*, vol. 589, pp. 261–270, 1990.

[188] K. Nilsson and K. Mosbach, "Immobilization of enzymes and affinity ligands to various hydroxyl group carrying supports using highly reactive sulfonyl chlorides," *Biochemical and Biophysical Research Communications*, vol. 102, no. 1, pp. 449–457, 1981.

[189] K. Nilsson and K. Mosbach, "Tresyl chloride-activated supports for enzyme immobilization," *Methods in Enzymology*, vol. 135, pp. 65–78, 1987.

[190] K. Nilsson and K. Mosbach, "Immobilization of ligands with organic sulfonyl chlorides," *Methods in Enzymology*, vol. 104, pp. 56–69, 1984.

[191] R. Benters, C. M. Niemeyer, and D. Whorle, "Dendrimer-activated solid supports for nucleic acid and protein microarrays," *ChemBioChem*, vol. 2, no. 9, pp. 686–694, 2001.

[192] M. Yang, R. Y. C. Kong, N. Kazmi, and A. K. C. Leung, "Covalent immobilization of oligonucleotides on modified glass/silicon surfaces for solid-phase DNA hybridization and amplification," *Chemistry Letters*, no. 3, pp. 257–258, 1998.

[193] S. P. Pack, N. K. Kamisetty, M. Nonogawa, et al., "Direct immobilization of DNA oligomers onto the amine-functionalized glass surface for DNA microarray fabrication through the activation-free reaction of oxanine," *Nucleic Acids Research*, vol. 35, no. 17, 2007.

[194] A. Dekker, et al., "Improved adhesion and proliferation of human endothelial cells on PE pre-coated with monoclonal antibodies directed against cell membrane antigens and extracellular matrix proteins," in *Adhesion and Proliferation of Human Endothelial Cells on Polymeric Surfaces, Optimization Studies*, pp. 61–85, 1990.

[195] R. K. O'Reilly, M. J. Joralemon, C. J. Hawker, and K. L. Wooley, "Facile syntheses of surface-functionalized micelles and shell cross-linked nanoparticles," *Journal of Polymer Science A*, vol. 44, no. 17, pp. 5203–5217, 2006.

[196] K. K. Perkin, J. L. Turner, K. L. Wooley, and S. Mann, "Fabrication of hybrid nanocapsules by calcium phosphate mineralization of shell cross-linked polymer micelles and nanocages," *Nano Letters*, vol. 5, no. 7, pp. 1457–1461, 2005.

[197] M. L. Becker, L. A. O. Bailey, and K. L. Wooley, "Peptide-derivatized shell-cross-linked nanoparticles. 2. Biocompatibility evaluation," *Bioconjugate Chemistry*, vol. 15, no. 4, pp. 710–717, 2004.

[198] M. L. Becker, J. Liu, and K. L. Wooley, "Peptide-polymer bioconjugates: hybrid block copolymers generated via living radical polymerizations from resin-supported peptides," *Chemical Communications*, vol. 9, no. 2, pp. 180–181, 2003.

[199] J. Riesle, A. P. Hollander, R. Langer, L. E. Freed, and G. Vunjak-Novakovic, "Collagen in tissue-engineered cartilage: types, structure, and crosslinks," *Journal of Cellular Biochemistry*, vol. 71, no. 3, pp. 313–327, 1998.

[200] J. Yang, Y. Wan, J. Yang, J. Bei, and S. Wang, "Plasma-treated, collagen-anchored polylactone: its cell affinity evaluation under shear or shear-free conditions," *Journal of Biomedical Materials Research A*, vol. 67, no. 4, pp. 1139–1147, 2003.

[201] Z. Ma, C. Gao, Y. Gong, and J. Shen, "Cartilage tissue engineering PLLA scaffold with surface immobilized collagen and basic fibroblast growth factor," *Biomaterials*, vol. 26, no. 11, pp. 1253–1259, 2005.

[202] S. Ber, G. Torun Köse, and V. Hasirci, "Bone tissue engineering on patterned collagen films: an in vitro study," *Biomaterials*, vol. 26, no. 14, pp. 1977–1986, 2005.

[203] D. L. Wilson, R. Martin, S. Hong, M. Cronin-Golomb, C. A. Mirkin, and D. L. Kaplan, "Surface organization and nanopatterning of collagen by dip-pen nanolithography," *Proceedings of the National Academy of Sciences of the United States of America*, vol. 98, no. 24, pp. 13660–13664, 2001.

[204] I. Keranov, T. Vladkova, M. Minchev, A. Kostadinova, and G. Altankov, "Preparation, characterization, and cellular interactions of collagen-immobilized PDMS surfaces," *Journal of Applied Polymer Science*, vol. 110, no. 1, pp. 321–330, 2008.

[205] X. Liu, Y. Won, and P. X. Ma, "Surface modification of interconnected porous scaffolds," *Journal of Biomedical Materials Research A*, vol. 74, no. 1, pp. 84–91, 2005.

[206] T. Serizawa and M. Akashi, "A novel approach for fabricating ultrathin polymer films by the repetition of the adsorption/drying processes," *Journal of Polymer Science A*, vol. 37, no. 13, pp. 1903–1906, 1999.

[207] Z. Ma, C. Gao, Y. Gong, and J. Shen, "Cartilage tissue engineering PLLA scaffold with surface immobilized collagen and basic fibroblast growth factor," *Biomaterials*, vol. 26, no. 11, pp. 1253–1259, 2005.

[208] M.-C. Chen, H.-F. Liang, Y.-L. Chiu, Y. Chang, H.-J. Wei, and H.-W. Sung, "A novel drug-eluting stent spray-coated with multi-layers of collagen and sirolimus," *Journal of Controlled Release*, vol. 108, no. 1, pp. 178–189, 2005.

[209] X. Wang, H. J. Kim, P. Xu, A. Matsumoto, and D. L. Kaplan, "Biomaterial coatings by stepwise deposition of silk fibroin," *Langmuir*, vol. 21, no. 24, pp. 11335–11341, 2005.

[210] K. Cai, K. Yao, S. Lin, et al., "Poly(D,L-lactic acid) surfaces modified by silk fibroin: effects on the culture of osteoblast in vitro," *Biomaterials*, vol. 23, no. 4, pp. 1153–1160, 2002.

[211] A. Chiarini, P. Petrini, S. Bozzini, I. Dal Pra, and U. Armato, "Silk fibroin/poly(carbonate)-urethane as a substrate for cell growth: in vitro interactions with human cells," *Biomaterials*, vol. 24, no. 5, pp. 789–799, 2003.

[212] I. Dal Pra, P. Petrini, A. Charini, S. Bozzini, S. Farè, and U. Armato, "Silk fibroin-coated three-dimensional polyurethane scaffolds for tissue engineering: interactions with normal human fibroblasts," *Tissue Engineering*, vol. 9, no. 6, pp. 1113–1121, 2003.

[213] P. Petrini, C. Parolari, and M. C. Tanzi, "Silk fibroin-polyurethane scaffolds for tissue engineering," *Journal of Materials Science*, vol. 12, no. 10–12, pp. 849–853, 2001.

[214] G. H. Altman, R. L. Horan, H. H. Lu, et al., "Silk matrix for tissue engineered anterior cruciate ligaments," *Biomaterials*, vol. 23, no. 20, pp. 4131–4141, 2002.

[215] G. H. Altman, H. H. Lu, R. L. Horan, et al., "Advanced bioreactor with controlled application of multi-dimensional strain for tissue engineering," *Journal of Biomechanical Engineering*, vol. 124, no. 6, pp. 742–749, 2002.

[216] J. S. Mao, H. F. Liu, Y. J. Yin, and K. D. Yao, "The properties of chitosan-gelatin membranes and scaffolds modified with hyaluronic acid by different methods," *Biomaterials*, vol. 24, no. 9, pp. 1621–1629, 2003.

[217] H. S. Yoo, E. A. Lee, J. J. Yoon, and T. G. Park, "Hyaluronic acid modified biodegradable scaffolds for cartilage tissue engineering," *Biomaterials*, vol. 26, no. 14, pp. 1925–1933, 2005.

[218] S. R. Hong, Y. M. Lee, and T. Akaike, "Evaluation of a galactose-carrying gelatin sponge for hepatocytes culture and transplantation," *Journal of Biomedical Materials Research A*, vol. 67, no. 3, pp. 733–741, 2003.

[219] T. G. Park, "Perfusion culture of hepatocytes within galactose-derivatized biodegradable poly(lactide-co-glycolide) scaffolds prepared by gas foaming of effervescent salts," *Journal of Biomedical Materials Research*, vol. 59, no. 1, pp. 127–135, 2002.

[220] M. P. Lutolf and J. A. Hubbell, "Synthetic biomaterials as instructive extracellular microenvironments for morphogenesis in tissue engineering," *Nature Biotechnology*, vol. 23, no. 1, pp. 47–55, 2005.

[221] U. Hersel, C. Dahmen, and H. Kessler, "RGD modified polymers: biomaterials for stimulated cell adhesion and beyond," *Biomaterials*, vol. 24, no. 24, pp. 4385–4415, 2003.

[222] E. Ruoslahti, "RGD and other recognition sequences for integrins," *Annual Review of Cell and Developmental Biology*, vol. 12, pp. 697–715, 1996.

[223] T. G. Kim and T. G. Park, "Biomimicking extracellular matrix: cell adhesive RGD peptide modified electrospun poly(D,L-lactic-co-glycolic acid) nanofiber mesh," *Tissue Engineering*, vol. 12, no. 2, pp. 221–233, 2006.

[224] H. S. Mansur, Z. P. Lobato, R. L. Oréfice, W. L. Vasconcelos, C. Oliveira, and L. J. Machado, "Surface functionalization of porous glass networks: effects on bovine serum albumin and porcine insulin immobilization," *Biomacromolecules*, vol. 1, no. 4, pp. 789–797, 2000.

[225] R. F. S. Lenza, J. R. Jones, W. L. Vasconcelos, and L. L. Hench, "In vitro release kinetics of proteins from bioactive foams," *Journal of Biomedical Materials Research A*, vol. 67, no. 1, pp. 121–129, 2003.

[226] E. Ruoslahti, "RGD and other recognition sequences for integrins," *Annual Review of Cell and Developmental Biology*, vol. 12, pp. 697–715, 1996.

[227] J. L. Myles, B. T. Burgess, and R. B. Dickinson, "Modification of the adhesive properties of collagen by covalent grafting with RGD peptides," *Journal of Biomaterials Science, Polymer Edition*, vol. 11, no. 1, pp. 69–86, 2000.

[228] J. C. Schense, J. Bloch, P. Aebischer, and J. A. Hubbell, "Enzymatic incorporation of bioactive peptides into fibrin matrices enhances neurite extension," *Nature Biotechnology*, vol. 18, no. 4, pp. 415–419, 2000.

[229] S. P. Massia and J. A. Hubbell, "Human endothelial cell interactions with surface-coupled adhesion peptides on a nonadhesive glass substrate and two polymeric biomaterials," *Journal of Biomedical Materials Research*, vol. 25, no. 2, pp. 223–242, 1991.

[230] M. J. Humphries, "The molecular basis and specificity of integrin-ligand interactions," *Journal of Cell Science*, vol. 97, no. 4, pp. 585–592, 1990.

[231] S. P. Massia and J. A. Hubbell, *Journal of Biomedical Materials Research*, vol. 25, pp. 249–252, 1991.

[232] B. K. Brandley and R. L. Schnaar, "Covalent attachment of an Arg-Gly-Asp sequence peptide to derivatizable polyacrylamide surfaces: support of fibroblast adhesion and long-term growth," *Analytical Biochemistry*, vol. 172, no. 1, pp. 270–278, 1988.

[233] H.-B. Lin, W. Sun, D. F. Mosher, et al., "Synthesis, surface, and cell-adhesion properties of polyurethanes containing

covalently grafted RGD-peptides," *Journal of Biomedical Materials Research*, vol. 28, no. 3, pp. 329–342, 1994.

[234] H.-B. Lin, Z. C. Zhao, C. Garcia-Echeverria, D. H. Rich, and S. L. Cooper, "Synthesis of a novel polyurethane co-polymer containing covalently attached RGD peptide," *Journal of Biomaterials Science, Polymer Edition*, vol. 3, no. 3, pp. 217–227, 1992.

[235] P. D. Drumheller, D. L. Elbert, and J. A. Hubbell, "Multifunctional poly(ethylene glycol) semi-interpenetrating polymer networks as highly selective adhesive substrates for bioadhesive peptide grafting," *Biotechnology and Bioengineering*, vol. 43, no. 8, pp. 772–780, 1994.

[236] H.-B. Lin, W. Sun, D. F. Mosher, et al., "Synthesis, surface, and cell-adhesion properties of polyurethanes containing covalently grafted RGD-peptides," *Journal of Biomedical Materials Research*, vol. 28, no. 3, pp. 329–342, 1994.

[237] S. P. Massia and J. A. Hubbell, *Journal of Biomedical Materials Research*, vol. 25, pp. 273–282, 1991.

[238] P. D. Drumheller, D. L. Elbert, and J. A. Hubbell, "Multifunctional poly(ethylene glycol) semi-interpenetrating polymer networks as highly selective adhesive substrates for bioadhesive peptide grafting," *Biotechnology and Bioengineering*, vol. 43, no. 8, pp. 772–780, 1994.

[239] J. Chen, G. H. Altman, V. Karageorgiou, et al., "Human bone marrow stromal cell and ligament fibroblast responses on RGD-modified silk fibers," *Journal of Biomedical Materials Research A*, vol. 67, no. 2, pp. 559–570, 2003.

[240] Y.-S. Lin, S.-S. Wang, T.-W. Chung, et al., "Growth of endothelial cells on different concentrations of Gly-Arg-Gly-Asp photochemically grafted in polyethylene glycol modified polyurethane," *Artificial Organs*, vol. 25, no. 8, pp. 617–621, 2001.

[241] L. De Bartolo, S. Morelli, A. Piscioneri, et al., "Novel membranes and surface modification able to activate specific cellular responses," *Biomolecular Engineering*, vol. 24, no. 1, pp. 23–26, 2007.

[242] S. S. Lateef, S. Boateng, T. J. Hartman, C. A. Crot, B. Russell, and L. Hanley, "GRGDSP peptide-bound silicone membranes withstand mechanical flexing in vitro and display enhanced fibroblast adhesion," *Biomaterials*, vol. 23, no. 15, pp. 3159–3168, 2002.

[243] Y. Hu, S. R. Winn, I. Krajbich, and J. O. Hollinger, "Porous polymer scaffolds surface-modified with arginine-glycine-aspartic acid enhance bone cell attachment and differentiation in vitro," *Journal of Biomedical Materials Research A*, vol. 64, no. 3, pp. 583–590, 2003.

[244] M.-H. Ho, L.-T. Hou, C.-Y. Tu, et al., "Promotion of cell affinity of porous PLLA scaffolds by immobilization of RGD peptides via plasma treatment," *Macromolecular Bioscience*, vol. 6, no. 1, pp. 90–98, 2006.

[245] D. S. W. Benoit and K. S. Anseth, "The effect on osteoblast function of colocalized RGD and PHSRN epitopes on PEG surfaces," *Biomaterials*, vol. 26, no. 25, pp. 5209–5220, 2005.

[246] D. L. Elbert and J. A. Hubbell, "Surface treatments of polymers for biocompatibility," *Annual Review of Materials Science*, vol. 26, no. 1, pp. 365–394, 1996.

[247] J. P. Tam, Q. Yu, and Z. Miao, "Orthogonal ligation strategies for peptide and protein," *Biopolymers*, vol. 51, no. 5, pp. 311–332, 1999.

[248] J. A. Camarero, Y. Kwon, and M. A. Coleman, "Chemoselective attachment of biologically active proteins to surfaces by expressed protein ligation and its application for "protein chip" fabrication," *Journal of the American Chemical Society*, vol. 126, no. 45, pp. 14730–14731, 2004.

[249] G. Thumshirn, U. Hersel, S. L. Goodman, and H. Kessler, "Multimeric cyclic RGD peptides as potential tools for tumor targeting: solid-phase peptide synthesis and chemoselective oxime ligation," *Chemistry*, vol. 9, no. 12, pp. 2717–2725, 2003.

[250] L. Scheibler, P. Dumy, M. Boncheva, et al., "Functional molecular thin films: topological templates for the chemoselective ligation of antigenic peptides to self-assembled monolayers," *Angewandte Chemie: International Edition*, vol. 38, no. 5, pp. 696–699, 1999.

[251] S. P. Massia and J. A. Hubbell, "Immobilized amines and basic amino acids as mimetic heparin-binding domains for cell surface proteoglycan-mediated adhesion," *Journal of Biological Chemistry*, vol. 267, no. 14, pp. 10133–10141, 1992.

[252] W.-J. Li, R. Tuli, X. Huang, P. Laquerriere, and R. S. Tuan, "Multilineage differentiation of human mesenchymal stem cells in a three-dimensional nanofibrous scaffold," *Biomaterials*, vol. 26, no. 25, pp. 5158–5166, 2005.

[253] W.-J. Li, C. T. Laurencin, E. J. Caterson, R. S. Tuan, and F. K. Ko, "Electrospun nanofibrous structure: a novel scaffold for tissue engineering," *Journal of Biomedical Materials Research*, vol. 60, no. 4, pp. 613–621, 2002.

[254] A. Mata, C. Boehm, A. J. Fleischman, G. Muschler, and S. Roy, "Analysis of connective tissue progenitor cell behavior on polydimethylsiloxane smooth and channel micro-textures," *Biomedical Microdevices*, vol. 4, no. 4, pp. 267–275, 2002.

[255] G. Assero, C. Satriano, G. Lupo, C. D. Anfuso, G. Marletta, and M. Alberghina, "Pericyte adhesion and growth onto polyhydroxymethylsiloxane surfaces nanostructured by plasma treatment and ion irradiation," *Microvascular Research*, vol. 68, no. 3, pp. 209–220, 2004.

[256] R. Raman, G. Venkataraman, S. Ernst, V. Sasisekharan, and R. Sasisekharan, "Structural specificity of heparin binding in the fibroblast growth factor family of proteins," *Proceedings of the National Academy of Sciences of the United States of America*, vol. 100, no. 5, pp. 2357–2362, 2003.

[257] M. J. B. Wissink, R. Beernink, A. A. Poot, et al., "Improved endothelialization of vascular grafts by local release of growth factor from heparinized collagen matrices," *Journal of Controlled Release*, vol. 64, no. 1–3, pp. 103–114, 2000.

[258] J. S. Pieper, T. Hafmans, P. B. Van Wachem, et al., "Loading of collagen-heparan sulfate matrices with bFGF promotes angiogenesis and tissue generation in rats," *Journal of Biomedical Materials Research*, vol. 62, no. 2, pp. 185–194, 2002.

[259] S. E. Sakiyama-Elbert and J. A. Hubbell, "Development of fibrin derivatives for controlled release of heparin-binding growth factors," *Journal of Controlled Release*, vol. 65, no. 3, pp. 389–402, 2000.

[260] J. Li, J. Pan, L. Zhang, X. Guo, and Y. Yu, "Culture of primary rat hepatocytes within porous chitosan scaffolds," *Journal of Biomedical Materials Research A*, vol. 67, no. 3, pp. 938–943, 2003.

[261] A. T. Gutsche, H. Lo, J. Zurlo, J. Yager, and K. W. Leong, "Engineering of a sugar-derivatized porous network for hepatocyte culture," *Biomaterials*, vol. 17, no. 3, pp. 387–393, 1996.

[262] J. J. Yoon, H. J. Chung, H. J. Lee, and T. G. Park, "Heparin-immobilized biodegradable scaffolds for local and sustained release of angiogenic growth factor," *Journal of Biomedical Materials Research A*, vol. 79, no. 4, pp. 934–942, 2006.

[263] H. J. Chung, H. K. Kim, J. J. Yoon, and T. G. Park, "Heparin immobilized porous PLGA microspheres for angiogenic

growth factor delivery," *Pharmaceutical Research*, vol. 23, no. 8, pp. 1835–1841, 2006.

[264] D. D. Hile, M. L. Amirpour, A. Akgerman, and M. V. Pishko, "Active growth factor delivery from poly(D,L-lactide-co-glycolide) foams prepared in supercritical CO_2," *Journal of Controlled Release*, vol. 66, no. 2-3, pp. 177–185, 2000.

[265] H. Lee, R. A. Cusick, F. Browne, et al., "Local delivery of basic fibroblast growth factor increases both angiogenesis and engraftment of hepatocytes in tissue-engineered polymer devices," *Transplantation*, vol. 73, no. 10, pp. 1589–1593, 2002.

[266] R. Padera, G. Venkataraman, D. Berry, R. Godavarti, and R. Sasisekharan, "FGF-2/fibroblast growth factor receptor/heparin-like glycosaminoglycan interactions: a compensation model for FGF-2 signaling," *FASEB Journal*, vol. 13, no. 13, pp. 1677–1687, 1999.

[267] L. D. Thompson, M. Pantoliano, and B. Springer, "Energetic characterization of the basic fibroblast growth factor-heparin interaction: identification of the heparin binding domain," *Biochemistry*, vol. 33, no. 13, pp. 3831–3840, 1994.

[268] R. Raman, G. Venkataraman, S. Ernst, V. Sasisekharan, and R. Sasisekharan, "Structural specificity of heparin binding in the fibroblast growth factor family of proteins," *Proceedings of the National Academy of Sciences of the United States of America*, vol. 100, no. 5, pp. 2357–2362, 2003.

[269] J. J. Yoon, H. J. Chung, H. J. Lee, and T. G. Park, "Heparin-immobilized biodegradable scaffolds for local and sustained release of angiogenic growth factor," *Journal of Biomedical Materials Research A*, vol. 79, no. 4, pp. 934–942, 2006.

[270] H. K. Kim, H. J. Chung, and T. G. Park, "Biodegradable polymeric microspheres with "open/closed" pores for sustained release of human growth hormone," *Journal of Controlled Release*, vol. 112, no. 2, pp. 167–174, 2006.

[271] H. Lee, H. J. Chung, and T. G. Park, "Perspectives on: local and sustained delivery of angiogenic growth factors," *Journal of Bioactive and Compatible Polymers*, vol. 22, no. 1, pp. 89–114, 2007.

[272] C. P. Vepari and D. L. Kaplan, "Covalently immobilized enzyme gradients within three-dimensional porous scaffolds," *Biotechnology and Bioengineering*, vol. 93, no. 6, pp. 1130–1137, 2006.

[273] M. Wang, "Surface modification of biomaterials and tissue engineering scaffolds for enhanced osteoconductivity," in *Proceedings of the 3rd Kuala Lumpur International Conference on Biomedical Engineering*, vol. 15, pp. 22–27, Kuala Lumpur, Malaysia, December 2006.

[274] Z. Hu, Y. Chen, C. Wang, Y. Zheng, and Y. Li, "Polymer gels with engineered environmentally responsive surface patterns," *Nature*, vol. 393, no. 6681, pp. 149–152, 1998.

[275] M. Ebara, J. M. Hoffman, A. S. Hoffman, and P. S. Stayton, "Switchable surface traps for injectable bead-based chromatography in PDMS microfluidic channels," *Lab on a Chip*, vol. 6, no. 7, pp. 843–848, 2006.

[276] F. Stoica, C. Alexander, N. Tirelli, A. F. Miller, and A. Saiani, "Selective synthesis of double temperature-sensitive polymer-peptide conjugates," *Chemical Communications*, no. 37, pp. 4433–4435, 2008.

Hindawi Publishing Corporation
International Journal of Polymer Science
Volume 2010, Article ID 138686, 20 pages
doi:10.1155/2010/138686

Review Article

Polymers for Fabricating Nerve Conduits

Shanfeng Wang and Lei Cai

Department of Materials Science and Engineering, The University of Tennessee, Knoxville, TN 37996, USA

Correspondence should be addressed to Shanfeng Wang, swang16@utk.edu

Received 16 June 2010; Accepted 12 August 2010

Academic Editor: Lichun Lu

Peripheral nerve regeneration is a complicated and long-term medical challenge that requires suitable guides for bridging nerve injury gaps and restoring nerve functions. Many natural and synthetic polymers have been used to fabricate nerve conduits as well as luminal fillers for achieving desired nerve regenerative functions. It is important to understand the intrinsic properties of these polymers and techniques that have been used for fabricating nerve conduits. Previously extensive reviews have been focused on the biological functions and in vivo performance of polymeric nerve conduits. In this paper, we emphasize on the structures, thermal and mechanical properties of these naturally derived synthetic polymers, and their fabrication methods. These aspects are critical for the performance of fabricated nerve conduits. By learning from the existing candidates, we can advance the strategies for designing novel polymeric systems with better properties for nerve regeneration.

1. Introduction

Peripheral nerve injury is a serious health problem that affects 2.8% of trauma patients annually [1]. There are around 360,000 cases of upper extremity paralytic syndromes in the United States and more than 300,000 peripheral nerve injuries in Europe on an annual basis [2]. These cases can potentially lead to lifelong disabilities although peripheral nerves exhibit the capacity of self-regeneration for less severe injury. Researchers have developed various strategies for better recovery of nerve functions. End-to-end suturing is one effective method for short nerve gaps whereas tubular structures are necessary for bridging longer gaps [3]. Autologous nerve grafts are considered as "gold standard" for bridging long gaps, but they suffer from limited tissue availability, donor site morbidity, and potential mismatch of tissue structure and size [1–3].

Therefore, various bioengineered nerve grafts have been developed from polymeric materials that have well-tailored properties and dimensions to meet the requirements for peripheral nerve regeneration. These materials range from naturally derived polymers to conventional nondegradable and biodegradable synthetic polymers. Generally, an ideal nerve guide should be non-cytotoxic, highly permeable, and sufficiently flexible with suitable degradation rate and products to provide guidance for regenerative axons and to minimize swelling and inflammatory responses [4]. Inner luminal fillers, offering larger surface area and platform for incorporating bioactive substances, are often used to improve the performance of nerve conduits. The required properties of both tubes and fillers are highly dependent on the intrinsic characteristics of these materials, such as the chemical structure and molecular weight, as well as the fabrication method for making them [5–7]. The polymers for fabricating tubes and their physical properties and manufacturing techniques are summarized in Table 1. Although these materials should have complete information about their molecular characteristics and properties, we only list the information found in the references.

Because of the importance of this topic, there exist a number of review articles on guided nerve regeneration using polymeric materials for constructing nerve conduits and luminal fillers [1–24]. Instead of elaborating on their biocompatibility and *in vivo* regenerative performance, this paper is to focus on the intrinsic properties of these polymeric materials and their specific fabrication techniques. We provide readers with the knowledge about these polymeric biomaterials and fabrication methods that have been investigated for peripheral nerve regeneration, as well as the material design strategies that can be used to control the physical properties and regenerative functions of synthetic nerve conduits.

Table 1: Summary of polymers used for fabricating nerve conduits.

Material	Chemical structure	T_g (°C)	T_m (°C)	Molecular weight (g/mol), intrinsic viscosity [η], and composition [reference(s)]	Fabrication method [reference(s)]	Mechanical properties [reference(s)]
Alginate/Chitosan blend				Alginate: 57% mannuronic acid; Chitosan: 89%* and 91%*	Mandrel coating [31]	0.38 ± 0.16 N (pull-out force) 37 ± 1, 40 ± 4, and 61 ± 1 kPa (shear modulus) under normal forces of 3, 10, and 30 N
Chitosan	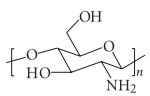	203		210 k, 93%* 22 k, 92.3%* 400 k, 89%* 85%*	Dip-coating [25] Injection molding [26] Injection molding [29] Soft lithography and molding [27]	
				1.8 M, 85.1%*	Braiding and molding [28]	Unreinforced porous conduits: 0.41 ± 0.17 MPa; Fiber-reinforced conduits: 3.69 ± 0.64 MPa (tensile strength)
Chitosan/PLA blend				Chitosan: 22 k, 92.3%*; PLA: 460 k	Mandrel coating [30]	
Collagen					Dip-coating and crosslinking [32, 33] Injection molding and crosslinking [34–36] Fiber winding [37] Unidirectional freezing and freeze-drying [38–40]	
					Film rolling and crosslinking [41, 42]	Crosslinked: 32.6 ± 0.6 or 22.5 ± 0.7 kPa; Uncrosslinked: 16.7 ± 0.7 kPa. (tensile modulus) [42]
Collagen/Chitosan blend				Chitosan: 150 k, 96.7%*, Collagen: Chitosan = 4 : 1	Unidirectional freezing and freeze-drying [43]	87 ± 7 kPa (tensile modulus)
				Collagen: Chitosan = 3:1	Freeze-drying and steam-extrusion [44]	326 ± 11 kPa (tensile modulus)
				Collagen: Chitosan = 4:3		886 ± 3 kPa (tensile modulus)
Gelatin				bloom number: 300	Injection molding and crosslinking [45–47]	Porous: 0.94 ± 0.22 MPa; Nonporous: 7.25 ± 4.1 MPa (tensile stress) [46]
					Dipcoating and crosslinking [48–50]	

Table 1: Continued.

Material	Chemical structure	T_g (°C)	T_m (°C)	Molecular weight (g/mol), intrinsic viscosity [η], and composition [reference(s)]	Fabrication method [reference(s)]	Mechanical properties [reference(s)]
Cinnamoyl HA Hyaff	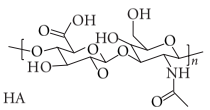				Injection molding and photo-crosslinking [52] Braiding [54]	
SF					Injection molding [55] Electrospinning and film rolling [56]	Dry condition: 10.9 ± 0.3 MPa (maximum fracture strength), 27.7 ± 0.8 g (compressive strength);Wet condition: 5.5 ± 0.4 MPa (maximum fracture strength), 2.5 ± 0.5 g (compressive strength).
PAN-PVC	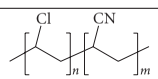				Wet-phase inversion [57, 58]	
PDMS or silicone	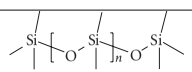				Commercially available [59–63]	
PE	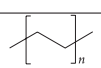				Commercially available [64, 65]	
PHEMA-MMA	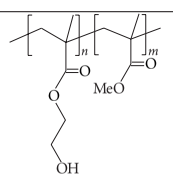				Centrifuge casting and crosslinking [66–73]	177 ± 26 kPa, 311 ± 51 kPa (tensile modulus) [71] 263 ± 13 kPa (tensile modulus) [73]
PPy	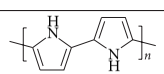				Electro-plating and molding [74]	
PCD	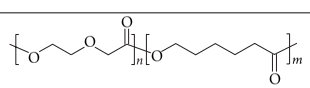			[η] = 2.09 dL/g, PCL:PDO = 95 : 5	Injection molding [75]	
PCL	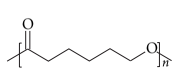	~ −60	~60	65 k [76] 80 k	Dip coating [76, 77] Braiding [78] Melt extrusion [79] Wire mesh and mandrel coating [80]	206–345 MPa (tensile modulus) 20–34 MPa (tensile strength)
PCL/CultiSpher					Wire mesh and mandrel coating [80]	0.13 ± 0.1 MPa (tensile modulus) 0.51 ± 0.3 MPa (tensile strength)

Table 1: Continued.

Material	Chemical structure	T_g (°C)	T_m (°C)	Molecular weight (g/mol), intrinsic viscosity [η], and composition [reference(s)]	Fabrication method [reference(s)]	Mechanical properties [reference(s)]
PCL/gelatin and PCL/PLL grafted gelatin				PCL: 80k; gelatin: bloom number 300; FITC-labeled PLL: 30–70 k; PLL bromide: 150–300 k	Melt extrusion and inner surface treatment [79]	
PCLA	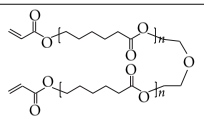	~ −60	39	3.5 k	Injection molding and photo-crosslinking [81]	70.0 ± 31.1 MPa (tensile modulus at 37°C)
PCLF	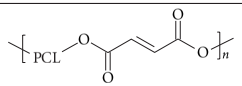	~ −59	42	9 k	Injection molding and photo-crosslinking [82–84]	138 ± 17 MPa (tensile modulus) 0.42 ± 0.03 N (pull-out force) 73.4 ± 12.7 MPa (flexural modulus)
PDLLA	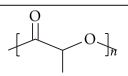			46.7 k [85]	Dip coating [65, 85, 86]	
PDLLC	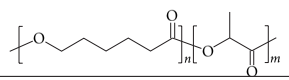			LA:CL = 50 : 50; L:D in LA = 85 : 15 LA:CL = 80 : 20	Dip coating [87] Ink-jet microdispensing [88]	
PDO	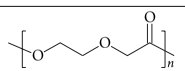	−16	110	[η] = 1.89 dL/g	Injection molding [75]	
PGA	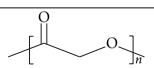	45–50 [89]	225–235 [89]	150 k	Braiding and dip-coating with collagen [90–94]	
PGC	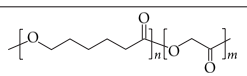			[η] = 1.63 dL/g, GA:CL = 65 : 35	Injection molding [75]	
PGS	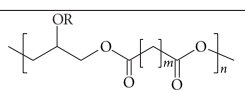		5.23, 37.62 [95]		Injection molding and crosslinking [95, 96]	0.28 MPa (tensile modulus) > 0.5 MPa (tensile strength)
PHB	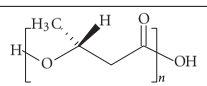				Film rolling [97, 98] Commercially available [99]	
PHBHHx	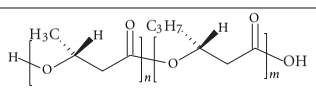				Dip coating and leaching [100]	Conduits with non-uniform wall porosity: 2.29 ± 0.37 MPa, with uniform wall porosity: 0.94 ± 0.19 MPa (wet state tensile stress)

Table 1: Continued.

Material	Chemical structure	T_g (°C)	T_m (°C)	Molecular weight (g/mol), intrinsic viscosity [η], and composition [reference(s)]	Fabrication method [reference(s)]	Mechanical properties [reference(s)]
PHBV/P(L-D,L)LA/PLGA blend	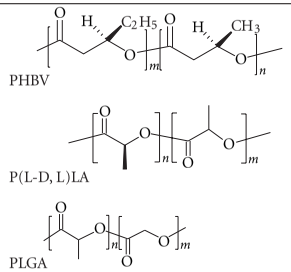			PHBV: 95% PHB; P(L-D,L)LA:PLLA:P(D,L)LA = 70 : 30, [η] = 5.5–6.5 g/dL; PLGA: 50 : 50$^+$, [η] = 0.32–0.44 g/dL	Solvent casting from micropatterned silicon templates and then film rolling on electrospun mat [101]	Solid film: 1.05 ± 0.23 MPa, Porous film: 0.08 ± 0.02 MPa (tensile modulus)
PLC	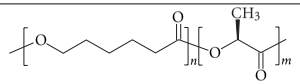	60	134	[η] = 1.58 dL/g, LA:CL = 60 : 40	Injection molding [75]	
PLGA	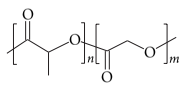			113 k, 75 : 25$^+$, 52 k, 50 : 50$^+$, Pluronic F127 ($EG_{99}PG_{65}EG_{99}$, 12.5 k) added.	Immersion precipitation [102, 103]	
				[η] = 0.5–0.79 dL/g, 50 : 50$^+$; [η] = 1.2–1.59 dL/g, 90 : 10$^+$ [104]51.9 k, [η] = 0.9–1.2 dL/g, 85 : 15$^+$ [105]	Dipcoating and immersion precipitation [104, 105]	
				[η] = 0.2 dL/g, 50 : 50$^+$	Wet phase inversion [106]	
				94 k, 85 : 15$^+$ [107] 122 k, 75 : 25$^+$ [108] 58.8 k, 50 : 50$^+$; 92 k, 75 : 25$^+$; 120 k, 85 : 15$^+$ [109] 75 k, 85 : 15$^+$ [110] 80–120 k, 11–24 k, 75 : 25$^+$ [111]136 k, 85 : 15$^+$ [112, 113]	Injection molding [107–113]	7-channel, porosity of 78.6% : 0.8 ± 0.2 kPa; 7-channel, porosity of 78.6%: 510 ± 130 kPa (compression modulus) [108]Porous multiple lumen conduits using 80–120 K (porogen:polymer = 12 : 1): 134 kPa (compression modulus) [111]
				37.4 k, 75 : 25$^+$	Extrusion [114]	Porous conduits: ~8 MPa (tensile modulus)
				100 k, 10 : 90$^+$	Electrospinning [115]	
				10 : 90$^+$	Microbraiding [116]	
				64.7 k, 85 : 15$^+$	Dip coating [117]	

Table 1: Continued.

Material	Chemical structure	T_g (°C)	T_m (°C)	Molecular weight (g/mol), intrinsic viscosity [η], and composition [reference(s)]	Fabrication method [reference(s)]	Mechanical properties [reference(s)]
PLGA/gelatin blend					Molding [118]	Composition dependent: ~0.25–~3.75 MPa (tensile strength)
PLGC	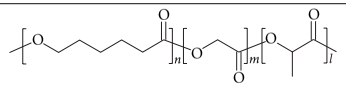			300 k, LA:GA:CL = 75 : 8:1	Film rolling [119]	
PLLA	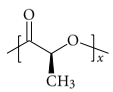	55–60	170–175	46.5 k	Extrusion [114]	Porous conduits: ~80 MPa (tensile modulus)
					Braiding [120]	
				46.5 k [121]	Solvent casting, extrusion, and particulate leaching [121, 122]	81.7 ± 35.1 MPa (tensile strength), 1.0 ± 0.4 MPa (tensile modulus) [121]
					Fused deposition [89]	
				100 k [117]	Dip coating [117, 123]	
PLLA and PGA				130 k [94]	Braiding and dip coating with collagen [94]	
PLLA-PEG-MA	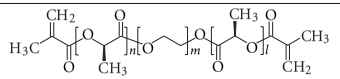			LLA:PEG = 2 : 1 and 4 : 1	Centrifuge casting and crosslinking [124]	
PPE, or P(BHET-EOP/TC)	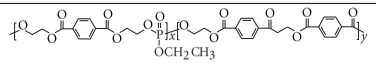			14.9 k and 18.9 k, EOP/TC = 80 : 20, x : y = 4 : 1	Dip coating [125–127]	
PPF-PCL	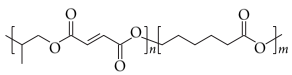	−57	17.1	29k, PPF:PCL = 10 : 90	Injection molding and photo-crosslinking [128]	2.68 ± 0.05 MPa (tensile modulus); single-channel conduits: 52.0 ± 1.2 MPa (flexural modulus); seven-channel conduits: 66.0 ± 3.7 MPa (flexural modulus); 0.11 N (pull-out force)
PSU	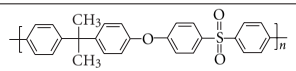	185			Commercially available [129–131]	
PTMC-CL	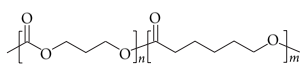		47	TMC:CL = 30 : 70, [η] = 1.31 dL/g	Dip coating [132, 133]	
			44	TMC:CL = 15 : 85, [η] = 1.27 dL/g		
PU based on PEG and PCL diol	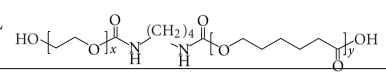			110 k	Dip coating [134] Rapid prototyping [135]	~8–~15 MPa (tensile strength)
PU based on PHBV-diol and PGC-diol	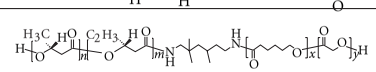	−35	120	178 k	Extrusion [136]	1.9 MPa (tensile modulus)
		−35	122	105 k		8.4 MPa (tensile modulus)
		−30	123	160 k		46 MPa (tensile modulus)

*Deacetylation degree; +Lactide:Glycolide (LA:GA) ratio.

2. Tube Materials

2.1. Natural Polymers for Fabricating Nerve Conduits. Natural polymers utilized for fabricating nerve conduits include chitosan [25–31], collagen [32–44], gelatin [45–50], hyaluronic acid (HA) [51–54], and silk fibroin (SF) [55, 56]. These natural polymers offer excellent biocompatibility, support cell attachment and functions, avoid serious immune response, provide appropriate signaling to cells without the need of growth factors and can degrade by naturally occurring enzymes [5–7, 22]. However, natural polymers generally suffer from batch-to-batch variance and need extensive purification and characterization [5–7]. Further, most of them lack adequate mechanical strength and degrade relatively fast *in vivo* [5–7]. Oftentimes natural polymers need to be chemically modified and crosslinked or blended with other structural components such as synthetic polymers to meet the mechanical requirements. Due to their low denaturing temperature and thermal stability, natural polymers are usually fabricated via injection molding, dip-coating, and electrospinning from their solutions at ambient or lower temperatures [5–7]. Although these fabrication methods are mentioned in this section, the detailed descriptions will be elaborated in Section 4.

Chitosan, a copolymer of D-glucosamine and *N*-acetyl-D-glucosamine, is a well-known biodegradable polysaccharide obtained from *N*-deacetylation of chitin, which can be extracted from the shells of crabs and shrimps [5, 6, 22]. Chitosan has been used to fabricate nerve tubes and scaffolds because of its excellent biocompatibility and antibacterial activity [5, 6, 22]. Due to its high glass transition temperature (T_g) of $\sim$ 203°C and relatively low thermal stability, pure chitosan cannot be melted and is usually processed in solutions. In one study, chitosan was dissolved in trifluoroacetic acid (TFA) first and added with methylene chloride (MC) to prepare a solution [25]. This chitosan/TFA/MC solution was electrospun onto a rotating Steel use Stainless (SUS) bar to form macro/nanofibrous scaffolds as the inner layer while chitosan-acetic acid solution is dip-coated on the SUS bar to form an outer layer [25]. Immobilization of laminin peptides to these bilayered chitosan tubes was also achieved [25]. Multichanneled chitosan nerve conduits with more complex patterned designs and precise dimensions have been achieved by molding chitosan/acetic acid solution in polydimethylsiloxane (PDMS) molds prepared through soft lithography [27]. Chitosan is relatively brittle and can degrade rapidly in solutions at high temperatures; therefore, many studies have been conducted to improve the mechanical properties of chitosan scaffolds via crosslinking or blending with reinforcing fibers or other polymers [26, 28–31]. Chitosan dissolved in acetic acid was injected in a tubular stainless-steel mold and crosslinked with formaldehyde into a porous viscous gel [26]. Nerve conduits were formed by subsequent freeze-drying or lyophilization and inserted with longitudinally aligned poly (glycolic acid) (PGA) fibers as luminal fillers [26]. Chitosan tubes prepared using mold casting were strengthened by over 9 times with braided chitosan yarns [28]. In another study, reinforcing poly (L-lactide-*co*-glycolide) (PLGA) coils were mounted into a mold before chitosan solution was injected and dried [29]. Poly (lactic acid) (PLA) was also incorporated with chitosan in preparing nerve tubes using the dip-coating method to improve the resistance to tension and compression [30]. Physically crosslinked hydrogel nerve tubes can be formed by adding alginate aqueous solution into chitosan/acetic acid solution because these two polysaccharides are oppositely charged [31].

Collagen is comprised of a group of 28 proteins with a same triple helical structure as an extended rod stabilized by hydrogen bonding [5, 6, 23, 24]. Collagen (types I and III) can be derived from animal tissues such as porcine skin [32] and bovine deep flexor (Achilles) tendon [33–35, 42, 44]. As one major form of extracellular matrix (ECM) protein, collagen provides excellent biocompatibility and weak antigenic activity [5, 6]. Collagen has been extensively employed to form both outer tubular structures and central lumen for nerve regeneration. By crosslinking collagen between amine groups, the relatively low mechanical properties of collagen can be circumvented and the structural stability of fabricated nerve conduits can be achieved. The crosslinking reagents for collagen include formaldehyde, glutaraldehyde, and 1-ethyl-3-(3-dimethylaminopropyl)-1-carbodiimide (EDC)/*N*-hydroxysuccinimide (NHS) pair for a zero-length crosslinking method. Among several commercially available nerve guides [5, 32, 36], there exists an FDA-approved nerve conduit made from crosslinked bovine collagen (type I). This collagen nerve conduit is known as NeuraGen (Integra) tube [5, 32, 36]. Besides conventional injection molding and dip-coating methods for preparing nerve conduits [32–36], collagen can be extruded in its water solution and coagulated into filaments [37]. These collagen filaments can be wound up around a mandrel to form a tubular structure and also used as longitudinally aligned luminal fillers [37]. Collagen sponge tubes with parallel oriented interconnected pores have been achieved through unidirectional freezing followed by lyophilization [38–40]. Microwave irradiation was also used to crosslink collagen and this method is advantageous because potentially toxic crosslinking agents such as glutaraldehyde can be avoided [41, 42]. The average tensile modulus of microwave-crosslinked collagen tubes was enhanced from 16.7 ± 0.7 kPa for uncrosslinked tubes to 32.6 ± 0.6 kPa [42]. Collagen was blended with chitosan homogeneously in acidic solutions to fabricate nerve conduits [43, 44], which exhibited much higher tensile modulus of 886 ± 3 kPa when the collagen:chitosan ratio was 4 : 3 after crosslinking and freeze-drying [44].

Gelatin is a biodegradable polymer derived from collagen by thermal denaturation of chemical and physical degradation. Gelatin has excellent biocompatibility, plasticity, and adhesiveness. The water solubility of gelatin renders convenient processing in aqueous solutions but the resulted products suffer from poor mechanical properties and handling characteristics [5, 6]. Thus, subsequent crosslinking using proper crosslinking agents is crucial to improve the chemical and physical characteristics of gelatin for preventing toxicity and fabricating suitable tubular structures for nerve regeneration [5, 6]. Gelatin tubes are usually

prepared by injection molding or dip-coating followed by immersing the mold or mandrel into crosslinking agent solutions [45–50]. Styrenated gelatin was synthesized and photopolymerized into nerve conduits and fibers under visible light irradiation in the presence of camphorquinone [45]. Other than chemical modification of gelatin, three commonly used agents, genipin, proanthocyanidin, and EDC/NHS, can be used to crosslink gelatin via primary amino groups along the chain backbone [46–50]. The residue free amino groups are a useful indicator for estimating the crosslinking density [47, 48]. Crosslinking degree has been revealed to be crucial in tuning the degradation rate so as to influence nerve regenerative responses because a too low crosslinking density results in more degradation products to evoke more severe foreign body reaction while a too high crosslinking density impedes the degradation and causes nerve compression with thickened perineurium and epineurium [48].

Hyaluronan (HA or hyaluronate) is a high molecular weight glycosaminoglycan (GAG) that can be found in ECM of humans [22]. HA demonstrates a unique combination of advantages including nonimmunogenic, nonadhesive, bioactive GAG that has been associated with several cellular processes and axonal ingrowth [22, 51–54]. HA has to be modified to be crosslinkable for forming three-dimensional (3D) structures with mechanical strength. HA, conjugated by cinnamic acid to the carboxyl group using aminopropanol as a spacer, can be injected into a silicone mold and cured under ultraviolet (UV) light [51, 52]. Crosslinked HA is so weak for handling that augmentation of an outer layer made from another biodegradable material is required for the operation procedure and during the nerve regeneration period because the nerve conduits should keep their structure with sufficient elasticity and flexibility for the fixation to the nerve stumps [52]. Another crosslinkable HA is glycidyl methacrylate HA or GMHA [53]. Nerve conduits based on an esterified hyaluronan derivative (Hyaff) have been prepared from individually knitted strands and strengthened by coating a thin layer of the same polymer [54]. Although Hyaff nerve tubes demonstrated excellent biocompatibility, a quick degradation, massive ingrowth of cells, and fibrous tissue formation can possibly hamper the ultimate goal of the tubes in peripheral nerve repair [54].

SF, a core structure protein derived from natural silk, can be used as a textile material. SF is also a candidate biomaterial for nerve regeneration applications [55, 56]. Similar to other naturally derived polymers, SF is also water soluble with excellent biocompatibility, but it has a high resilience and a relatively slower degradation rate [55]. Fabrication method is crucial for achieving desired properties from SF. Normal injection molding techniques followed by demolding via lyophilization result in fragile sheets with weak compressive and tensile properties under wet conditions [55]. Tubes woven from electro-spun SF fibers are easily crushed and the degradation is slow *in vivo* although they have an improved tensile strength [55]. Tubes with a unique eggshell-like microstructure have been developed by combining a molded tubular structure with inner oriented SF filaments [55]. Tubes with this eggshell-like microstructure have a good compressive strength of 10.9 ± 0.3 MPa at the dry state and a lower value of 5.5 ± 0.4 MPa at the wet state [55]. Using electro-spinning, SF nanofibers have been fabricated after blended with poly(ethylene oxide) (PEO), which helps achieve stable and continuous processing [56]. SF membranes decorated with SF nanofibers were hydrated and rolled around a mandrel and glued using cyanoacrylate glue to form a tube, which was further coated with PLGA [56].

2.2. Synthetic Polymeric Tubular Materials. Compared with their naturally derived counterparts, synthetic polymers have advantages such as unlimited supply and tailorable properties via varying their chemical structures [12–22]. The ease of copolymerization facilitates the development of regulating and optimizing material characteristics such as degradation behavior, mechanical performance, thermal properties, and wettability [12–22]. These polymers (Table 1) are generally classified into two categories based on degradability. Non-biodegradable polymers used in fabricating nerve conduits include silicone rubber or PDMS [59–63], polyethylene (PE) [64, 65], polysulfone (PSU) [129–131], poly(acrylonitrile-*co*-vinyl chloride) (PAN-PVC) [57, 58], poly(2-hydroxyethyl methacrylate-*co*-methyl methacrylate) (PHEMA-MMA) [66–73], and polypyrrole (PPy) [74]. Biodegradable polymers used in fabricating nerve conduits include poly(ε-caprolactone) (PCL) [76–80], PCL acrylate (PCLA) [81], PCL fumarate (PCLF) [82–84], polypropylene fumarate-*co*-PCL (PPF-PCL) [128], polydioxanone (PDO) [75], PCL-*co*-PDO (PCD) [75], PGA [90–94], poly(glycerol sebacate) (PGS) [95, 96], PLGA [102–118], poly(L-lactic acid) (PLLA) [89, 114, 117, 120–123], poly(D,L-lactic acid) (PDLLA) [65, 85, 86], poly(D,L-lactide-*co*-caprolactone) (PDLLC) [87, 88], poly(L-lactide-*co*-caprolactone) (PLC) [75], poly(glycolide-*co*-caprolactone) (PGC) [75], poly(lactide-*co*-glycolide-*co*-caprolactone) (PLGC) [119], poly(L-lactide-*co*-ethylene glycol) methacrylate (PLLA-PEG-MA) [124], poly(3-hydroxybutyrate) (PHB) [97–99], poly(3-hydroxybutyrate-*co*-3-hydroxyhexanoate) (PHBHHx) [100], poly(3-hydroxybutyrate-*co*-3-hydroxyvalerate)/poly(L-lactide-*co*-D,L-lactide)/PLGA [PHBV/P(L-D,L)LA/PLGA] blend [101], polyphosphoester (PPE) [125–127], polytrimethylene carbonate-ε-caprolactone (PTMC-CL) [132, 133], and polyurethane (PU) [134–136]. Among these polymers, one of the authors and his colleagues recently developed injectable and photocrosslinkable PCLA [81], PCLF [82–84] and PPF-PCL [128], which have well controlled material properties, slow degradation rates, and nonswelling characteristics in water. Figure 1 demonstrates nerve conduits made from crosslinked PCLF before and after implantation in the rat sciatic nerve for 17 weeks [83].

Nerve guides made from non-biodegradable materials can lead to chronic nerve compression and may damage the regenerating nerves [5–7, 15]. Therefore, a secondary surgery is needed to remove these nondegradable conduits after nerve regeneration is fulfilled. Silicone rubber tubes are the earliest and widely used synthetic nerve tubes because

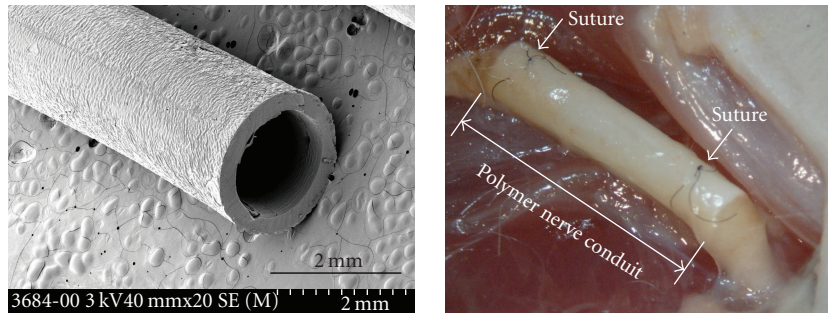

(a) (b)

Figure 1: Polymer nerve conduits made from crosslinked poly (ε-caprolactone) fumarate (PCLF) before (a) and after (b) implantation in the rat sciatic nerve. (Source: [83], copyright with permission from Elsevier Science).

of their inertness, availability, and flexibility [15, 59–63]. It can be processed directly without the need of a solvent, which may cause problems such as evaporation and toxicity. Because silicone nerve conduits are not biodegradable or permeable for large molecules, they only supply an isolated environment for nerve regeneration [59–63]. Other commercially available PE or PSU tubes were also used to evaluate the role of luminal fillers such as gel rod and aligned filaments or electro-spun fibers in guiding neurite extension and promoting axon growth in long-gap nerve injuries [64, 65, 129–131]. Although PHB conduits are normally prepared using the film rolling method [97, 98], they are also commercially available [99].

PAN-PVC copolymer was used to fabricate nerve guides via a wet-phase inversion technique [57, 58]. Semipermeable membranes can be formed from the polymer solution using an annular spinneret with deionized water as a liquid precipitant [57, 58]. Using different starting polymer solutions, various hollow fiber membranes were fabricated with different wall thicknesses and hydraulic permeabilities [58]. The wall architectures of these membranes were anisotropic and consisted of a fingerlike macrovoid structure [58].

Poly(2-hydroxyethyl methacrylate) (PHEMA) is an elastic and inert polymer. Hydrogel-based tubular structures made from PHEMA are too soft to be handled in implantation [66]. A hydrophobic monomer methyl methacrylate (MMA) was copolymerized with HEMA in the presence of crosslinking agent ethylene dimethacrylate to obtain PHEMA-MMA hydrogel with a higher mechanical strength [66–73]. A biphasic wall structure can be created with an inner porous sponge-like layer and an outer gel-like layer because of phase separation during the polymerization with centrifugal forces [68–73]. Because PHEMA-MMA nerve conduits are still weak, PCL coils have been used to further enhance their mechanical strength and prevent tubes from partial collapse during implantation [72]. Mechanical stability can be also improved by wrapping small PHEMA-MMA tubes in an expanded polytetrafluoroethylene (e-PTFE) membrane [73].

As electrical stimulation has been demonstrated to have a beneficial effect on axonal regeneration, electrically conductive nerve conduits are promising for enhancing restoration of lost nerve function [74]. Nerve conduits made from PPy could optimally utilize the polymer properties, such as controllable charge density, erodability, and wettability [74]. To fabricate 3D PPy structures, PPy monomer has been oxidized to form a tubular structure on an electrode while subsequent reduction allowed mechanical dissociation from the cylindrical electrode mold to separate PPy from its conductive template [74]. PPy can be also incorporated with PCL network in preparing nerve conduits [84], which will be discussed later.

Biodegradable nerve conduits are generally more promising in bridging nerve gaps as they can degrade away after accomplishing their task. Further, biodegradable nerve conduits offer possibilities of incorporating bioactive chemicals such as nerve growth factor (NGF), laminin, and fibronectin inside the wall and then releasing them in a controlled manner during polymer degradation [5–7, 12–22]. In order to achieve this goal, polymer degradation rate should match the rate for axon growth along the gap. The thermal and mechanical properties of biodegradable polymers can be readily controlled at the molecular level using advanced synthetic routes. These properties are crucial for handling and implantation of conduits and axonal ingrowth. Many biodegradable polymers are semi-crystalline and their thermal properties such as melting temperature (T_m), crystallinity, crystallization rate, and morphology of crystalline domains are important for determining their bulk and surface physicochemical properties. The existence of crystalline regions can enhance mechanical strength and structural stability while it reduces the degradation rate and permeability of the nerve tubes made from these semi-crystalline polymers, consequently affecting cellular and regenerative functions [5–7].

Polyesters such as PGA, PLA, PCL, PDO, and their copolymers are most commonly used biodegradable polymers in constructing tubular structures for peripheral nerve regeneration. These polyesters are usually synthesized via ring-opening polymerization and can degrade via the hydrolysis of ester bonds along the polymer backbone [5–7]. As shown in Table 1, there are many methods to fabricate polyesters into nerve conduits, such as dip-coating, immersion precipitation, injection molding, extrusion, braiding,

and electro-spinning. These polyesters dissolved in solutions can also be electro-spun to fibers or fibrous mats, which can be subsequently braided or rolled into flexible, porous, and highly permeable tubes. There are also commercially available fibers of these polyesters for braiding. Fabrication of nerve conduits using fibers is an advantageous way to overcome the inherent rigidity of polylactides such as PGA, PLA, and their copolymer PLGA with T_g higher than the body temperature [90–94, 115, 116, 120]. In order to improve their processability and the flexibility of the produced conduits, polylactides can be plasticized adding 2% triethyl citrate, a plasticizer [65].

Material properties can be readily tailored by varying the composition and block length in the copolymers such as PCD [75], PLC [75], PGC [75], PDLLC [87, 88], and PLGC [119]. Besides copolymers, PLGA was also blended with gelatin in a co-solvent MC to obtain composition dependent mechanical properties with tensile strength varied from ~0.25 to ~3.75 MPa [118]. Besides making single-component nerve conduits [76–80], PCL was also blended with gelatin, poly(L-lysine) (PLL)-grafted gelatin [79], or porous collagen-based beads (CultiSphers) [80] for preparing nerve conduits, which have the combination of good processability of PCL and the optimal biocompatibility of natural polymers. Crosslinkable PLLA-PEG-MA was synthesized by the ring-opening polymerization of LLA in the presence of PEG with two hydroxyl end groups as the initiator and then end-coupling PLLA-PEG with methacrylate groups [124]. Porous PLLA-PEG-MA nerve conduits were fabricated using the same centrifugal casting method for preparing PHEMA-MMA nerve conduits [124].

PGS synthesized via polycondensation between glycerol and sebacic acid is a viscous prepolymer that can be further crosslinked in a mold into an elastomeric device with a desired shape and excellent mechanical properties [95, 96]. PGS films with a tensile modulus of 0.28 MPa were fabricated to mimic the mechanical properties of ECM and the biocompatibility evaluation suggested PGS an excellent candidate material for neural reconstruction applications [96].

PCL-derived crosslinkable copolymers such as PCLF, PCLA, and PPF-PCL have been synthesized and nerve conduits have been fabricated via a technique that combines injection molding and photo-crosslinking [81–84, 128]. The synthesis routes of PCLF and PCLA were simplified by reacting the hydroxyl groups in PCL diols or triols that have different molecular weights with acryloyl chloride or fumaryl chloride in the presence of potassium carbonate [81–83, 137] as the proton scavenger other than triethylamine (TEA) [138]. The use of this new proton scavenger can avoid colorization and contamination from the reaction between TEA and unsaturated acyl chloride/anhydride and greatly simplify the purification steps [139]. Using PCL diol or triol precursors with different molecular weights, controllable thermal properties such as T_g, T_m, and crystallinity for both uncrosslinked and crosslinked PCLF or PCLA were obtained and used to further modulate the mechanical and rheological properties of PCL networks [81–83]. When the molecular weight of PCL diol or triol precursor was low, the resulted PCL network was amorphous at room temperature with low-tensile modulus because the crosslinks completely suppressed the crystalline domains [81–83]. In contrast, a higher molecular weight (>2000 g/mol) PCL diol can result in a semi-crystalline network with significantly higher tensile modulus and strength, and resistance to tear in suturing [81–83]. PCLAs generally exhibited better crosslinking efficiency than PCLFs because of more reactive acrylate segments during the reaction and higher crosslinking densities [81–83].

Well-tuned architecture, crystallinity, mechanical and surface characteristic of crosslinked PCLAs and PCLFs have been shown to support and correlate with nerve cell attachment, proliferation, differentiation, and axon myelination [81–84]. Mechanical properties enhanced by PCL crystalline structures were found to play an important role in controlling Schwann cell precursor line (SpL201) cell behavior [81, 83]. *In vivo* studies of crosslinked PCLF nerve conduits (Figure 1) showed no inflammatory reaction or existence of macrophages [83]. Nerve cable with myelinated axons has been found after 6 or 17 weeks of implantation [83]. Taking advantages of the roughness and flexibility of crosslinked PCLF [82, 83], a conductive PCLF-PPy composite nerve conduit has been prepared recently in the Yaszemski group by polymerizing pyrrole with benzoyl peroxide and naphthalene-2-sulfonic acid sodium salt in a swollen PCLF nerve conduit in MC [84].

In order to achieve a wider range of mechanical properties, PCLF or PCLDA can be blended and crosslinked with PPF [140, 141]. Meanwhile, a series of multiblock PPF-PCL copolymers have been synthesized via a three-step polycondensation between PPF and PCL diol [142]. Through controlling the block size and composition in PPF-PCL copolymers, both uncrosslinked and crosslinked PPF-PCL have a broad range of thermal and mechanical properties that can be used to satisfy the requirements in hard and soft tissue replacements such as bone and nerve repair [128, 142]. Similar to crosslinked PCLF nerve conduits [83], single-lumen and multi-channel PPF-PCL nerve conduits have been fabricated using the molding and photo-crosslinking technique and implanted in the rat sciatic nerve transection model for 4 and 16 weeks to demonstrate biocompatibility and guided axonal growth [128].

PHB is a granular constituent of bacterial cytoplasm, having the advantage of ease of synthesis via microorganisms and its adjustable mechanical properties, biocompatibility and biodegradability. PHB conduits have been fabricated by rolling PHB sheets around a mandrel followed by thermal sealing [97, 98]. PHBHHx was developed with a better flexibility than PHB [100]. Conduits with uniform wall porosity and those with nonuniform wall porosity were fabricated using dip-coating and particulate leaching with NaCl-sized particles as porogen [100]. PHBV containing 95% PHB was blended with P(L-D,L)LA and PLGA to form a porous micropatterned film by solution casting from a silicon template and then the film can be rolled together with a electro-spun PHBV/PLGA aligned fibrous mat inside to prepare nerve conduits [101].

PPE is biocompatible with a controllable rate of degradation via hydrolysis due to their relatively low molecular weight. Porous tubular structure can be easily achieved via dip-coating followed by immersion precipitation [125–127]. The drawbacks of PPE are fast degradation and swelling in water that will reduce its mechanical properties in the duration for axon growth and then may cause tube distortion or even failure [125].

PU has elastic and flexible properties that are favorable for nerve guidance tubes [134–136]. A biodegradable polyurethane has been developed from PCL and PEG with 1,6-hexamethyl diisocyanate as the chain extender and dip-coated into tubes for repairing peripheral nerve injuries [134]. The hydrophilic PEG segment can accelerate the degradation rate of hydrophobic PCL, making the degradation kinetics more compatible with the nerve regeneration rate [134]. Porous nerve conduits can also be processed via rapid prototyping using a double nozzle, low temperature, deposition manufacturing system that combines phase separation and chemical crosslinking simultaneously [134]. PUs made from crystalline PHB segments and amorphous segments of glycolide and ε-caprolactone have shown controllable physical properties with varied crystallinity and Young's modulus from 1.9 to 46 MPa when the composition is varied [136].

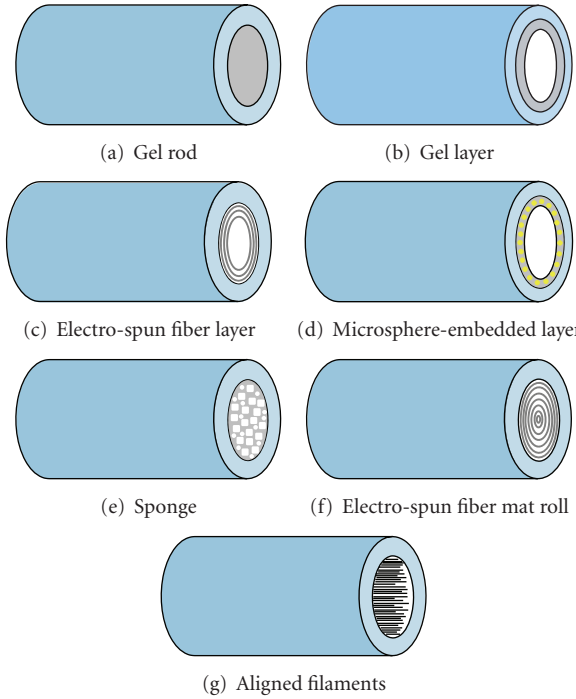

Figure 2: Forms of luminal fillers in polymer nerve conduits.

3. Luminal Fillers

To modify hollow nerve tubes to achieve enhanced performance, luminal fillers have been employed as a structural component [23, 24]. The internal filler substances can provide more surface area and have potentials to incorporate cells and growth factors [17, 23, 24]. Various factors such as composition, mechanical properties, and the permeability of nerve conduits may influence the organization of the inside filler. Fillers may also affect the physical properties of the whole tube and reduce the cross-sectional area for growth of regenerative nerves [17, 23, 24]. Therefore sophisticated design of the filler form should be performed by taking consideration of these factors to achieve optimal enhancement based on the hollow tubes. Widely used structural luminal fillers are summarized in Table 2 and seven major filler forms are demonstrated in Figure 2. Two comprehensive reviews on the roles of luminal fillers in nerve regeneration have been published earlier [23, 24], which also include support cells and neurotrophins. In this section, we focus on the polymeric fillers inside nerve conduits in the forms of gel rod and sponge, gel inner layer, and aligned fibers.

Natural polymers, such as agarose, collagen, laminin, and fibrin, are often used as luminal fillers in the form of solutions, hydrogels, filaments, and porous sponges as platforms for incorporating cells, growth factors, and drugs [17, 23, 24]. Their soft characteristics and biocompatibility can help regenerative guidance for the reconstruction of nerve gaps [17, 23, 24]. Agarose can form hydrogels containing gradients of laminin-1 and NGF molecules in PSU conduits as anisotropic scaffolds [129]. Distributed micro- or nanosized fibers or films in 3D gels are growth permissive as the gels can serve to distribute the fibers in 3D space, and the fibers would provide a 2D surface for regenerating axons [3]. Collagen has been formed into filaments [37, 63, 90], sponges [90–93], and gel inner layers [135] in PGA, PU, silicone conduits. Collagen sponges were prepared by pouring homogenized collagen aqueous solution into PGA tubes and freezing the solution at -20°C followed by freeze-drying for 3 h [90–93]. The tubes were then subjected to dehydrothermal treatment at 140°C for 24 h to induce crosslinking among the collagen molecules [90–93].

Laminins as major proteins found in basal lamina are important molecules widely investigated for regeneration of nerve tissues [5–7]. Laminins contain various cell binding sites including the Ile-Lys-Val-Ala-Val (IKVAV) sequence, a bioactive peptide that can promote neurite outgrowth [5]. One commercially available laminin-containing gel, Matrigel, and the above-mentioned agarose hydrogels containing laminin have been used as filler materials in nerve conduits [65, 129, 132]. Fibrin, a fibrous protein made from fibrinogen, can be formed into a matrix as structural support for neural tissues [5–7]. In one case, the liquid-state mixture of collagen, laminin, and fibronectin can be injected through a precooled micropipette into the lumens inside silicone rubber chambers prior to crosslinking of collagen *in vivo* [60]. These gel-like luminal fillers can also be used as injectable materials with the capability of carrying support cells, NGF, and drugs for central nerve repair and other degenerative diseases [22].

Synthetic filler polymers are usually inserted into nerve conduits as aligned fibers or filaments. For this purpose, these polymers have been fabricated into fibers using traditional fiber spinning techniques or electro-spinning:

Table 2: Summary of structural luminal fillers in polymer nerve conduits.

Filler material	Structure	Filler form	Tube material(s) [reference(s)]
Agarose coupled with laminin	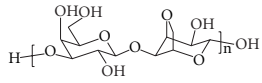	Gel rod	PSU [129]
Alginate with or without fibronectin		Gel rod	PHB [99]
Chitosan immobilized with peptides	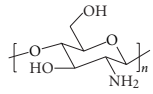	Electrospun fiber mesh inner layer	Chitosan [25]
Collagen		Aligned fibrils	Collagen [37], Silicone [63]
		Fiber	PGA coated with collagen [90]
		Sponge	PGA coated with collagen [90–93]
		Gel layer	PU [135]
Collagen-GAG		Gel rod	Collagen and silicone [34]
Fibrin		Gel rod	Silicone [60], PLGC [119], PHB [97]
HA	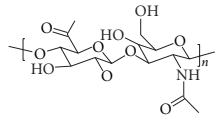	Gel rod	PE [64]
Gelatin		Fiber or gel rod	Gelatin [45]
Matrigel		Gel rod	PTMC-CL [132], PDLLA and PE [65]
SF		Longitudinal aligned fiber	SF [55]
Polyamide	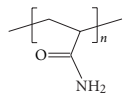	Filament	Silicone [62]
PAN-MA	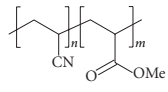	Electrospun fiber	PSU [130]
PGA	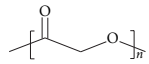	Longitudinal aligned fiber	Chitosan [26]
		Filament	PTMC-CL [133]
PHBV/PLGA blends	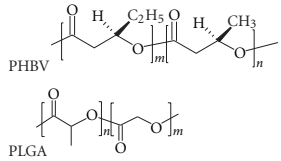	Electro-spun mat	PHBV/P(L-D,L)LA/PLGA blends [101]
PLLA	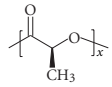	Filament	Silicone and P(L-D,L)LA (75 : 25) [61]
PLGA	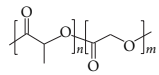	Electro-spun fiber mat roll (LA:GA = 85 : 15)	PSU [131]
		PHEMA inner layer embedded with PLGA microspheres (LA:GA = 85 : 15)	PHEMA-MMA [68]
		PCL inner layer embedded with PLGA microspheres (LA:GA = 50 : 50)	PCL [76]
PP		Filament	PAN-PVC [57]

polyamide [62], polyacrylonitrile-*co*-methylacrylate (PAN-MA) [130], PGA [26, 133], PLLA [61], and PLGA [131]. For example, eight polyamide filaments (250 μm, diameter) were placed inside silicone tubes to increase the overall cross-sectional area that can support myelinated axon [62]. Longitudinal PGA filaments (14 μm, diameter) have been inserted into a chitosan conduit to serve as a directional guide for axons [26]. Electro-spun fibers of PLGA with diameters from 100 nm to 3 μm, which can be controlled by the polymer concentration, were aligned on a rotating mandrel and later this electro-spun fiber mat was rolled into a nanofilament "cigar" and inserted into a PSU tube to guide neurite extension; however, the degradation of PLGA fibers was so fast that distortion of fibers reduced the alignment [131]. To overcome this problem, non-degradable PAN-MA electro-spun fibers (~400–600 nm, diameter) were applied in the same group and successfully promoted regeneration of axons over a 17 mm nerve gap [130].

Other than gel rod/sponge and aligned fibers/filaments, an inner layer can be prepared inside nerve conduits. As shown in Table 2, electro-spun fiber mesh [25], collagen gel [135], and an inner PCL layer embedding PLGA double-walled microspheres [76] have been incorporated with a stronger outer tube made from chitosan, PU, and PCL, respectively. These inner layers supply helpful environment and bioactive substances for axon growth while the outer tube is strong enough to endure the implantation period.

4. Fabrication Methods

As mentioned in Section 2, a variety of techniques have been utilized to fabricate different natural and synthetic polymers into 3D tubular nerve guide, depending on their material characteristics. In this section, we supply detailed descriptions about these techniques using schemes demonstrated in Figure 3. There are seven widely-used techniques such as injection molding, mandrel coating or dip coating, centrifuge casting, film rolling and sealing, extrusion, electrospinning, and microbraiding of filaments. Although not included in Figure 3, polymer nerve conduits can also be fabricated using wet phase inversion [57, 58, 106], immersion precipitation [102–105], and advanced computer-aided microfabrication techniques such as fused deposition and soft lithography [27, 88, 89, 135].

Injection molding (Figure 3(a)) is the most commonly used technique for fabricating nerve conduits because it can be applied to most polymers except for very brittle materials such as PHB. Polymers with relatively a high thermal stability and a relatively low T_m, such as PCL (T_m = ~ 60°C), can be melt extruded while alternatively they can be dissolved in an evaporative solvent, referred to as solvent casting. Polymer melts or solutions with appropriate viscosities can be injected into one specific tubular mold to form a desired shape after solidification at $T < T_m$ or T_g or solvent removal. Due to finite length effect, polymer physical properties such as thermal and mechanical properties normally demonstrate sharp molecular weight dependence when the molecular weight is smaller than a critical value. A molecular weight higher than the entanglement molecular weight (M_e) of a polymer is generally required for injection molding because otherwise the polymer may lack adequate mechanical strength for structural applications. For low molecular weight oligomers or natural polymers, crosslinking or curing is needed. Chemical crosslinking for collagen or gelatin can occur in a mold by adding crosslinking agent prior to injection. Photo-crosslinkable polymers such as PCLFs and PCLAs can be cured in a transparent glass mold by UV light exposure [81–84]. Permeable conduits can be also easily

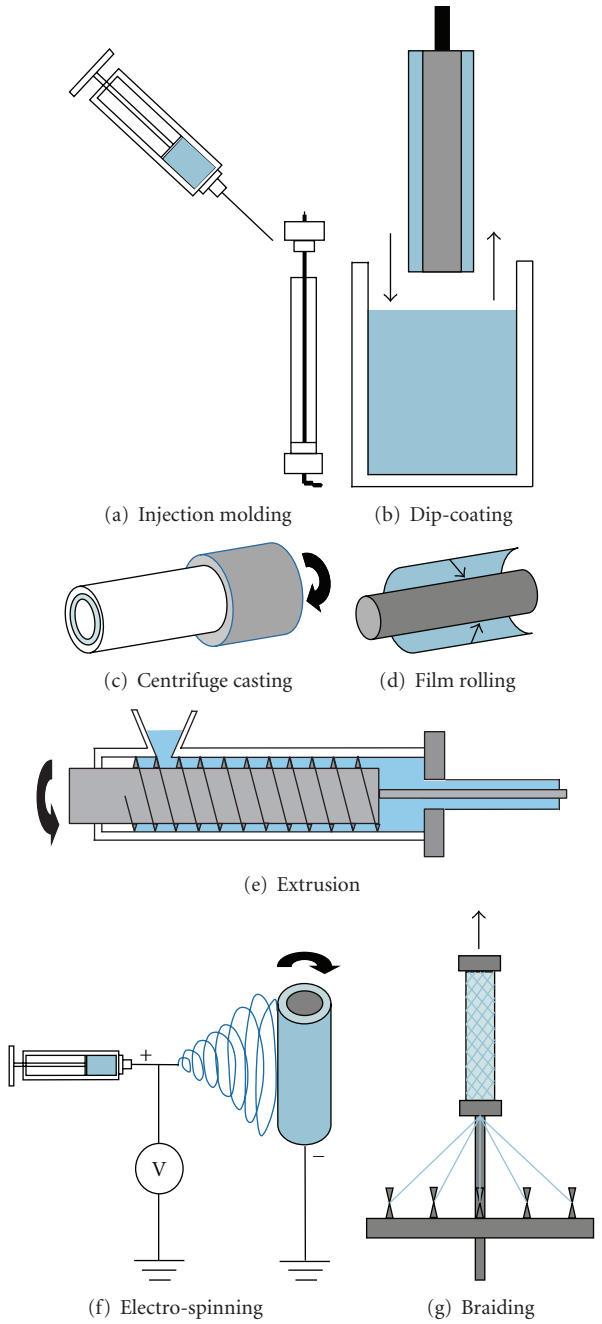

Figure 3: Widely used methods for fabricating polymer nerve conduits.

prepared using particulate leaching, gas foaming, and phase-separation methods [5–7]. Freeze drying or lyophilization is commonly used for natural polymers to dehydrate and demold. Unidirectional freezing followed by freeze-drying has recently been developed to obtain oriented porous structure in the collagen tubes [38–40, 43].

Mandrel coating or dip coating (Figure 3(b)) is another facile technique to fabricate nerve conduits with better controlled thickness and homogeneity. This technique involves a rotating metal or Teflon or water-soluble poly(vinyl alcohol) (PVA) mandrel [80] that can be coated with or dipped into polymer solutions to form a thin polymer layer after drying. The wall thickness depends on the solution concentration and coating cycles. Dip coating is usually followed by solvent evaporation or immersion precipitation in a nonsolvent, allowing quick formation of a polymer membrane that can have a porous structure on the rotating mandrel. Moreover, the potential of this technique exists to incorporate a myriad of features for each individual layer, such as one layer that can be more permeable and porous than the other [125–127]. Preparing conductive PPy nerve conduits also needs an electrode mold although the synthesis of PPy occurs directly onto the electrode via electroplating [74].

Liquid-liquid centrifuge casting method (Figure 3(c)) developed in the Shoichet group has been used for acrylate-based hydrogels such as PHEMA-MMA [66–73]. The centrifugal casting process is based on phase separation of the polymer phase from the monomer phase during polymerization in a centrifuging mold. The polymer phase with higher viscosity and density can be pushed to the outer edges by centrifugal forces to forming a stable tube. PHEMA-MMA conduits prepared using this method are semipermeable, soft and flexible, and with mechanical properties similar to those of nerve tissue [66–73].

Film rolling (Figure 3(d)) around a mandrel is a very simple method to achieve tubular structure using a polymer sheet or an electro-spun mat. It is particularly convenient for a two-dimensional (2D) substrate with surface patterns that can be only fabricated on a surface to be rolled into a 3D nerve conduit [101]. The sealing step is critical in this method and it can be achieved by heating [97, 98], fusing or gluing the overlapping ends with organic chemicals [56, 119], or dipping the roll in a solution containing crosslinking agents [41, 42].

Melt extrusion (Figure 3(e)) is a conventional method for processing thermoplastic polymers with suitable flow temperatures, melt viscosities, and thermal stabilities. A single-screw extruder can be used to fabricate nerve conduits through melt extrusion [79, 114]. The nozzle or die in this extruder and the rod moving together with the piston determine the outer and inner diameters of the nerve conduit [114]. Melt extrusion is often combined with particulate leaching to prepare porous biodegradable conduits [114, 121, 122].

Electro-spinning (Figure 3(f)) has been extensively used to fabricate fibers with submicron size. These fibers can serve as fillers directly or be microbraided into highly permeable and flexible tubes, especially for PGA, PLLA, and PLGA fibers [90–94, 116, 120]. The microbraiding machine (Figure 3(g)) involves a Teflon mandrel with a controlled diameter that allows fiber to be pulled upward from bottom through a convergence point and forming point [116]. The porosity of the tubular structure can be modulated by the braiding angle, number of fibers in a bundle, and the number of fiber bundles [116]. As discussed in Section 3, electro-spun luminal filler fibers and nerve conduits have porous structures, which are advantages for neurite extension and axon growth along the fiber direction [131].

Because of limitations of precise manufacturing processes, techniques aforementioned cannot reproduce tubes with uniform channel diameter and designed patterns at microscale. Soft lithography has been newly developed to manufacture silicon-based structures and replicate them with PDMS for producing chitosan nerve conduit subunits which can be stacked coaxially [27]. Because of its precise capability, soft lithography is well suited for fabricating nerve conduits with complex structures for controlling regenerative pathways and degradation rate [27]. Soft lithography can be potentially applied to manufacture injectable and photo-crosslinkable polymers to achieve precisely controlled networks. Novel microfabrication system also involves rapid prototyping, which is the general term for a manufacturing process used to produce complicated 3D structures automatically based on computer-aided designs (CADs). Several rapid prototyping processes such as fused deposition modeling [89] and ink-jet microdispensing [88] have been utilized for biodegradable polymers to form nerve conduits with precise dimensions and complex internal structures. In one study, polylactides including PLA, PGA, and PLGA were heated up at 200°C and extruded through a fine nozzle as the nozzle traces an XY surface [89]. The process was repeated layer by layer until the microstructure was completed [89]. A double nozzle, low temperature, deposition manufacturing system has been developed to process PU and collagen simultaneously, combining both phase separation and chemical crosslinking to form a double layered tubular structure [135].

5. Conclusions and Perspectives

This paper summarizes natural and synthetic polymeric materials and fabrication methods to produce tubular structures and luminal fillers for guided nerve regeneration and repair. The importance of material properties such as chemical structure, thermal, and mechanical properties have been discussed to correlate with their performance. Understanding the design strategies for developing novel tubular materials and luminal fillers is crucial to further improve the biological performance and regenerative functions of nerve guidance conduits. Nerve cell-material interactions are also important in examining the suitability of a polymer candidate for nerve repair and regeneration [143–147]. Numerous studies have been performed on the differentiation of pheochromocytoma (PC12) cells, dorsal root ganglia, and neuronal stem/progenitor cells on the polymer substrates with controllable mechanical properties [146–151]. It should be noted that surface stiffness plays different roles in regulating neuronal cells and glial cells:

soft substrates can stimulate neurite extension and branching while inhibit glial cell spreading and proliferation [147–151]. In order to meet the requirements in optimizing regenerative conditions *in vivo*, the physical properties, especially thermal and mechanical properties of the material should be characterized extensively prior to fabrication of nerve conduits and animal implantation. Injectable and photo-crosslinkable materials with sufficient mechanical properties and lower degradation rates have demonstrated great promise for feasible and effective treatment to bridge nerve gaps. Novel *in-situ* crosslinkable polymers and their manufacturing methods, particularly microfabrication methods, need to be developed for fabricating nerve conduits with more complicated structures and advanced functions. In particular, heterogeneous conduits that can precisely combine different materials, varied geometric architecture, and bioactive substances will be promising for nerve regeneration and repair.

Abbreviations

2D:	Two-dimensional
3D:	Three-dimensional
CAD:	Computer-aided design
CultiSpher:	Porous collagen-based bead
ECM:	Extracellular matrix
EDC:	1-ethyl-3-(3-dimethylaminopropyl)-1-carbodiimide
e-PTFE:	Expanded polytetrafluoroethylene
FDA:	Food and Drug Administration
GAG:	Glycosaminoglycan
GMHA:	Glycidyl methacrylated HA
HA:	Hyaluronic acid
Hyaff:	Esterified hyaluronan derivative
MC:	Methylene chloride
M_e:	Entanglement molecular weight
MMA:	methyl methacrylate
NGF:	Nerve growth factor
NHS:	*N*-hydroxysuccinimide
PAN-MA:	Poly(acrylonitrile-*co*-methylacrylate)
PAN-PVC:	poly(acrylonitrile-*co*-vinyl chloride)
P(BHET-EOP/TC):	Poly(bishydroxyethyl terephthalate-ethylorthophosphorylate/terephthaloyl chloride)
PC12:	Pheochromocytoma
PCD:	Poly(ε-caprolactone)-*co*-polydioxanone
PCL:	Poly(ε-caprolactone)
PCLA:	Poly(ε-caprolactone) acrylate
PCLF:	Poly(ε-caprolactone) fumarate
PDLLA:	Poly(D,L-lactic acid) or poly(D,L-lactate)
PDLLC:	poly(D,L-lactide-*co*-caprolactone)
PDMS:	Polydimethylsiloxane
PDO:	Polydioxanone or poly(*p*-dioxanone)
PE:	Polyethylene
PEO:	Poly(ethylene oxide)
PEG:	Poly(ethylene glycol)
PGA:	Poly(glycolic acid)
PGC:	Poly(glycolide-*co*-caprolactone)
PGS:	Poly(glycerol sebacate)
PHB:	Poly(3-hydroxybutyrate)
PHBHHx:	Poly(3-hydroxybutyrate-*co*-3-hydroxyhexanoate)
PHBV:	Poly(3-hydroxybutyrate-*co*-3-hydroxyvalerate) or poly[(*R*)-3-hydroxybutyric acid-*co*-(*R*)-3-hydroxyvaleric acid]
PHEMA:	Poly(2-hydroxyethyl methacrylate)
PHEMA-MMA:	Poly(2-hydroxyethyl methacrylate-*co*-methyl methacrylate)
PLA:	Poly(lactic acid) or polylactide
PLC:	Poly(L-lactide-*co*-caprolactone)
P(L-D,L)LA:	Poly(L-lactide-*co*-D,L-lactide)
PLGA:	Poly(L-lactide-*co*-glycolide)
PLGC:	Poly(lactide-*co*-glycolide-*co*-caprolactone)
PLL:	Poly(L-lysine)
PLLA:	Poly(L-lactic acid) or poly(L-lactide)
PLLA-PEG-MA:	Poly(L-lactide-*co*-ethylene glycol) methacrylate
PP:	Polypropylene
PPE:	Polyphosphoester
PPF-*co*-PCL:	Polypropylene fumarate-*co*-poly(ε-caprolactone)
PPy:	Polypyrrole
PSU:	Polysulfone
PTMC-CL:	Polytrimethylene carbonate-ε-caprolactone
PU:	Polyurethane
PVA:	Poly(vinyl alcohol)
SF:	Silk fibroin
SpL201:	Schwann cell precursor line
SUS:	Steel use Stainless
TEA:	Triethylamine
TFA:	Trifluoroacetic acid
T_g:	Glass transition temperature
T_m:	Melting temperature
UV:	Ultraviolet.

Acknowledgment

This work was supported by the start-up fund from the University of Tennessee.

References

[1] J. S. Belkas, M. S. Shoichet, and R. Midha, "Peripheral nerve regeneration through guidance tubes," *Neurological Research*, vol. 26, no. 2, pp. 151–160, 2004.

[2] J. Noble, C. A. Munro, V. S. S. V. Prasad, and R. Midha, "Analysis of upper and lower extremity peripheral nerve injuries in a population of patients with multiple injuries," *Journal of Trauma—Injury, Infection and Critical Care*, vol. 45, no. 1, pp. 116–122, 1998.

[3] R. V. Bellamkonda, "Peripheral nerve regeneration: an opinion on channels, scaffolds and anisotropy," *Biomaterials*, vol. 27, no. 19, pp. 3515–3518, 2006.

[4] G. C. W. de Ruiter, M. J. A. Malessy, M. J. Yaszemski, A. J. Windebank, and R. J. Spinner, "Designing ideal conduits for peripheral nerve repair," *Neurosurgical Focus*, vol. 26, no. 2, pp. 1–9, 2009.

[5] V. Chiono, C. Tonda-Turo, and G. Ciardelli, "Artificial scaffolds for peripheral nerve reconstruction," *International Review of Neurobiology*, vol. 87, pp. 173–198, 2009.

[6] G. Ciardelli and V. Chiono, "Materials for peripheral nerve regeneration," *Macromolecular Bioscience*, vol. 6, no. 1, pp. 13–26, 2006.

[7] C. E. Schmidt and J. B. Leach, "Neural tissue engineering: strategies for repair and regeneration," *Annual Review of Biomedical Engineering*, vol. 5, pp. 293–347, 2003.

[8] R. D. Fields, J. M. Le Beau, F. M. Longo, and M. H. Ellisman, "Nerve regeneration through artificial tubular implants," *Progress in Neurobiology*, vol. 33, no. 2, pp. 87–134, 1989.

[9] R. Bellamkonda and P. Aebischer, "Review: tissue engineering in the nervous system," *Biotechnology and Bioengineering*, vol. 43, no. 7, pp. 543–554, 1994.

[10] C. A. Heath and G. E. Rutkowski, "The development of bioartificial nerve grafts for peripheral-nerve regeneration," *Trends in Biotechnology*, vol. 16, no. 4, pp. 163–168, 1998.

[11] G. R. D. Evans, "Challenges to nerve regeneration," *Seminars in Surgical Oncology*, vol. 19, no. 3, pp. 312–318, 2000.

[12] R. Y. Kannan, H. J. Salacinski, P. E. M. Butler, and A. M. Seifalian, "Artificial nerve conduits in peripheral-nerve repair," *Biotechnology and Applied Biochemistry*, vol. 41, no. 3, pp. 193–200, 2005.

[13] M. F. Meek and J. H. Coert, "US Food and Drug Administration /Conformit Europe-approved absorbable nerve conduits for clinical repair of peripheral and cranial nerves," *Annals of Plastic Surgery*, vol. 60, no. 4, pp. 466–472, 2008.

[14] S. Ichihara, Y. Inada, and T. Nakamura, "Artificial nerve tubes and their application for repair of peripheral nerve injury: an update of current concepts," *Injury*, vol. 39, no. 4, pp. 29–39, 2008.

[15] E. O. Johnson and P. N. Soucacos, "Nerve repair: experimental and clinical evaluation of biodegradable artificial nerve guides," *Injury*, vol. 39, pp. S30–S36, 2008.

[16] L. A. Pfister, M. Papaloïzos, H. P. Merkle, and B. Gander, "Nerve conduits and growth factor delivery in peripheral nerve repair," *Journal of the Peripheral Nervous System*, vol. 12, no. 2, pp. 65–82, 2007.

[17] X. Jiang, S. H. Lim, H.-Q. Mao, and S. Y. Chew, "Current applications and future perspectives of artificial nerve conduits," *Experimental Neurology*, vol. 223, pp. 86–101, 2010.

[18] Y.-C. Huang and Y.-Y. Huang, "Biomaterials and strategies for nerve regeneration," *Artificial Organs*, vol. 30, no. 7, pp. 514–522, 2006.

[19] H. M. Geller and J. W. Fawcett, "Building a bridge: engineering spinal cord repair," *Experimental Neurology*, vol. 174, no. 2, pp. 125–136, 2002.

[20] L. N. Novikova, L. N. Novikov, and J.-O. Kellerth, "Biopolymers and biodegradable smart implants for tissue regeneration after spinal cord injury," *Current Opinion in Neurology*, vol. 16, no. 6, pp. 711–715, 2003.

[21] N. N. Madigan, S. McMahon, T. O'Brien, M. J. Yaszemski, and A. J. Windebank, "Current tissue engineering and novel therapeutic approaches to axonal regeneration following spinal cord injury using polymer scaffolds," *Respiratory Physiology and Neurobiology*, vol. 169, no. 2, pp. 183–199, 2009.

[22] D. R. Nisbet, K. E. Crompton, M. K. Horne, D. I. Finkelstein, and J. S. Forsythe, "Neural tissue engineering of the CNS using hydrogels," *Journal of Biomedical Materials Research Part B*, vol. 87, no. 1, pp. 251–263, 2008.

[23] H. Yan, F. Zhang, M. B. Chen, and W. C. Lineaweaver, "Conduit luminal additives for peripheral nerve repair," *International Review of Neurobiology*, vol. 87, pp. 199–225, 2009.

[24] M. B. Chen, F. Zhang, and W. C. Lineaweaver, "Luminal fillers in nerve conduits for peripheral nerve repair," *Annals of Plastic Surgery*, vol. 57, no. 4, pp. 462–471, 2006.

[25] W. Wang, S. Itoh, A. Matsuda et al., "Enhanced nerve regeneration through a bilayered chitosan tube: the effect of introduction of glycine spacer into the CYIGSR sequence," *Journal of Biomedical Materials Research Part A*, vol. 85, no. 4, pp. 919–928, 2008.

[26] X. Wang, W. Hu, Y. Cao, J. Yao, J. Wu, and X. Gu, "Dog sciatic nerve regeneration across a 30-mm defect bridged by a chitosan/PGA artificial nerve graft," *Brain*, vol. 128, no. 8, pp. 1897–1910, 2005.

[27] D.-Y. Wang and Y.-Y. Huang, "Fabricate coaxial stacked nerve conduits through soft lithography and molding processes," *Journal of Biomedical Materials Research Part A*, vol. 85, no. 2, pp. 434–438, 2008.

[28] A. Wang, Q. Ao, Y. Wei et al., "Physical properties and biocompatibility of a porous chitosan-based fiber-reinforced conduit for nerve regeneration," *Biotechnology Letters*, vol. 29, no. 11, pp. 1697–1702, 2007.

[29] T. Freier, R. Montenegro, H. S. Koh, and M. S. Shoichet, "Chitin-based tubes for tissue engineering in the nervous system," *Biomaterials*, vol. 26, no. 22, pp. 4624–4632, 2005.

[30] F. Xie, F. L. Qing, B. Gu, K. Liu, and X. S. Guo, "*In vitro* and *in vivo* evaluation of a biodegradable chitosan-PLA composite peripheral nerve guide conduit material," *Microsurgery*, vol. 28, no. 6, pp. 471–479, 2008.

[31] L. A. Pfister, M. Papaloïzos, H. P. Merkle, and B. Gander, "Hydrogel nerve conduits produced from alginate/chitosan complexes," *Journal of Biomedical Materials Research Part A*, vol. 80, no. 4, pp. 932–937, 2007.

[32] O. Alluin, C. Wittmann, T. Marqueste et al., "Functional recovery after peripheral nerve injury and implantation of a collagen guide," *Biomaterials*, vol. 30, no. 3, pp. 363–373, 2009.

[33] S.-T. Li, S. J. Archibald, C. Krarup, and R. D. Madison, "Peripheral nerve repair with collagen conduits," *Clinical Materials*, vol. 9, no. 3-4, pp. 195–200, 1992.

[34] L. J. Chamberlain, I. V. Yannas, H.-P. Hsu, and M. Spector, "Connective tissue response to tubular implants for peripheral nerve regeneration: the role of myofibroblasts," *Journal of Comparative Neurology*, vol. 417, no. 4, pp. 415–430, 2000.

[35] B. A. Harley, M. H. Spilker, J. W. Wu et al., "Optimal degradation rate for collagen chambers used for regeneration of peripheral nerves over long gaps," *Cells Tissues Organs*, vol. 176, no. 1-3, pp. 153–165, 2004.

[36] L. Yao, G. C.W. de Ruiter, H. Wang et al., "Controlling dispersion of axonal regeneration using a multichannel collagen nerve conduit," *Biomaterials*, vol. 31, no. 22, pp. 5789–5797, 2010.

[37] H. Okamoto, K.-I. Hata, H. Kagami et al., "Recovery process of sciatic nerve defect with novel bioabsorbable collagen tubes packed with collagen filaments in dogs," *Journal of Biomedical Materials Research Part A*, vol. 92, no. 3, pp. 859–868, 2010.

[38] A. Bozkurt, R. Deumens, C. Beckmann et al., "*In vitro* cell alignment obtained with a Schwann cell enriched microstructured nerve guide with longitudinal guidance channels," *Biomaterials*, vol. 30, no. 2, pp. 169–179, 2009.

[39] A. Bozkurt, G. A. Brook, S. Moellers et al., "*In vitro* assessment of axonal growth using dorsal root ganglia explants in a novel three-dimensional collagen matrix," *Tissue Engineering*, vol. 13, no. 12, pp. 2971–2979, 2007.

[40] V. Kroehne, I. Heschel, F. Schügner, D. Lasrich, J. W. Bartsch, and H. Jockusch, "Use of a novel collagen matrix with oriented pore structure for muscle cell differentiation in cell culture and in grafts," *Journal of Cellular and Molecular Medicine*, vol. 12, no. 5A, pp. 1640–1648, 2008.

[41] M. R. Ahmed, S. Vairamuthu, MD. Shafiuzama, S. H. Basha, and R. Jayakumar, "Microwave irradiated collagen tubes as a better matrix for peripheral nerve regeneration," *Brain Research*, vol. 1046, no. 1-2, pp. 55–67, 2005.

[42] M. R. Ahmed, U. Venkateshwarlu, and R. Jayakumar, "Multi-layered peptide incorporated collagen tubules for peripheral nerve repair," *Biomaterials*, vol. 25, no. 13, pp. 2585–2594, 2004.

[43] X. Hu, J. Huang, Z. Ye et al., "A novel scaffold with longitudinally oriented microchannels promotes peripheral nerve regeneration," *Tissue Engineering Part A*, vol. 15, no. 11, pp. 3297–3308, 2009.

[44] X. Wang, J. Zhang, H. Chen, and Q. Wang, "Preparation and characterization of collagen-based composite conduit for peripheral nerve regeneration," *Journal of Applied Polymer Science*, vol. 112, no. 6, pp. 3652–3662, 2009.

[45] E. Gámez, Y. Goto, K. Nagata, T. Iwaki, T. Sasaki, and T. Matsuda, "Photofabricated gelatin-based nerve conduits: nerve tissue regeneration potentials," *Cell Transplantation*, vol. 13, no. 5, pp. 549–564, 2004.

[46] J.-Y. Chang, T.-Y. Ho, H.-C. Lee et al., "Highly permeable genipin-cross-linked gelatin conduits enhance peripheral nerve regeneration," *Artificial Organs*, vol. 33, no. 12, pp. 1075–1085, 2009.

[47] B.-S. Liu, "Fabrication and evaluation of a biodegradable proanthocyanidin-crosslinked gelatin conduit in peripheral nerve repair," *Journal of Biomedical Materials Research Part A*, vol. 87, no. 4, pp. 1092–1102, 2008.

[48] M.-C. Lu, S.-W. Hsiang, T.-Y. Lai, C.-H. Yao, L.-Y. Lin, and Y.-S. Chen, "Influence of cross-linking degree of a biodegradable genipin-cross-linked gelatin guide on peripheral nerve regeneration," *Journal of Biomaterials Science, Polymer Edition*, vol. 18, no. 7, pp. 843–863, 2007.

[49] Y.-S. Chen, J.-Y. Chang, C.-Y. Cheng, F.-J. Tsai, C.-H. Yao, and B.-S. Liu, "An *in vivo* evaluation of a biodegradable genipin-cross-linked gelatin peripheral nerve guide conduit material," *Biomaterials*, vol. 26, no. 18, pp. 3911–3918, 2005.

[50] J.-Y. Chang, J.-H. Lin, C.-H. Yao, J.-H. Chen, T.-Y. Lai, and Y.-S. Chen, "*In vivo* evaluation of a biodegradable EDC/NHS-cross-linked gelatin peripheral nerve guide conduit material," *Macromolecular Bioscience*, vol. 7, no. 4, pp. 500–507, 2007.

[51] K. Miyamoto, M. Sasaki, Y. Minamisawa, Y. Kurahashi, H. Kano, and S.-I. Ishikawa, "Evaluation of *in vivo* biocompatibility and biodegradation of photo-crosslinked hyaluronate hydrogels (HADgels)," *Journal of Biomedical Materials Research Part A*, vol. 70, no. 4, pp. 550–559, 2004.

[52] Y. Sakai, Y. Matsuyama, K. Takahashi et al., "New artificial nerve conduits made with photo-crosslinked hyaluronic acid for peripheral nerve regeneration," *Bio-Medical Materials and Engineering*, vol. 17, no. 3, pp. 191–197, 2007.

[53] J. B. Leach and C. E. Schmidt, "Characterization of protein release from photo-crosslinkable hyaluronic acid-polyethylene glycol hydrogel tissue engineering scaffolds," *Biomaterials*, vol. 26, no. 2, pp. 125–135, 2005.

[54] K. Jansen, J. F. A. van der Werff, P. B. van Wachem, J.-P. A. Nicolai, L. F. M. H. de Leij, and M. J. A. Van Luyn, "A hyaluronan-based nerve guide: *in vitro* cytotoxicity, subcutaneous tissue reactions, and degradation in the rat," *Biomaterials*, vol. 25, no. 3, pp. 483–489, 2004.

[55] Y. Yang, F. Ding, J. Wu et al., "Development and evaluation of silk fibroin-based nerve grafts used for peripheral nerve regeneration," *Biomaterials*, vol. 28, no. 36, pp. 5526–5535, 2007.

[56] S. Madduri, M. Papaloïzos, and B. Gander, "Trophically and topographically functionalized silk fibroin nerve conduits for guided peripheral nerve regeneration," *Biomaterials*, vol. 31, no. 8, pp. 2323–2334, 2010.

[57] X. Wen and P. A. Tresco, "Effect of filament diameter and extracellular matrix molecule precoating on neurite outgrowth and Schwann cell behavior on multifilament entubulation bridging device *in vitro*," *Journal of Biomedical Materials Research Part A*, vol. 76, no. 3, pp. 626–637, 2006.

[58] K. W. Broadhead, R. Biran, and P. A. Tresco, "Hollow fiber membrane diffusive permeability regulates encapsulated cell line biomass, proliferation, and small molecule release," *Biomaterials*, vol. 23, no. 24, pp. 4689–4699, 2002.

[59] C.-B. Jenq and R. E. Coggeshall, "Nerve regeneration through holey silicone tubes," *Brain Research*, vol. 361, no. 1-2, pp. 233–241, 1985.

[60] L. R. Williams, "Exogenous fibrin matrix precursors stimulate the temporal progress of nerve regeneration within a silicone chamber," *Neurochemical Research*, vol. 12, no. 10, pp. 851–860, 1987.

[61] J. Cai, X. Peng, K. D. Nelson, R. Eberhart, and G. M. Smith, "Permeable guidance channels containing microfilament scaffolds enhance axon growth and maturation," *Journal of Biomedical Materials Research Part A*, vol. 75, no. 2, pp. 374–386, 2005.

[62] G. Lundborg, L. Dahlin, D. Dohi, M. Kanje, and N. Terada, "A new type of 'bioartificial' nerve graft for bridging extended defects in nerves," *Journal of Hand Surgery*, vol. 22, no. 3, pp. 299–303, 1997.

[63] J. B. Phillips, S. C. J. Bunting, S. M. Hall, and R. A. Brown, "Neural tissue engineering: a self-organizing collagen guidance conduit," *Tissue Engineering*, vol. 11, no. 9-10, pp. 1611–1617, 2005.

[64] B. R. Seckel, D. Jones, K. J. Hekimian, K.-K. Wang, D. P. Chakalis, and P. D. Costas, "Hyaluronic acid through a new injectable nerve guide delivery system enhances peripheral nerve regeneration in the rat," *Journal of Neuroscience Research*, vol. 40, no. 3, pp. 318–324, 1995.

[65] R. D. Madison, C. da Silva, and P. Dikkes, "Peripheral nerve regeneration with entubulation repair: comparison of biodegradable nerve guides versus polyethylene tubes and the effects of a laminin-containing gel," *Experimental Neurology*, vol. 95, no. 2, pp. 378–390, 1987.

[66] P. D. Dalton, L. Flynn, and M. S. Shoichet, "Manufacture of poly(2-hydroxyethyl methacrylate-co-methyl methacrylate) hydrogel tubes for use as nerve guidance channels," *Biomaterials*, vol. 23, no. 18, pp. 3843–3851, 2002.

[67] R. Midha, C. A. Munro, P. D. Dalton, C. H. Tator, and M. S. Shoichet, "Growth factor enhancement of peripheral nerve regeneration through a novel synthetic hydrogel tube," *Journal of Neurosurgery*, vol. 99, no. 3, pp. 555–565, 2003.

[68] A. Piotrowicz and M. S. Shoichet, "Nerve guidance channels as drug delivery vehicles," *Biomaterials*, vol. 27, no. 9, pp. 2018–2027, 2006.

[69] J. S. Belkas, C. A. Munro, M. S. Shoichet, and R. Midha, "Peripheral nerve regeneration through a synthetic hydrogel nerve tube," *Restorative Neurology and Neuroscience*, vol. 23, no. 1, pp. 19–29, 2005.

[70] Y. Luo, P. D. Dalton, and M. S. Shoichet, "Investigating the properties of novel poly(2-hydroxyethyl methacrylate-co-methyl methacrylate) hydrogel hollow fiber membranes," *Chemistry of Materials*, vol. 13, no. 11, pp. 4087–4093, 2001.

[71] E. C. Tsai, P. D. Dalton, M. S. Shoichet, and C. H. Tator, "Synthetic hydrogel guidance channels facilitate regeneration of adult rat brainstem motor axons after complete spinal cord transection," *Journal of Neurotrauma*, vol. 21, no. 6, pp. 789–804, 2004.

[72] Y. Katayama, R. Montenegro, T. Freier, R. Midha, J. S. Belkas, and M. S. Shoichet, "Coil-reinforced hydrogel tubes promote nerve regeneration equivalent to that of nerve autografts," *Biomaterials*, vol. 27, no. 3, pp. 505–518, 2006.

[73] E. C. Tsai, P. D. Dalton, M. S. Shoichet, and C. H. Tator, "Matrix inclusion within synthetic hydrogel guidance channels improves specific supraspinal and local axonal regeneration after complete spinal cord transection," *Biomaterials*, vol. 27, no. 3, pp. 519–533, 2006.

[74] P. M. George, R. Saigal, M. W. Lawlor et al., "Three-dimensional conductive constructs for nerve regeneration," *Journal of Biomedical Materials Research Part A*, vol. 91, no. 2, pp. 519–527, 2009.

[75] G. Verreck, I. Chun, Y. Li et al., "Preparation and physicochemical characterization of biodegradable nerve guides containing the nerve growth agent sabeluzole," *Biomaterials*, vol. 26, no. 11, pp. 1307–1315, 2005.

[76] L. E. Kokai, A. M. Ghaznavi, and K. G. Marra, "Incorporation of double-walled microspheres into polymer nerve guides for the sustained delivery of glial cell line-derived neurotrophic factor," *Biomaterials*, vol. 31, no. 8, pp. 2313–2322, 2010.

[77] C.-J. Chang, "Effects of nerve growth factor from genipin-crosslinked gelatin in polycaprolactone conduit on peripheral nerve regeneration—*in vitro* and *in vivo*," *Journal of Biomedical Materials Research Part A*, vol. 91, no. 2, pp. 586–596, 2009.

[78] C. L. A. M. Vleggeert-Lankamp, G. C. W. de Ruiter, J. F. C. Wolfs et al., "Pores in synthetic nerve conduits are beneficial to regeneration," *Journal of Biomedical Materials Research Part A*, vol. 80, no. 4, pp. 965–982, 2007.

[79] V. Chiono, G. Ciardelli, G. Vozzi et al., "Enzymatically-modified melt-extruded guides for peripheral nerve repair," *Engineering in Life Sciences*, vol. 8, no. 3, pp. 226–237, 2008.

[80] M. D. Bender, J. M. Bennett, R. L. Waddell, J. S. Doctor, and K. G. Marra, "Multi-channeled biodegradable polymer/CultiSpher composite nerve guides," *Biomaterials*, vol. 25, no. 7-8, pp. 1269–1278, 2004.

[81] L. Cai and S. Wang, "Poly(ε-caprolactone) acrylates synthesized using a facile method for fabricating networks to achieve controllable physicochemical properties and tunable cell responses," *Polymer*, vol. 51, no. 1, pp. 164–177, 2010.

[82] S. Wang, M. J. Yaszemski, J. A. Gruetzmacher, and L. Lu, "Photo-crosslinked poly(ε-caprolactone fumarate) networks: roles of crystallinity and crosslinking density in determining mechanical properties," *Polymer*, vol. 49, no. 26, pp. 5692–5699, 2008.

[83] S. Wang, M. J. Yaszemski, A. M. Knight, J. A. Gruetzmacher, A. J. Windebank, and L. Lu, "Photo-crosslinked poly(ε-caprolactone fumarate) networks for guided peripheral nerve regeneration: material properties and preliminary biological evaluations," *Acta Biomaterialia*, vol. 5, no. 5, pp. 1531–1542, 2009.

[84] M. B. Runge, M. Dadsetan, J. Baltrusaitis et al., "The development of electrically conductive polycaprolactone fumarate-polypyrrole composite materials for nerve regeneration," *Biomaterials*, vol. 31, no. 23, pp. 5916–5926, 2010.

[85] S. Wang, Q. Cai, J. Hou et al., "Acceleration effect of basic fibroblast growth factor on the regeneration of peripheral nerve through a 15-mm gap," *Journal of Biomedical Materials Research Part A*, vol. 66, no. 3, pp. 522–531, 2003.

[86] G. E. Rutkowski and C. A. Heath, "Development of a bioartificial nerve graft. II. Nerve regeneration *in vitro*," *Biotechnology Progress*, vol. 18, no. 2, pp. 373–379, 2002.

[87] W. F. A. den Dunnen, B. van der Lei, J. M. Schakenraad et al., "Poly(DL-lactide-ε-caprolactone) nerve guides perform better than autologous nerve grafts," *Microsurgery*, vol. 17, no. 7, pp. 348–357, 1997.

[88] D. Radulescu, S. Dhar, C. M. Young et al., "Tissue engineering scaffolds for nerve regeneration manufactured by ink-jet technology," *Materials Science and Engineering C*, vol. 27, no. 3, pp. 534–539, 2007.

[89] A. Yamada, F. Niikura, and K. Ikuta, "A three-dimensional microfabrication system for biodegradable polymers with high resolution and biocompatibility," *Journal of Micromechanics and Microengineering*, vol. 18, no. 2, Article ID 025035, 2008.

[90] T. Toba, T. Nakamura, Y. Shimizu et al., "Regeneration of canine peroneal nerve with the use of a polyglycolic acid-collagen tube filled with laminin-soaked collagen sponge: a comparative study of collagen sponge and collagen fibers as filling materials for nerve conduits," *Journal of Biomedical Materials Research*, vol. 58, no. 6, pp. 622–630, 2001.

[91] M. Yoshitani, S. Fukuda, S.-I. Itoi et al., "Experimental repair of phrenic nerve using a polyglycolic acid and collagen tube," *Journal of Thoracic and Cardiovascular Surgery*, vol. 133, no. 3, pp. 726–e3, 2007.

[92] S. Tanaka, T. Takigawa, S. Ichihara, and T. Nakamura, "Mechanical properties of the bioabsorbable polyglycolic acid-collagen nerve guide tube," *Polymer Engineering and Science*, vol. 46, no. 10, pp. 1461–1467, 2006.

[93] T. Nakamura, Y. Inada, S. Fukuda et al., "Experimental study on the regeneration of peripheral nerve gaps through a polyglycolic acid-collagen (PGA-collagen) tube," *Brain Research*, vol. 1027, no. 1-2, pp. 18–29, 2004.

[94] S. Ichihara, Y. Inada, A. Nakada et al., "Development of new nerve guide tube for repair of long nerve defects," *Tissue Engineering Part C*, vol. 15, no. 3, pp. 387–402, 2009.

[95] Y. Wang, G. A. Ameer, B. J. Sheppard, and R. Langer, "A tough biodegradable elastomer," *Nature Biotechnology*, vol. 20, no. 6, pp. 602–606, 2002.

[96] C. A. Sundback, J. Y. Shyu, Y. Wang et al., "Biocompatibility analysis of poly(glycerol sebacate) as a nerve guide material," *Biomaterials*, vol. 26, no. 27, pp. 5454–5464, 2005.

[97] D. F. Kalbermatten, P. J. Kingham, D. Mahay et al., "Fibrin matrix for suspension of regenerative cells in an artificial nerve conduit," *Journal of Plastic, Reconstructive & Aesthetic Surgery*, vol. 61, no. 6, pp. 669–675, 2008.

[98] R. C. Young, G. Terenghi, and M. Wiberg, "Poly-3-hydroxybutyrate (PHB): a resorbable conduit for long-gap repair in peripheral nerves," *British Journal of Plastic Surgery*, vol. 55, no. 3, pp. 235–240, 2002.

[99] A. Mosahebi, M. Wiberg, and G. Terenghi, "Addition of fibronectin to alginate matrix improves peripheral nerve regeneration in tissue-engineered conduits," *Tissue Engineering*, vol. 9, no. 2, pp. 209–218, 2003.

[100] Y.-Z. Bian, Y. Wang, G. Aibaidoula, G.-Q. Chen, and Q. Wu, "Evaluation of poly(3-hydroxybutyrate-co-3-hydroxyhexanoate) conduits for peripheral nerve regeneration," *Biomaterials*, vol. 30, no. 2, pp. 217–225, 2009.

[101] D. Yucel, G. T. Kose, and V. Hasirci, "Polyester based nerve guidance conduit design," *Biomaterials*, vol. 31, no. 7, pp. 1596–1603, 2010.

[102] S. H. Oh, J. H. Kim, K. S. Song et al., "Peripheral nerve regeneration within an asymmetrically porous PLGA/Pluronic F127 nerve guide conduit," *Biomaterials*, vol. 29, no. 11, pp. 1601–1609, 2008.

[103] S. H. Oh and J. H. Lee, "Fabrication and characterization of hydrophilized porous PLGA nerve guide conduits by a modified immersion precipitation method," *Journal of Biomedical Materials Research Part A*, vol. 80, no. 3, pp. 530–538, 2007.

[104] C.-J. Chang, S.-H. Hsu, H.-J. Yen, H. Chang, and S.-K. Hsu, "Effects of unidirectional permeability in asymmetric poly(DL-lactic acid-co-glycolic acid) conduits on peripheral nerve regeneration: an *in vitro* and *in vivo* study," *Journal of Biomedical Materials Research Part B*, vol. 83, no. 1, pp. 206–215, 2007.

[105] C.-J. Chang and S.-H. Hsu, "The effect of high outflow permeability in asymmetric poly(DL-lactic acid-co-glycolic acid) conduits for peripheral nerve regeneration," *Biomaterials*, vol. 27, no. 7, pp. 1035–1042, 2006.

[106] X. Wen and P. A. Tresco, "Fabrication and characterization of permeable degradable poly(DL-lactide-co-glycolide) (PLGA) hollow fiber phase inversion membranes for use as nerve tract guidance channels," *Biomaterials*, vol. 27, no. 20, pp. 3800–3809, 2006.

[107] Z. H. Zhou, X. P. Liu, and L. H. Liu, "Preparation and biocompatibility of poly(L-lactide-co-glycolide) scaffold materials for nerve conduits," *Designed Monomers and Polymers*, vol. 11, no. 5, pp. 447–456, 2008.

[108] L. He, Y. Zhang, C. Zeng et al., "Manufacture of PLGA multiple-channel conduits with precise hierarchical pore architectures and *in vitro*/*vivo* evaluation for spinal cord injury," *Tissue Engineering Part C*, vol. 15, no. 2, pp. 243–255, 2009.

[109] G. C. de Ruiter, I. A. Onyeneho, E. T. Liang et al., "Methods for *in vitro* characterization of multichannel nerve tubes," *Journal of Biomedical Materials Research Part A*, vol. 84, no. 3, pp. 643–651, 2008.

[110] M. J. Moore, J. A. Friedman, E. B. Lewellyn et al., "Multiple-channel scaffolds to promote spinal cord axon regeneration," *Biomaterials*, vol. 27, no. 3, pp. 419–429, 2006.

[111] Y. Yang, L. de Laporte, C. B. Rives et al., "Neurotrophin releasing single and multiple lumen nerve conduits," *Journal of Controlled Release*, vol. 104, no. 3, pp. 433–446, 2005.

[112] C. Sundback, T. Hadlock, M. Cheney, and J. Vacanti, "Manufacture of porous polymer nerve conduits by a novel low-pressure injection molding process," *Biomaterials*, vol. 24, no. 5, pp. 819–830, 2003.

[113] T. Hadlock, C. Sundback, D. Hunter, M. Cheney, and J. P. Vacanti, "A polymer foam conduit seeded with Schwann cells promotes guided peripheral nerve regeneration," *Tissue Engineering*, vol. 6, no. 2, pp. 119–127, 2000.

[114] M. S. Widmer, P. K. Gupta, L. Lu et al., "Manufacture of porous biodegradable polymer conduits by an extrusion process for guided tissue regeneration," *Biomaterials*, vol. 19, no. 21, pp. 1945–1955, 1998.

[115] T. B. Bini, S. Gao, T. C. Tan et al., "Electrospun poly(L-lactide-co-glycolide) biodegradable polymer nanofibre tubes for peripheral nerve regeneration," *Nanotechnology*, vol. 15, no. 11, pp. 1459–1464, 2004.

[116] T. B. Bini, S. Gao, X. Xu, S. Wang, S. Ramakrishna, and K. W. Leong, "Peripheral nerve regeneration by microbraided poly(L-lactide-co-glycolide) biodegradable polymer fibers," *Journal of Biomedical Materials Research Part A*, vol. 68, no. 2, pp. 286–295, 2004.

[117] T. Hadlock, J. Elisseeff, R. Langer, J. Vacanti, and M. Cheney, "A tissue-engineered conduit for peripheral nerve repair," *Archives of Otolaryngology—Head & Neck Surgery*, vol. 124, no. 10, pp. 1081–1086, 1998.

[118] X.-K. Li, S.-X. Cai, B. Liu et al., "Characteristics of PLGA-gelatin complex as potential artificial nerve scaffold," *Colloids and Surfaces B*, vol. 57, no. 2, pp. 198–203, 2007.

[119] K. Nakayama, K. Takakuda, Y. Koyama et al., "Enhancement of peripheral nerve regeneration using bioabsorbable polymer tubes packed with fibrin gel," *Artificial Organs*, vol. 31, no. 7, pp. 500–508, 2007.

[120] M.-C. Lu, Y.-T. Huang, J.-H. Lin et al., "Evaluation of a multilayer microbraided polylactic acid fiber-reinforced conduit for peripheral nerve regeneration," *Journal of Materials Science: Materials in Medicine*, vol. 20, no. 5, pp. 1175–1180, 2009.

[121] G. R. D. Evans, K. Brandt, M. S. Widmer et al., "*In vivo* evaluation of poly(L-lactic acid) porous conduits for peripheral nerve regeneration," *Biomaterials*, vol. 20, no. 12, pp. 1109–1115, 1999.

[122] G. R. D. Evans, K. Brandt, S. Katz et al., "Bioactive poly(L-lactic acid) conduits seeded with Schwann cells for peripheral nerve regeneration," *Biomaterials*, vol. 23, no. 3, pp. 841–848, 2002.

[123] C. F. da Silva, R. Madison, and P. Dikkes, "An *in vivo* model to quantify motor and sensory peripheral nerve regeneration using bioresorbable nerve guide tubes," *Brain Research*, vol. 342, no. 2, pp. 307–315, 1985.

[124] A. Goraltchouk, T. Freier, and M. S. Shoichet, "Synthesis of degradable poly(L-lactide-co-ethylene glycol) porous tubes by liquid-liquid centrifugal casting for use as nerve guidance channels," *Biomaterials*, vol. 26, no. 36, pp. 7555–7563, 2005.

[125] S. Wang, A. C. A. Wan, X. Xu et al., "A new nerve guide conduit material composed of a biodegradable poly(phosphoester)," *Biomaterials*, vol. 22, no. 10, pp. 1157–1169, 2001.

[126] A. C. A. Wan, H.-Q. Mao, S. Wang, K. W. Leong, L. K. L. L. Ong, and H. Yu, "Fabrication of poly(phosphoester) nerve guides by immersion precipitation and the control of porosity," *Biomaterials*, vol. 22, no. 10, pp. 1147–1156, 2001.

[127] X. Xu, W.-C. Yee, P. Y. K. Hwang et al., "Peripheral nerve regeneration with sustained release of poly(phosphoester) microencapsulated nerve growth factor within nerve guide conduits," *Biomaterials*, vol. 24, no. 13, pp. 2405–2412, 2003.

[128] S. Wang, D. H. Kempen, G. C. W. de Ruiter et al., "Molecularly engineered photo-cross-linkable polymers with controlled physical properties for bone and nerve regeneration," submitted.

[129] M. C. Dodla and R. V. Bellamkonda, "Differences between the effect of anisotropic and isotropic laminin and nerve growth factor presenting scaffolds on nerve regeneration across long peripheral nerve gaps," *Biomaterials*, vol. 29, no. 1, pp. 33–46, 2008.

[130] Y.-T. Kim, V. K. Haftel, S. Kumar, and R. V. Bellamkonda, "The role of aligned polymer fiber-based constructs in the bridging of long peripheral nerve gaps," *Biomaterials*, vol. 29, no. 21, pp. 3117–3127, 2008.

[131] H. Shen, Y. T. Kim, R. Bellamkonda, and S. Kumar, "Aligned biodegradable poly(lactide-co-glycolide) (PLGA) nano/micro filaments for guided neurite extension," *Polymeric Materials Science & Engineering*, vol. 94, pp. 768–769, 2006.

[132] M. Lietz, A. Ullrich, C. Schulte-Eversum et al., "Physical and biological performance of a novel block copolymer nerve guide," *Biotechnology and Bioengineering*, vol. 93, no. 1, pp. 99–109, 2006.

[133] M. Lietz, L. Dreesmann, M. Hoss, S. Oberhoffner, and B. Schlosshauer, "Neuro tissue engineering of glial nerve guides and the impact of different cell types," *Biomaterials*, vol. 27, no. 8, pp. 1425–1436, 2006.

[134] D. Yin, X. Wang, Y. Yan, and R. Zhang, "Preliminary studies on peripheral nerve regeneration using a new polyurethane conduit," *Journal of Bioactive and Compatible Polymers*, vol. 22, no. 2, pp. 143–159, 2007.

[135] T. Cui, Y. Yan, R. Zhang, L. Liu, W. Xu, and X. Wang, "Rapid prototyping of a double-layer polyurethane-collagen conduit for peripheral nerve regeneration," *Tissue Engineering Part C*, vol. 15, no. 1, pp. 1–9, 2009.

[136] M. Borkenhagen, R. C. Stoll, P. Neuenschwander, U. W. Suter, and P. Aebischer, "*In vivo* performance of a new biodegradable polyester urethane system used as a nerve guidance channel," *Biomaterials*, vol. 19, no. 23, pp. 2155–2165, 1998.

[137] S. Wang, L. Lu, J. A. Gruetzmacher, B. L. Currier, and M. J. Yaszemski, "Synthesis and characterizations of biodegradable and cross-linkable poly(ε-caprolactone fumarate), poly(ethylene glycol fumarate), and their amphiphilic copolymer," *Biomaterials*, vol. 27, no. 6, pp. 832–841, 2006.

[138] E. Jabbari, S. Wang, L. Lu et al., "Synthesis, material properties, and biocompatibility of a novel self-cross-linkable poly(caprolactone fumarate) as an injectable tissue engineering scaffold," *Biomacromolecules*, vol. 6, no. 5, pp. 2503–2511, 2005.

[139] L. Cai and S. Wang, "Elucidating colorization in the functionalization of hydroxyl-containing polymers using unsaturated anhydrides/acyl chlorides in the presence of triethylamine," *Biomacromolecules*, vol. 11, no. 1, pp. 304–307, 2010.

[140] S. Wang, D. H. Kempen, N. K. Simha et al., "Photo-cross-linked hybrid polymer networks consisting of poly(propylene fumarate) and poly(caprolactone fumarate): controlled physical properties and regulated bone and nerve cell responses," *Biomacromolecules*, vol. 9, no. 4, pp. 1229–1241, 2008.

[141] L. Cai and S. Wang, "Parabolic dependence of material properties and cell behavior on the composition of polymer networks via simultaneously controlling crosslinking density and crystallinity," *Biomaterials*, vol. 31, pp. 7423–7434, 2010.

[142] S. Wang, L. Lu, J. A. Gruetzmacher, B. L. Currier, and M. J. Yaszemski, "A biodegradable and cross-linkable multiblock copolymer consisting of poly(propylene fumarate) and poly(ε-caprolactone): synthesis, characterization, and physical properties," *Macromolecules*, vol. 38, no. 17, pp. 7358–7370, 2005.

[143] D. E. Discher, P. Janmey, and Y.-L. Wang, "Tissue cells feel and respond to the stiffness of their substrate," *Science*, vol. 310, no. 5751, pp. 1139–1143, 2005.

[144] P. C. Georges and P. A. Janmey, "Cell type-specific response to growth on soft materials," *Journal of Applied Physiology*, vol. 98, no. 4, pp. 1547–1553, 2005.

[145] I. Levental, P. C. Georges, and P. A. Janmey, "Soft biological materials and their impact on cell function," *Soft Matter*, vol. 3, no. 3, pp. 299–306, 2007.

[146] L. L. Norman, K. Stroka, and H. Aranda-Espinoza, "Guiding axons in the central nervous system: a tissue engineering approach," *Tissue Engineering Part B*, vol. 15, no. 3, pp. 291–305, 2009.

[147] S. Nemir and J. L. West, "Synthetic materials in the study of cell response to substrate rigidity," *Annals of Biomedical Engineering*, vol. 38, no. 1, pp. 2–20, 2009.

[148] L. A. Flanagan, Y.-E. Ju, B. Marg, M. Osterfield, and P. A. Janmey, "Neurite branching on deformable substrates," *NeuroReport*, vol. 13, no. 18, pp. 2411–2415, 2002.

[149] P. C. Georges, W. J. Miller, D. F. Meaney, E. S. Sawyer, and P. A. Janmey, "Matrices with compliance comparable to that of brain tissue select neuronal over glial growth in mixed cortical cultures," *Biophysical Journal*, vol. 90, no. 8, pp. 3012–3018, 2006.

[150] A. Kostic, J. Sap, and M. P. Sheetz, "RPTPα is required for rigidity-dependent inhibition of extension and differentiation of hippocampal neurons," *Journal of Cell Science*, vol. 120, no. 21, pp. 3895–3904, 2007.

[151] R. J. Strassman, P. C. Letourneau, and N. K. Wessells, "Elongation of axons in an agar matrix that does not support cell locomotion," *Experimental Cell Research*, vol. 81, no. 2, pp. 482–487, 1973.